DRAINAGE AND SETTLEMENT CHARACTERISTICS OF HYDRAULIC FILLS

A Thesis Submitted by

Shailesh SINGH

in January 2009

for the degree of Doctor of Philosophy

in the School of Engineering

James Cook University

STATEMENT OF ACCESS

I, the undersigned, the author of this thesis, understand that James Cook University will make it available for use within the University Library and, by microfilm or other means, allow access to users in other approved libraries.

All users consulting this thesis will have to sign the following statement:

> In consulting this thesis, I agree not to copy or closely paraphrase it in whole or in part without the written consent of the author; and to make proper public written acknowledgement for any assistance which I have obtained from it.

Beyond this, I do not wish to place any restriction on access to this thesis.

Signature

14/01/2009

Date:

STATEMENT OF SOURCES

DECLARATION

I declare that this thesis is my own work and has not been submitted in any form for another degree or diploma at any university or other institution of tertiary education. Information derived from the published or unpublished work of others has been acknowledged in the text and a list of references is given.

Signature

14/01/2009
Date

DECLARATION-ELECTRONIC COPY

I, the undersigned, the author of this work, declare that to the best of my knowledge, the electronic copy of this thesis submitted to the library at James Cook University is an accurate copy of the printed thesis submitted.

Signature

14/01/2009
Date

ACKNOWLEDGEMENTS

I express my thanks and appreciation to Associate Prof. Nagaratnam Sivakugan for his guidance and insight throughout the research. It would have been impossible to complete my work without his support. Further I would like to thank Dr. Bithin Datta, Dr. Joao Flavio V. Vasconcellos, Dr. Sarvesh Chandra and Dr. Sanjay Kumar Shukla for their suggestions and inputs in completing my research.

I would like to acknowledge Mr. Warren O'Donnell for his constant support and assistance in laboratory. I am very thankful to my colleague Dr. Kandiah Pirapakaran for all his help in the research. I would like to extend my thanks to School of Engineering, James Cook University for allowing me to undertake this dissertation.

I express my thanks to my family for their understanding, motivation and patience. Lastly, but in no sense the least, I am thankful to all my friends Avinash, Rahul, Girish, Harsha, Garima, Pranvan, Meenan, Sneha, Anuj and Rohit for motivating and keeping me focused on my research.

Thank you all.

Abstract

Mining is one of the major export industries in Australia. When the ore is removed from the ground voids are backfilled. Hydraulic backfill and paste fill are most common backfills. These backfills provide safe working conditions and increase the strength of the ground. Hydraulic backfills consist of classified mine tailings with not more than 10% by weight of size less than 10 μm and approximately 70% by solid weight. These are prepared on the surface by dewatering the mine tailings and transported to the stope transported by gravity through boreholes and pipelines. The solid particles of hydraulic fills settle rapidly after entering the stopes. Excess water initially tends to pond on the surface building up from the lowest corners of a stope and then commences a vertical path of drainage due to gravity. Several miners and equipment had been trapped in mines due to barricade failures and the resulting in rush of mine fills into the drives. An extensive study of drainage and settlement characteristics of hydraulic fills is required to improve design of drainage and barricades.

Most permeability measurements reported in the literature are from undisturbed or reconstituted samples in the laboratory under no surcharge. However, in the mine stopes the hydraulic fill is subjected to significant surcharge due to the overburden. In this research, extensive laboratory tests have been performed to measure permeability of hydraulic fill samples subjected to vertical stress. An analytical solution has been developed to estimate vertical stress development in a vertical and inclined mine stope using continuous compression arch of principal stresses. It has been verified with different analytical model discussed in literature. Degree of saturation of hydraulic fills within mine stopes decreases with continuous drainage of water through barricades. Laboratory tests have been performed to study the moisture content variation in a mine stope with depth and time. Soil-water characteristic curves have been developed using Filter Paper Method for hydraulic fills. Permeability of hydraulic fill has been computed using vertical stress and moisture content variation in a stope. It has been shown graphically.

The anecdotal evidence suggests that the consolidation of the deslimed hydraulic fill is instantaneous. In this dissertation, laboratory tests have been conducted using conventional oedometer and modified triaxial cell to measure the settlement of hydraulic fills. It has been found that the immediate settlement and time dependent settlement contributes equally to the total settlement. Pore water pressure dissipation has observed using modified triaxial cell. Time of consolidation and coefficient of consolidation have been estimated and reported. Settlement- effective stress- time plot has been used to investigate the variation of coefficient of secondary compression (C_α) and it has been observed that $C\alpha$ of hydraulic fill increases with effective stresses and is independent of time.

Concept of equivalent permeability has been used to estimate drainage and maximum pore water pressure in a stope using method of fragments. Empirical equation has been proposed to estimate water level in stope at any time after filling. Reliability analysis has been carried out using First Order-Second Moment Analysis Method to measure the effect of parameter and modeling errors in drainage and settlement analysis. It has been verified using Monte Carlo Simulation.

List of Publications

Journals

Singh Shailesh, Sivakugan Nagaratnam and Chandra Sarvesh (2008). "The permeability of hydraulic fills under surcharge." *International Journal of Geotechnical Engineering*, Vol. 2, No. 2, pp. 77-87.

Singh Shailesh and Sivakugan Nagaratnam (2008). "Time dependent settlement in hydraulic fills." *International Journal of Geotechnical Engineering*, Vol. 2, No. 4, pp. 293 – 303.

Singh Shailesh, Sivakugan Nagaratnam, and Shukla Sanjay Kumar. (2008). "Arching in an inclined mining stope." *Canadian Geotechnical Journal*, (under review).

Singh Shailesh, Sivakugan Nagaratnam, and Shukla Sanjay Kumar (2008). "Can soil arching be insensitive to phi?" *International Journal of Geomechanics*, ASCE, (under review).

Singh Shailesh, Sivakugan Nagaratnam, and Shukla Sanjay Kumar (2008). "Stress reduction factor for a mine stope." *International Journal of Geomechanics*, ASCE, (under review).

Singh Shailesh and Sivakugan Nagaratnam (2009). "Soil-water characteristics curve of hydraulic fills." *Geomechanics and Geoengineering* (Submitted).

Refereed Conference Proceedings

Singh Shailesh and Sivakugan Nagaratnam (2007), "Consolidation behavior of hydraulic fills", *10th Australia New Zealand Conference on Geomechanics*, 21st – 24th October 2007 Brisbane

Pirapakaran Kandiah, Singh, Shailesh, and Sivakugan Nagaratnam (2007),"Hydraulic Fill Research at James Cook University in the new Millennium." *Minefill 2007: Innovations and Experience, Proceedings of the 9th International Symposium on Mining with Backfill,* 29 April – 3 May, 2007, Montreal, Quebec

Pirapakaran Kandiah, Singh Shailesh and Sivakugan Nagaratnam (2006); " Geotechnical characteristics of Australian mine fills ", *Northern Engineering Conference*, 2 – 5 November 2006, University of Central Queensland ,Mackay Australia.

Table of contents

List of Figures

List of Tables

Chapter 1

Introduction

1.1 General

Mining is a multi-billion dollar export industry in many developed and developing countries such as Australia, Brazil, Canada, China, India, etc., where it remains the backbone of the economy. Mining is a large, vital and lucrative business. Its rewards are spread across a wide cross-section of our population. The mines contribute the raw materials for the construction and manufacturing and most of the minerals needed for our society. Undeniably, the evolution of mining is playing an important role in Australia. When ore is removed from mines, large underground voids known as stopes are created. Stopes can be approximated as rectangular parallelepipe and they can have plan dimensions of 20 – 60 m and heights as much as 200 m, and are filled tailings, left over from the mineral extraction process. Different types of backfill materials are used for backfilling depending on the availability and requirements. Hydraulic and paste backfills are the major one. Drainage and settlement is major concern for all the hydraulic backfilled mines. Since stope can have height of up to 200m, even 1% settlement in the hydraulic fill cause a total settlement of up to 2 m, which will leave a large space over backfilled surface. In this dissertation, drainage and settlement characteristics of hydraulic backfills have been studied.

1.2 Methods of mining

There are several mining methods. These can be classified as open pit surface mining and underground mining. In open pit surface mining method, mines are left open after

excavation of ore. These days, most of the mines are using underground mining methods over open pit surface mining. Figure 1.1, shows under ground mine at Osborne Mine in Queensland, Australia. Underground mining can be divided into room and pillar method; and cut and fill method. Room and pillar mining (Figure 1.2a) is designed for mining of flat, bedded deposits of limited thickness whereas cut and fill mining (Figure 2.b) is applied for mining of steeply dipping ore bodies, in strata with good to moderate stability, and a comparatively high grade mineralization. Cut and fill mining provides better selectivity; therefore it is preferred for ore bodies of irregular shape and scattered mineralization. Cut-and-fill mining excavates the ore in horizontal slices, starting from a bottom undercut, advancing upward (2.b). The ore is drilled, blasted, the muck loaded and removed from the stope. When the full stope area has been mined out, voids are backfilled with sand, tailings or waste rock.

a) Underground mine

b) Underground mine showing access drive

Figure 1.1 Underground mine at Osborne, Queensland Australia

1.3 Role and importance of backfilling

The large voids created in the process of underground mining operations are generally backfilled by mill tailings that are produced in mining operation after crushing crude ore in a milling process and grounding it in ball mills or rod mills to a particle size small enough to free the minerals. After removing the minerals from crushed ore, the waste is

either pumped into tailing disposal ponds, as shown in Figure 1.3 or classified for use as hydraulic fills (Pettibone and Kealy, 1971).The underground voids, that are backfilled are known as stopes, and can be approximated as rectangular prisms, which can have heights exceeding 200 meters. These voids are backfilled on the completion of ore extraction. Backfills provide local and regional stability of rock while removing the adjacent stopes in order to continue the mining sequence.

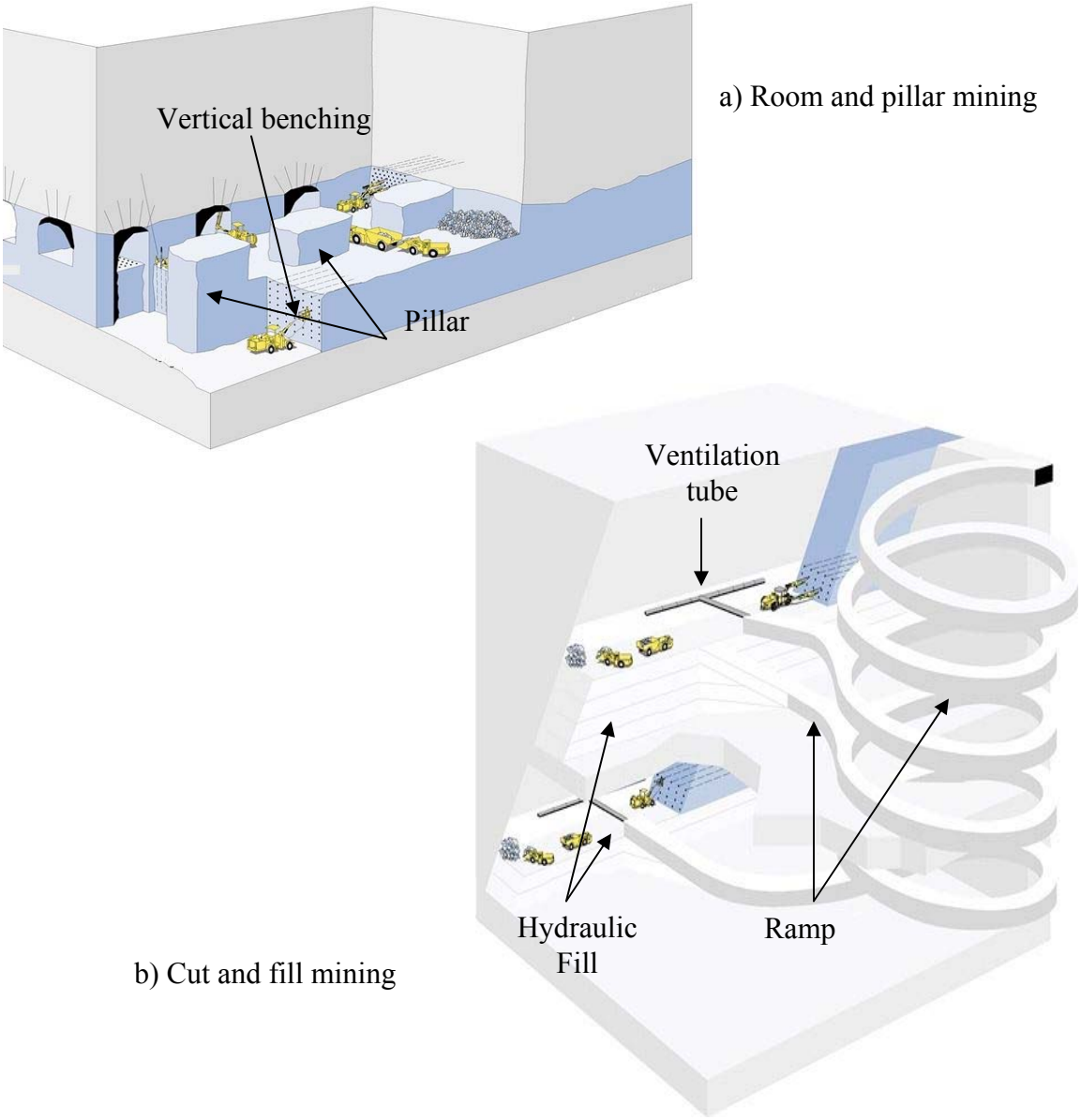

a) Room and pillar mining

b) Cut and fill mining

Figure 1.2 Room and pillar and cut and fill mining methods (Adapted from Hamrin, 2001)

Mine wastes contains heavy minerals which causes several environmental hazards. Disposal of mine wastes have been a major issue for environmentalist. Backfilling of mine stopes using mine tailings (mine wastes) gives a solution to this problem and reduces surface environmental impacts. It also provides safe working conditions and platform for equipments required for mining process by increasing ground strength.

a) Disposed tailing b) Tailing dam

Figure 1.3 Disposed tailing and tailing dam at Osborne Mine Queensland

1.4 Types of backfill

There are several types of minefill materials based on combinations of surface processing plant by-products called tailings, and waste or quarried rock. These minefill materials include tailings-based products such as paste fill, hydraulic fill and cemented hydraulic fill, sand fill, cemented sand fill, rock fill, cemented rock fill, aggregate and cemented aggregate fill (Bloss, 1992). The three major fill types used in Australia are hydraulic fills, pastefills and cemented hydraulic fills (Grice, 2001). Typical backfilled used by mine industries are discussed below.

1.4.1 Dry Fill

Dry fills consists of unclassified gravel, waste rock and slag. These days, use of dry fills is very rare. These are generally unclassified except to remove large boulders. These are transported underground by dropping down a height above the surface directly into the stope. These are suitable for mechanized cut and fill method. It is very rarely used these days.

1.4.2 Cemented rock fill

When cement slurry is added to waste rock to improve the bond strength of rock fragment, it is known as cemented rock fills. It contains coarse and fine aggregates. Both classified and unclassified waste rock can be used to prepare cemented rock fill. These contain a mixture of coarse aggregate and fine aggregates to minimize the void space in the fill. The cement slurry is approximately 55% by weight. It is used in open stopes, undercut and fill. It is suitable for long hole stopes and cut and fill method where a structural fill is required.

1.4.3 Hydraulic fill

Hydraulic backfill can consist either of mine tailings or sand deposits mined off the site. Hydraulic fill is prepared on the surface by dewatering the mine tailings to approximately 65-70% solids by weight. It consist of classified mine tailing with not more than 10% by weight of size less than 10 μm. These are placed underground in the form of slurry, introducing substantial quantities of water into the stope. These are hydraulically pumped to stopes through pipes. Hydraulic fills are discussed in detail later in this dissertation.

1.4.4 Paste fill

Paste fills are newest form of mining backfill, which are produced from the full mill tailings and has a much finer grain size distribution than any other form of backfill. Typically it has a minimum of 15% of the material smaller than 20 μm. Typically the maximum size of particles in paste is between 350 – 400 μm. Paste fill can be defined as a mixture of tailings, cement and water and in its uncured state particles do not settle out. Cement and water are added to the mix to achieve the required rheological and strength characteristics.

1.5 Problems associated with hydraulic backfilling

In 1997, five hydraulic backfill failed in Australian mines due to delivery of excess quantity of transport water from low density slurry (Grice, 1998a). On June 26, 2000 three men were killed when around 18000 m^3 of fill entered the lower levels of a gold mine in the northern Goldfield of Western Australia (Potential Hazards Associated with Mine fill, Department of Mineral and Petroleum Resources Western Australia, Safety Bulletin) due to the failure of fill barricades. Most of the failures take place in the early hours of filling and are caused by the presence of excess water within the mine fill. The major cause barricades failure is attributed to the build-up of high pore water pressure behind the barricades resulting the liquefaction due to blasting or piping.

1.6 Problem statement

Mine stopes are backfilled using hydraulic fills. These are transported through pipelines in the form of slurry, at 65-75% solids content, implying water contents of 33-54%. It settles within the stope under its self-weight, draining through the barricades that cover the horizontal access drives. The solid particles of hydraulic fills settle rapidly after entering the stopes. Excess water initially tends to pond on the surface building up from the lowest corners of the mine stope and then commences a vertical path of drainage due to gravity. Since hydraulic fills are placed as slurry, there is substantial amount of water entering the stope. Several hydraulic backfilled mine have failed due to presence of excess water in stope and development of high pore water pressure. Sivakugan and

Rankine (2006); and Sivakugan et al. (2006) used method of fragments to estimate drainage and maximum pore water pressure in the stope. Isaac and Carter (1983) developed a numerical model for same. Several analysis and numerical modeling haves been done to predict measure pore water pressure and drainage from stope.

In most of the numerical modeling work carried out to date, simulating the drainage through hydraulic fills, it is assumed that the permeability of the fill remains constant with depth (Isaacs and Carter, 1983; Sivakugan et al., 2006; Sivakugan and Rankine, 2006; and Rankine, 2004 and 2007). The hydraulic fills in at the mine stopes are under several meters of overburden which reduces voids in the hydraulic fills thus reduces permeability. Hydraulic fill transfer a part of its self weight to the adjacent rock mass in the process of self-weight settlement due their friction between hydraulic fill and adjacent rock wall (Sivakugan 2008). This process of reduction in vertical normal stress is known as arching. Stress reduction in a two dimensional vertical and inclined mine stope have been studied in this dissertation. In this dissertation, modified oedometer has been used to measure permeability variation with vertical effective stress. Effect of moisture content on permeability has been studied using soil – water characteristic curve, which has been developed using filter paper method. Permeability variation in a mine stope with depth has been studied and equivalent permeability has been used to compute drainage and maximum pore water pressure using method of fragments.

When hydraulic fill is placed in the underground voids in the form of slurry, the settlement takes place solely under the self-weight. It has been assumed that the consolidation of hydraulic fills is over within seconds. In this dissertation, several laboratory tests have been conducted on oedometer and modified triaxial cell to measure settlement and pore water dissipation in hydraulic fill samples. Concept of secondary compression has been used to understand the settlement behavior of hydraulic fills. Reliability analysis has been carried out to study uncertainties in numerical and laboratory modeling.

1.7 Scope of research

The main objectives of this research are as following:

i. Study the effect of arching on vertical stress in an inclined and vertical mine stope using compression arch of principal stresses and compare it with arching models used by Marston (1930), Handy (1985), Aubertin et al. (2003), and Pirapakaran and Sivakugan (2007a and 2007b).
ii. Develop soil-water characteristic curve (SWCC) for hydraulic fills using Filter Paper method and estimate residual moisture content in hydraulic fills.
iii. Carryout laboratory tests to measure permeability of hydraulic fills under surcharge.
iv. Study moisture content variation with depth and time within the stopes and develop permeability variation with depth in a mine stope using SWCC, surcharge and moisture content variation.
v. Predict the time dependent settlement (Consolidation and secondary compression) and pore water pressure dissipation in hydraulic fills fill samples.
vi. Estimate of drainage and pore water pressure using method of fragments and equivalent permeability.
vii. Carryout the reliability analysis to study uncertainty in numerical and laboratory modeling.

1.8 Thesis overview

Chapter 1 introduces mining methods and different type of backfills used by mining industry. It gives an overview of the importance and problem associated with backfilling of mines using hydraulic fills. An overview of the thesis has been given in this section.

Physical properties of hydraulic fills are discussed in Chapter 2. Review of physical properties available, in literature such as grain shape, texture, mineralogy, particle size distribution, specific gravity, permeability, consolidation, etc are briefed in this chapter.

An empirical equation has been proposed to estimate hydraulic fill internal friction angle using relative density. A mathematical model has been developed to predict particle size distribution of hydraulic fills which has been used in establishing soil – water characteristic curve for hydraulic fills numerically. Filter paper method has been to measure matric suction of hydraulic fills and soil – water characteristic curves has established. Residual and saturation moisture content of hydraulic fills have been reported in this chapter.

State of stress within an underground mine has been discussed in Chapter 3. Concept of arching has been reviewed in this chapter. A brief description of backfill stope interface angle has been given. An analysis has been carried out to estimate vertical stress in an inclined and vertical stope using compression arch of principal stresses. An equation has been proposed to estimate the vertical stresses within the inclined stope for any backfill under a surcharge. In this chapter, a methodology has been proposed to calculate the vertical stress distribution along the width of inclined stope. The variation of stresses along the width of stope is graphically shown. Effects of hydraulic fill friction angle (ϕ) and wall-backfill interface angle (δ) on vertical stress have been studied and discussed in this chapter. Concept of stress reduction factor (α_s) and average stress reduction factor ($\alpha_{average}$) have been introduced to estimate average stress at any depth in the stope.

Chapter 4 discusses permeability and moisture content variation in a stope. Laboratory tests have been conducted to study effect of surcharge on permeability. Empirical equations have been proposed to estimate permeability from surcharge and other physical properties such as specific gravity and relative density of hydraulic fills. Variation of moisture content with depth and time in laboratory models representing stopes have been discussed in this chapter. It has been used with SWCC and stress due arching in estimating permeability variation with depth in a mine stope. Concept of cutoff permeability is also discussed in this chapter.

Settlement of hydraulic fills is discussed in Chapter 5. Extensive laboratory tests that have been used to measure settlement and pore water pressure dissipation have been

reported in this chapter. An empirical equation has been given in this chapter to estimate total settlement of hydraulic fills. Settlement – effective stress – time plot has been used to investigate the variation of coefficient of secondary compression. Coefficient of consolidation and pore water pressure dissipation are also reported in this chapter.

Chapter 6 describes method of fragments that has been used by Sivakugan and Rankine (2006) and Sivakugan et al. (2006) to compute drainage and maximum pore water pressure in a stope. It also discusses the concept of equivalent permeability that has been proposed to use for estimating drainage and maximum pore water pressure. A methodology has been given in this chapter to calculate time dependent drainage and pore water pressure in hydraulic backfilled stope.

Chapter 7 gives details of uncertainty analysis of drainage and pore water pressure analysis used in this dissertation. First Order – Second Moment (FOSM) and Monte Carlo simulation has been described briefly in this chapter. FOSM has been used for reliability analysis and it has been verified using Monte Carlo simulation. Summary and conclusions of the research and recommendations for future research are presented in Chapter 8.

Chapter 2

Physical Properties of Hydraulic Fills

2.1 General

Tailings are produced in mining operation after crushing crude ore in a milling process and grounding it in ball mills or rod mills to a particle size small enough to free the minerals. After removing the minerals from crushed ore, the waste is either pumped into tailing disposal ponds or classified for use as hydraulic fills (Pettibone and Kealy, 1971). Hydraulic fills are class of mine fills that are delivered as high density slurry through boreholes and pipelines to the mine stopes. Water-borne delivery method is the reason behind the name, hydraulic fill. These are also known as conventional backfill, slurry backfill, or sand fill.

Hydraulic fills generally have maximum particle size less than 1 mm and not more than 10% of weight less than 10 μm (i.e. $D_{10} > 10$ μm). Hydraulic fill slurries are prepared at densities between 40 to 50 % solid by volume or greater than 65 – 70 % solid by weight, implying water contents of 33 – 54% (Grice 2005).

Hydraulic fills are prepared from classified mine tailings or sands or esker deposits mined on the surface. It is frequently the case that mine tailings do not have sufficient coarse fraction to meet the hydraulic backfill requirements so the mines may add borrowed sand or fill parts of the stopes with waste rocks wherever possible. These are most commonly prepared using hydrocyclones. Schematic diagram of hydrocylone is shown in Figure 2.1 Hydrocyclones use vortex mechanism to achieve the classification process. Mine tailing slurries, at densities 15–35% solid by weight, are pumped through a cluster of

hydrocyclones (Figure 2.2). The slurry enters the top of the unit tangentially and commences a spiral downward flow around the perimeter of hydrocyclone. Heavier particles remain closer to the body wall and finer particles tend toward central axis with water. Finer particles and water travel upwards through the inner vortex and heavier particles and remaining water exit the hydrocyclone via the spigot. The underflow product is deslimed and dewatered hydraulic fills whereas overflow is rejected to the final tailing storage facilities such as tailing dams.

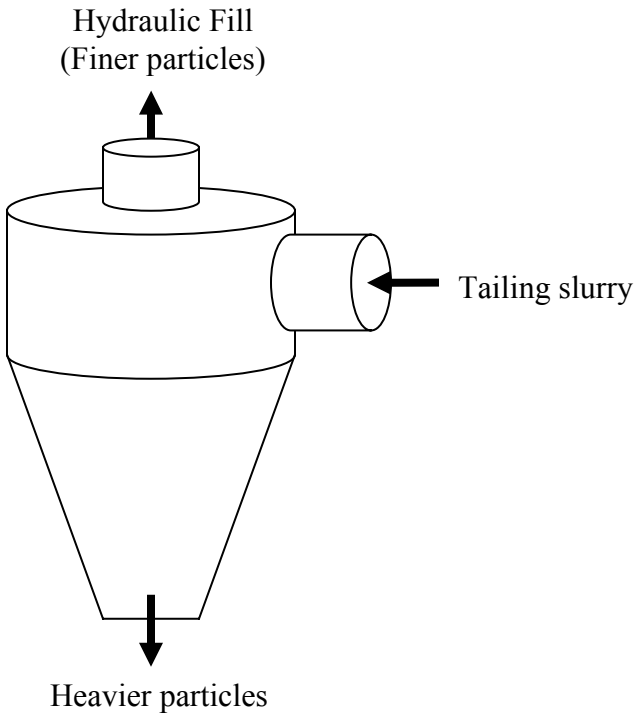

Figure 2.1 Schematic diagram of hydrocyclone

Hydraulic fills are placed in mine stope in form of a loose structure with a void ratio of about 0.7 (http://www.mininglife.com/Miner/Backfill/Types_of_%20Mine_Backfill.htm). In practice, an apparent cohesion often develops in uncemented sandfill which increases the shear strength of the backfill. Vibratory forces due to blasting in neighboring stopes can densify the fill and increase the shear strength. Very small amount of cement and other binders are added to hydraulic fills to increase the cohesion.

Hydraulic fills provides good working surface for mechanized mining machines. It reduces surface storage and environmental problems caused by presence of heavy metals in mine wastes. Main disadvantage of hydraulic fills is the amount of water that drains from the mine stope and must be pumped back to the surface (Cooke 2001).

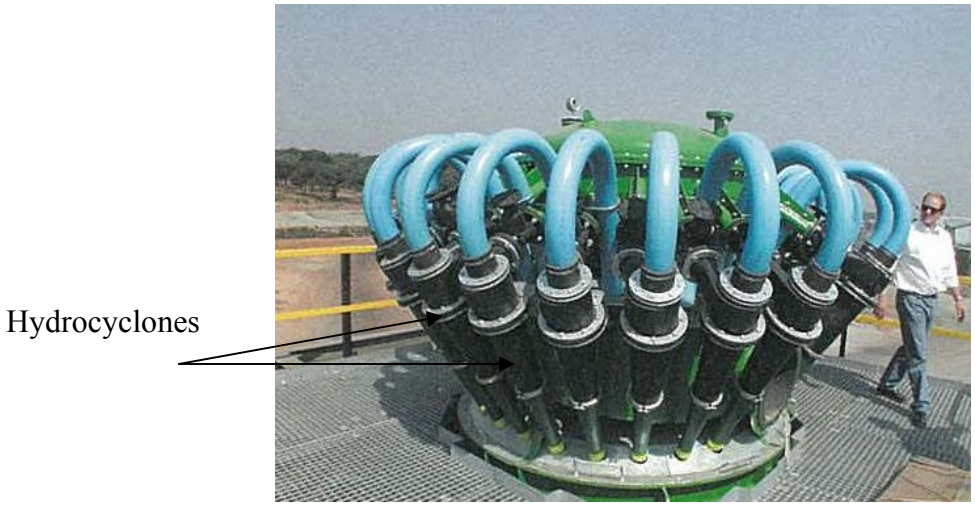

Figure 2.2 Hydrocyclone cluster (After Grice, 2005)

2.2 Review of physical properties of hydraulic fills

Hydraulic backfills consist of either mine tailings or sand deposits mined off the site, where the effective grain size (D_{10}) is greater than 10 μm. These are prepared on the surface by passing the tailings through hydrocyclones where the very fine fraction is removed, leaving only silt and sand sized grains. These are transported through pipelines in the form of slurry, at 65-75% solids content, implying water contents of 33-54%. This slurry settles within the stope under its self-weight, draining through the barricades that cover the horizontal access drives. Physical and geotechnical properties of hydraulic fills are discussed in this chapter.

2.2.1 Grain shape, texture and mineralogy

Hydraulic fills are prepared from crushing of waste rock or waste products from mining operation from the milling process. These consist of hard, angular particles and siliceous particles (http://www.tfhrc.gov/hnr20/recycle/waste/mwst4.htm, 15 November 2008). Typical shape of hydraulic fill sample A1, B1, B2 and C2 is shown in Figure 2.3. Hydraulic fills are prepared from raw rocks or new rocks so they are angular and sharp (as shown in Figure 2.3), which increases interlocking of the fill materials. Pettibone and Kealy (1971); Nicholson and Wayment (1964); Rankine (2007); and Sivakugan (2008) made similar observation of grain shape of hydraulic fills.

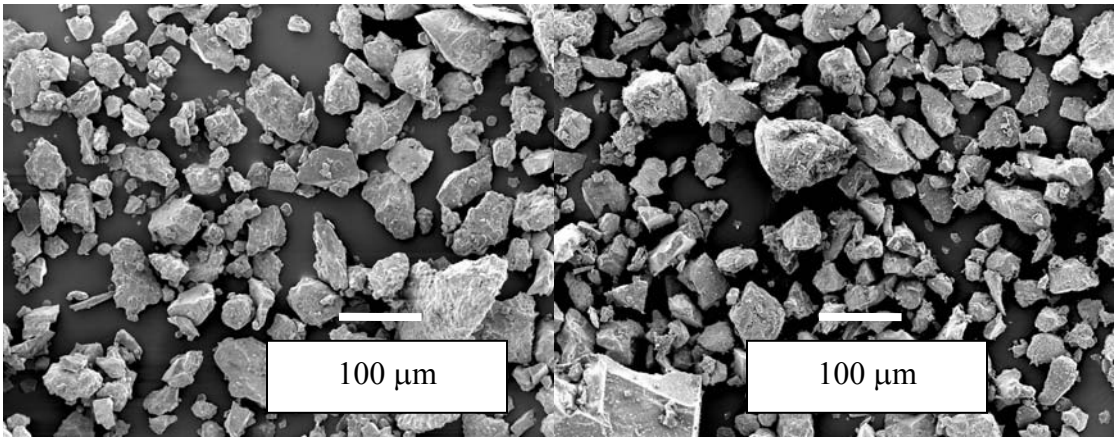

(a) A1 (b) B1

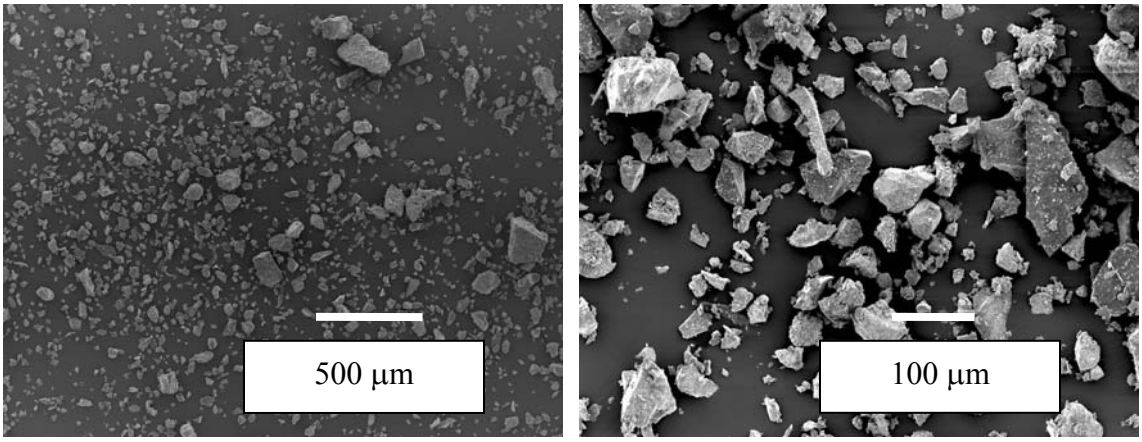

(c) B2 (d) C2

Figure 2.3 Electronic micrograph of hydraulic fill samples A1, B1, B2 and C2

Majority of clay minerals or mica present in the mine tailings are lost when excess water is added and fines are removed using hydrocyclones. It leaves hydraulic fills with coarser grains.

2.2.2 Particle size distribution

Particle size distribution plays a major role in deciding the soil behavior (Clarke, 1988; Fredlund et al., 2000; and Hinde, 1993).Void ratio and internal friction angle of sands depends on the grading of particle size distribution (Holtz and Gibbs, 1956; and Lambe and Whitman, 1969). Better distribution of particle size (well graded) produces a better interlocking of the soil grains (Lambe and Whitman, 1969) thus lower the permeability. Particle size distribution curves of 15 hydraulic fill samples from Australian Mines are shown in Figure 2.4 (Rankine, 2005). Effective grain size (D_{10}), which is defined as diameter corresponding to 10% finer in the particle size distribution curve, defines the ability of a hydraulic fill to percolate water and settle from slurry (Nicholson and Wayment, 1964; Thomas and Holtham, 1989). For hydraulic fills d_{10} should be greater than 10 μm.

Uniformity coefficient (C_u) and coefficient of gradation (C_Z) of hydraulic fill have been calculated using Equations 2.1 and 2.2 and have been reported in Table 2.1.

$$C_u = \frac{D_{60}}{D_{10}} \tag{2.1}$$

$$C_z = \frac{D_{30}^2}{D_{60} \times D_{30}} \tag{2.2}$$

It can be seen from Figure 2.4 that effective grain size (D_{10}) of hydraulic fills in Australian Mines is more than 10 μm. In previous studies, D_{10} has been used to compute permeability of hydraulic fills (Sivakugan et al. 2006 and Rankine 2007). Kuganathan

(2002) and Brady and Brown (2002) quoted that typical hydraulic fill D_{10} values of excess of 10 μm and Herget and De Korompay (1978) suggested that d_{10} of hydraulic fills is 35 μm. D_{10} of hydraulic fills measured at James Cook University varies from 19 μm to 40.5 μm as shown in Table 2.1 and Figure 2.4. Uniformity coefficient (C_u) and coefficient of gradation (C_Z) shows the packing of grains in the hydraulic fills. Figure 2.2 shows that hydraulic fills are poorly graded.

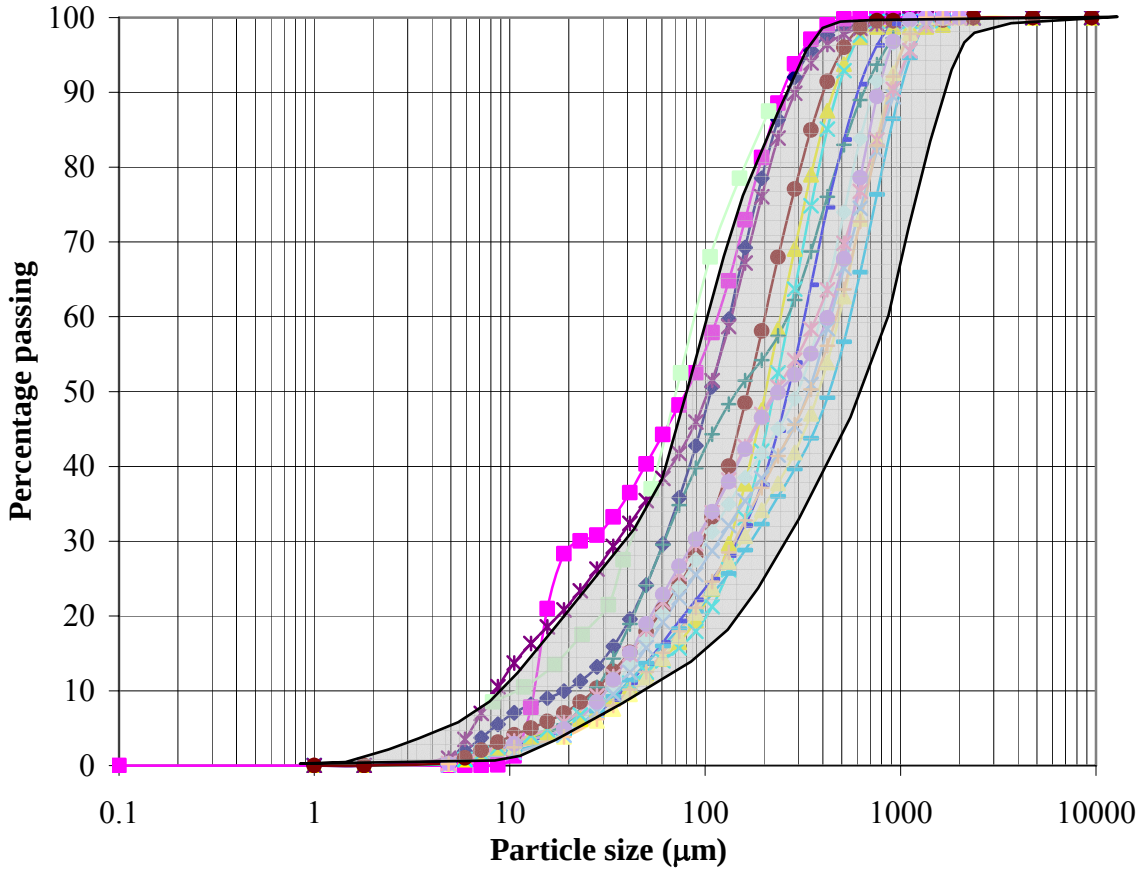

Figure 2.4 Particle size distribution curves of 15 hydraulic fills of Australian mines (From Rankine, 2005)

2.2.3 Unified Soil Classification System

As discussed in Section 2.2.1, clay and finer particles in mine tailings are removed using hydroclones which leaves coarser particle only. In the Unified Soil Classification System (USCS), the hydraulic fills would be classified as silty sands (SM) or sandy silts (ML)

with no plasticity. 15 hydraulic fill samples from 3 different mines have been classified as per USCS and reported in Table 2.1.

Table 2.1 Geotechnical properties of hydraulic fills

Sample*	D_{10} (μm)	d_{30} (μm)	d_{60} (μm)	C_u	C_Z	e_{max}	e_{min}	e	D_r (%)	G_s	k (mm/hr)	USCS symbols
A1	19.5	62	132	6.8	1.5	1.029	0.417	0.69	55.4	2.80	19.1	SM
A2	19	61	133	7.0	1.5	0.959	0.437	0.67	55.4	2.79	9.1	SM
B1	12	56	132	11.0	2.0	1.017	0.434	0.63	66.4	3.69	17.8	SM
B2	19	37	71	3.7	1.0	1.04	0.399	0.59	70.2	3.02	22.5	ML
B3	20	44	83.5	4.2	1.2	1.048	0.673	0.79	68.8	4.37	17.4	ML
B4	19.5	58	130	6.7	1.3	1.091	0.479	0.62	77.0	3.45	18.0	SM
C1	36	165	550	15.3	1.4	1.166	0.477	0.7	67.6	3.53	37.8	SM
C2	40.5	160	475	11.7	1.3	0.937	0.412	0.66	52.8	3.53	33.1	SM
C3	26	62	260	10.0	0.6	0.829	0.431	0.58	62.6	3.42	20.7	SM
C4	38	150	315	8.3	1.9	1.559	0.438	0.66	80.2	3.71	22.7	SM
C5	34	101	395	11.6	0.8	1.021	0.418	0.72	49.9	3.50	24.4	SM
C6	34.5	120	440	12.8	0.9	1.402	0.53	0.7	80.5	3.50	30.3	SM
C7	29	91	365	12.6	0.8	1.184	0.544	0.68	78.8	3.32	27.8	SM
C8	32	89	425	13.3	0.6	0.975	0.567	0.72	62.5	3.12	33.2	SM
C9	40.5	140	465	11.5	1.0	1.036	0.534	0.72	62.9	3.42	28.2	SM

*A, B and C are samples from different mines; each sample was collected at different time and are independent.

2.2.4 Dry density, relative density and porosity

Cowling (1998) reported that dry density of hydraulic fills is approximately half of the specific gravity. Rankine (2005) and Rankine et al. (2006) performed series of laboratory tests at James Cook University laboratory to study dry density variation of hydraulic fills with specific gravity. Variation of dry density of hydraulic fills with specific gravity for hydraulic fill samples at James Cook Univeristy, in situ measurements (Pettibone and Kealy, 1971) is shown in Figure 2.5.

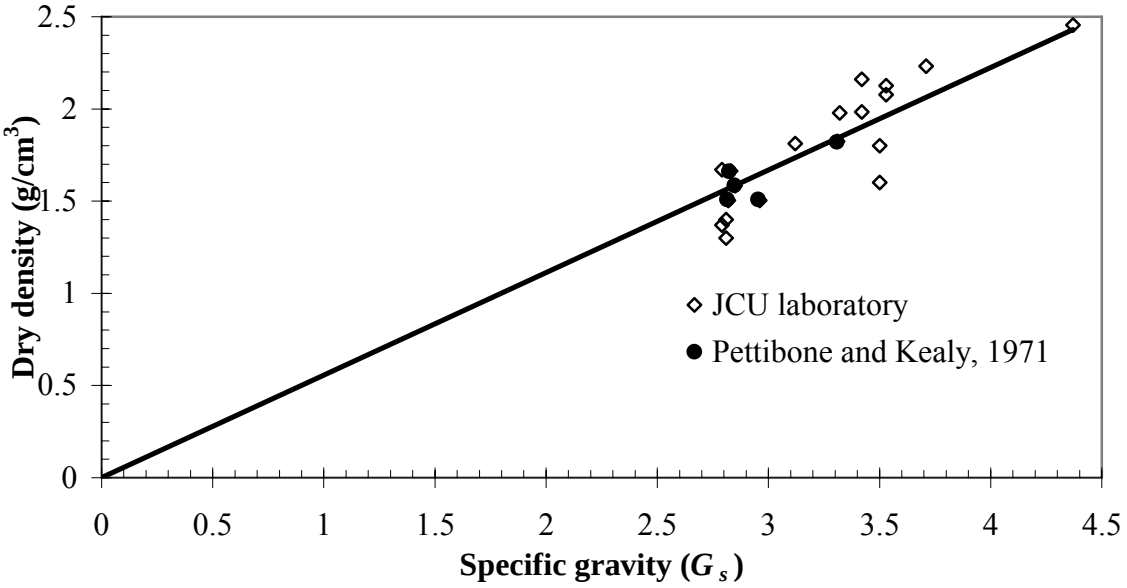

Figure 2.5 Dry density versus specific gravity (Adapted from Rankine et al. 2006)

Equation 2.3 was proposed by Rankine et al. (2006) and Rankine (2007) to estimate laboratory dry density of hydraulic fills.

$$\rho_d \left(\frac{\text{g}}{\text{cm}^3} \right) = 0.56 G_s \tag{2.3}$$

where, ρ_d is laboratory dry density and G_s is specific gravity of hydraulic fills. Coefficient of determination (R^2) of above empirical equation is 0.85, which shows very good correlation between specific gravity and dry density.

Porosity of hydraulic fills have been reported in the literature by Nicholson and Wayment (1964), Pettibone and Kealy (1971), and Potvin et al. (2005). It has been reported that it varies from 0.3 to 0.5. Rankine et al. (2006) estimated porosity of hydraulic fills using 24 samples at James Cook University Laboratory and reported that it varies from 0.37 to 0.49.

Relative density (D_r) of soil is defined as following:

$$D_r = \frac{e_{\max} - e}{e_{\max} - e_{\min}} \times 100\% \tag{2.4}$$

where, e_{max}, e_{min} and e are maximum void ratio, minimum void ratio and void ratio of hydraulic fills respectively. Rankine et al. (2006) observed that relative density of hydraulic fills measured at James Cook University Laboratory varies from 40 – 80%. Nicholson and Wayment (1964), Pettibone and Kealy (1971), and Corson et al. (1981) estimated relative density of mine tailings and reported similar values. Relative density variation of hydraulic fills with void ratio is shown in Figure 2.6. As shown in the Figure 2.6, relative density of hydraulic fills varies from 50% to 80%. Maximum and minimum void ratio of hydraulic fills used in this dissertation is given in Table 2.1.

2.2.5 Specific gravity

The mineralogy of the mine tailings is such they have quite high values of specific gravities from 2.80 to 4.50. This is significantly higher than the range of 2.60-2.80 reported for inorganic soils including sands, silts and clays. Specific gravity of hydraulic fills have been measured as per AS 1289 3.5.1 and reported in Table 2.1. Specific gravity plays a major role in behavior of hydraulic fills. Effect of higher specific gravity on permeability and other geotechnical properties have been studied in this dissertation and discussed in Chapter 4.

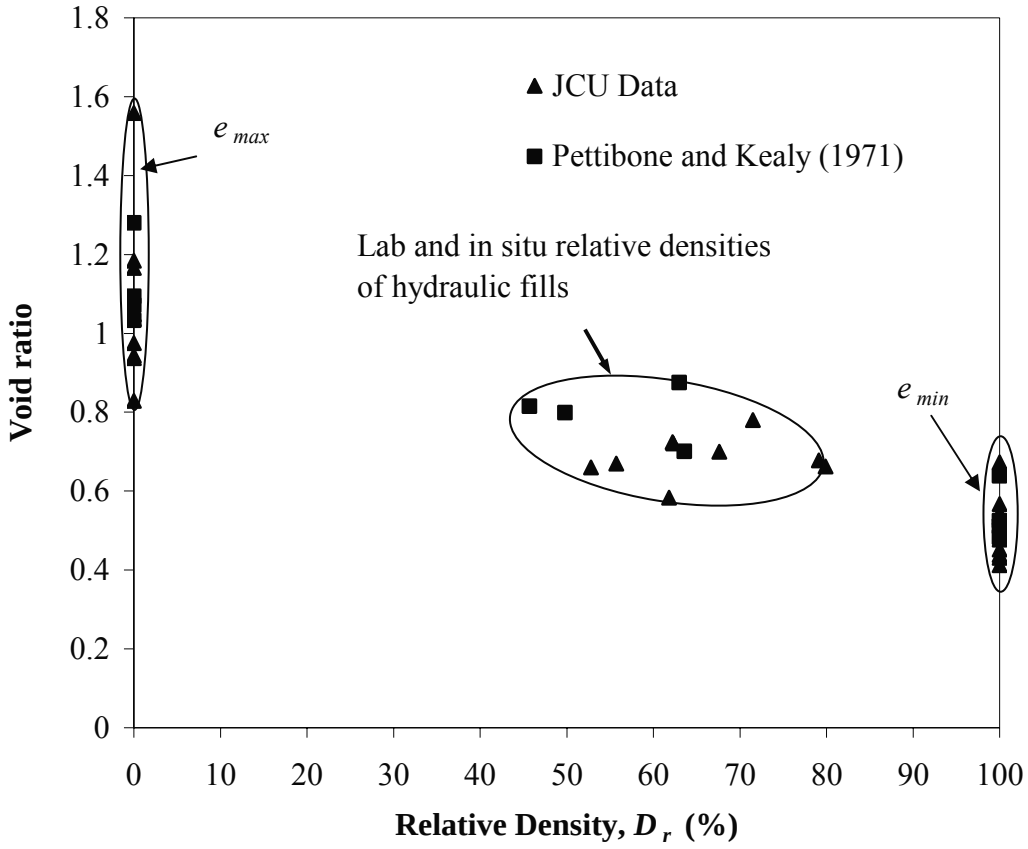

Figure 2.6 Void ratio versus relative density of hydraulic fills (Adapted from Rankine et al. 2006)

2.2.6 Permeability

Rankine et al. (2004) and Sivakugan et al. (2006) reported permeability measurements on 25 different hydraulic fills representing four different mines in Australia. All samples were prepared as slurries with water content of 30-35%, similar to those of slurries placed at the mines. All samples were allowed to settle under their self weight in a 153 mm diameter × 306 mm high cylindrical permeameter. Hydraulic fills were poured in a permeameter in form of slurry and allowed to settle with the permeameter. The porosity variation of settled hydraulic fill in the permeameter varied from 36% to 49%. Constant head and falling head permeability tests were carried out on each sample and the average values are plotted against the effective grain size in Figure 2.7. Hazen (1930) suggested

that for clean uniform filler sand, permeability and effective grain size are related by following equation:

$$k = CD_{10}^2 \tag{2.5}$$

where, k is permeability of hydraulic fills in mm/hr, C is empirical coefficient and d_{10} is effective grain size in μm. It can be seen from Figure 2.7 that the C is in range of 0.02-0.06 for above hydraulic fills. Permeability variation with surcharge, moisture content in a mine stope have been studied and discussed in Chapter 4 for sample A1, B1, B2, C1 and C2.

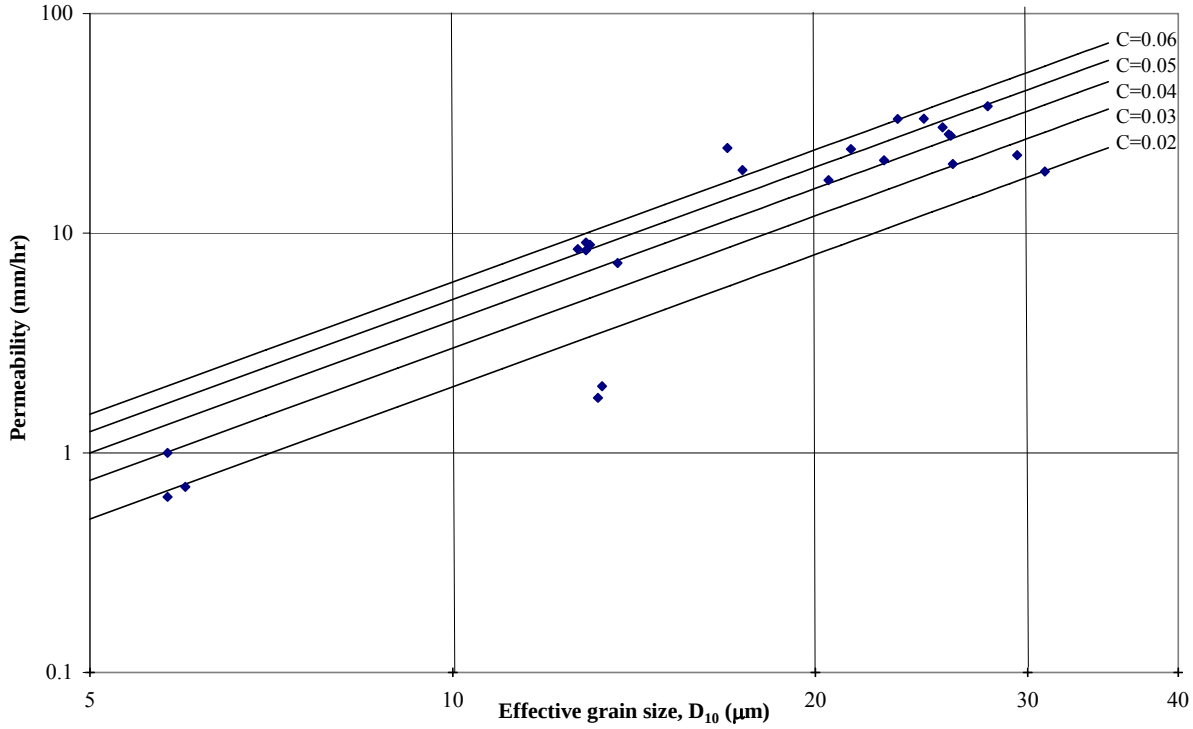

Figure 2.7 Variation of permeability of sedimented hydraulic fills in laboratory with effective grain size

2.2.7 Consolidation and settlement

When hydraulic fill is placed in the underground voids in the form of slurry, the settlement takes place solely under its self weight. Consolidation is the volume change in any saturated and unsaturated soil under a constant load with time due to change in pore water pressure. Very small consolidation settlement occurs in sand to silt sized soils, such as hydraulic fills (Carrier et al., 1983). Thomas et al. (1979) and Clarke (1988) reported that consolidation of hydraulic fills is complete within seconds and no further change occurs with subsequent drainage.

Wickland and Wilson (2005) performed self weight consolidation tests on mine tailing and rock mixture in a column of approximately 1 m diameter and 6 m height for disposal of mine wastes. Wickland and Wilson (2005) observed that the majority of settlement of mixture column occurs during dissipation of pore water pressure with additional volume change and shrinkage occurring under negative pore water pressure. Total settlement in each column was less than 5% after 100 days. Stone et al. (1994) used centrifuge modeling technique to replicate the staged filling of the tailings impoundment to assess both the short and long time consolidation behavior of tailings from Boddinston Gold Mine in Western Australia and measured the long term variation of pore pressure within the different layers of tailing during self weight consolidation. Qiu and Sego (2001) performed consolidation test in a large-strain consolidation cell on copper, coal and gold mine tailings in Canada for load increment of 0.5-100 kPa. Coefficient of consolidation and coefficient of volume compressibility were calculated for these samples by Qiu and Sego (2001). It has been reported that the coefficient of consolidation of tailings varies from 0.310 m^2/yr to 104.23 m^2/yr.

2.2.8 Cohesion and friction angle

Friction angle of hydraulic fills is very important in analyzing static and dynamic stability of mine stopes (Mitchell et al. 1975). Pirapakaran (2008) performed Direct Shear test on 12 hydraulic fill samples from three different mines (A, B and C) to determine peak

friction angle as per AS 1289.6.2.2. Friction angle of 12 hydraulic fill samples at different packing has been shown in Table 2.2. Friction angle of hydraulic fills varies from 27.6^0 to 43.6^0. Bloss (1992), Pettibone and Kealy (1971), and Nicholson and Wayment (1964) reported that friction angle of hydraulic fills varies from 30^0 to 47^0, which is same as laboratory test results at James Cook University Laboratory.

Variations of friction angle with relative density of hydraulic fills have been studied. Hydraulic fills from Australian mines falls in a narrow band as shown in Figure 2.8. Pirapakaran (2008) plotted friction angle variation with relative density for hydraulic fills samples A1, B1 and C1. Pirapakaran (2008) computed internal friction angle using empirical equations proposed by Kulhawy and Mayne (1990), Skempton (1986), and Meyerhof (1957) and proposed a linear correlation between friction angle and relative density as following equations:

Kulhawy and Mayne (1990) $$\phi(\text{degree}) = 0.20D_r + 23.5 \quad (2.6)$$

Skempton (1986) $$\phi(\text{degree}) = 0.18D_r + 23.7 \quad (2.7)$$

Meyerhof (1957) $$\phi(\text{degree}) = 0.13D_r + 24.5 \quad (2.8)$$

Pirapakaran (2008) $$\phi(\text{degree}) = 0.17D_r + 26.4 \quad (2.9)$$

It has been observed that friction angle of hydraulic fills is higher than the friction angle of other soils at similar relative density. Angular particles of hydraulic fills increase the interlocking of particles which increases the friction angle. As shown in Figure 2.8, friction angle of hydraulic fills is 3.5^0 more than the friction angle predicted using the empirical equation proposed by Skempton (1986). Following equation can be used to determine friction angle of hydraulic fills from relative density.

$$\phi(\text{degree}) = 0.18D_r + 27.2 \quad (2.10)$$

Table 2.2 Friction angle (ϕ) of hydraulic fills in degree (Pirapakaran, 2008)

Sample	Very loose		Loose		Medium		Dense	
	ϕ	D_r (%)	ϕ	D_r (%)	ϕ	D_r (%)	ϕ	D_r (%)
A1	27.6	0	29.2	24	31.0	64	36.6	74
B1	33.1	0	33.9	30	36.2	49	38.7	69
B2	29.7	0	30.4	29	31.0	46	33.6	70
C1	36.2	13	36.2	30	38.5	54	41.3	68
C2	35.5	0	35.5	32	38.2	51	43.6	75
C3	30.5	0	30.5	19	33.4	61	36.7	81
C4	31.0	0	31.0	34	36.5	54	39.0	81
C5	32.0	0	32.3	24	35.8	47	40.2	67
C6	32.6	0	32.6	21	36.7	54	37.9	75
C7	29.9	6	30.0	27	34.6	60	36.9	72
C8	34.4	5	35.5	24	37.5	48	42.9	82
C9	33.8	0	34.9	27	39.8	56	41.3	72

2.3 Mathematical model to represent particle size distribution

Particle size distribution has been used as basis for estimation of soil water characteristic of soil by many researchers (Gupta and Larsen 1979a, 1979b; Arya and Paris 1981). Several attempts have been made to establish a mathematical model to represent the particle size distribution of soils. Gardner (1956) proposed a two parameter lognormal distribution to represent the particle size distribution of soil. Hagen et al. (1987) developed a computerized iterative procedure using two sieves to establish particle size distribution of soil. Fredlund et al. (2000) presented two mathematical models, namely, unimodal form and bimodal form, to represent the particle size distribution curve. In all these models various curve fitting parameters, such as parameter related to shape and slope of the particle size distribution curve, minimum allowable particle size, etc, have been used. In this dissertation, an attempt has been made to develop a particle size

distribution for hydraulic fills using median particle size D_{50} (diameter corresponding to 50% finer).

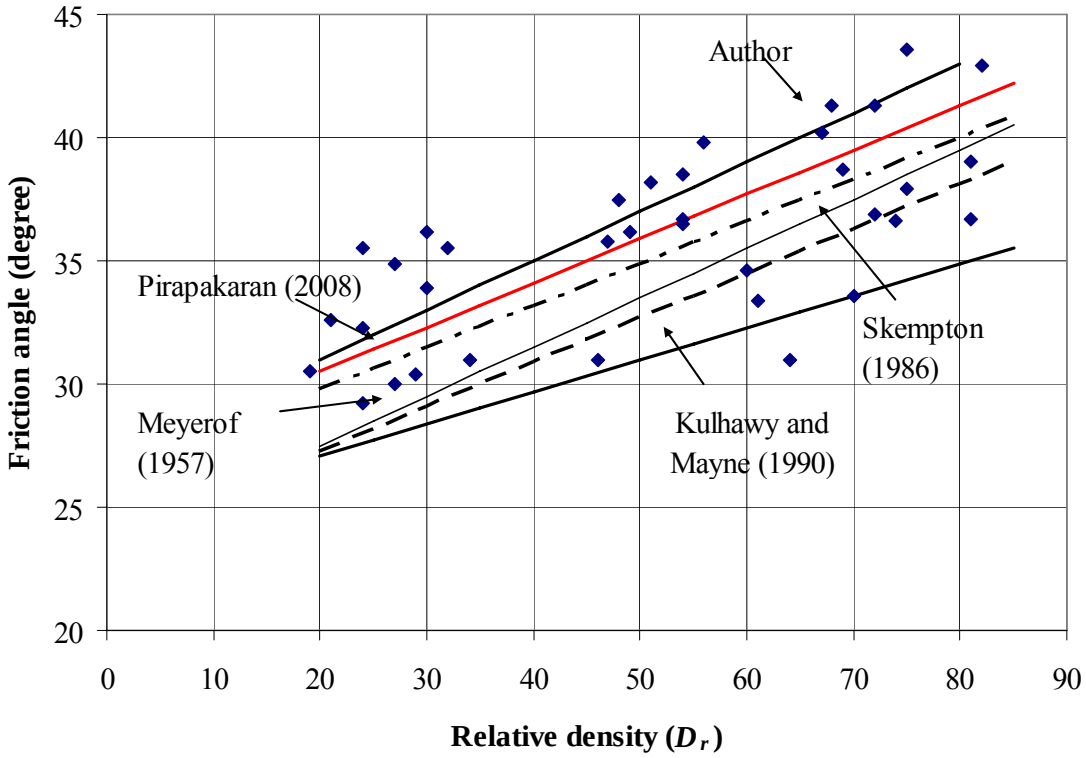

Figure 2.8 Friction angle versus relative density of hydraulic fills

Rankine et al. (2004), (2007) and Sivakugan et al. (2006) determined the particle size distribution of hydraulic fills in Australian Mines (Figure 2.4). It was reported that the particle size distribution of these hydraulic fills fall within a relatively narrow band as shown in Figure 2.4. An empirical equation, Equation 2.12, has been proposed for the particle size distribution curve of hydraulic fill for further use in the mathematical modeling work discussed herein.

$$\% \text{ Passing } = 50\left[1+\tanh\left(n\log\frac{D}{D_{50}}\right)\right] \qquad (2.12)$$

where, D is diameter of tailing and D_{50} is diameter corresponding to 50% finer (i.e. median particle size) and n is curve fitting parameter.

Figure 2.9 shows the particle size distribution curves of five different hydraulic fills which have been estimated using Equation 2.13, with n = 2.5 and the actual curve determined in laboratory for sample A1, B1, B2, C1 and C2. It shows that there is good agreement between laboratory results and particle size curved developed using mathematical model.

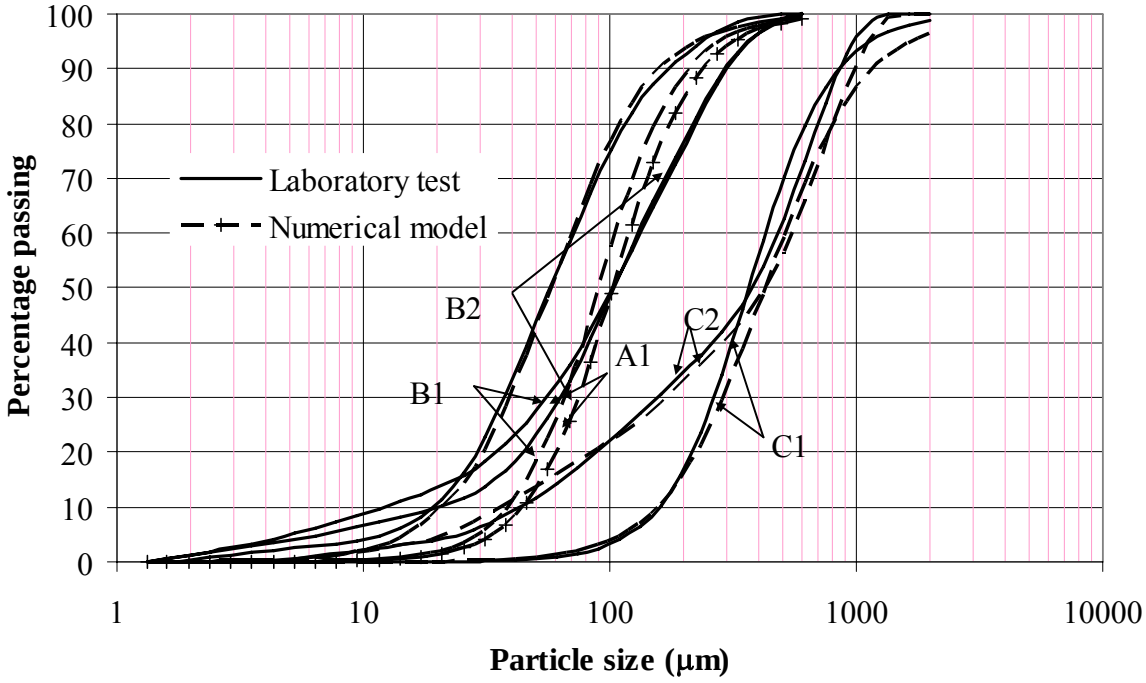

Figure 2.9 Comparison of particle size distribution curve of hydraulic fills measured in laboratory and estimated using Equation 2.12

2.4 Soil-water characteristic curve

The degree of saturation of hydraulic fills within mine stopes decreases with continuous drainage of water through barricades (as shown in Figure 2.10). The permeability of partially saturated hydraulic fills decreases with reduction in degree of saturation or moisture content. Soil-water characteristic curves (SWCC) are plots of moisture content

versus matric suction or/and permeability versus matric suction or/and permeability variation with moisture content. SWCC have been used by many researchers to study the behavior of unsaturated soils. Many direct and indirect tests methods has been proposed in the litreature (Brooks and Corey, 1964; Gardner 1958; Fredlund and Xing 1994) to develop soil-water characteristic curve or measure matric suction of unsaturated soils. Arya and Paris (1981) used particle size distribution curve to estimate the matric suction. In this dissertation, filter paper method has been used to measure matric suction of five hydraulic fill samples from three different mines. Matric suction, measured using filter paper method has been compared with matric suction estimated using particle size distribution curve. Permeability of unsaturated hydraulic fills has been estimated using matric suction of hydraulic fills and has been discussed in Chapter 4. Cut off permeability and residual moisture content of hydraulic fills have been reported in Chapter 4.

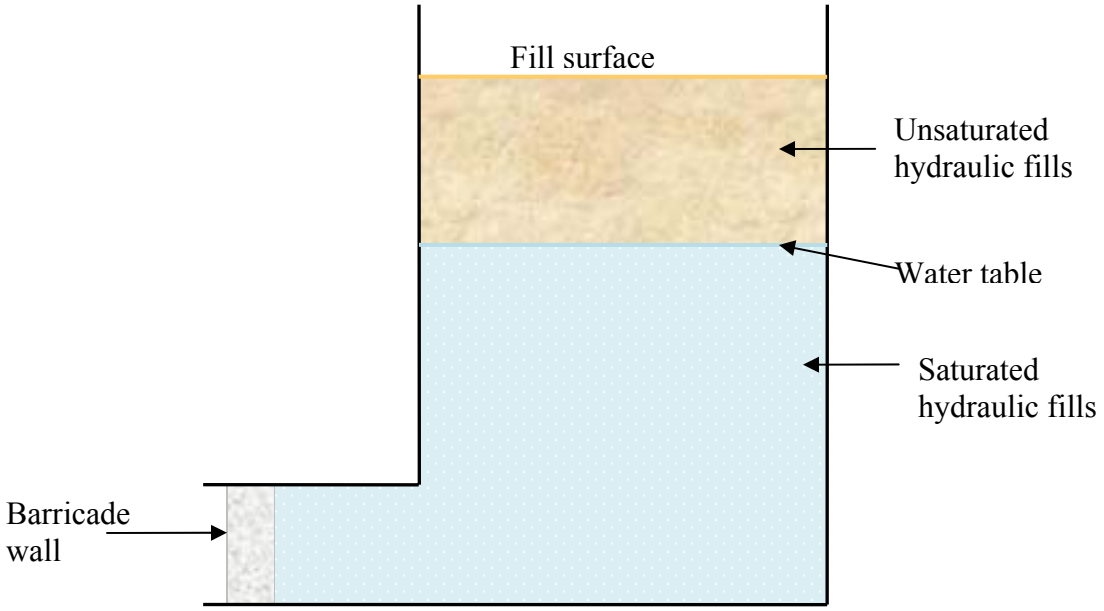

Figure 2.10 Unsaturation of hydraulic fills in a mine stope

2.4.1 Review of SWCC

Soil suction is one of the most important parameters governing the response of unsaturated soils. The total soil suction is defined as the free energy of the soil water, which can be measured in terms of the partial vapour pressure of soil water (Richards, 1965). Matric suction (u_a-u_w), where u_a and u_w are pore air pressure and pore water pressure respectively, is the change in the suction due to movement of the water in liquid phase. Osmotic suction (π) is the change in suction related to the change in moiture content that arises due to movement of water in vapor phase (Vanapalli et al. 2002). Total suction (ψ) can be defined as following:

$$\psi = (u_a - u_w) + \pi \tag{2.13}$$

Equation 2.14 shows the relation between total suction of soil and relative humidity.

$$\psi = -\frac{RT}{v_{w0}\omega_v}\ln RH \tag{2.14}$$

where, R is universal gas constant, T is temperature in Kelvin , RH, relative humidity in the soil, is ratio of partial pressure for pore – water vapor and saturation pressure of water vapor over a flat surface of pure water at same temperature, v_{w0} is specific volume of water and ω_v is molecular mass of water vapor. Most of suction measuring devices and methodologies use the concept of relative humidity.

Matric suction is the suction exerted by soil mass that induces water to flow in unsaturated soils. It is the negative pressure that results from the combined effect of adsorption and capillarity due to the soil matrix. Osmotic suction is related to the salt content in pore water. Change in osmostic suction can effect the mechanical behavior of soil. Osmotic suction of the soils remains constant. The change in total suction is essentially equivalent to change in the matric suction (Fredlund and Rahardjo, 1993).

There are many direct and indirect methods to measure the soil suction. The soil suction can be determined by measuring the relative humidity in the soil or the vapor pressure of the soil water. Psychrometer is the device that is used for direct measurement of total

suction of soil whereas filter paper is used for indirect measurement of relative humidity in the soil. Different types of psychrometer are used to measure the relative humidity in the soil. Most of these instruments and techniques have limitations with regard to range of measurement whereas filter paper method can be used to measure over wide range of values. In this study, filter paper method has been used to measure matric suction of hydraulic fills.

2.4.2 Laboratory tests to develop SWCC using Filter Paper Method

Filter paper method was evolved in Europe in 1920s. It is used as sensor to measure relative humidity in the soil. Gardner (1937) established the calibration curve for filter paper method. Different types of filter papers were used to measure the suction of soil. Houston et al. (1994) developed two different calibration curves for total suction and matric suction. Saturated salt solutions (*NaCl*) were used to calibrate the filter paper for total suction. Tensiometer and pressure membranes were used to calibrate matric suction of soil.

The contact (filter paper is placed in contact with soil) and noncontact filter paper methods are used to measure matric and total suction of soil respectively. Filter paper 1 in Figure 2.11 is in contact will soil and filter paper is 2 is separated by a plastic tube. Filter papers 1 and 2 are used to measure matric and total suction respectively. In contact filter paper method, the soil – water and water transferred to the filter paper are identical so there will be no osmotic suction. In noncontact method, the water transferred to the filter paper by evaporation, is the distilled water. Water movement in vapor phase will generate osmotic suction in the soil. Suction measured using filter paper will give total suction.

In this dissertation, matric suction of hydraulic fills has been measured using Whatman No. 42 filter papers and the methodology given in ASTM D 5298-03. Calibration charts for Whatman No. 42 filter paper provided by Hamblin (1981), Chandler and Gutierrez (1986), Fawcett and Collis-George (1967) and Leong et al. (2002) have been used to

calculate matric suction of hydraulic fills. Calibration curve for Whatman No. 42 filter paper is shown in Figure 2.12 (Fawcett and Collis-George, 1967).

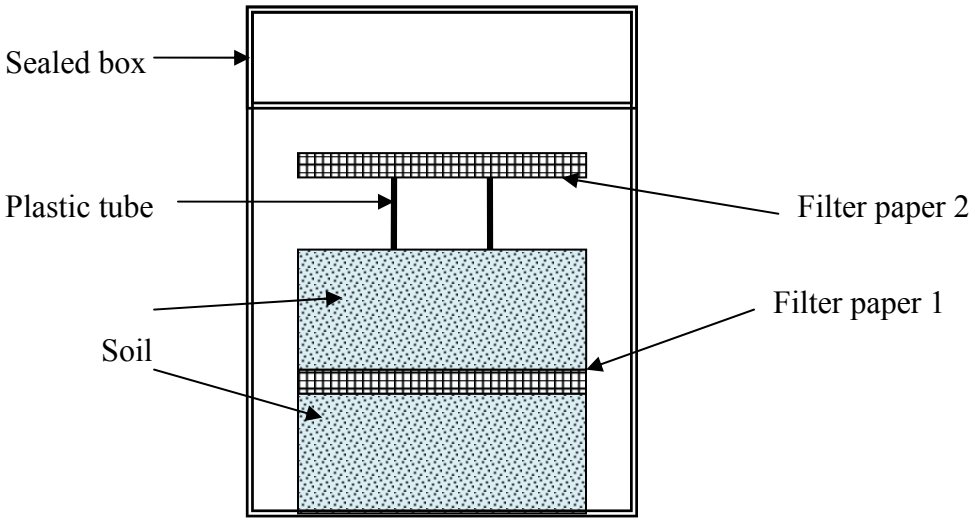

Figure 2.11 Schematic diagram of laboratory setup for measuring matric suction using filter paper method

Whatman No. 42 filter paper was dried in drying oven for 16 hr before starting the tests. Filter paper test was performed as per ASTM D5298 – 03. Three stacked filter papers were placed in contact with hydraulic fill as shown in Figure 2.11 (filter paper 1). The outer filter papers prevent central filter paper from any contamination from hydraulic fill. Central filter paper is used to measure matric suction of hydraulic fills. Sample was sealed in a plastic container using plastic bag and electrical tape. Sealed container was placed in a temperature controlled room for 7 days. After 7 days moisture content of central filter paper was measured using a high precision balance with 0.0001 g of accuracy. Measured moisture content of filter paper has been used to compute matric suction of hydraulic fill using calibration curve shown in Figure 2.12. Matric suction variation of the hydraulic fills with moisture content is shown in Figure 2.13.

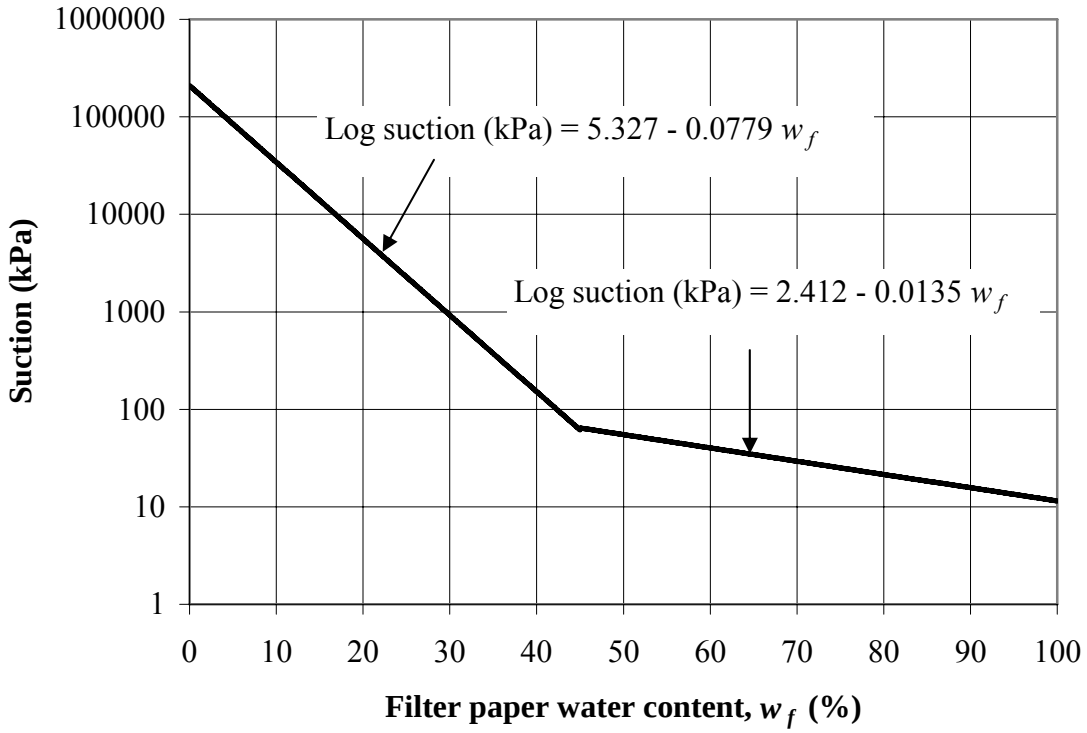

Figure 2.12 Calibration curve for estimating suction using filter paper Whatman No. 42 (Fawcett and Collis-George 1967)

2.4.3 Test result

Moisture content of filter papers (w_f) is measured after 7 days (ASTM D D5298 – 03). It has been assumed that filter papers come in equilibrium within 7 days with moisture content. Hydraulic fills samples of initial moisture content of 2 to 30% have been prepared to study the suction variation with moisture content. As soil approaches towards saturation ($S \rightarrow 1$) pore water pressure (u_w) approaches pore air pressure (u_a) and the matric suction goes towards zero ($u_a - u_w \rightarrow 0$) (Fredlund and Rahardjo, 1993). Figure 2.13 has been used to estimate saturation moisture content (w_s) of hydraulic fills. It has been observed that saturation moisture content varies from 22 – 27 % for hydraulic fills.

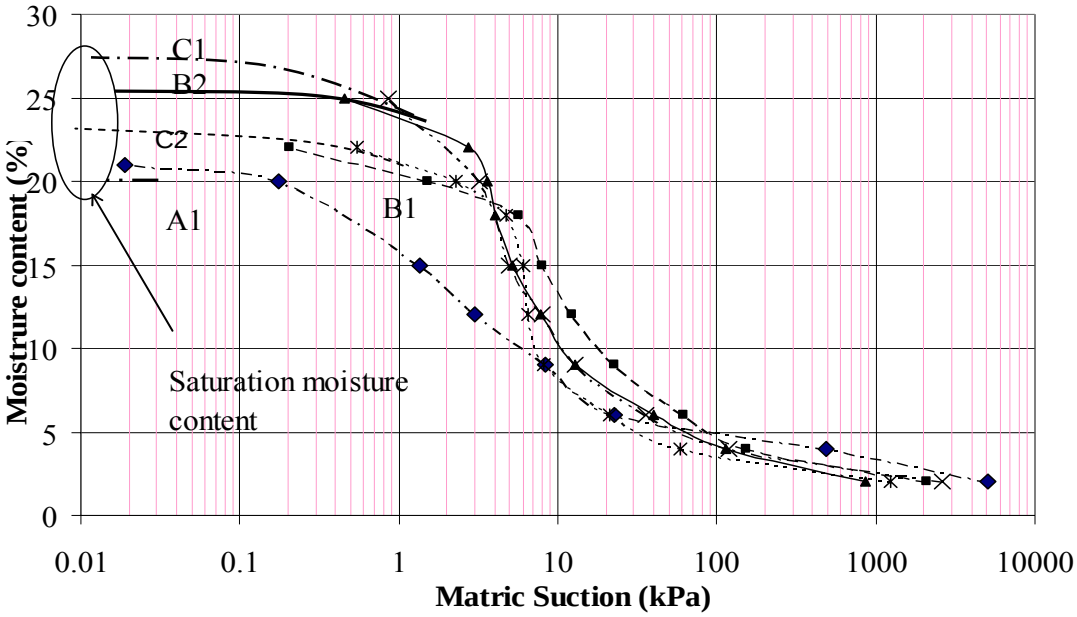

Figure 2.13 Matric suction of hydraulic fills samples measured using Filter Paper method

2.4.4 Development of SWCC using particle size distribution curve

Matric suction of hydraulic fills has been calculated using particle size distribution of hydraulic fills using method proposed by Arya and Paris (1981). Equation 2.7 has been used to predict the particle size distribution of hydraulic fills. Methodology of estimating matric suction using particle size distribution is discussed in Appendix A1. The variation of matric suction with degree of saturation has been plotted in Figure 2.14. Results of the matric suction calculated using particle size distribution has been compared with matric suction measured using filter paper method for samples B1 and B2 (Figure 2.14). Results of other samples are shown in Appendix A2.1. It has been observed that there is good agreement between matric suction measured using filter paper method and computed using numerical method. It suggests that the particle size distribution curve can be used to estimate properties of unsaturated hydraulic fills.

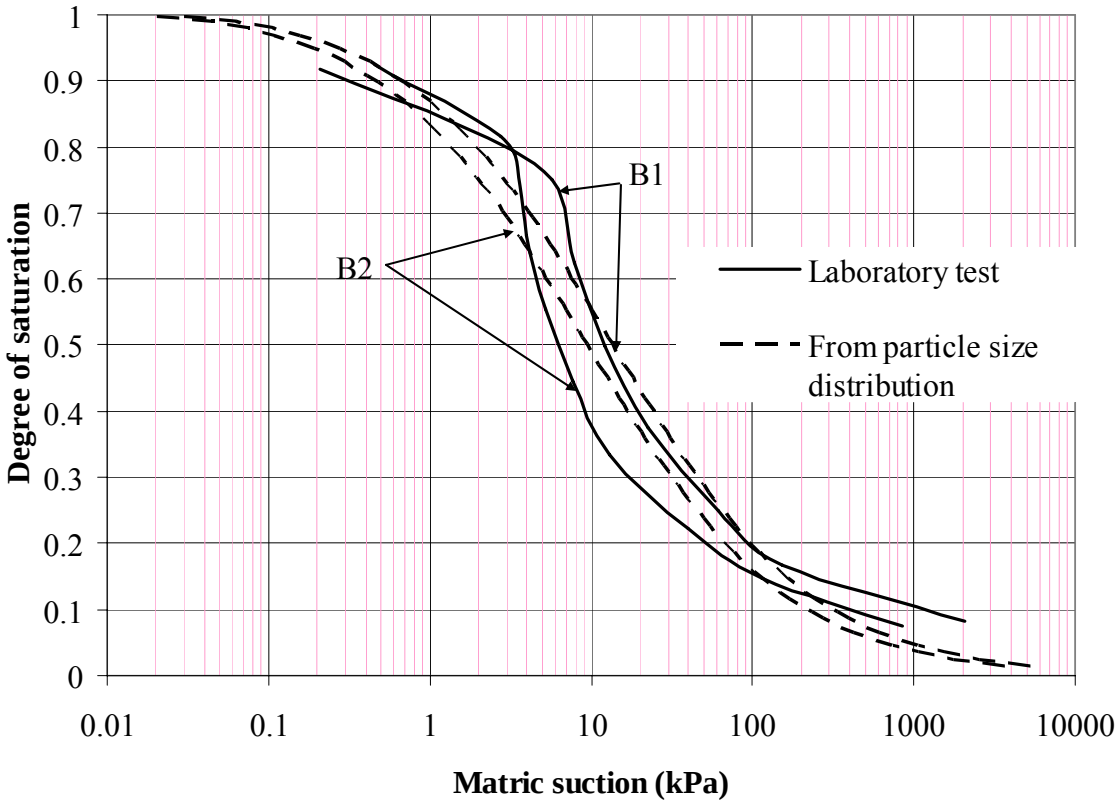

Figure 2.14 Comparison of matric suction of hydraulic fills samples B1 and B2 measured in laboratory and computed using particle size distribution

2.5 Residual moisture content

Many researchers have proposed different definitions for residual moisture content of soil. Brooks and Corey (1964) defined residual moisture content as moisture content corresponding to infinite suction. As per, Luckner et al. (1989), residual moisture content is maximum moisture content that will not contribute to flow. Fredlund and Xing (1994) proposed that the residual moisture content is the moisture content where a large suction change is required to remove additional water from the soil. Gitirana and Fredlund (2004) defined residual moisture content as moisture content corresponding to centre of rotation of a hyperbola that fits the lower portion of the soil water characteristic curve.

Most investigators treated residual moisture content as fitting parameters with no real physical significance (Vanapalli et at. 1998). Different models of soil-water characteristic curves can produce different result for residual moisture content so the residual moisture

content estimated from soil-water characteristic curves is merely a curve fitting parameter. Delleur (1998) defined residual moisture content as the amount of water that remains in a soil mass even when a high vacuum pressure is applied to the soil. Sillers (1997) defined residual moisture content as the moisture content where soil water goes from being held within the soil primarily by the capillary action to soil-water being held in the soil primarily by adsorptive forces.

Residual moisture content of the hydraulic fills has been calculated using soil water characteristic curve (Ebrahimi et al., 2004). Figure 2.15 shows the graphical method of estimating the residual moisture content using soil water characteristic curve. It shows that the residual moisture content of hydraulic fills varies from 5% to 7%. Westraad (2005) reported the residual moisture content of gold tailing from Vaal Reef as 8% of volumetric moisture content. Sivakugan (2008) used 25% of moisture as residual moisture content for hydraulic fills in estimating drainage from the mine stopes. All the assumed and estimated values of residual moisture content of hydraulic fills are very inconsistent.

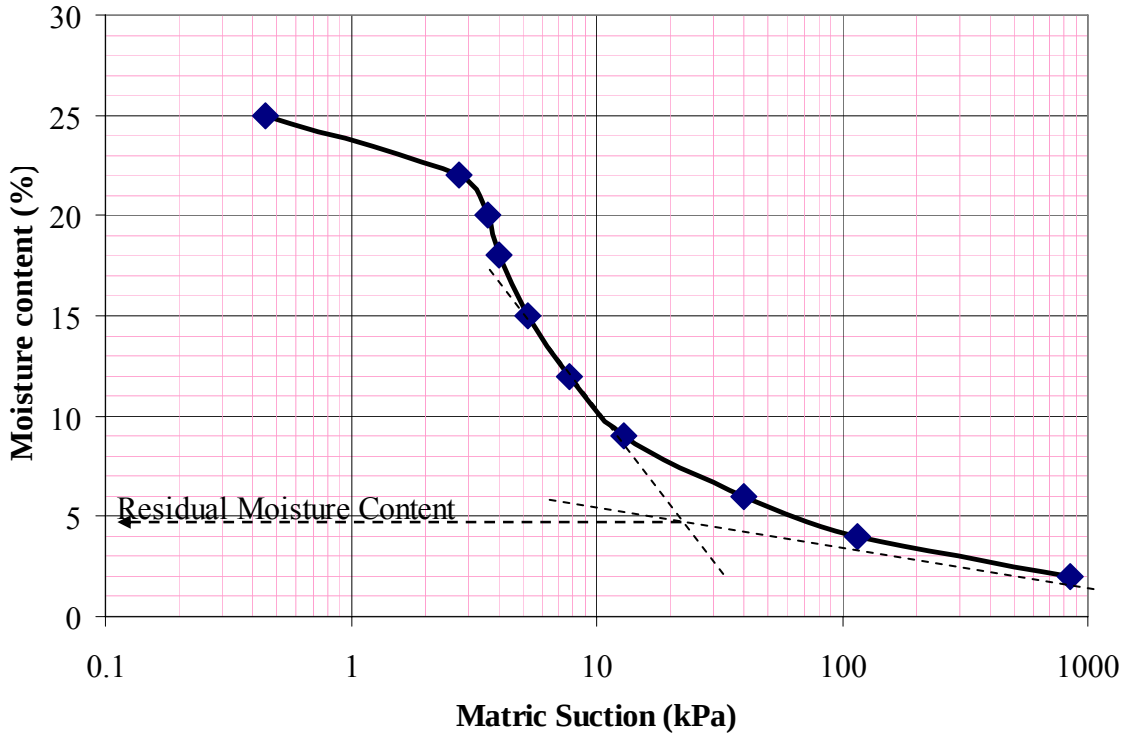

Figure 2.15 Residual moisture content using SWCC

Paterson (2004) observed that solid and liquid phases of relatively fine materials may not separate until a long period in a quiescent state has passed. The temperature within the stopes remains almost constant with time and mine stopes are closed to atmosphere which reduces rate of evaporation. Drainage of water mainly occurs due to high permeability and disturbance created by blasting of neighboring stopes which separate liquid phase and solid phase in hydraulic fill. A minimum moisture content or threshold moisture content is required to enable water flow from soil media (Miller and Low 1963). Threshold moisture content in hydraulic fills mine stope is same as residual moisture content. Laboratory tests were conducted to measure the minimum water holding capacity of hydraulic fills. Sieve vibrator was used to apply vibration loading on a hydraulic fill samples in a cylinder of 80 mm diameter with downward drainage. The moisture content of hydraulic fills was measured for sample heights of 23.9 mm, 47.7 mm, 71.6 mm and 95.4 mm and vibration time of 30 min, 1 hr and 2 hr. The result for sample B2 is shown in Table 2.3 and 2.4. Similar test has been performed for other hydraulic fill samples. Results of other samples (A1, B1, C1 and C2) are shown in Appendix A2.2. It has been observed that the final moisture content for hydraulic fills varies from 12% to 14%. It can be assumed that there will not be any evaporation in the stopes so the residual moisture content of the hydraulic fills will vary from 12% - 14%, which is higher than the residual moisture content predicted using soil-water characteristic curve.

Table 2.3 Measurement of final moisture content of B2 for 47.7 mm high sample

Initial moisture content (%)	Final moisture content (%)		
	Vibration time		
	30 min	60 min	120 min
20	14.4	14.7	14.3
25	14.6	14.8	14.5
30	14.7	14.5	14.3
35	14.7	14.1	14.4
40	14.8	14.4	14.8

Table 2.4 Effect of sample height on final moisture content of B2

Sample height	Average final moisture content
23.9	14.6
47.7	14.5
71.6	14.3
95.4	14.2

2.6 Conclusions

Hydraulic fills are prepared by crushing waste rock or waste products from mining operation from the milling process. These consist of hard, angular and siliceous particles. In the Unified Soil Classification System (USCS), the hydraulic fills would be classified as silty sands (SM) or sandy silts (ML) with no plasticity. Hydraulic fills have high values of specific gravities from 2.80 to 4.50 due to presence of heavy minerals. Permeability of hydraulic fills, settled under their self weight, have been measured at James Cook University Laboratory using 153 mm diameter × 306 mm high cylindrical permeameter using constant head and falling head method. It varies from 9 mm/hr to 38 mm/hr. Consolidation tests have been performed on very large samples by researchers (column of approximately 1 m diameter and 6 m height) of mine tailings for waste disposals and reported that the coefficient of consolidation varies from 0.310 m^2/yr to 104.23 m^2/yr. Geotechnical properties of hydraulic fills, such as uniformity coefficient, coefficient of gradation, permeability, specific gravity, relative density, USCS classification, etc are presented in Table 2.1.

Hydraulic backfills consists of either mine tailings or sand deposits mined off the site. These are prepared on the surface by dewatering the mine tailings to approximately 65-70% solids by weight. It consist of classified mine tailing with not more than 10% by weight of size less than 10 μm. These are placed underground in the form of slurry,

introducing substantial quantities of water into the stope. These are hydraulically pumped to stopes through pipes.

Friction angle of 12 hydraulic fill samples at different packing has been measured using direct shear test at James Cook University Laboratory and results are shown in Table 2.2. Friction angle of hydraulic fills varies from 27^0 to 44^0. An empirical equation has been proposed to compute friction angle from relative density (Equation 2.10). It has been observed that hydraulic fills are cohesionless.

Filter paper method was used to establish soil water characteristic curves for hydraulic fills using the calibration charts. Matric suction has been estimated using particle size distribution curve of hydraulic fills and compared with laboratory test results. An empirical equation (Equation 2.12) has been proposed to represent the mathematical model of particle size distribution curve of hydraulic fills. It has been observed that the saturation moisture content of hydraulic fills varies from 22% to 27% and residual moisture content varies from 12 – 14 %.

Chapter 3

State of Stress within an Underground Mine Stope

3.1 General

Mine stopes are large underground voids that are created in the process of removing the ore for the extraction of valuable minerals. Figure 3.1 shows the schematic diagram of a stope. The stopes can be approximated as rectangular prisms with plan dimensions in the order of 20-60 m and heights as much as 200 m. The horizontal access drives, which can be 3-5 m in width and height, are used for ore removal and later for backfilling during which they have to be barricaded. Hydraulic fills are generally transported in the form of slurry, through boreholes and pipes, over a large distance, before being placed in an empty stope. Fill slurry enters the stope and overlies the existing fills. The solid particles of hydraulic fills settle rapidly after entering the stopes (Grice, 1998). The excess water initially tends to pond on the surface building up from the lowest corners of a stope and then commences a vertical path of drainage due to gravity.

3.1.1 Vertical and inclined stope

For stability and drainage analysis, the mine stopes are often assumed to be vertical rectangular prisms. In reality, the mine stopes can be inclined as shown in Figure 3.2, where the walls are no more vertical. Horizontal access drives, as shown in Figure 3.2, are used as barricades for drainage in backfilled stope. 2-D schematic diagram of mine stope is shown in Figure 3.3. The effect of horizontal access drives at different heights of mining stope has been ignored in stress analysis.

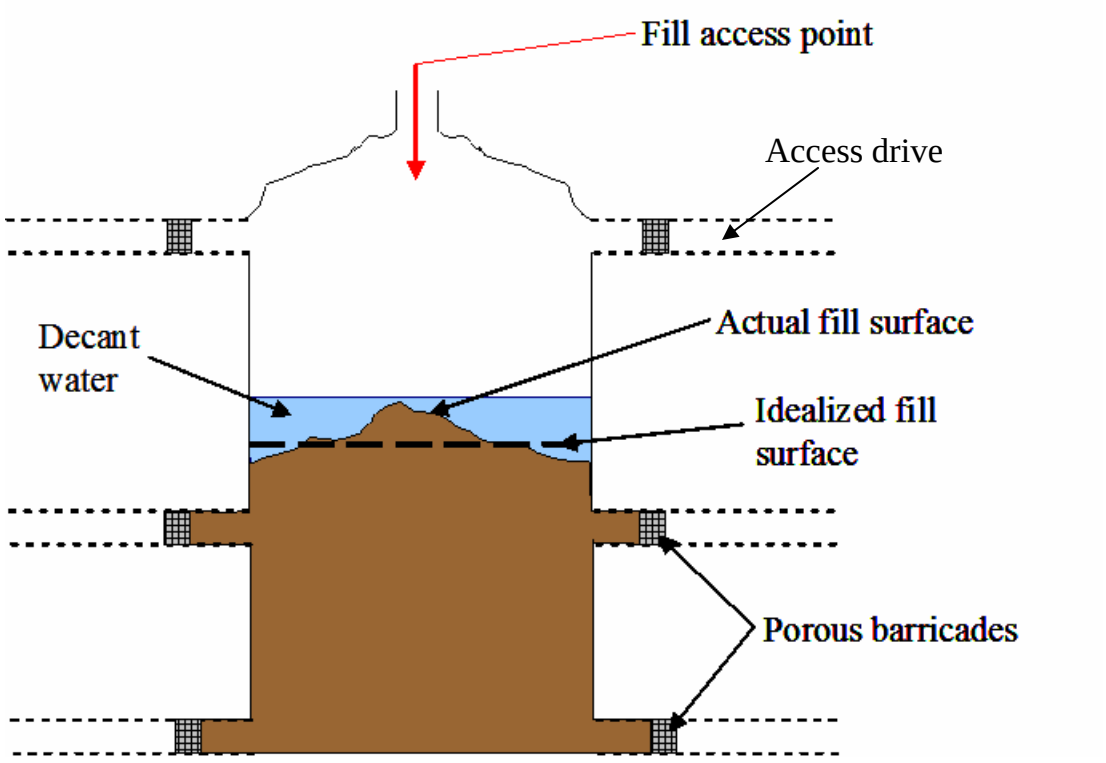

Figure 3.1 Schematic diagram of a stope

3.1.2 Barricades

The horizontal drives at various sublevels, shown in Figures 3.1 and 3.2, are blocked by retaining wall structures, known as barricades or bulkhead or fill fences. These are used in underground mine operations to retain hydraulic fills in the stopes. Barricades consist of permeable bricks. An example of barricade wall with two drain pipes is shown in Figure 3.4. These are designed to facilitate free drainage from hydraulic fill stopes and retain the hydraulic fill. Sivakugan et al. (2006) and Berndt et al. (2007) studied the permeability and material properties of hydraulic fill barricades respectively. Sivakugan et al. (2006) reported that the permeability of barricades is 2 – 3 times of the hydraulic fill.

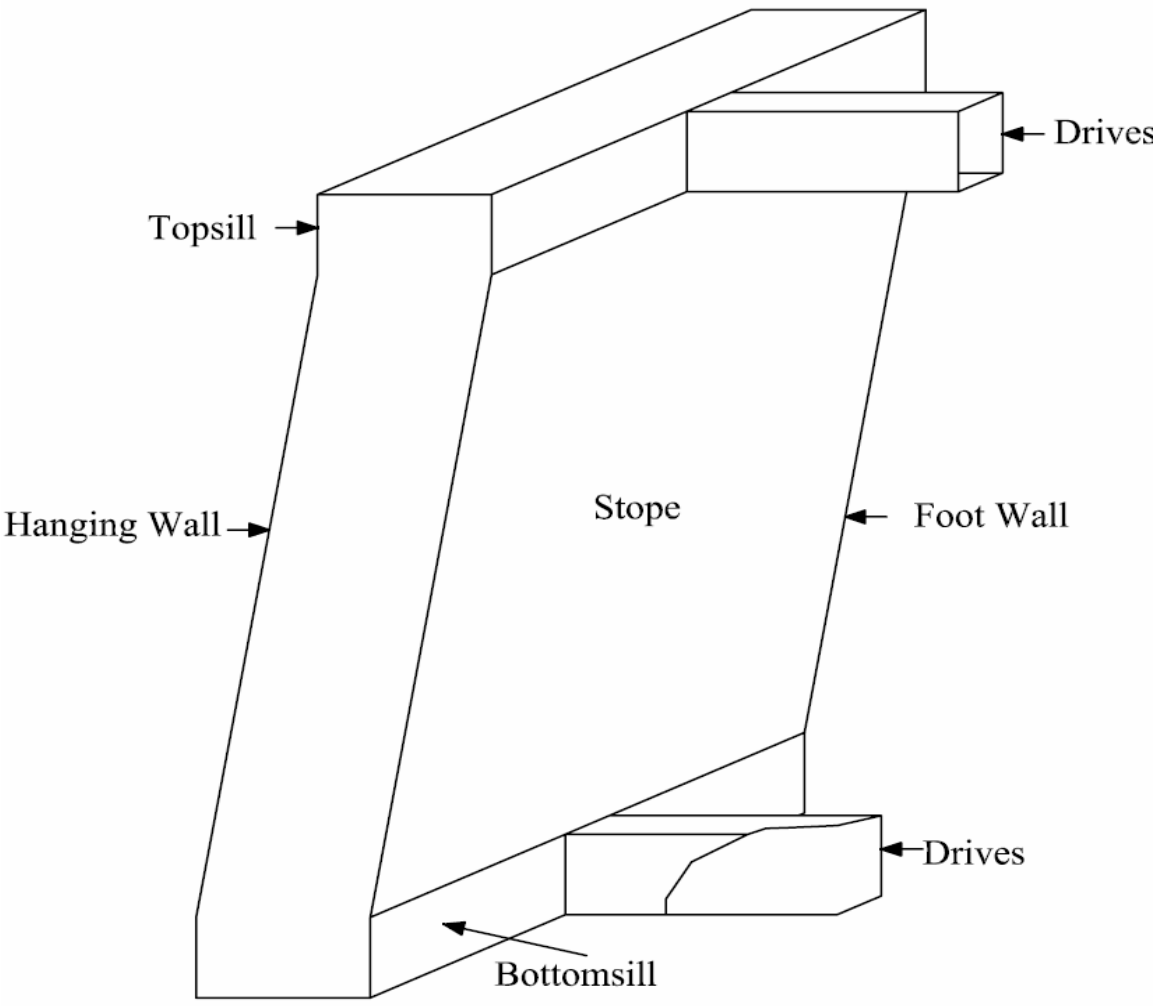

Figure 3.2 Schematic diagram of a mine stope

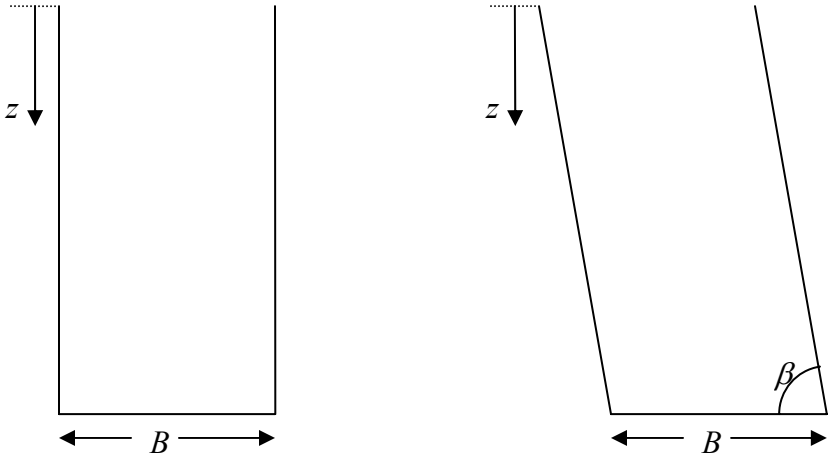

a) Vertical stope b) Inclined stope

Figure 3.3 Schematic diagram of 2-D mine stope

Figure 3.4 Example of barricade in a stope (After Potvin et al. 2005)

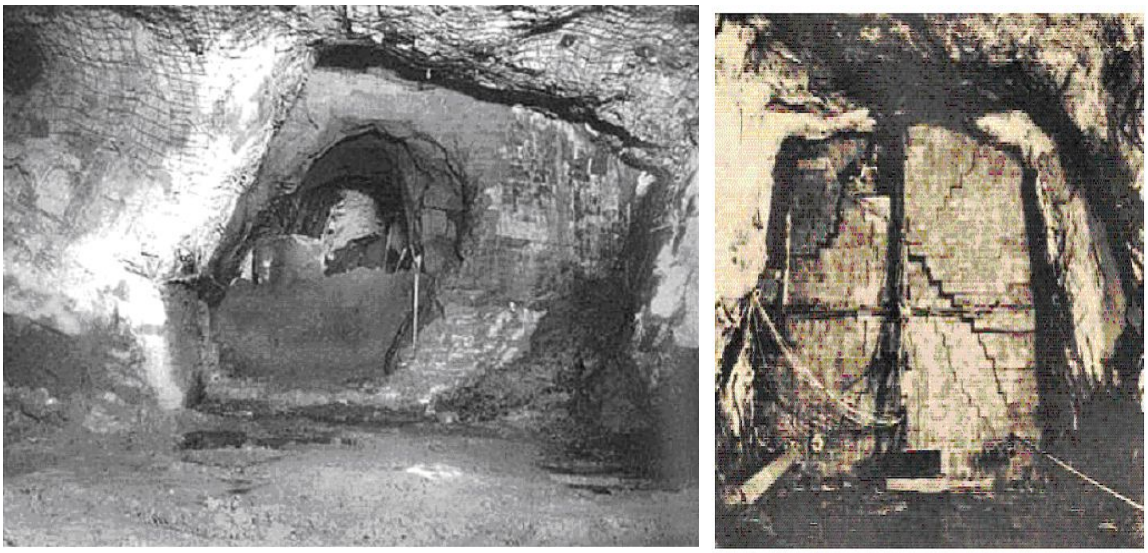

a) After Grice, 1989 b) After Digging Deeper, 2003

Figure 3.5 Failed barricade walls

Failure of the barricades can be catastrophic, resulting in severe economic and human life losses, and this has happened in many parts of the world in the past. The in-rush of the wet slurry can bury the workers and the machinery beyond the barricade without much warning. Common factor in most of the accident involved the loading conditions from the fill acting on a barricade, exceeding its capacity and leading to a barricade failure, fill mobilization and liquefaction. Five hydraulic backfill barricades failed in Australian

mines in 1997 due to delivery of excess quantity of transport water from low density slurry (Grice, 1998). Figure 3.5 show some of the barricade failures in the stopes.

3.1.3 Wall fill friction angle

Three possible scenarios are presented in Figure 3.6 to describe the shear resistance along the wall-backfill interface. Figure 3.6 (a) shows a smooth wall which does not carry any shear stress and hence the wall-backfill friction angle δ is 0. Figure 3.6(b) shows a rough wall along which shear stress can be carried, and it thus enables arching to take place with δ lying between 0 and ϕ depending on the surface roughness. Figure 3.6(c) shows a very rough wall, as seen in mine stopes where the wall surface consists of broken rock in the form of large undulations. Here, the failure within the backfills will take place few grain diameters away from the wall and hence δ can be taken as ϕ.

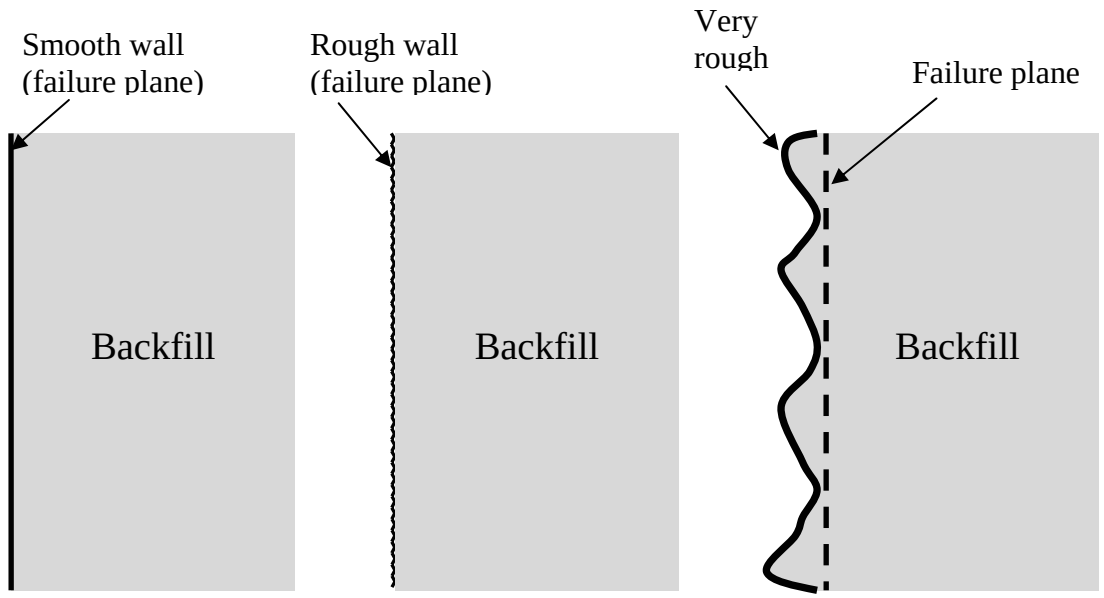

Figure 3.6 Field conditions controlling the value of wall-backfill interface friction angle (δ)

3.2 Review of arching in vertical and inclined stopes

The phenomenon of "arching" has been recognized in several geotechnical and mining applications during the past several decades. These include earth pressures behind retaining walls (Handy, 1985; Take and Valsangkar, 2001), piled embankments (Low et al. 1994), buried conduits (Spangler, 1962; Handy, 1985; McCarthy, 1988) and underground openings (Terzaghi, 1943; Hunt, 1986; Ladanyi and Hoyaux 1969). Arching takes places within a geomaterial in contact with another stiffer material (e.g. rock), where the geomaterial moves downward relative to the stiffer material, transferring some of the load to the stiffer material through the shear stresses developed at the interface.

3.2.1 Marston (1930)

Marston (1930) proposed the first rational method for determining the average normal stresses within a long trench filled with a granular backfill, approximated as a two-dimensional plane strain problem. The average vertical normal stress (σ_v) within a granular backfill in a long and narrow trench at depth z can be expressed as:

$$\sigma_v = \frac{\gamma B}{2\mu K}\left[1 - \exp\left(-\frac{2\mu K}{B} z\right)\right] \tag{3.1}$$

where μ (= $\tan\delta$) is the friction coefficient at the wall-backfill interface; δ is the friction angle at the wall-backfill interface; K is a ratio of horizontal stress to vertical stress at the desired depth within the fill; and B is the width of the trench.

3.2.2 Terzaghi (1943)

Terzaghi (1943) incorporated cohesion in Marston's expression, and expressed the average normal vertical stress (σ_v) within the stope at a depth z below its top surface as:

$$\sigma_v = \frac{\gamma B - 2c}{2\mu K}\left\{1 - \exp\left(-\frac{2\mu K z}{B}\right)\right\} \quad (3.2)$$

where B is stope width, γ is unit weight of the fill, c is cohesion at the wall-fill interface, $\mu = \tan\delta$ is wall-fill friction coefficient, δ is wall-fill friction angle and K is a coefficient of earth pressure. Terzaghi suggested that $\delta = \phi$, where ϕ is soil friction angle. Terzaghi (1945) suggested that the Krynine (1945) earth pressure coefficient can be used as the ratio of lateral and vertical earth pressure.

Following expression can be used to compute Krynine (1945) earth pressure coefficient:

$$K_{krynine} = \frac{1}{1 + 2\tan^2\phi} = \frac{1 - \sin^2\phi}{1 + \sin^2\phi} \quad (3.3)$$

3.2.3 Aubertin et al. (2003)

Aubertin et al. (2003) applied the Marston's theory (Equation 3.1) to estimate the vertical and lateral loads on the stope floor and wall. It was assumed that $\delta = \phi$, therefore $\mu = \tan\phi$ as suggested by Terzaghi. Numerical models were developed using PHASE2, a numerical code based on finite element method, considering $K = K_a$, K_p and K_0 where K_a, K_p and K_0 are Rankine's active earth pressure coefficient, passive earth pressure coefficient and earth pressure coefficient at rest, respectively. Active earth pressure coefficient, passive earth pressure coefficient and earth pressure coefficient at rest can be computed as following:

$$K_a = \tan^2(45^0 - \frac{\phi}{2}) = \frac{1 - \sin\phi}{1 + \sin\phi} \quad (3.4)$$

$$K_p = \tan^2(45^0 + \phi/2) = \frac{1 + \sin\phi}{1 - \sin\phi} \quad (3.5)$$

$$K_0 = 1 - \sin\phi \tag{3.6}$$

It was concluded by Aubertin et al. (2003) that the fully passive condition ($K = K_p$) could be the most exaggerated, and the fully active condition ($K = K_a$) was not realistic considering the movement required to induce it. It was observed that the actual response of the stope and backfill would be close to the rest condition, and hence $K = K_0$ is more appropriate than other earth pressure coefficients.

3.2.4 Pirapakaran and Sivakugan (2007a)

Pirapakaran and Sivakugan (2007a) compared the vertical stress (σ_v) values predicted by Equation. 3.2 with those obtained from numerical modeling, and showed that for hydraulic fills where $c = 0$, Equation 3.2 gives realistic estimates when $\delta = 0.67\ \phi$ and $K = K_0$, where K_0 is the coefficient of earth pressure at rest. It was shown that, for a 3-dimensional stope, Equation 3.2 becomes:

$$\sigma_v = \frac{\gamma B - 2c}{2K\tan\delta}\left(\frac{L}{B+L}\right)\left\{1 - \exp\left\{-2\left(\frac{L+B}{BL}\right)Kz\tan\delta\right\}\right\} \tag{3.7}$$

where L and B are length and width of stope respectively. For long narrow trench, $L \to \infty$, and Equation 3.5 reduces to Equation 3.2. If the void is square or circular in plan, Equation (3.5) becomes:

$$\sigma_v = \frac{(\gamma B - 2c)}{4\mu K}\left[1 - \exp\left(-\frac{4\mu K}{B}z\right)\right] \tag{3.8}$$

Pirapakaran and Sivakugan (2007b) carried out some laboratory model tests for measuring vertical normal stresses within hydraulic fill stopes which were compared with the predictions from numerical models and Marston's equation. All three approaches compared very well for the three-dimensional hydraulic fill stopes.

3.3.5 Handy (1985)

Handy (1985) used catenary arch of principal stresses to estimate the vertical and horizontal stresses in a vertical walled trench (discussed in section 3.3). Following expression was used to estimate the vertical stress due to arching:

$$\frac{\sigma_v}{\gamma B} = \frac{1}{2K_w \tan\delta}\left\{1 - \exp\left(-\frac{2K_w \tan\delta}{B} z\right)\right\} \tag{3.9}$$

where, $K_w = \frac{\sigma_h}{\sigma_v} = \frac{\cos^2\theta_w + K_a \sin^2\theta_w}{\sin^2\theta_w + K_a \cos^2\theta_w}$, σ_h and σ_v are horizontal and vertical normal stress respectively, and θ_w is the angle of intersection of principal stress and wall (Figure 3.7). For rough wall $\theta_w = 45^0 + \phi/2$ and for smooth wall $\theta_w = 90^0$.

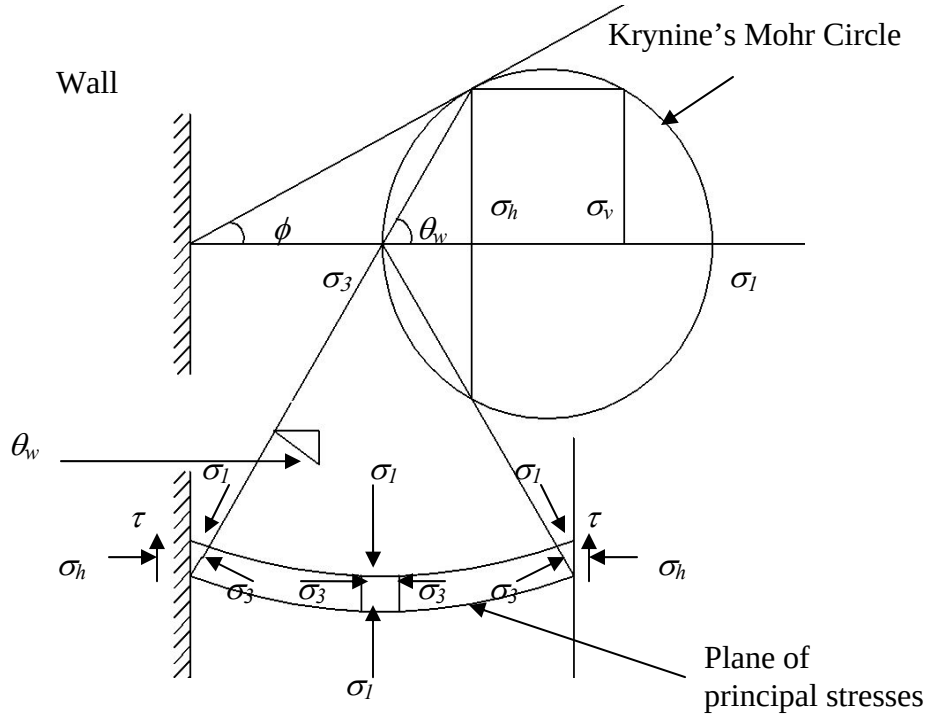

Figure 3.7 Arching stress at rough wall

3.3.6 Caceres (2005)

Caceres (2005) modified Marston's (1930) theory for inclined stopes, and presented an expression to estimate vertical normal stress within the inclined stopes filled with cohesionless materials as:

$$\frac{\sigma_v}{\gamma B} = \frac{\sin^2\alpha}{2K\tan\phi}\left\{1-\exp\left(-\frac{2K\tan\phi}{B\sin^2\alpha}z\right)\right\} \tag{3.10}$$

where $K \approx 1.4\sin^2\phi - 2\sin\phi + 1$, and α is the angle of inclination of the stope to the horizontal.

3.2.7 Shukla et al. (2008)

Shukla et al. (2008) presented a simplified extension of Equation 3.2 for non-vertical walls of the trench having trapezoidal vertical section as:

$$\sigma = \gamma B\left[\frac{2R\tan\alpha + 2P\left(\frac{z}{B}\right)\tan\alpha + PQ - 2Q\tan\alpha}{P(2\tan\alpha - P)} + \frac{2R\tan\alpha - PQ + 2Q\tan\alpha}{P(2\tan\alpha - P)}\left\{\frac{2\left(\frac{z}{B}\right)\tan\alpha + R}{R}\right\}^{\frac{P}{2\tan\alpha}}\right] \tag{3.11}$$

with P, Q and R as:

$$P = 2\{(K'-1)\tan\alpha + \mu K'\} \tag{3.12a}$$

$$Q = 2\left(\frac{c}{\gamma H}\right) - 2\left(\frac{H}{B}\right)\tan\alpha - 1 \tag{3.12b}$$

and

$$R = -\left[1 + 2\left(\frac{H}{B}\right)\tan\alpha\right] \tag{3.12c}$$

where α is the inclination to the vertical of the wall, B is the width of the trench at bottom, and K' is the ratio of normal stress at the sloping wall to vertical stress at depth z within the fill, which is expressed in terms of K as:

$$K' = \frac{(1+K)-(1-K)\cos 2\alpha}{2} \tag{3.13}$$

It should be noted that as $\alpha \rightarrow 0$, Equation 3.11 reduces to Equation 3.2.

3.3 Arch in soil arching

Janssen (1895) used a flat rectangular element to derive the differential equation to estimate pressure in a silo as shown in Figure 3.8. Flat rectangular element was also considered by Marston and Anderson (1913), Marston (1930), and Terzaghi (1943). It was assumed that the frictional force at the ends of a flat rectangular element is equal to the lateral force times the coefficient of friction, where the lateral force is the vertical stress times lateral stress ratio K. Janssen (1895) determined K ($= \frac{p_s f}{p}$, where p_s is horizontal pressure on wall, p is normal pressure on wall and f is friction coefficient) experimentally. Marston and Anderson (1913) assumed that $K = \frac{\sigma_3}{\sigma_1}$, where K is Rankine's coefficient of active earth pressure, and σ_1 and σ_3 are vertical and horizontal principal stresses respectively. Marston (1930); Terzaghi (1943); Aubertin et al. (2003); Caceres (2005); and Pirapakaran and Sivakugan (2007a) assumed earth pressure coefficient as ratio of horizontal and vertical stress in a rectangular element and modified equation for different lateral stress ratios using numerical models.

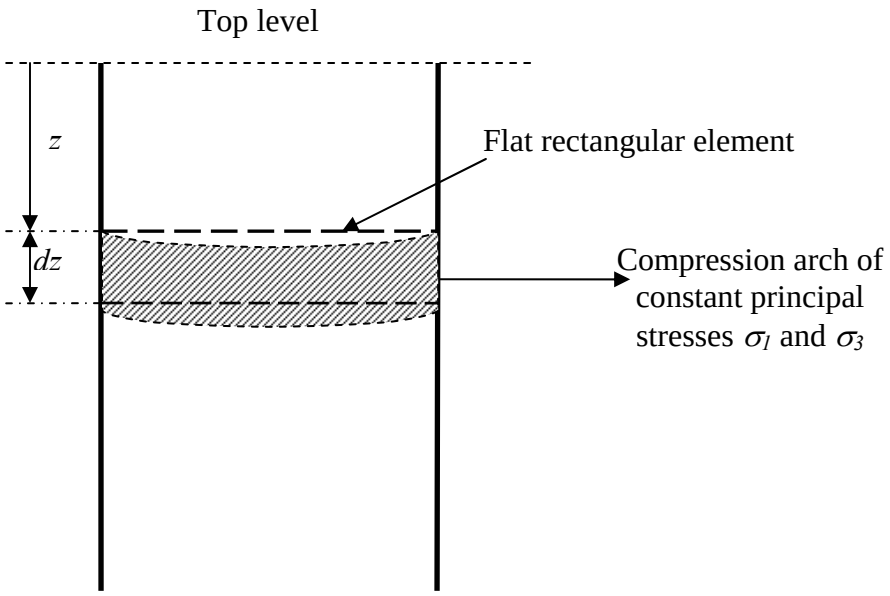

Figure 3.8 Differential element in classical soil arching

If $K = \frac{\sigma_3}{\sigma_1}$, where σ_1 and σ_3 are principal stresses, then friction force on the plane vertical wall should be zero. Krynine (1945) resolved the problem using Mohr circle, showing that the rotation of principal stresses gives a wall pressure σ_h, which is different from σ_3. Krynine (1945) presented an expression for the ratio of horizontal to vertical stress ($\frac{\sigma_h}{\sigma_v}$) to calculate the lateral force coefficient (Equation 3.5) at a wall with fully mobilized friction.

Since vertical stress at wall is less than average vertical stress across the continuum, it is incorrect to use Equation 3.7 in estimating σ_h at the wall in presence of arching. Handy (1985) defined a continuous compression arch as shown in Figure 3.8, using the intersections of shear lines drawn by numerical method suggested by Sokolovskii (1965), which is based on the Mohr Circle. When soil is in the state of plastic equilibrium, the slip occurs only along the direction defined by the slip lines. The arching element of Figure 3.8 is bounded by surfaces representing principal planes of zero shearing stress.

Thus, the moment equilibrium requires the normal stress (σ_1) to be constant throughout the arch. Harrop-Williams (1989) showed that the actual arch can be approximated by a catenary and is very close to a circular arch. In this dissertation, circular arch has been assumed to simplify the arching analysis of inclined stopes.

3.4 Arching in an inclined stope

Figure 3.9 shows a vertical section of an inclined mining stope of height *H* and width *B*. The hanging and foot walls of the stope are inclined to the horizontal at an angle α. An elemental strip of thickness *dz* is considered at a depth *z* below the top level of the stope. Using the geometry of the Figure 3.9, the radius of the arch, *R*, area of the elemental strip, *dA*, and the weight of the strip, *dW* are obtained as follows:

$$R = \frac{B}{2}\sin\alpha \,\mathrm{cosec}\,\delta \tag{3.14}$$

$$dA = \delta\, B\,\mathrm{cosec}\,\delta\, dz \tag{3.15}$$

and

$$dW = \gamma\,\delta\, B\,\mathrm{cosec}\,\delta\, dz \tag{3.16}$$

where γ is the unit weight of the hydraulic fills.

Principal stresses (σ_1 and σ_3) remain constant along the arch (Hardy 1985). If σ_z is the vertical stress acting at any point on the arch, then $\sigma_1 = \sigma_z$ at the position SS1 as shown in Figure 3.9.

Using stress transformation, the vertical stress, $\sigma_{z,\theta}$, at any angle θ as shown in Figure 3.9 can be expressed as:

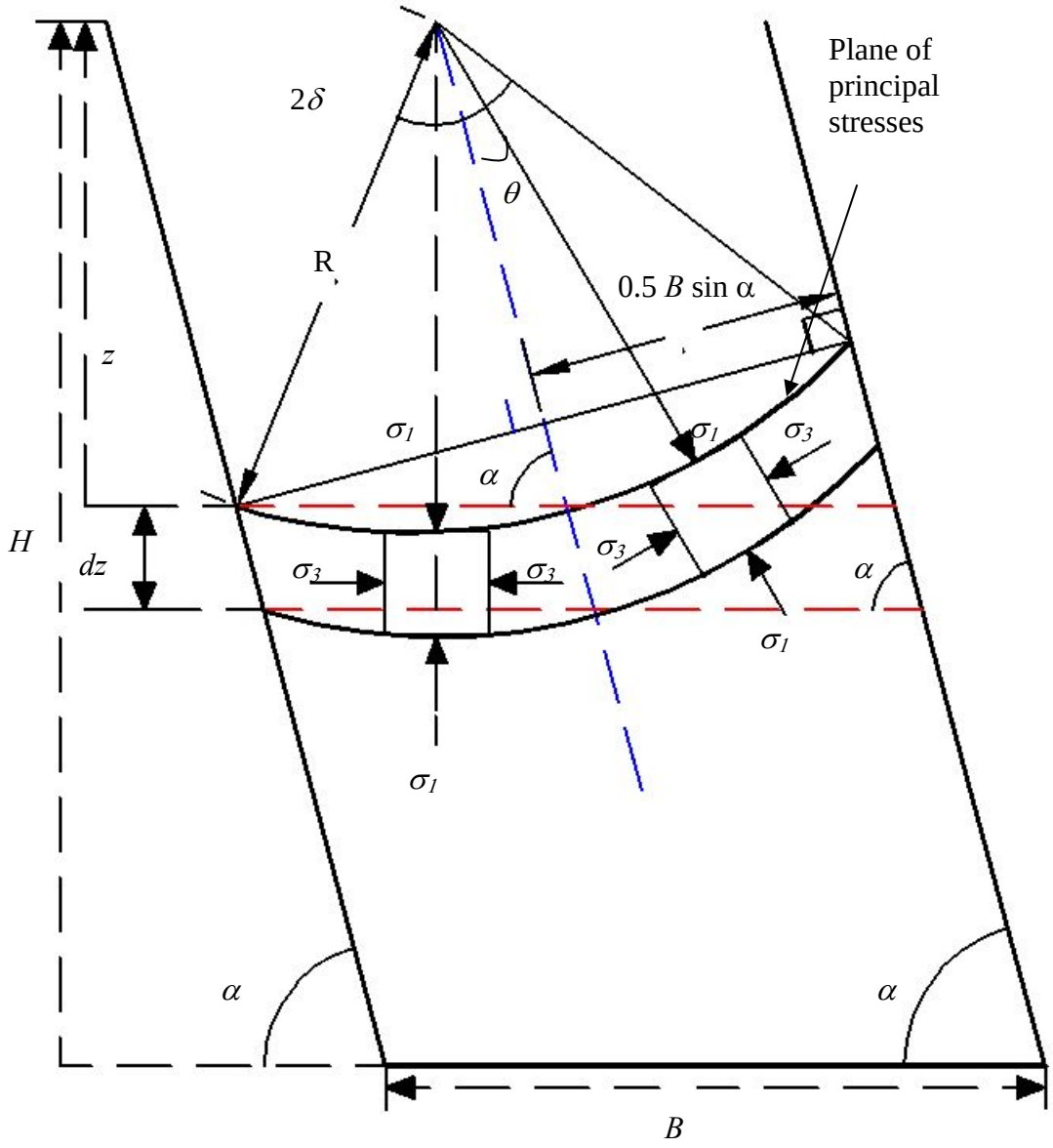

Figure 3.9 Schematic diagram of an inclined stope and compression arch

$$\sigma_{z,\theta} = \frac{\sigma_1 + \sigma_3}{2} + \frac{\sigma_3 - \sigma_1}{2}\cos 2\theta + \tau \sin 2\theta \qquad (3.17)$$

Since the shear stress acting along the arch is zero, i.e. $\tau = 0$, Equation (3.17) becomes:

$$\sigma_{z,\theta} = \sigma_1 \left[\frac{1+K}{2} - \frac{1-K}{2} \cos 2\theta \right] \tag{3.18}$$

where $\frac{\sigma_3}{\sigma_1} = K$.

Figure 3.10 shows the free body diagram of the compression arch. It is assumed that the whole fill mass moves together under gravity and the shape of the arch will remain constant during movement throughout the stope. Tensional force developed due relative displacement of the soil between hanging wall and footwall will cause a separation of grains within the soil mass. Soil cannot take tension and it is realistic to assume that there is no separation of grains within hydraulic fill mass. This will result in mobilization of equal frictional force on both the walls with full friction mobilization at the footwall and partial mobilization at the hanging wall. F_{n1} and F_{n2} are the normal forces, and F_s is the frictional resistance acting at the sides of the elemental arch. dW is the weight of this element. F_z and $F_z + dF_z$ are the vertical forces acting on the top and the bottom of this element.

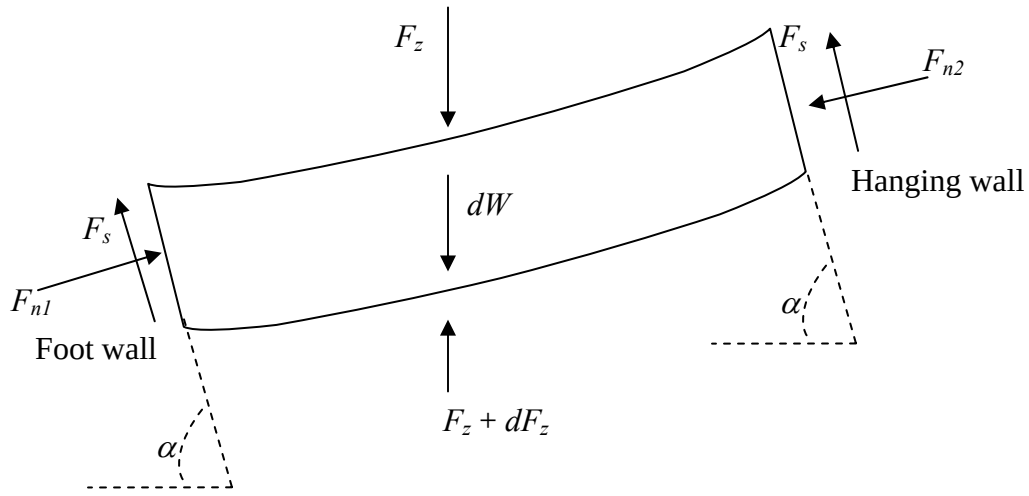

Figure 3.10 Free body diagram of the arch

From Figure 3.10, the expression for force F_z is obtained as:

$$F_z = \int_{\frac{\pi}{2}-\alpha-\delta}^{\frac{\pi}{2}-\alpha+\delta} \sigma_{z,\theta} R\, d\theta = \int_{\frac{\pi}{2}-\alpha-\delta}^{\frac{\pi}{2}-\alpha+\delta} \sigma_1 \left[\frac{1+K}{2} - \frac{1-K}{2} \cos 2\theta \right] R\, d\theta$$

or

$$F_z = \frac{B}{2} \sigma_1 \left[(1+K)\delta - \frac{1-K}{2} \sin 2\delta \cos 2\alpha \right] \sin\alpha \operatorname{cosec}\delta \tag{3.19}$$

Similarly, the expression for force $F_z + dF_z$ is obtained as:

$$F_z + dF_z = \frac{B}{2} (\sigma_1 + d\sigma_1) \left[(1+K)\delta - \frac{1-K}{2} \sin 2\delta \cos 2\alpha \right] \sin\alpha \operatorname{cosec}\delta$$

or

$$dF_z = \frac{B}{2} d\sigma_1 \left[(1+K)\delta - \frac{1-K}{2} \sin 2\delta \cos 2\alpha \right] \sin\alpha \operatorname{cosec}\delta \tag{3.20}$$

In Figure 3.10, the horizontal force equilibrium of the elemental arch gives:

$$F_{n1} \sin\alpha - F_{n2} \sin\alpha - 2F_s \cos\alpha = 0$$

or

$$F_{n1} - F_{n2} = 2F_s \cot\alpha \tag{3.21}$$

In Figure 3.10, the vertical force equilibrium of the elemental arch gives:

$$(F_z + dF_z) - F_z - dW + 2F_s \sin\alpha + F_{n1} \cos\alpha - F_{n2} \cos\alpha = 0$$

or

$$dF_z = dW - 2F_s \operatorname{cosec}\alpha \tag{3.22}$$

Using stress transformation at the footwall, the normal vertical stress (σ_{n1}) can be expressed as:

$$\sigma_{n1} = \frac{\sigma_1 + \sigma_3}{2} - \frac{\sigma_1 - \sigma_3}{2}\cos 2\delta \tag{3.23}$$

Substituting $\frac{\sigma_3}{\sigma_1} = K$ in Equation 3.23 gives:

$$\sigma_{n1} = \sigma_1\left[\frac{1+K}{2} - \frac{1-K}{2}\cos 2\delta\right] \tag{3.24}$$

or

$$\sigma_{n1} = \sigma_1\left[\sin^2\delta + K\cos^2\delta\right] \tag{3.25}$$

Shear force at the footwall can be determined using the *Mohr-Coulomb failure criterion* as follows:

$$\tau_{S1} = c + \sigma_{n1}\tan\delta \tag{3.26}$$

where τ_{s1} is the shear stress at the foot wall, and c is cohesion of the soil.

Frictional resistance (F_s) is calculated as:

$$F_s = \tau_{s1}\operatorname{cosec}\alpha dz$$

or

$$F_s = \left(c + \sigma_{n1} \tan\delta\right) \operatorname{cosec}\alpha \, dz \tag{3.27}$$

or

$$F_s = \left[c + \sigma_1 \left(\sin^2\delta + K\cos^2\delta\right)\tan\delta \right] \operatorname{cosec}\alpha \, dz \tag{3.28}$$

Substituting Equations 3.16, 3.17, and 3.28 in Equation 3.22 gives:

$$\frac{B}{2}\left[\left(1+K\right)\delta - \frac{1-K}{2}\sin 2\delta\cos 2\alpha \right] \sin\alpha \operatorname{cosec}\delta \, d\sigma_1 = \gamma\,\delta\, B \operatorname{cosec}\delta \, dz -$$
$$2\left[c + \sigma_1 \left(\sin^2\delta + K\cos^2\delta\right)\tan\delta \right] \operatorname{cosec}^2\alpha \, dz$$

or

$$\frac{d\sigma_1}{\left(\gamma\,\delta\, B \sin^2\alpha \operatorname{cosec}\delta - 2c\right) - 2\sigma_1\left(\sin^2\delta + K\cos^2\delta\right)\tan\delta} = \frac{dz}{\frac{B}{2}\left[\left(1+K\right)\delta - \frac{1-K}{2}\sin 2\delta\cos 2\alpha \right]\sin^3\alpha \operatorname{cosec}\delta} \tag{3.29}$$

If the surcharge on the stope is σ_0, the solution of the linear differential equation, Equation (3.29), is obtained as:

$$\sigma_1 = \frac{\left(\gamma\,\delta\, B \sin^2\alpha \operatorname{cosec}\delta - 2c\right)}{2\left(\sin^2\delta + K\cos^2\delta\right)\tan\delta}\left\{ 1 - \exp\left(- \frac{8\left(\sin^2\delta + K\cos^2\delta\right)\tan\delta\sin\delta}{B\left[2\left(1+K\right)\delta - \left(1-K\right)\sin 2\delta\cos 2\alpha \right]\sin^3\alpha} z \right) \right\} \tag{3.30}$$
$$+ \sigma_0 \exp\left(- \frac{8\left(\sin^2\delta + K\cos^2\delta\right)\tan\delta\sin\delta}{B\left[2\left(1+K\right)\delta - \left(1-K\right)\sin 2\delta\cos 2\alpha \right]\sin^3\alpha} z \right)$$

As per Unified Soil Classification System (USCS) hydraulic fills are classified as silty sand or sandy silt with zero cohesion (Section 2.2.8). In the absence of surcharge on hydraulic fill, Equation 3.30 can be written as:

$$\sigma_1 = \frac{\gamma\,\delta\,B\sin^2\alpha\,\mathrm{cosec}\,\delta}{2\left(\sin^2\delta + K\cos^2\delta\right)\tan\delta}\left\{1-\exp\left(-\frac{8\left(\sin^2\delta + K\cos^2\delta\right)\tan\delta\sin\delta}{B\left[2\left(1+K\right)\delta-\left(1-K\right)\sin 2\delta\cos 2\alpha\right]\sin^3\alpha}z\right)\right\} \quad (3.31)$$

3.5 Comparison of results with previous analysis

The above analysis has been compared with the analysis given Marston (1930), Handy (1985), Aubertin et al. (2003) and Pirapakaran and Sivakugan (2007a) for vertical stopes. The following expressions have been used for comparison of hydraulic fill in vertical stope:

Marston (1930):

$$\frac{\sigma_v}{\gamma B} = \frac{1}{2K_0\tan\delta}\left\{1-\exp\left(-\frac{2K_0\tan\delta}{B}z\right)\right\} \quad (3.32)$$

Aubertin et al. (2003):

$$\frac{\sigma_v}{\gamma B} = \frac{1}{2K_0\tan\phi}\left\{1-\exp\left(-\frac{2K_0\tan\phi}{B}z\right)\right\} \quad (3.33)$$

Pirapakaran and Sivakugan (2007a):

$$\frac{\sigma_v}{\gamma B} = \frac{1}{2K_0\tan\delta}\left\{1-\exp\left(-\frac{2K_0\tan\delta}{B}z\right)\right\} \quad (3.34)$$

$\alpha = 90^0$ has been substituted in Equation 3.31 to calculate the vertical stress in a vertical stope using present analysis as given in Equation 3.35.

$$\sigma_v = \frac{\gamma \delta B \ \mathrm{cosec}\delta}{2\left(\sin^2\delta + K\cos^2\delta\right)\tan\delta}\left\{1-\exp\left(-\frac{8\left(\sin^2\delta + K\cos^2\delta\right)\tan\delta\sin\delta}{B\left[2\left(1+K\right)\delta+\left(1-K\right)\sin 2\delta\right]}z\right)\right\} \quad (3.35)$$

The vertical stress for $\phi = 36^0$ and $\delta = 24^0$ for Pirapakaran and Sivakugan (2007a) and $\delta = 36^0$ for Marston (1930), Aubertin et al. (2003) and present analysis, has been calculated using above equations. $K = K_0$ has been used for Aubertin et al. (2003), and Pirapakaran and Sivakugan (2007a). A comparison of results is shown in Figure 3.11. The vertical stress estimated using present analysis (Equation 3.35) is higher than vertical stress estimated by Aubertin et al. (2003), as shown in Figure 3.12. It has been observed that the stress calculated using present analysis and Handy (1985) are very close and lower than the vertical stress computed using Marston (1930) and Pirapakaran and Sivakugan (2007a). In present analysis, circular arch has been used to estimate the vertical stress, therefore higher stress has been observed in comparison to Handy (1985).

Present analysis has been compared with Caceres (2005) for $\phi = 36^0$ and inclination of 75^0, 80^0 and 85^0 with horizontal (Figure 3.12). Present analysis gives higher vertical stresses than the vertical stresses estimated by Caceres (2005) as shown in Figure 3.10. Vertical stress decreases with increase in inclination of stope.

3.6 Stress distribution along the width of stope

Principal stresses remain constant along the arch as shown in Figure 3.9. To estimate the vertical stress along width of stope (XY in Figure 3.13), it is necessary to locate the arches which are intersecting XY. The loci of center of arches pass through the central line (OO′) of stope as shown in Figure 3.13. The difference between the heights of arch from horizontal line (Δz) will be same as the difference of center of arch which will pass

through the midpoint O´. Figure 3.13 has been used to calculate the elevation of arch from horizontal.

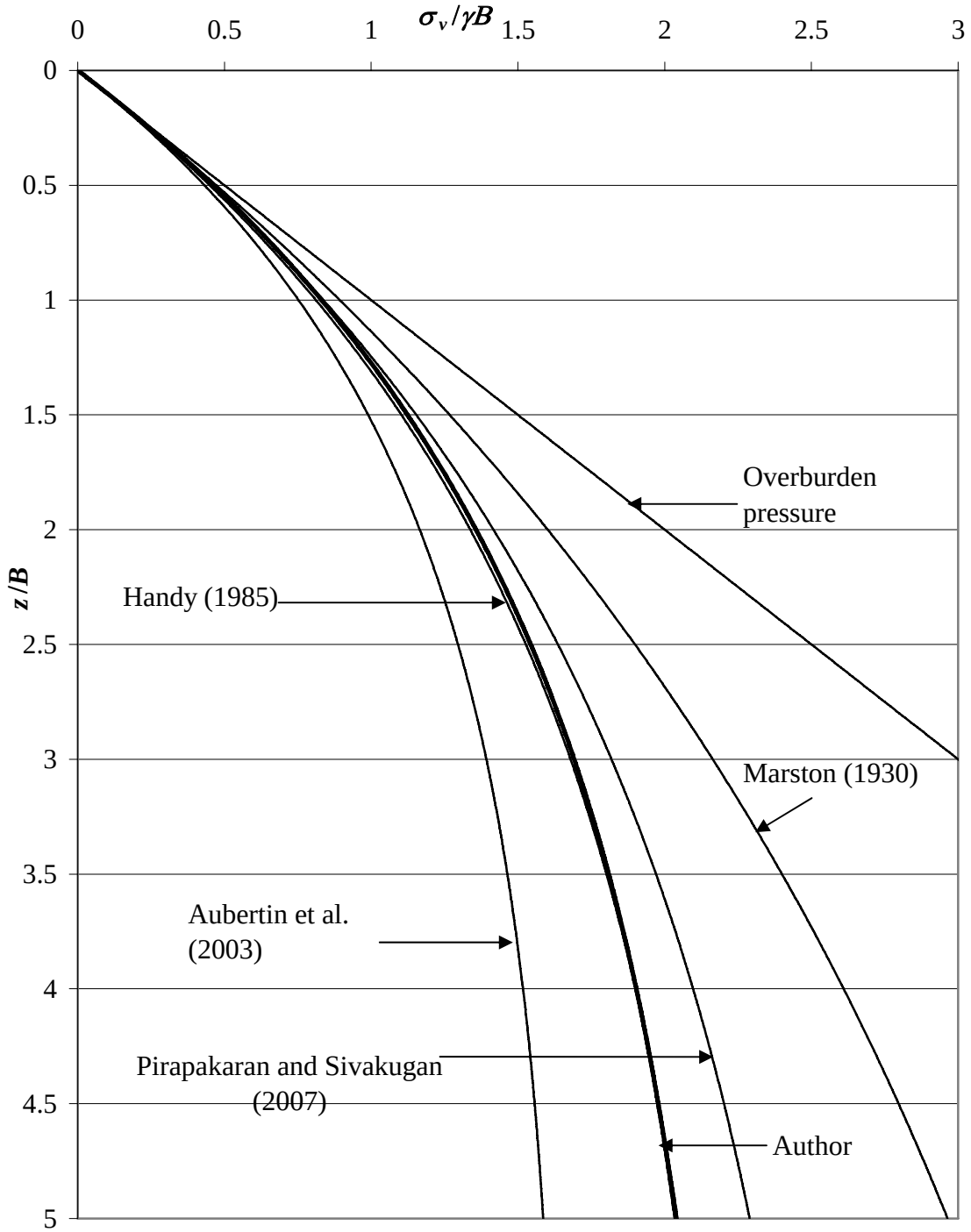

Figure 3.11 Vertical stress variation with depth for $\phi = 36^0$

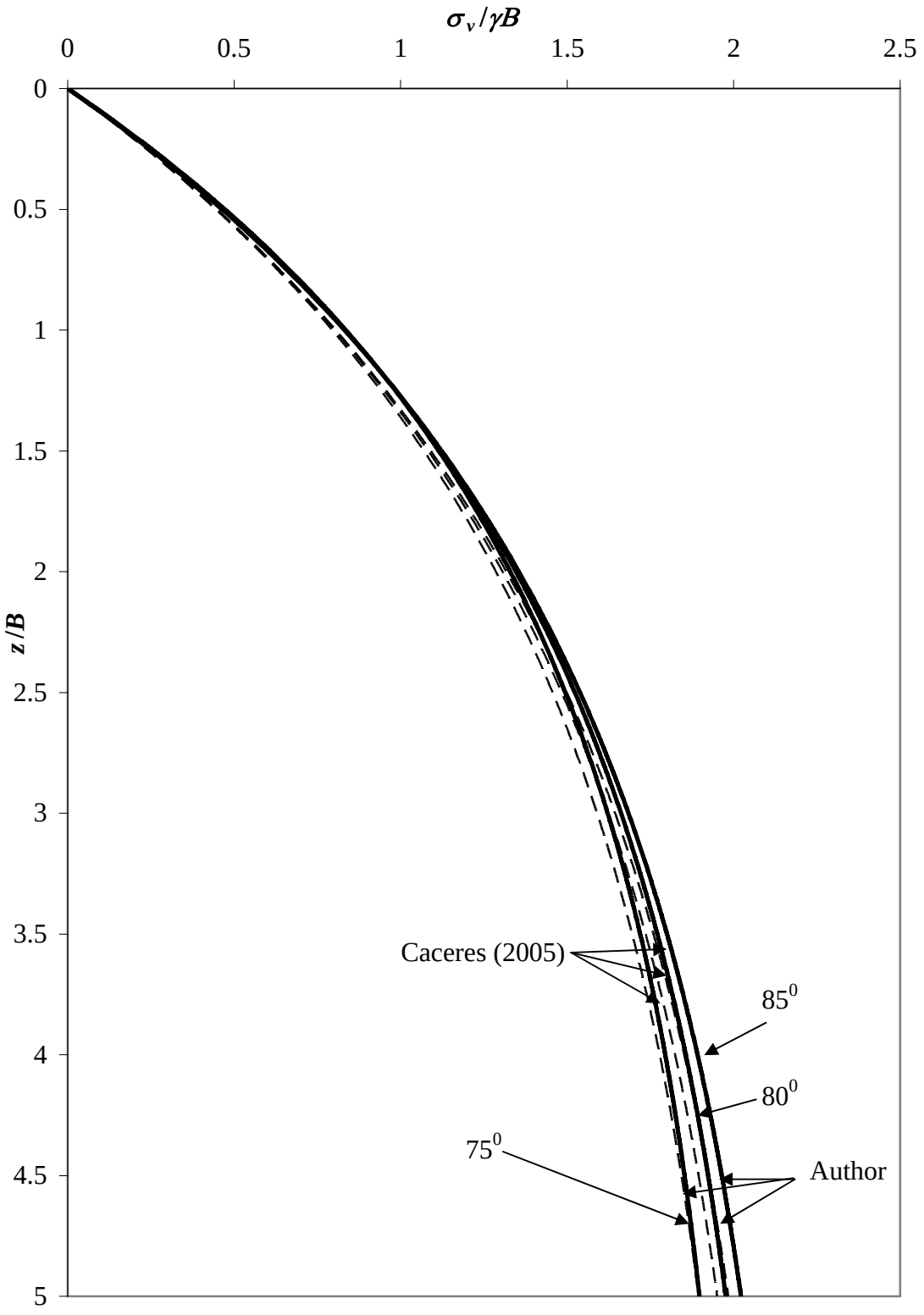

Figure 3.12 Vertical stress variation with depth for an inclined stope for $\phi = 36^0$ and inclination (α) of 75^0, 80^0 and 85^0 with horizontal

In Figure 3.13, the distance O′P′ (= x) is obtained as:

$$x = R\left(\sin\alpha\tan\theta - \cos\alpha\right) \tag{3.36}$$

Substituting R from Equation 3.14 in Equation 3.36 gives:

$$\frac{2x}{B} = \sin\alpha\,\mathrm{cosec}\,\delta\left(\sin\alpha\tan\theta - \cos\alpha\right) \tag{3.37}$$

From Figure 3.11,

$$\frac{\Delta z}{B} = \frac{\sin\alpha\,\mathrm{cosec}\,\delta\left(\sin\alpha - \cos\theta\right)}{2} \tag{3.38}$$

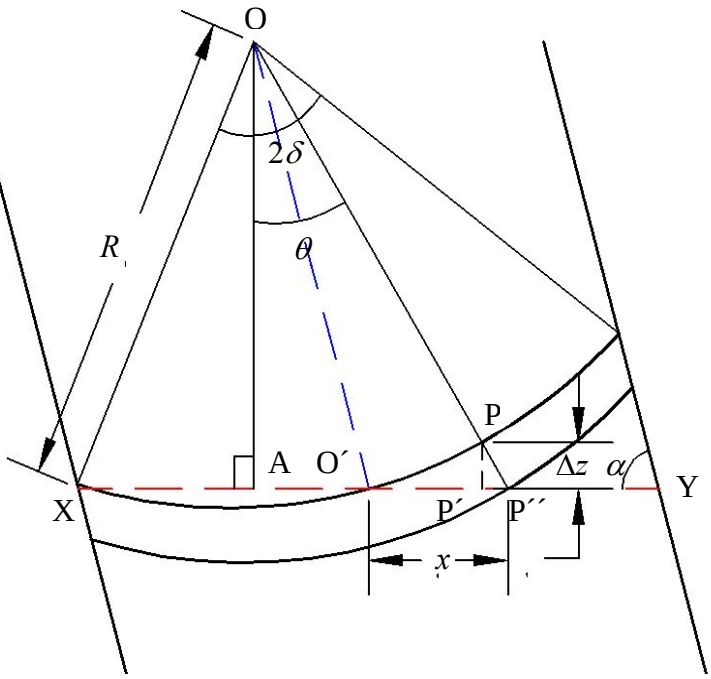

Figure 3.13 Continuous compression arch within an inclined stope.

where Δz is the elevation of point P from horizontal line AO′ in Figure 3.13, which is same as the difference in the vertical height of center of arch passing through P´´ and O´.

It has been used to locate the position of arch passing at distance 'x' from O′ with respect to O. Vertical stress at distance of 'x' from O′ has been calculated using new arch.

The arc angle θ at the hanging wall and the footwall can be calculated using following expressions:

$$\theta_{hanging\,wall} = \tan^{-1}\left(\frac{\sin\alpha\cos\alpha + \sin\delta}{\sin^2\alpha}\right) \tag{3.39}$$

$$\theta_{foot\,wall} = \tan^{-1}\left(\frac{\sin\alpha\cos\alpha - \sin\delta}{\sin^2\alpha}\right) \tag{3.40}$$

Equations 3.17, 3.37 and 3.38 have been used to calculate the variation of vertical stress along the width of stope for angle of inclination of 75^0, 80^0, 85^0 and 90^0 with horizontal, which are shown in Figure 3.14.

The stress variation along the width of stope is shown in Figure 3.12 for different depth and width ratio. It has been observed that the vertical stress is higher on the footwall than that of hanging wall for all the cases for inclined stope whereas it is symmetric for vertical stope ($\alpha = 90^0$). Vertical stress for the inclined stopes is skewed towards footwall and the maximum vertical stresses are shifted from central line (Figure 3.12).

3.7 Effect of soil friction angle (ϕ) on arching

The value K has been in debate until the recent past. Marston's work suggests K can be taken as the Rankine's active earth pressure coefficient K_a. Terzaghi (1943) proposed that K can be assumed to be equal to an empirical constant at every point of the fill, and reported that K can be as high as 1.5. Terzaghi (1943) used K = 1 to explain the arching effect in the soils.

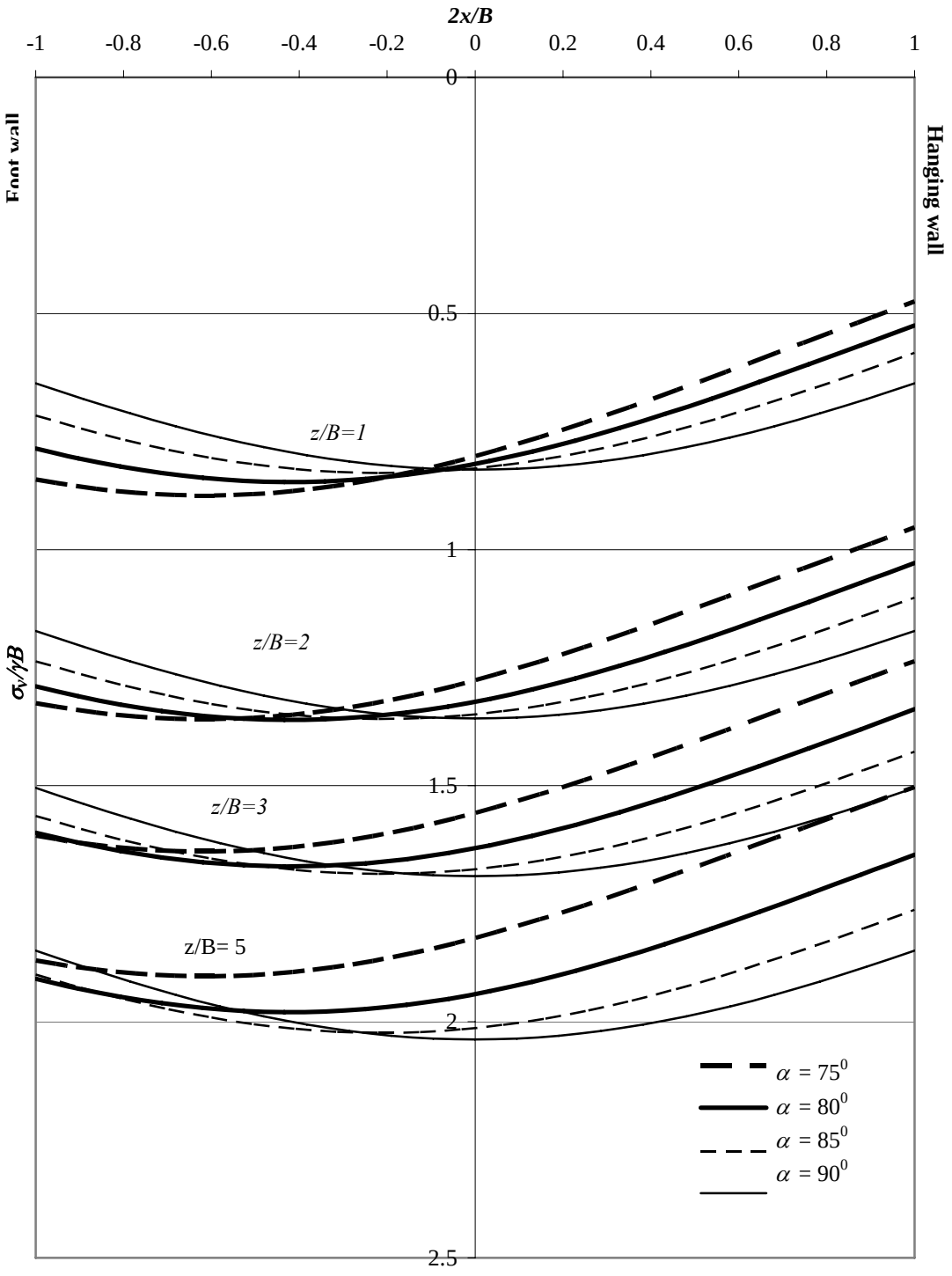

Figure 3.14 Vertical stress variation along the width for an inclined stope for $\phi = 36^0$ and inclination (α) of 75^0, 80^0, 85^0 and 90^0 with horizontal at z/B = 1, 2, 3 and 5.

Handy (1985, 2004), and Handy and Spangler (2007) reported that rotation of the principal stress directions near the wall increases K and will have the effect of increasing supporting friction, so the actual value is approximated by the earth pressure coefficient K_0.

Handy (1985) reported that the mobilization of wall friction causes an increase in horizontal stress and a decrease in vertical stress close to the wall due to rotation of principal stress directions, thus resulting in increase in K. In the wall and conduit problems, the calculated vertical stress is an average vertical stress over the trench width, K is horizontal stress at the wall divided by the average vertical stress – not by vertical stress at the wall, which is lower than the average vertical stress, used in Equation 3.3. Therefore, the K value is somewhat less than the value calculated using Equation 3.3.

Aubertin et al. (2003) applied the Marston's theory (Equation 3.1) to estimate the vertical and lateral loads on the stope floor and wall. It was assumed that $\delta = \phi$, and therefore $\mu = \tan\phi$ as suggested by Terzaghi. Numerical models were developed using PHASE2, a numerical code based on finite element method, considering $K = K_a$, K_p and K_0.

It was concluded by Aubertin et al. (2003) that the fully passive condition ($K = K_p$) could be the most exaggerated, and the fully active condition ($K = K_a$) was not realistic considering the movement required to induce it. It was observed that the actual response of the stope and backfill would be close to the rest condition, and thus $K = K_0$ is more appropriate than other earth pressure coefficients. Pirapakaran and Sivakugan (2007a and 2007b) also compared the vertical stress (σ_v) values predicted by Equation 3.1 with those obtained from numerical modeling, and showed that for hydraulic fills where $c = 0$, Equation 3.1 gives realistic estimates when $\delta = 0.67\ \phi$ and $K = K_0$.

It has been observed that the stress reduction due to arching (Equations 3.1, 3.2, 3.7, 3.9, 3.10 and 3.35) depends on the trench geometry and friction angles (ϕ and δ) in terms of μK. Several attempts have been made to study the behavior of soil friction angle (ϕ) and soil wall interface angle (δ) separately. It has been observed that the term μK appears

together in all expression used to estimate vertical stresses using arching phenomenon. It increases the importance of studying the variation of μK than studying the variation of ϕ and δ separately.

3.7.1 Sensitivity of soil arching to ϕ

It is seen from the above developments (Equations 3.1, 3.2, 3.5, 3.7, 3.8 and 3.33) that the fraction of the self weight of the backfill that is transferred to the bottom is a function of the geometry, and the shear strength characteristics of the wall-backfill interface and the backfill. Two main factors that contribute to the average vertical normal stress at any depth are the earth pressure coefficient, K, and tangent of the wall-backfill interface friction angle, $\tan\delta = \mu$. These two parameters appear in the expressions for the vertical stress at any depth within the backfill as their product μK.

For δ in the range of 0 to ϕ, the value of μ can lie in the range of 0 to $\tan\phi$. The relationship between δ and ϕ can precisely be obtained by conducting in-situ direct shear tests, or laboratory direct shear tests simulating the field situations.

If the wall is rigid and there is no lateral strain within the backfill, it is reasonable to assume that the backfill is at rest and $K = K_0$. If the wall is smooth and yields laterally, enabling the backfill to reach active state, $K = K_a$. If the wall is rough, the earth pressure coefficient can be closer to the one proposed by Krynine (1945), given in Equation 3.3.

Depending on the field application, δ can be taken as a fraction of ϕ, and K can be taken as K_a, K_0 or $K_{Krynine}$. For example, in computing vertical normal stresses within minefills surrounded by rock walls, the fragmented rock wall is similar to what is shown in Figure 3.6(c), where failure takes place a few grains away from the rock wall. Here, it is appropriate to take δ as ϕ.

The backfills are often granular. Their friction angle can be determined from triaxial or direct shear tests on reconstituted samples packed at densities representative of field

situation, or from in situ tests such as standard penetration test. The stresses within the backfills can be studied using numerical models or by the analytical expressions provided above. It may appear that friction angle is a key input parameter that has to be determined precisely for realistic estimates of the stresses within the backfills. A closer look at the Marston's equation and its other improved forms (Equations 3.1, 3.2, 3.5, 3.7, 3.8 and 3.33) reveals that all these equations are insensitive to ϕ, irrespective of the assumption with regards to K and δ, and hence it is not necessary to precisely know the value of ϕ, especially for routine design applications.

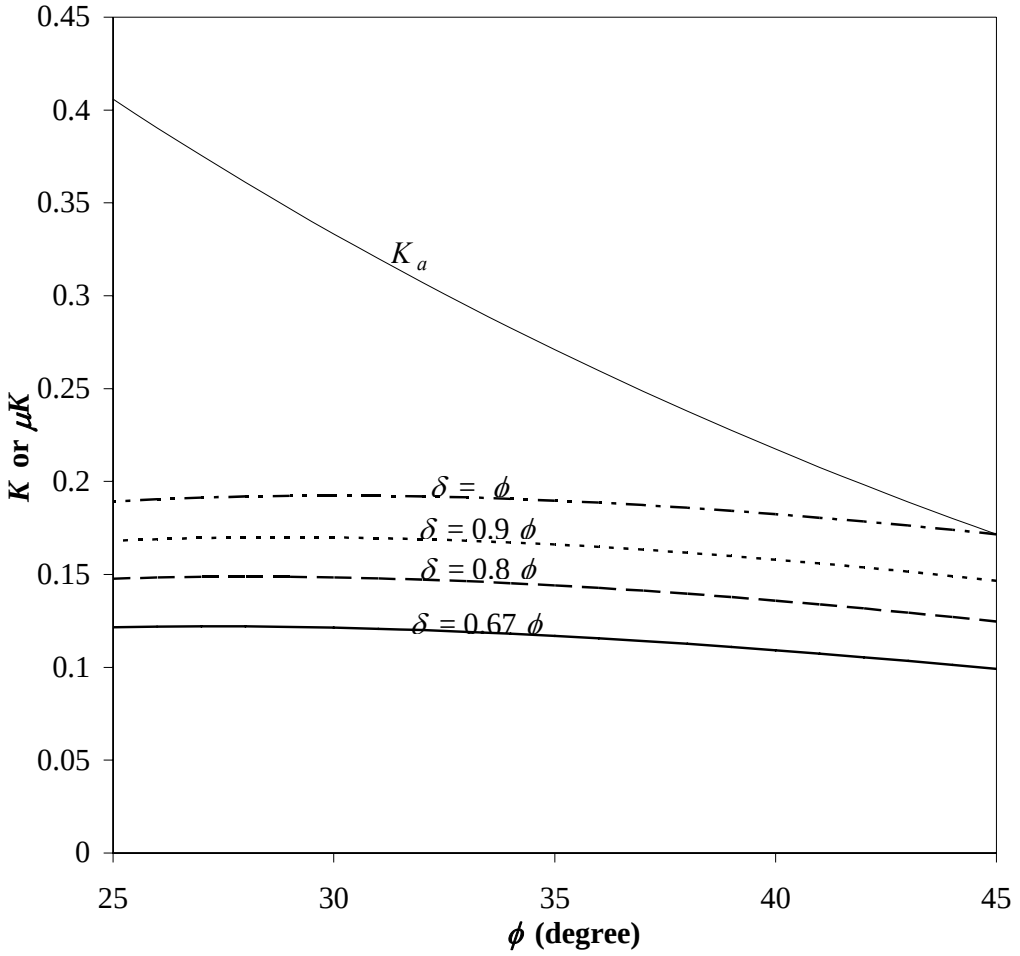

Figure 3.15 Variation of μK against ϕ for $K = K_a$ (Active earth pressure coefficient)

Figure 3.15 shows the variation of μK against ϕ for δ/ϕ = 0.67-1.0, where $K = K_a$. It is evident that μK remains approximately a constant over a wide range of ϕ. With increasing ϕ, K decreases and μ (or tanδ) increase such that μK remains approximately the same. The constant value of μK varies with δ/ϕ. Figure 3.16 shows the variation of μK against ϕ for δ/ϕ = 0.67 – 1.0 , where $K = K_0$. Again, μK remains a constant for a wide range of ϕ. The constant value of μK depends on the fraction assumed for δ/ϕ. Figure 3.17 shows the variation of μK against ϕ, where $K = K_{Krynine}$. As in the case of $K = K_a$ and $K = K_0$, here again μK remains a constant over a wide range of ϕ. The average values of μK computed for $K = K_a$, K_0 and $K_{Krynine}$ and δ/ϕ = 0.67, 0.8, 0.9 and 1 are summarized in Table 3.1. Friction coefficient (μK) decreases with decrease in wall – backfill interface angle. Krynine's earth pressure coefficient gives higher values of μK whereas Rankine active earth pressure coefficient gives lower values.

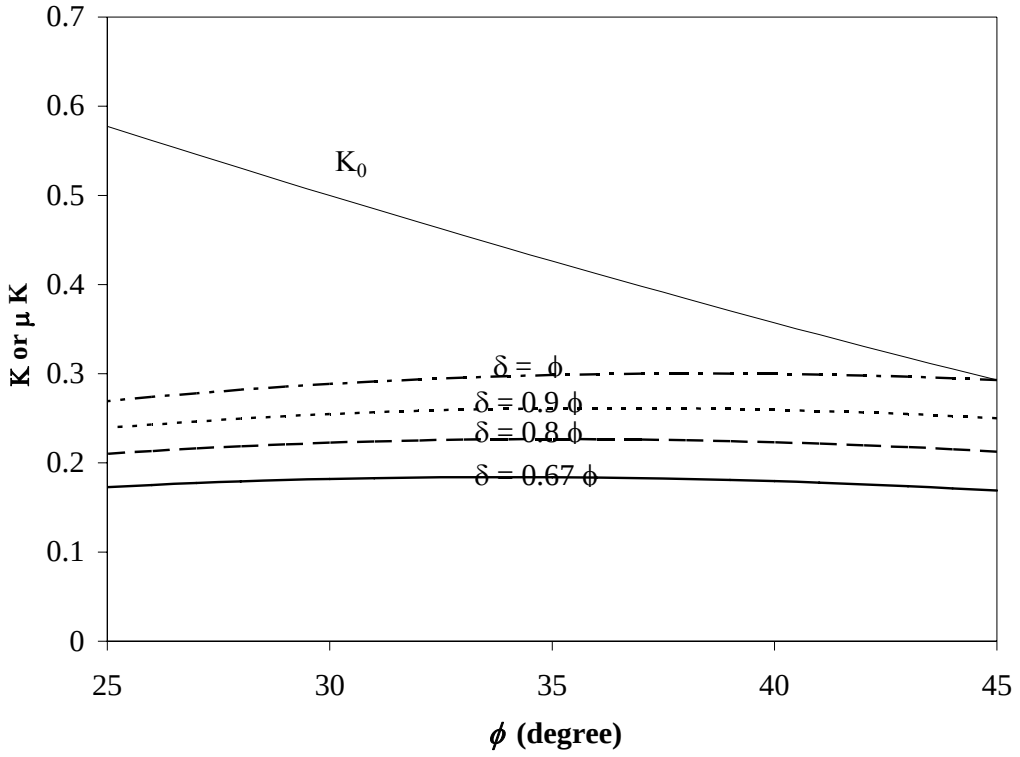

Figure 3.16 Variation of μK against ϕ for $K = K_0$ (Earth pressure coefficient at rest)

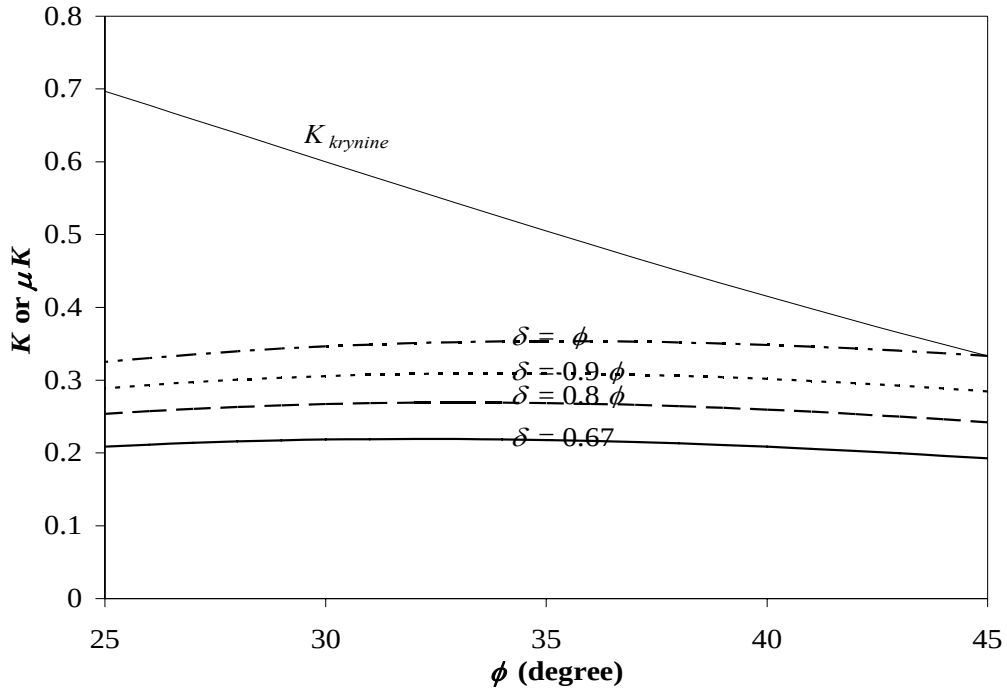

Figure 3.17 Variation of μK against ϕ for K = $K_{Krynine}$

3.7.2 Variation of vertical stresses with ϕ

Effect of ϕ on the vertical stress σ_v at two different depths $z = B$ and $z = 3B$ within the backfill, shown in Figure 3.18 and 3.19 respectively, indicates that σ_v does not vary significantly with variation in ϕ. Thus, this discussion is sufficient to state that soil arching is almost insensitive to ϕ, irrespective of the assumption with regards to K and δ, and hence it is not necessary to precisely know the value of ϕ, especially for routine design applications.

Table 3.1 Average values of μK

K	δ/ϕ	μK
K_0 Jaky (1944)	1	0.292
	0.9	0.255
	0. 8	0.221
	0.67	0.179
K_a Rankine (1857)	1	0.186
	0.9	0.163
	0. 8	0.141
	0.67	0.114
$K_{Krynine}$ Krynine (1945)	1	0.345
	0.9	0.301
	0. 8	0.261
	0.67	0.211

3.8 Stress reduction factor

Equations 3.1, 3.7, 3.9, 3.10 and 3.31 provide the vertical stress at any depth *z* for vertical and inclined stopes and can be used to analyze the stability of mining stopes. Although these expressions are giving the required vertical stress values; for routine applications, especially at the mining sites, a simple form of these equations will be appreciated by practicing engineers. In this dissertation, an attempt is made to present a single equation that represents all these equations through a stress reduction factor introduced by Sivakugan (2008).

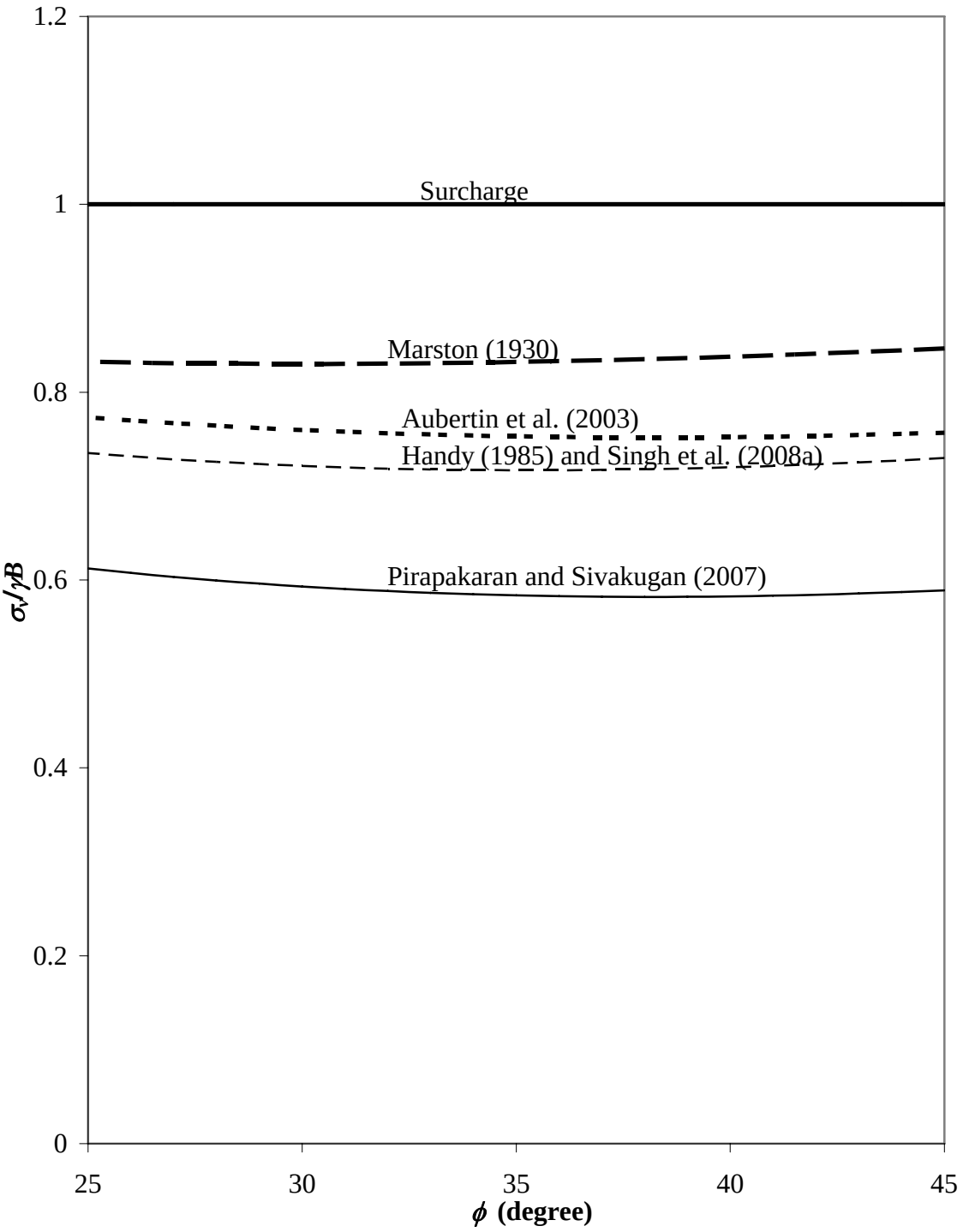

Figure 3.18 Effect of ϕ on the vertical stress σ_v at depth of $z = B$

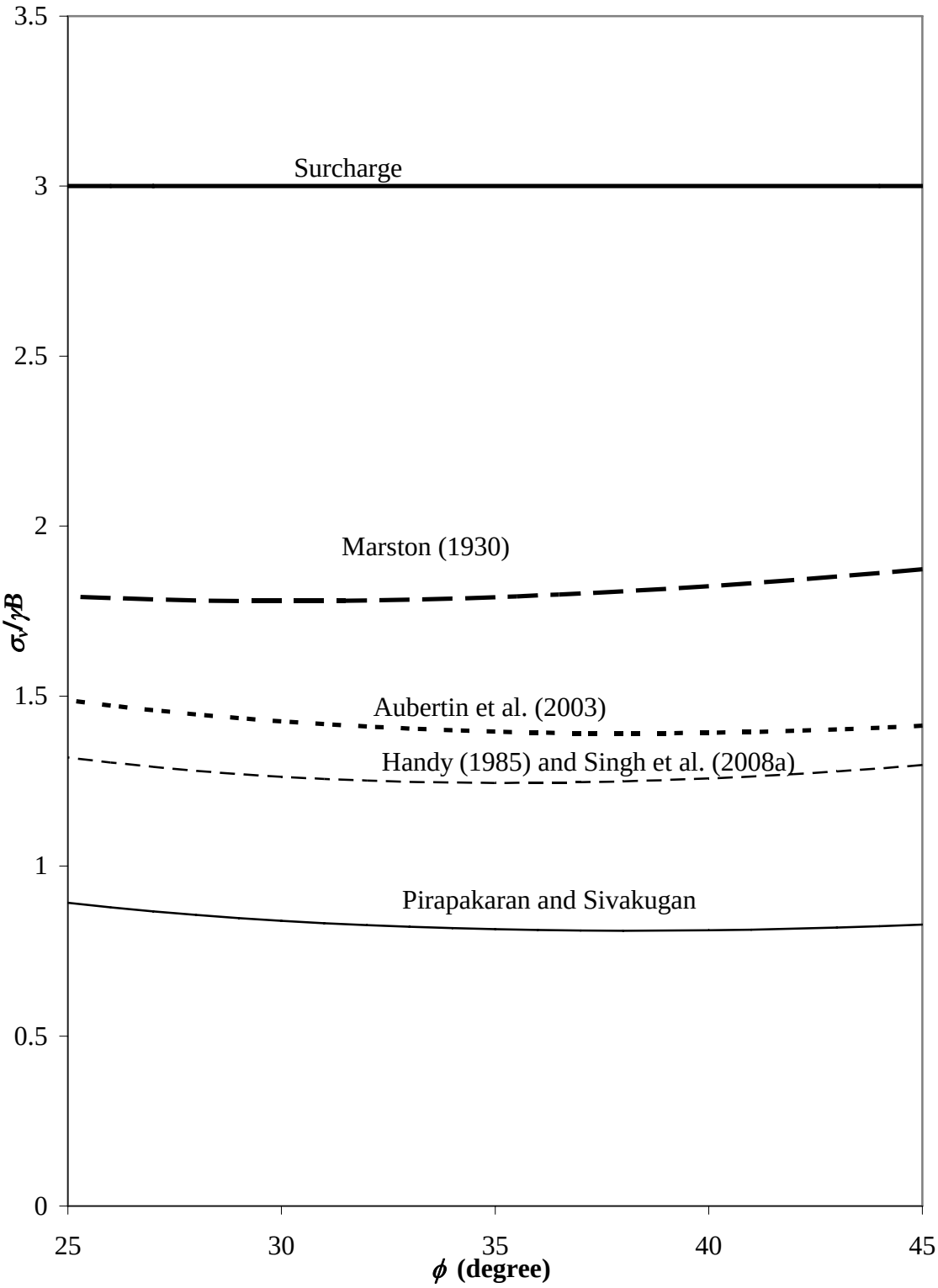

Figure 3.19 Effect of ϕ on the vertical stress σ_v at depth of $z = 3B$

3.8.1 Stress reduction factor (α_s)

The stress reduction factor (α_s) at a particular depth (z) is defined as the ratio of the actual vertical normal stress to surcharge (γz) at this depth. This is a factor, less than 1, which has to be multiplied by the overburden pressure (γz) to estimate the actual vertical stress acting at depth z. A typical stress variation in a hydraulic fill stope is shown in Fig. 3.20.

From Figure 3.20,

$$\alpha_s = \frac{\overline{ab}}{\overline{ac}} \tag{3.41}$$

or

$$\sigma_v = \alpha_s \gamma z \tag{3.42}$$

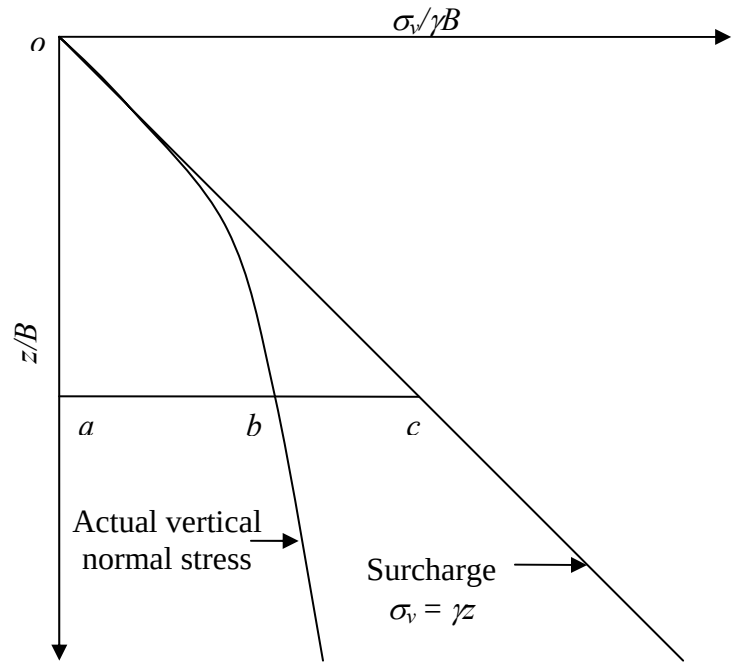

Figure 3.20 Vertical normal stress variation in a mine stope

Stress reduction factor (α_s) varies with depth of the stope. The variation of α_s with depth using expressions proposed by Marston (1930), Aubertin et al. (2003), Pirapakaran and Sivakugan (2007a) and Singh et al. (2008a), is shown in Figure 3.20 for a vertical stope. Earth pressure coefficient and wall friction angle used to estimate the stress reduction factor is shown in Table 3.2. Figure 3.21 shows that the stress reduction factor decreases rapidly with increase in aspect ration (z/B), where z and B are the depth and width of the stope respectively. It has been observed that there is not much difference in stress reduction factors calculated using analysis proposed by Aubertin et al. (2003) and Singh et al. (2008a). Analysis by Pirapakaran and Sivakugan (2007a) gives lowest value of stress reduction factor and Marston (1930) is on higher side.

Table 3.2 Earth pressure coefficient and wall friction angle used to estimate stress reduction factor

Method	Earth pressure coefficient	Wall friction angle (δ)
Marston (1930)	K_a	ϕ
Aubertin et al. (2003)	K_0	ϕ
Pirapakaran and Sivakugan (2007a)	K_0	0.67ϕ
Singh et al. (2008a)	K_0	ϕ

It can be seen in Figure 3.21 and 3.22 that the stress reduction factor α_s is close to unity at the top of stope and decreases rapidly with depth. At $z = 5B$ (i.e. depth of 5 times the stope width), α_s is in the range of 0.2 to 0.4, depending on the expressions used to compute normal vertical stress. In the case of inclined stope, the inclination to the vertical has little effect on α_s.

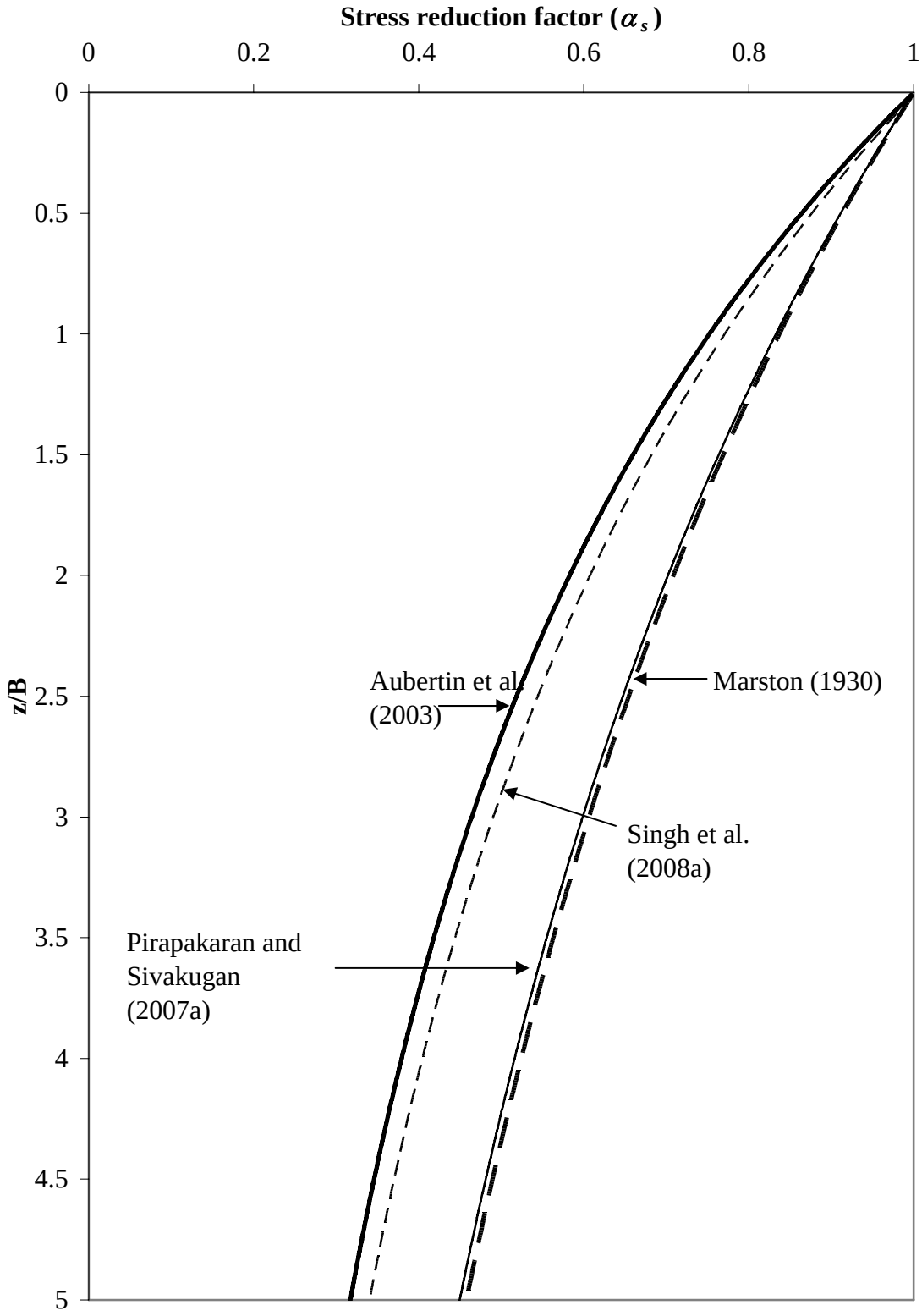

Figure 3.21 Stress reduction factor for vertical stope

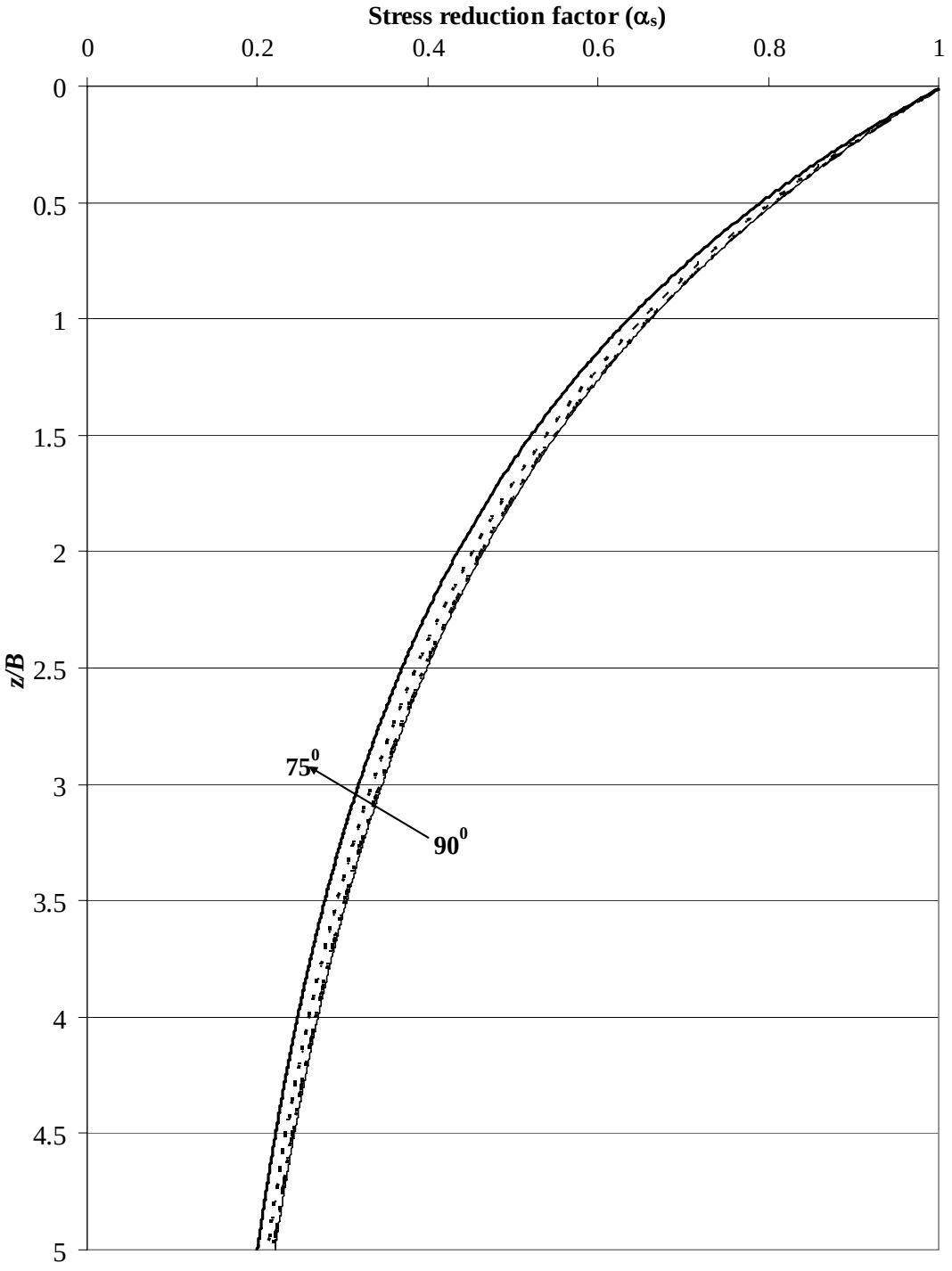

Figure 3.22 Stress reduction factor for inclined stope (inclination of 75^0, 80^0, 85^0 and 90^0 with horizontal)

It has been observed that the arching is relatively insensitive to backfill friction angle (ϕ) because the vertical stress depends on δ/ϕ and K. All previous authors have proposed a constant value of δ/ϕ and recommended usage of a specific earth pressure coefficient. By logarithmic curve fitting to the curves in Figure 3.21 and 3.22, it can be shown that:

$$\log \alpha_s = -\lambda\left(\frac{z}{B}\right) \tag{3.43}$$

where λ is an empirical coefficient determined through the regression analysis. The values of λ for vertical and inclined stopes are summarized in Tables 3.3a and 3.3b respectively. Coefficient of determination (R^2) has been calculated for logarithmic fitted curve in Fig. 3.9 and 4. R^2 varies from 0.9952 to 0.9434 for different values of δ/ϕ and K (Marston, 1930; Aubertin et al., 2003; Pirapakaran and Sivakugan, 2007; and Singh et al. 2008a) used to estimate the stress reduction factor. The values of R^2 are reported in Table 3.3a and 3.3b for vertical and inclined stopes respectively. Equation 3.43 can be used to calculate stress reduction factor at different depths in a vertical and inclined stope.

Table 3.3a Empirical coefficient for vertical stopes to estimate α_s

Method	Empirical coefficient (λ)	R^2
Marston (1930)	0.384	0.995
Aubertin et al. (2003)	0.566	0.987
Pirapakaran and Sivakugan (2007)	0.412	0.960
Singh et al. (2008a)	0.528	0.990

3.8.2 Average stress reduction factor ($\alpha_{average}$)

While a stope is filled, it is necessary to know the vertical stresses at any depth within the mine fill so that the loading on the barricades can be realistically determined. Since the stresses are the largest at the bottom of the stope and loading on the barricades at the

bottom drive is most critical, it is of great interest to be able to determine the vertical stresses at the bottom of the stope. The vertical stress at depth of the stope is given by Equation 3.42. It can be seen from Figure 3.21 and 3.22 that when stope is being filled, the stress reduction factor α_s decreases rapidly from unity and will take the lowest value when stope is filled. As a very conservative approximation, the lowest value of α_s, which occurs when the stope is filled, can be used throughout the filling process, for estimating the vertical stress at the bottom of the stope. A more realistic approach is to use $\alpha_{average}$ proposed herein, which is simply the ratio of area beneath actual σ_v - z plot to the area under overburden stress in Figure 3.23, where arching is not considered.

Table 3.3b Empirical coefficient for inclined stopes to estimate α_s

Angle of inclination (α)	Empirical coefficient (λ)	R^2
75^0	0.816	0.959
80^0	0.789	0.966
85^0	0.774	0.969
90^0	0.528	0.989

Average stress reduction factor ($\alpha_{average}$) at the bottom the stope of depth z is defined as ratio of area under actual vertical normal stress to area under surcharge at that depth. It can be expressed as:

$$\alpha_{average}(z) = \frac{\int_0^z \sigma_v(z)\,dz}{\frac{1}{2}\gamma z^2} \tag{3.44}$$

The variation of average stress reduction factor ($\alpha_{average}$) for vertical and inclined stopes is shown in Figures 3.24 and 3.25 respectively. It has been observed that the logarithmic of $\alpha_{average}$ varies linearly with depth and width ratio (z/B). Following empirical equation is established to estimate $\alpha_{average}$.

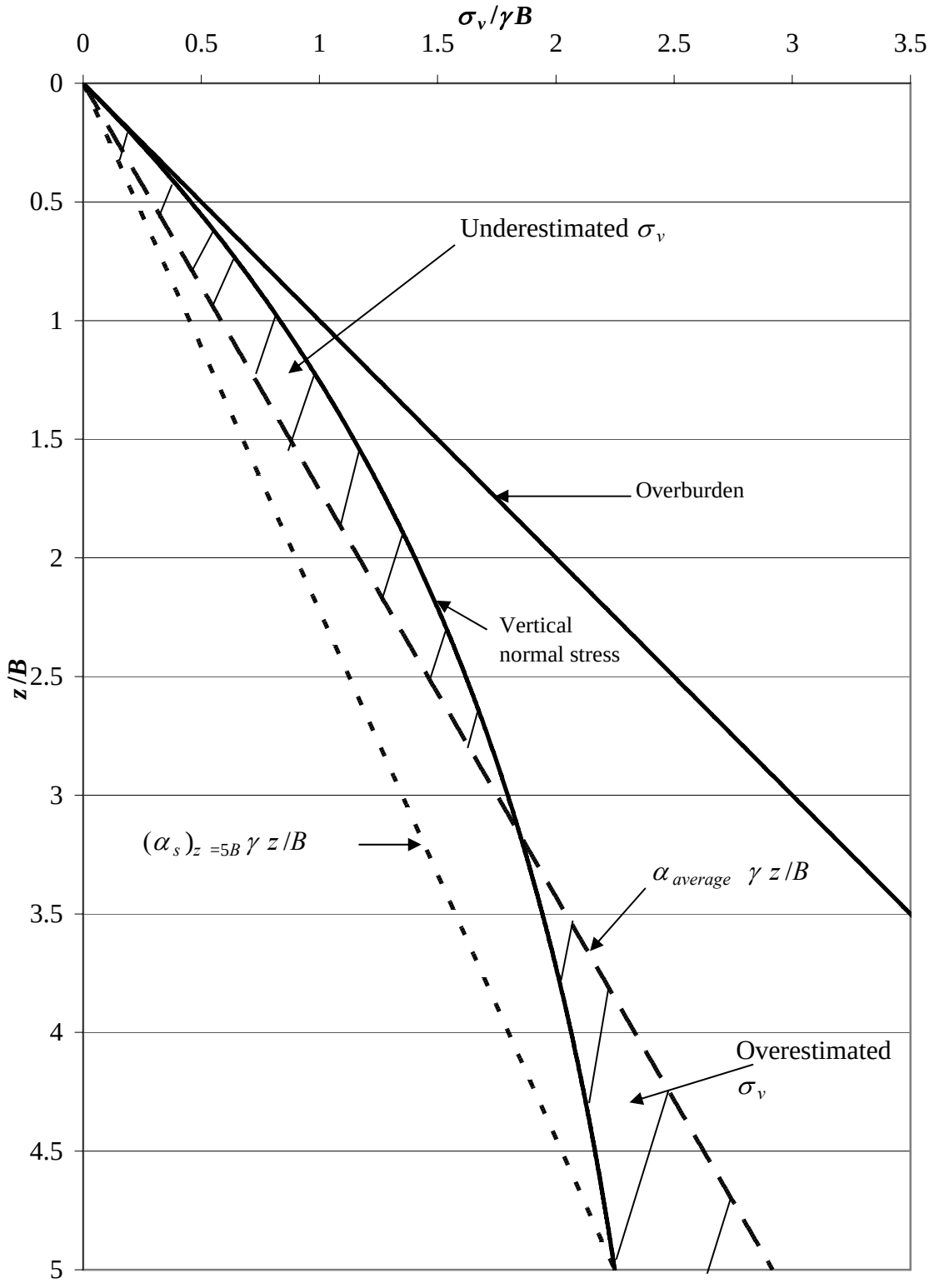

Figure 3.23 Variation of stresses using α_s and $\alpha_{average}$ from vertical normal stress estimated using Marston's theory at z/B= 5

$$\log \alpha_{average} = -\lambda_{average}\left(\frac{z}{B}\right) \tag{3.45}$$

where $\lambda_{average}$ is an empirical coefficient. The values of λ_{averag} are given in Table 3.4a and 3.4b for vertical and inclined stopes respectively. Coefficient of determination (R^2) has been calculated for Equation 3.45 for average stress reduction factor in vertical and inclined stope (Figures 3.24 and 3.25). R^2 varies from 0.9961 to 0.9627 for different analysis (Marston,1930; Aubertin et al., 2003; Pirapakaran and Sivakugan, 2007a; and Singh et al., 2008a) used to estimate stress reduction factor, which shows very good correlation between the empirical equation and the estimated values. The values of R^2 are reported in Table 3.4a and 3.4b for vertical and inclined stopes respectively.

The horizontal stress is required to study the stability of stopes. If earth pressure coefficient remains constant throughout the stope, total horizontal load on the stopes can be computed by multiplying earth pressure coefficient to the total vertical load within the stopes. Total horizontal stress on the stope (σ_h) at any depth H can be expressed using following expression:

$$\sigma_h = \frac{1}{2} K \alpha_{average} \gamma H^2 \tag{3.46}$$

where K is earth pressure coefficient. Equation 3.46 can be used to estimate average stress reduction factor to calculate horizontal stresses.

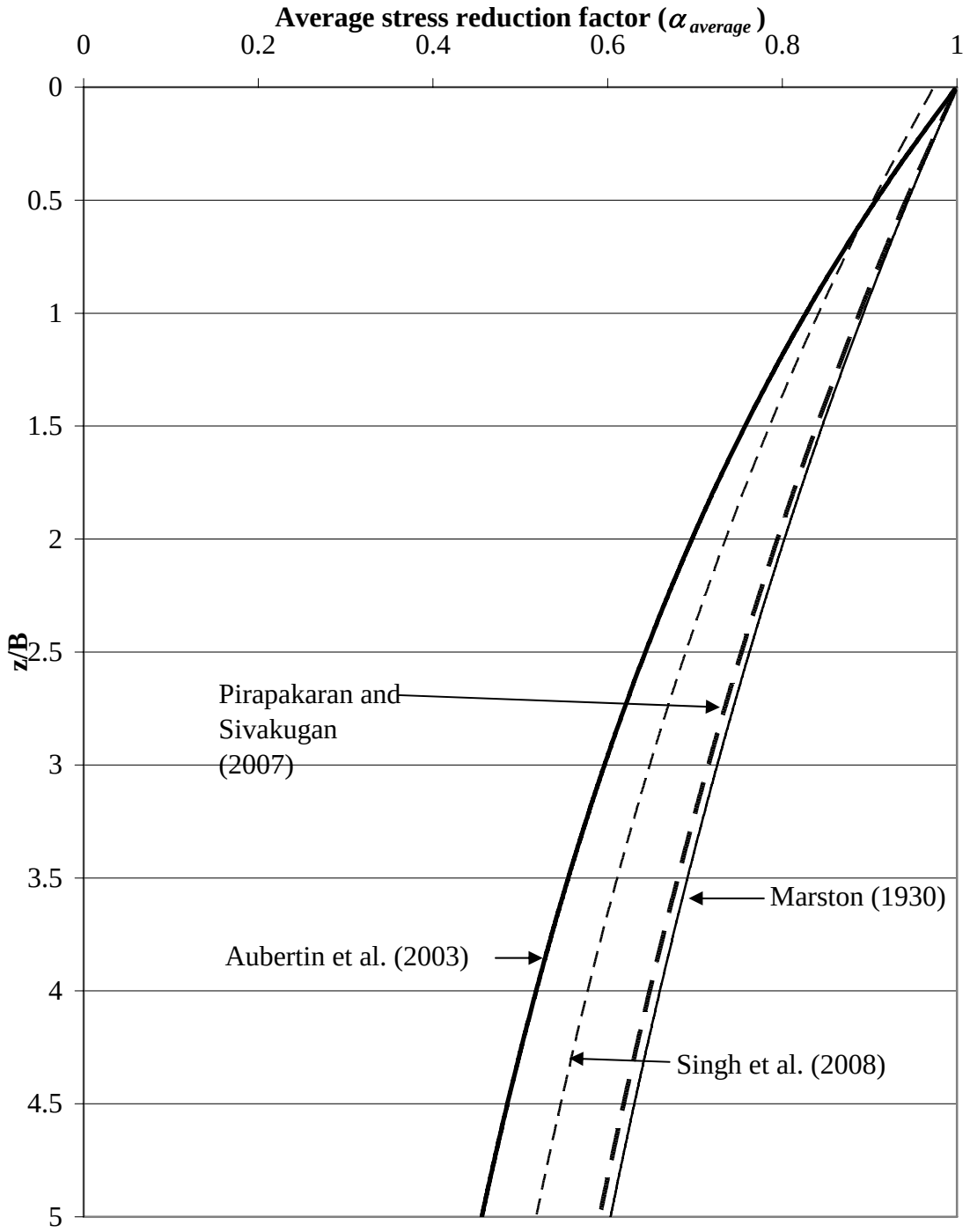

Figure 3.24 Average stress reduction factor for vertical stope

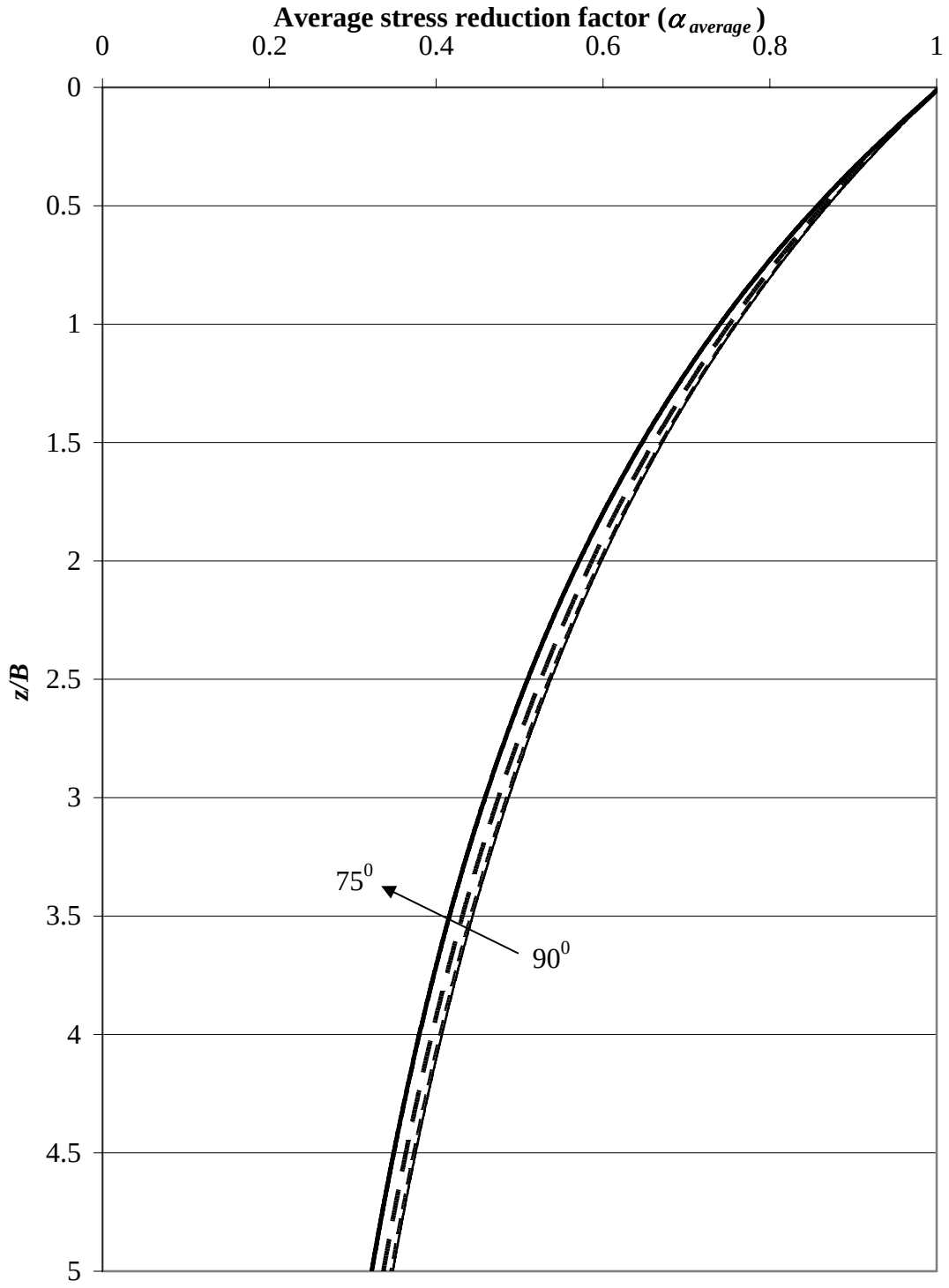

Figure 3.25 Average stress reduction factor for inclined stope (inclination of 75^0, 80^0, 85^0 and 90^0 with horizontal)

Table 3.4a Empirical coefficient for vertical stopes to estimate $\alpha_{average}$

Method	Empirical coefficient ($\lambda_{average}$)	R^2
Marston (1930)	0.258	0.996
Aubertin et al. (2003)	0.383	0.990
Pirapakaran and Sivakugan (2007a)	0.423	0.976
Singh et al. (2008a)	0.356	0.993

Table 3.4b Empirical coefficient for inclined stopes to estimate $\alpha_{average}$

Angle of inclination (β)	Empirical coefficient ($\lambda_{average}$)	R^2
75^0	0.564	0.974
80^0	0.543	0.977
85^0	0.532	0.979
90^0	0.356	0.993

3.9 Summary and conclusions

Hydraulic fills transfer a part of their self weight to the adjacent rock mass in the process of self-weight settlement due the friction between hydraulic fill and adjacent rock wall. This process of reduction in vertical normal stress is known as arching. Several theories have been proposed to estimate the vertical stress in a vertical mine stope. In this dissertation, a continuous compression arch of principal stresses has been used to estimate the vertical stress within an inclined mine stope, which is also extended to the vertical stope. For simplicity, circular compression arch has been assumed for the analysis. It has been observed that the wall friction angle is fully mobilized at the foot wall whereas it is partially mobilized at the hanging wall. An equation (Equation 3.30) has been proposed to estimate the vertical stresses within the inclined stope for any backfill under a surcharge. Equation 3.31 has been proposed to calculate the vertical

stress due to hydraulic fill in inclined stopes. Present analysis has been compared with Marston (1930), Aubertin et al. (2003), Pirapakaran and Sivakugan (2007a) for the vertical stope. It has been observed that present analysis gives higher stresses than the stresses reported by Aubertin et al. (2003), Pirapakaran and Sivakugan (2007a) and Handy (1985) and lower than Marston (1930). The vertical stress calculated using present analysis is higher than the stresses calculated by Caceres (2005) for an inclined stope. A methodology has been proposed to calculate the vertical stress distribution along the width of inclined stope. The variation of stresses along the width of stope is graphically shown.

Effect of hydraulic fill friction angle (ϕ) and wall-backfill interface angle (δ) on vertical stress has been studied. It has been observed that Arching is almost insensitive to the friction angle ϕ of the backfill. Therefore, it is not necessary to direct any effort towards determining the friction angle of the backfill precisely. Rather, attention should be paid to the value of δ/ϕ and the appropriate expression for K.

Concept of stress reduction factor (α_s) and average stress reduction factor ($\alpha_{average}$) have been introduced as the ratio of the actual vertical normal stress to the surcharge at that depth whereas average stress reduction factor ($\alpha_{average}$) at the bottom of the stope is the ratio of area under vertical normal stress to the area under surcharge at the depth z – vertical normal stress σ_v plot. Empirical equations have been proposed to calculate α and $\alpha_{average}$ for both vertical and inclined stopes. The variation of α and $\alpha_{average}$ with depth has been shown graphically. For practical applications, $\alpha_{average}$ can be used to calculate the total horizontal stress in the mining stope.

Chapter 4

Laboratory Studies of Permeability and Moisture Content Variation of Hydraulic Fills within a Model Stope

4.1 General

Mining accidents due to barricade failures are often catastrophic, resulting in sudden flow of wet slurry into the drives, trapping the miners and machinery in the vicinity. Several mechanisms such as piping and liquefaction have been suggested as the triggers (Bloss et al. 1998; Grice 1998; Kuganthan 2001). Most of the failures take place in the early hours of filling and are caused by the presence of excess water within the mine fill. Therefore, the mines make every effort to remove the excess water as quickly as possible from the stope. Herget and de Korompay (1988) suggested a minimum threshold permeability value of 100 mm/hour that would ensure adequate drainage characteristics for a hydraulic fill stope to perform satisfactorily.

Hydraulic fills being granular, they consolidate almost instantaneously in an oedometer, making it difficult to determine the value of coefficient of consolidation (c_v) from Taylor's or Casagrande's procedures. It is possible to overcome this difficulty by testing a very tall sample thus increasing the drainage path length and hence the consolidation time. Under any specific surcharge, knowing the coefficient of volume compressibility (m_v), and coefficient of consolidation (c_v), permeability (k) can be computed as:

$$k = c_v m_v \gamma_w \tag{4.1}$$

Nevertheless, it is well known that the permeability determined from Equation 4.1 using oedometer test data can be misleading (Tavenas et al. 1983).

Rankine et al. (2004) and Sivakugan et al. (2006) reported permeability measurements on 26 different hydraulic fills representing four different mines in Australia. All samples were prepared as slurries with water content of 30-35%, similar to those of slurries placed at the mines. All samples were allowed to settle under their self weight in a 153 mm diameter × 306 mm high cylindrical permeameter. Constant head and falling head permeability tests were carried out on each sample and the average values are plotted against the effective grain size in Figure 4.1. Hazen (1930) suggested that for clean uniform filler sand, permeability and effective grain size are related by following equation.

$$k = C D_{10}^2 \tag{4.2}$$

where, k is in mm/hr and D_{10} is in μm. it can be seen from Figure 4.1 that the constant C is in range of 0.02-0.06 for the above hydraulic fills.

Most permeability measurements reported in the literature are from hydraulic fill samples subjected to no surcharge (Rankine et al. 2006, Sivakugan et al. 2006a, 2006d). In reality, the hydraulic fills at the mine are under several meters of overburden and therefore it is useful to study the effects of surcharge on the measured permeability. Further, in most numerical modeling work carried out to date, simulating the drainage through hydraulic fills, it is assumed that the permeability of the fill remains the same with depth. At same time, the hydraulic fills in a mine stope become unsaturated due to continuous drainage. It has been observed that the permeability changes very rapidly with change in degree of saturation (Chapter 2).

In this dissertation, an attempt is made to relate the permeability to effective stress and void ratio, based on an extensive laboratory test program. Laboratory tests have been designed to measure the permeability variation with stress and moisture content variation with depth and time. It will help in estimating permeability variation with depth and time in a mine stope. This will enable

more realistic numerical modeling and analysis of the drainage through hydraulic fill, where permeability can be expressed as a function of the effective stress or void ratio.

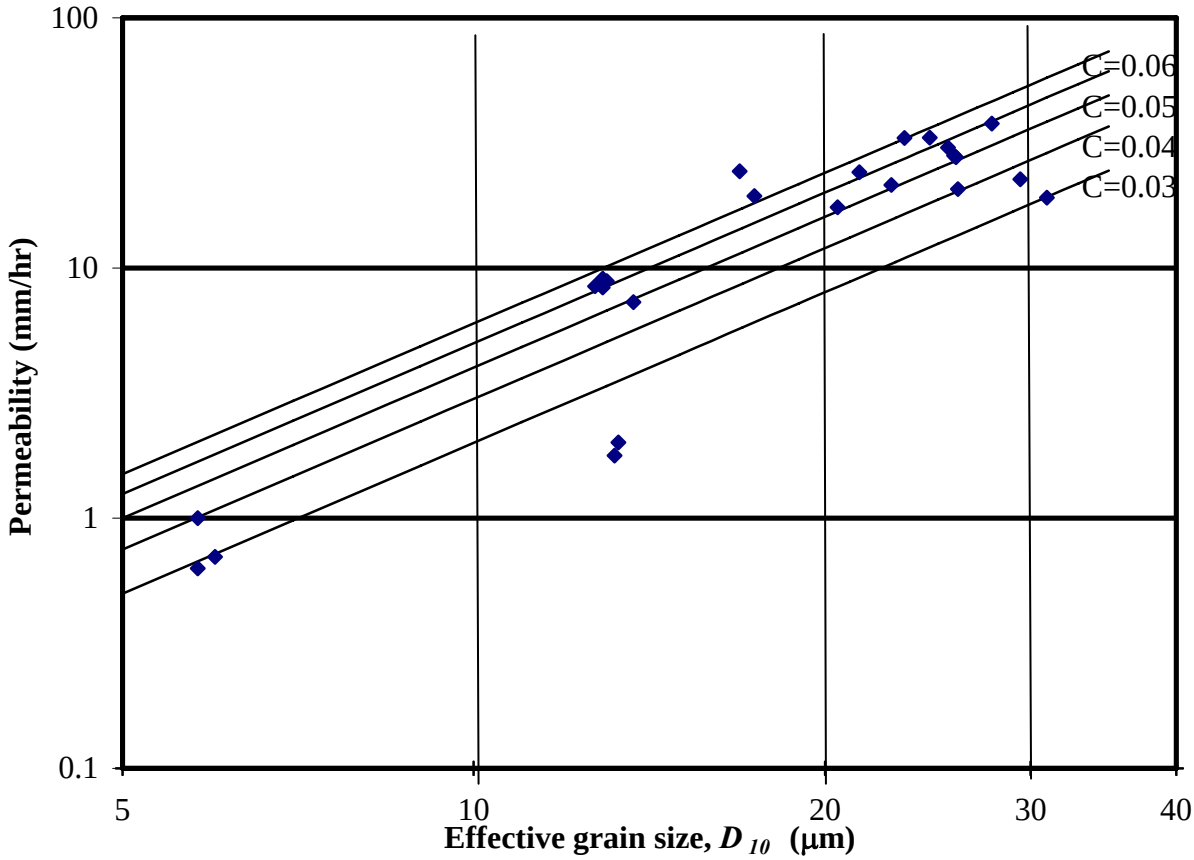

Figure 4.1 The variation of permeability of sedimented hydraulic fills in laboratory under surcharge with effective grain size

4.2 Laboratory tests

Falling head method and constant head method are two standard laboratory tests that are used to determine permeability of soil. Constant head method is primarily used for coarse grained soils and falling head method is preferred for fine grained soils (Das, 2005). Since hydraulic fills are fine grained silty sand or sandy silts hence falling head method is recommended to measure permeability of hydraulic fills. In this dissertation, modified oedometer has been used to measure permeability of hydraulic fills under surcharge using fall head method.

4.2.1 Modified Oedometer test

A modified oedometer, shown in Figure 4.2, was used to measure permeability of the hydraulic fill sample under surcharge pressure. The drainage line from the sample was taken from the centre of the bottom porous stone into the tail water reservoir where the water height was maintained at constant level (Figure 4.3). This tail water level was taken as the datum while measuring the head in the falling head permeability tests. The ring around sample has a hole that allows head water to reach the top porous stone and then flow through the sample downward. The oedometer ring has inner diameter of 72 mm and height of 19 mm. Similar setup was used by Tavenas et al. (1983) to measure effect of surcharge on permeability of clays.

The modified oedometer arrangement shown in Figure 4.3 enables independent measurement of permeability through a falling head permeability test. While the oedometer can be used for carrying out standard consolidation tests, in between pressure increments, falling head permeability tests can be carried out without unloading the sample. This is a very desirable feature of this modified oedometer setup where permeability can be measured under surcharge pressure.

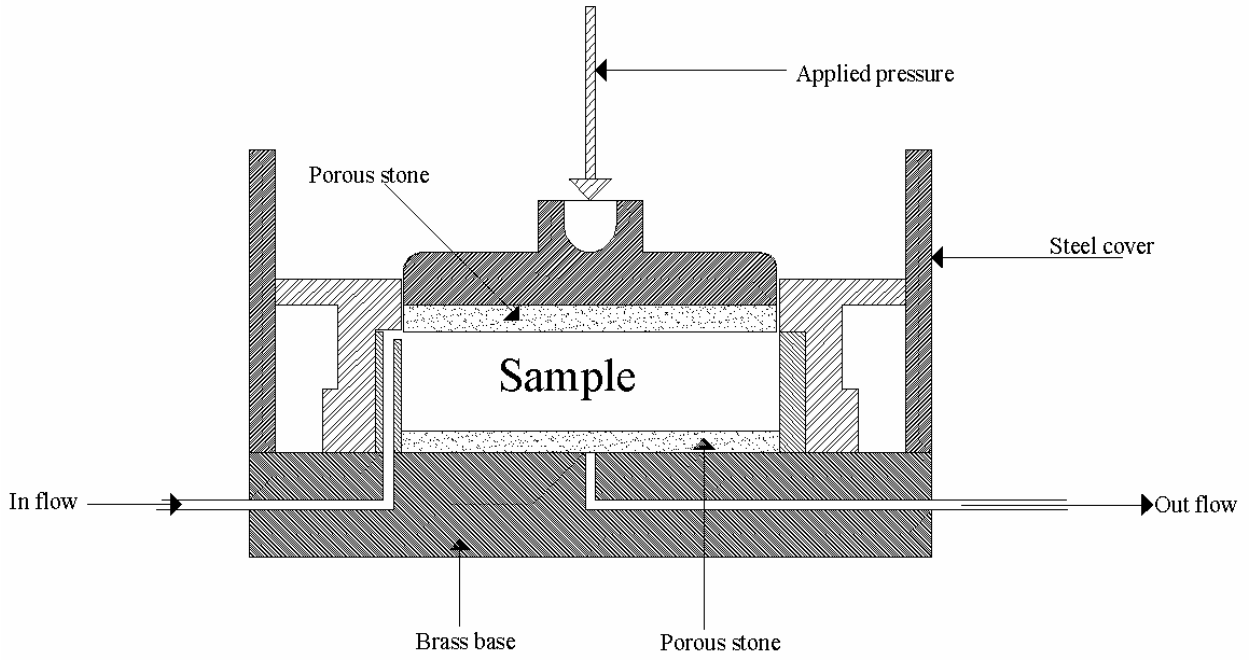

Figure 4.2 Modified oedometer

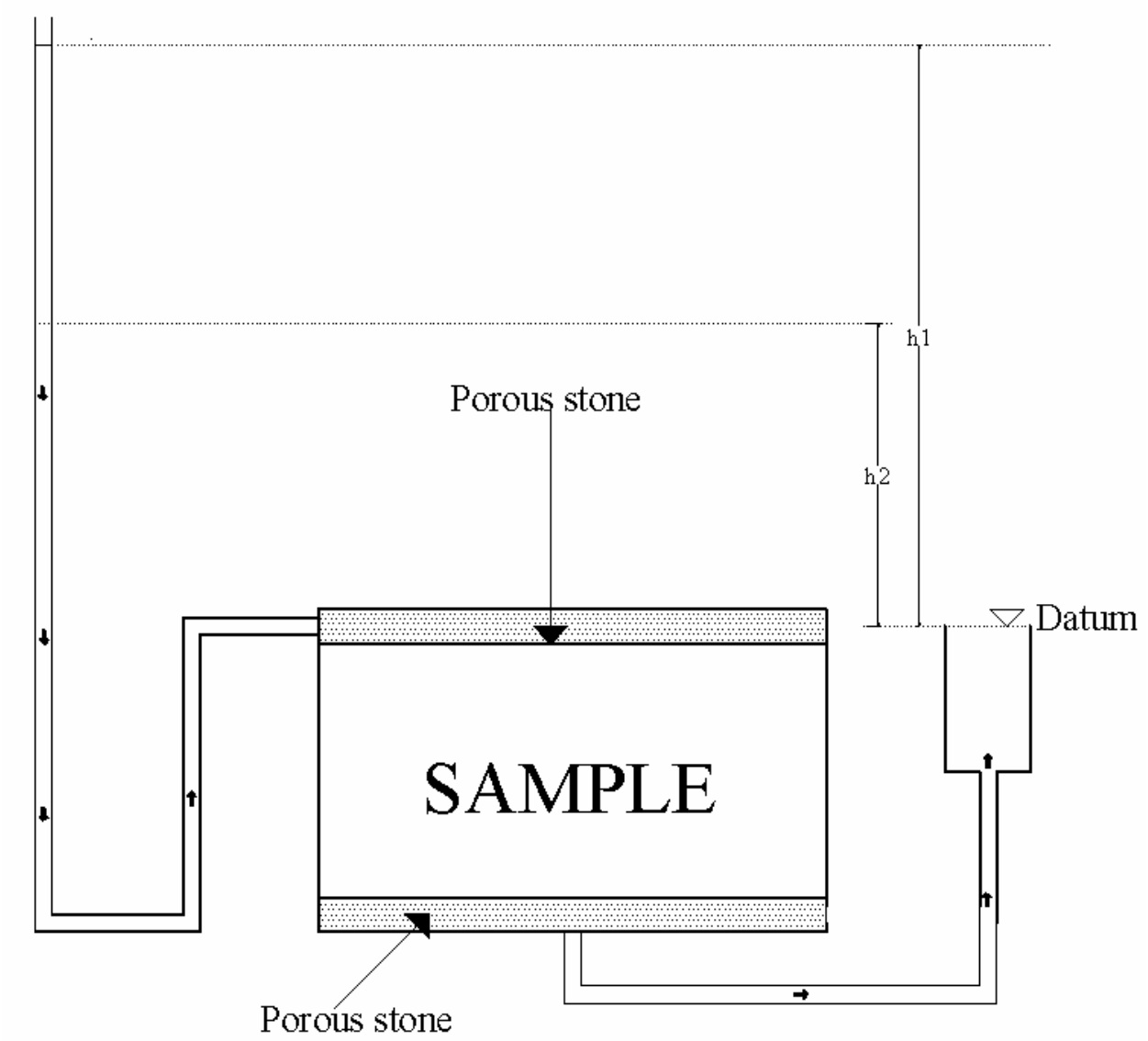

Figure 4.3 Arrangement for measurement of permeability by falling head method

4.2.2 Sample properties and sample preparation for modified oedometer test

In this study, five different samples (A1, B1, B2, C1 and C2) from three different mines (A, B, C) were used. The properties of the samples are given in Table 4.1 and Figure 4.4. The samples for measuring the permeability were prepared by making slurry of the hydraulic fills with initial moisture content of 40%. The slurries were allowed to consolidate under self-weight for different times depending on the hydraulic fill properties. Once the consolidation was complete, the sample was extruded into the oedometer ring which was then placed in the modified oedometer.

The consolidation test was performed as per Australian Standards AS 1289.6.6.1, where the void ratios were computed at the end of consolidation due to each stress increment. The permeability of hydraulic fills, at the end of consolidation due to each stress increment was measured using the falling head permeability test.

Table 4.1 Properties of hydraulic fills samples A1, B1, B2, C1, and C2

Sample*	D_{10} (μm)	D_{30} (μm)	D_{60} (μm)	C_u	C_Z	e_{max}	e_{min}	E	D_r (%)	G_s	k (mm/hr)	USCS symbols
A1	19.5	62	132	6.8	1.5	1.029	0.417	0.69	55.4	2.80	19.1	SM
B1	12	56	132	11.0	2.0	1.017	0.434	0.63	66.4	3.69	17.8	SM
B2	19	37	71	3.7	1.0	1.04	0.399	0.59	70.2	3.02	22.5	ML
C1	36	165	550	15.3	1.4	1.166	0.477	0.7	67.6	3.53	37.8	SM
C2	40.5	160	475	11.7	1.3	0.937	0.412	0.66	52.8	3.53	33.1	SM

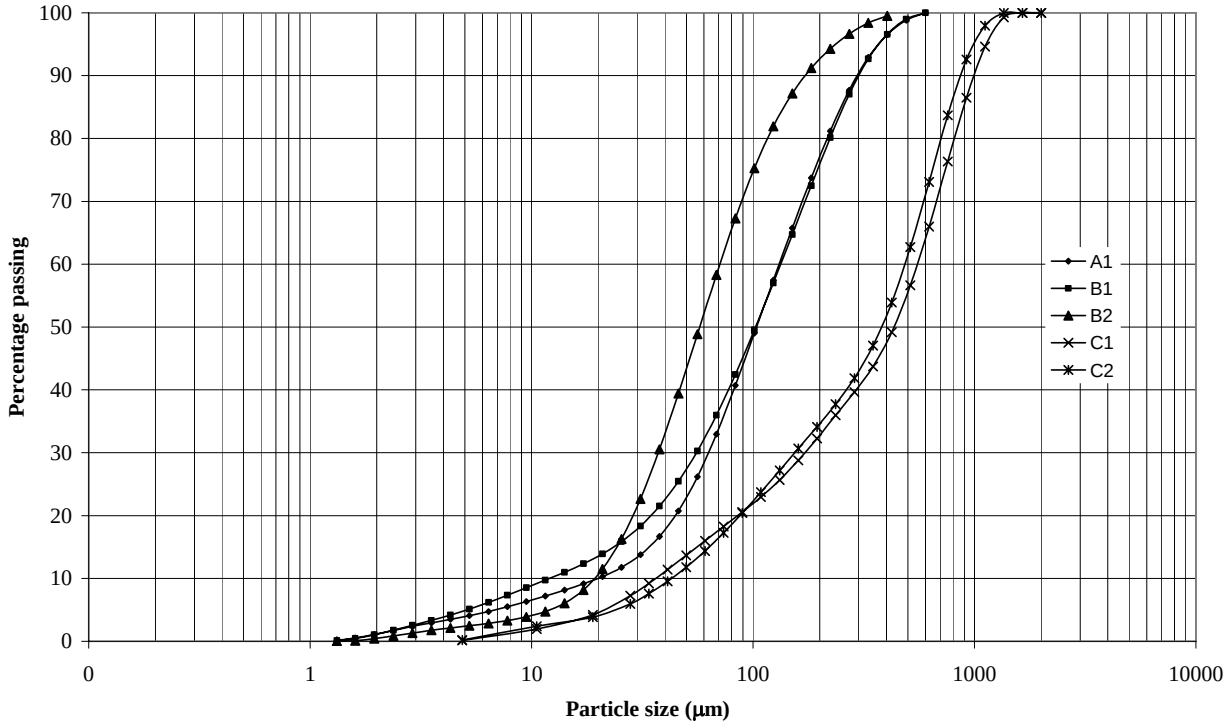

Figure 4.4 Particle size distribution curve for hydraulic fills samples for permeability test under surcharge

4.2.3 Separable ring apparatus to measure moisture content variation with depth

A separable ring apparatus, shown in Figure 4.5, was used to measure moisture content variation with depth and time in a cylindrical cell. It has 50 mm high rings on both top and bottom and 12 rings of 25 mm height and 80 mm diameter in the centre. All the rings were separable. Downward drainage was allowed from bottom ring. Drained water was collected in outer ring as shown in the figure. Two filter stones were used to retain the hydraulic fills within the rings and allow the drainage through it. Hydraulic fill was poured in the apparatus in form of slurry with initial moisture content of 40% and 35%. The hydraulic fill was allowed to drain for different time varying from 1 hr to 40 hr. Moisture content was measured for the sample in each ring. The top of the apparatus was covered to avoid any evaporation.

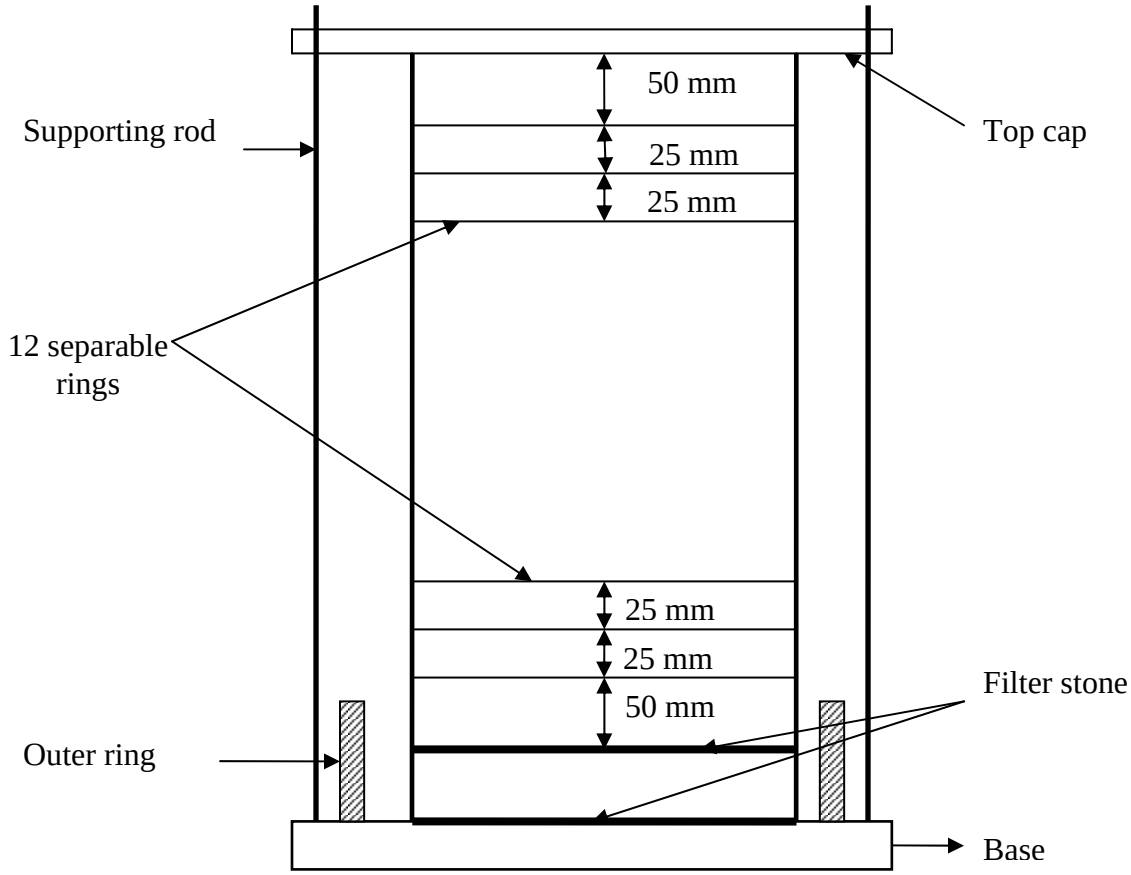

Figure 4.5 Schematic diagram of separable ring cell

4.2.4 Laboratory test to measure average moisture content variation with time

Average moisture content variation was measured using a cylindrical apparatus shown in Figure 4.6. It has a long cylinder of diameters 80 mm to 150 mm. Sideway drainage has been used to simulate the similar conditions that of a vertical mining stope. The drainage diameters varied from 10 mm to 40 mm. A porous membrane was glued inside the cylinder at drainage hole to retain hydraulic fill. This porous membrane plays a similar role that barricades play in a mine stope. A high precision balance (with accuracy of 0.01g) was used to measure the mass of apparatus and fill inside. The top of apparatus was covered to prevent the evaporation of water from the top of hydraulic fill. Drained water was collect in a flask. Hydraulic fill was poured into the cylinder in form of slurry with an initial moisture content of 40%. The mass of fill-apparatus system was measured at different times. It was assumed that any reduction the mass of fill-apparatus system is due to change in moisture content in the fill. The results of the tests are discussed later in this chapter.

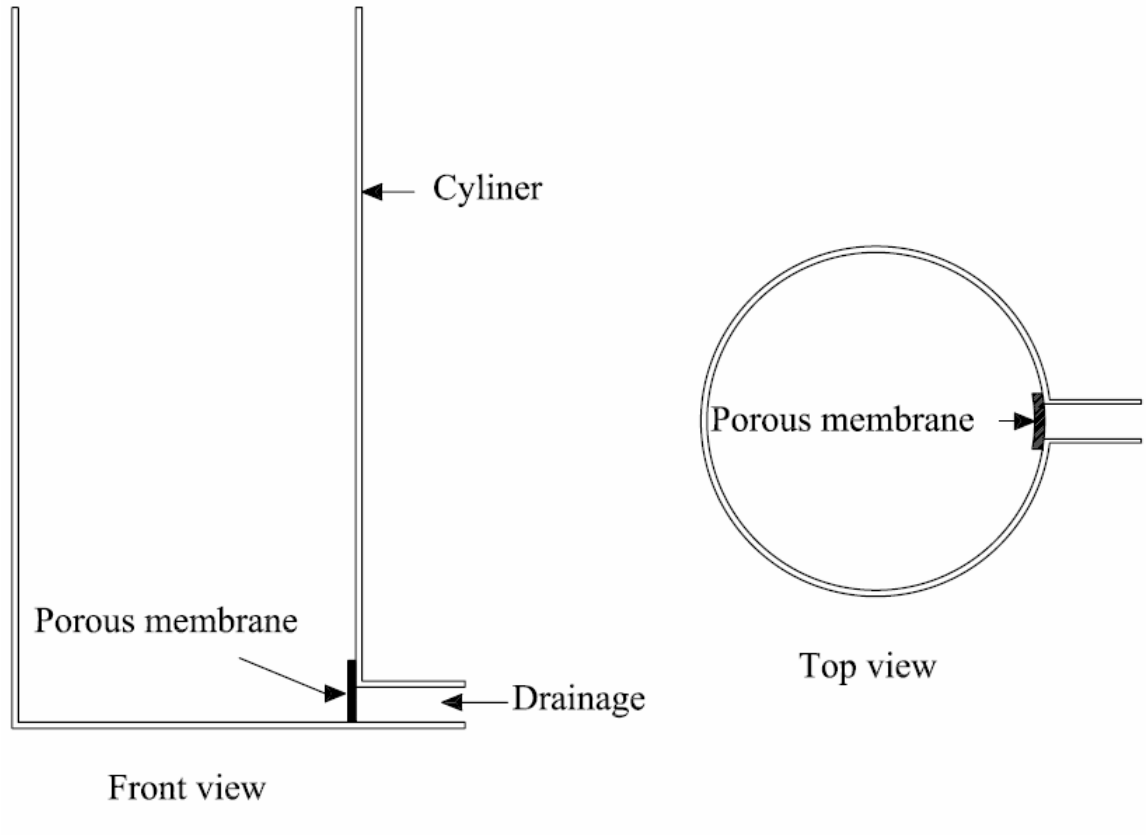

Figure 4.6 Schematic diagram of apparatus used for measuring moisture content with time

4.3 Permeability of hydraulic fill under surcharge

The permeability of hydraulic fills, at the end of consolidation due to each stress increment, was measured using the falling head permeability test on modified oedometer cell (Figure 4.2). Figure 4.7 shows the variation of void ratio with vertical effective stresses, where the vertical effective stresses are plotted on a logarithmic scale. It can be observed that there is a linear variation of void ratio for the samples as expected for self-weight settled slurry that has not experienced a preconsolidation pressure. While the effective stress is increased from 4.5 to 1600 kPa, by two orders of magnitude, there is only a slight reduction of less than 20% in the void ratio. The compression indices (C_C) of the five samples are shown in Figure 4.7. The values of C_C are in the range of 0.05-0.11, significantly less than that for clays.

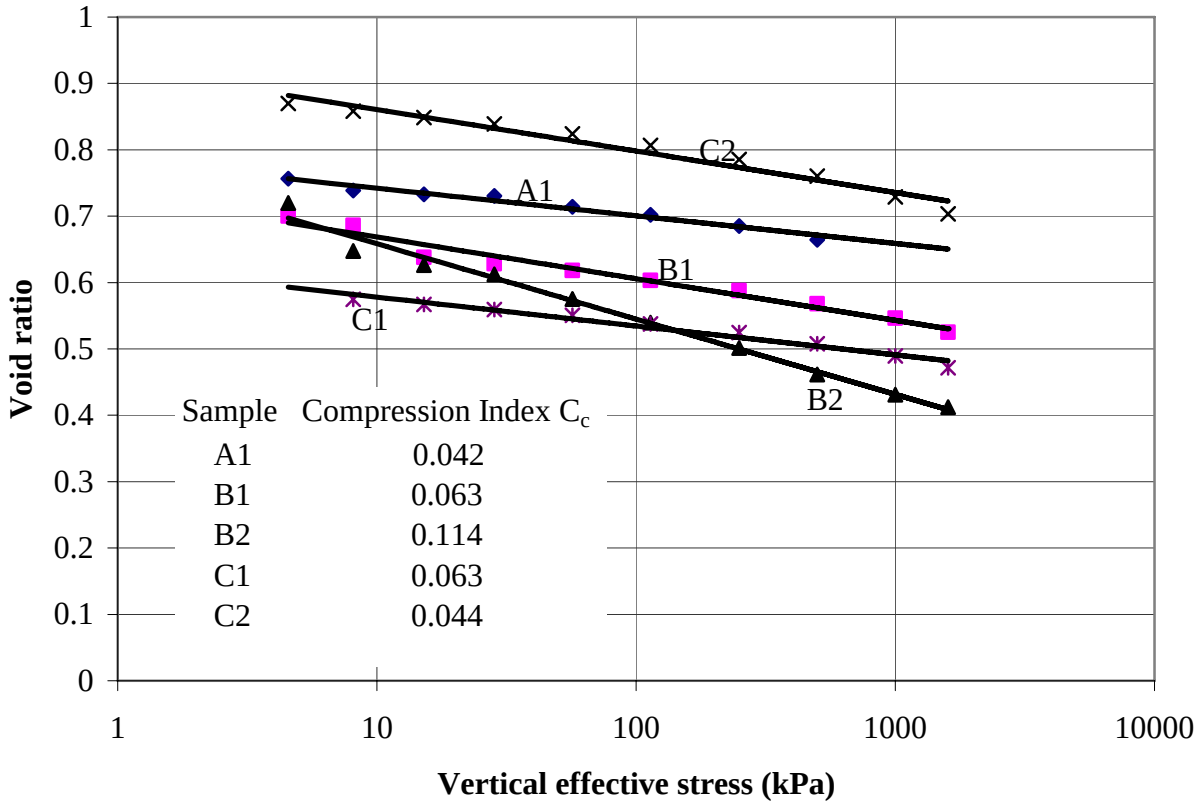

Figure 4.7 Void ratio variation with vertical effective stress

s

The plot of permeability with vertical effective stress is presented in Figure 4.8, where the vertical effective stress is shown in logarithmic scale. It can be seen that the void ratio is inversely proportional to the logarithm of vertical effective stress. The rate of decrease in permeability with effective stress is slightly more than that with the void ratio seen above. Figure 4.9 shows the variation of permeability of different type of soils with consolidation pressure (Cedergren 1967). The hydraulic fills results are also shown in Figure 4.9. It has been observed that the five hydraulic fill samples plot between fine sands and silts.

Figure 4.8 shows the permeability of hydraulic fills varies linearly with log of vertical effective stresses. Mathematically, the permeability can be expressed as:

$$k\,(\text{mm/hr}) = -a\,\log\sigma(\text{kPa}) + k_0 \qquad (4.3)$$

where a is empirical coefficients and k_0 is the permeability at surcharge of 1 kPa, which can be assumed as permeability of hydraulic fill measured in laboratory tests using falling head and constant head method. The coefficient a and k_0 obtained for different hydraulic fill samples are presented in Table 4.2. An attempt has been made to relate these empirical coefficient a and k_0 to specific gravity in Section 4.4.

Table 4.2 Empirical coefficient 'a' and 'k_0' of mine tailings

Sample	a	k_0 (mm/hr)
A1	3.417	19.1
B1	1.414	17.8
B2	2.545	22.5
C1	1.678	37.8
C2	1.584	33.1

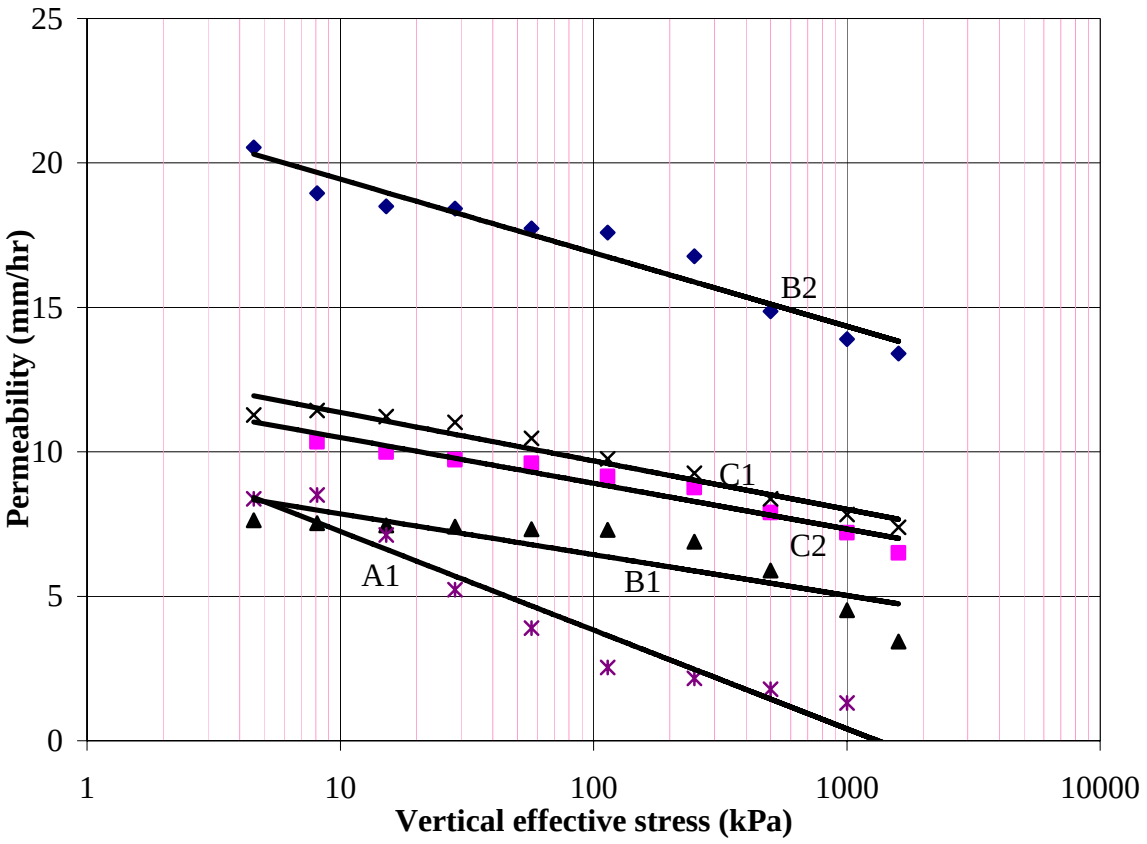

Figure 4.8 Permeability variation with vertical effective stress

In Figure 4.10, the variation of permeability of hydraulic fills with void ratio is shown where the permeability is presented on a logarithmic scale. It can be observed that the void ratio shows a linear variation with log of permeability. Qiyu and Sego (2001) observed that permeability of for hydraulic fills from mines in Canada decreases linearly with increase in void ration. Sallfors and Oberg-Hostga (2002) made similar observation for sand bentonite mixture. Lambe and Whitman (1969) showed that void ratio decreases linearly with logarithmic of permeability for a wide range of coarse and fine grained soils, as shown in Figure 4.11. Hydraulic fills results are also presented in this figure.

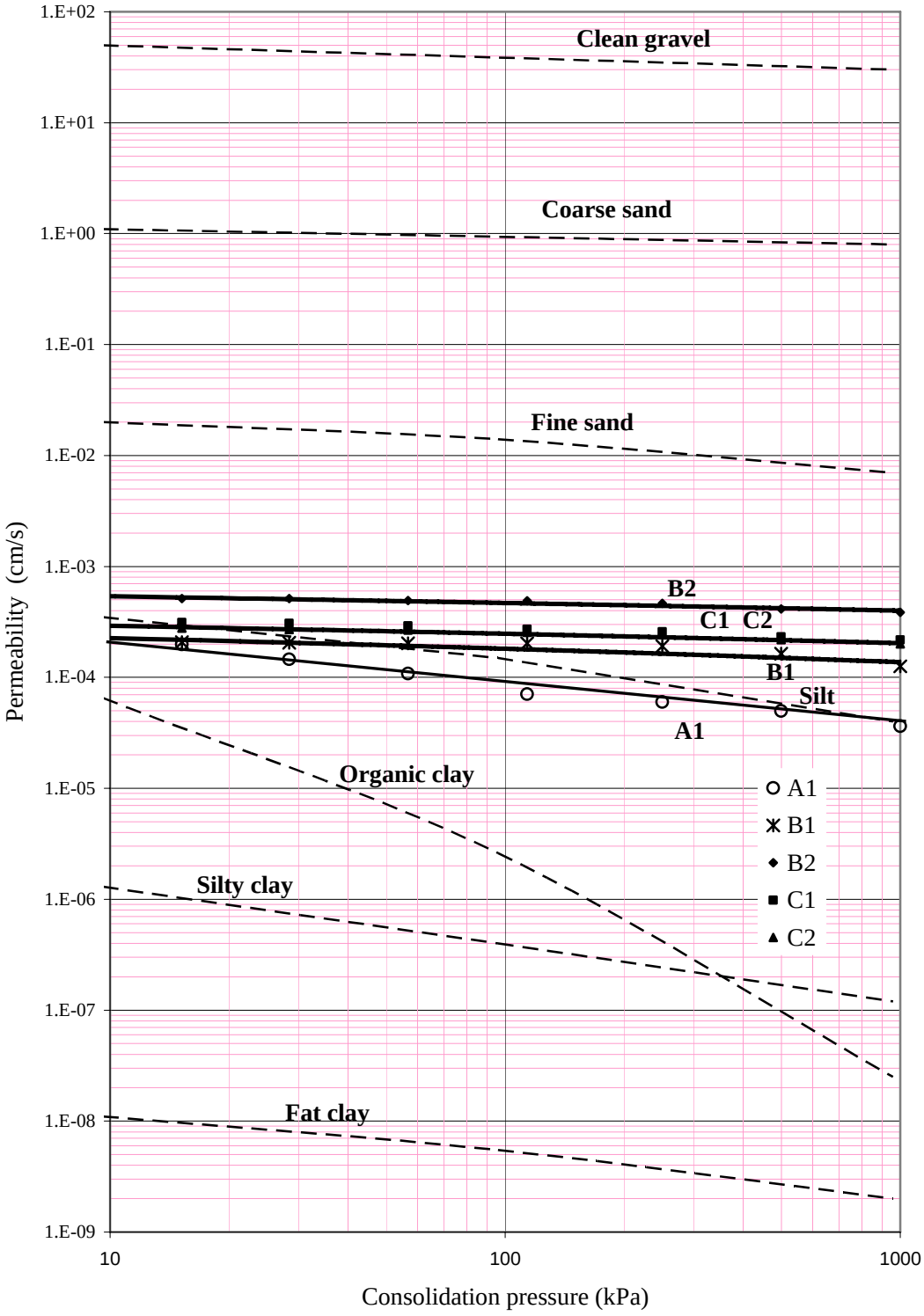

Figure 4.9 Permeability versus consolidation pressure (Adapted from Cedergen 1967)

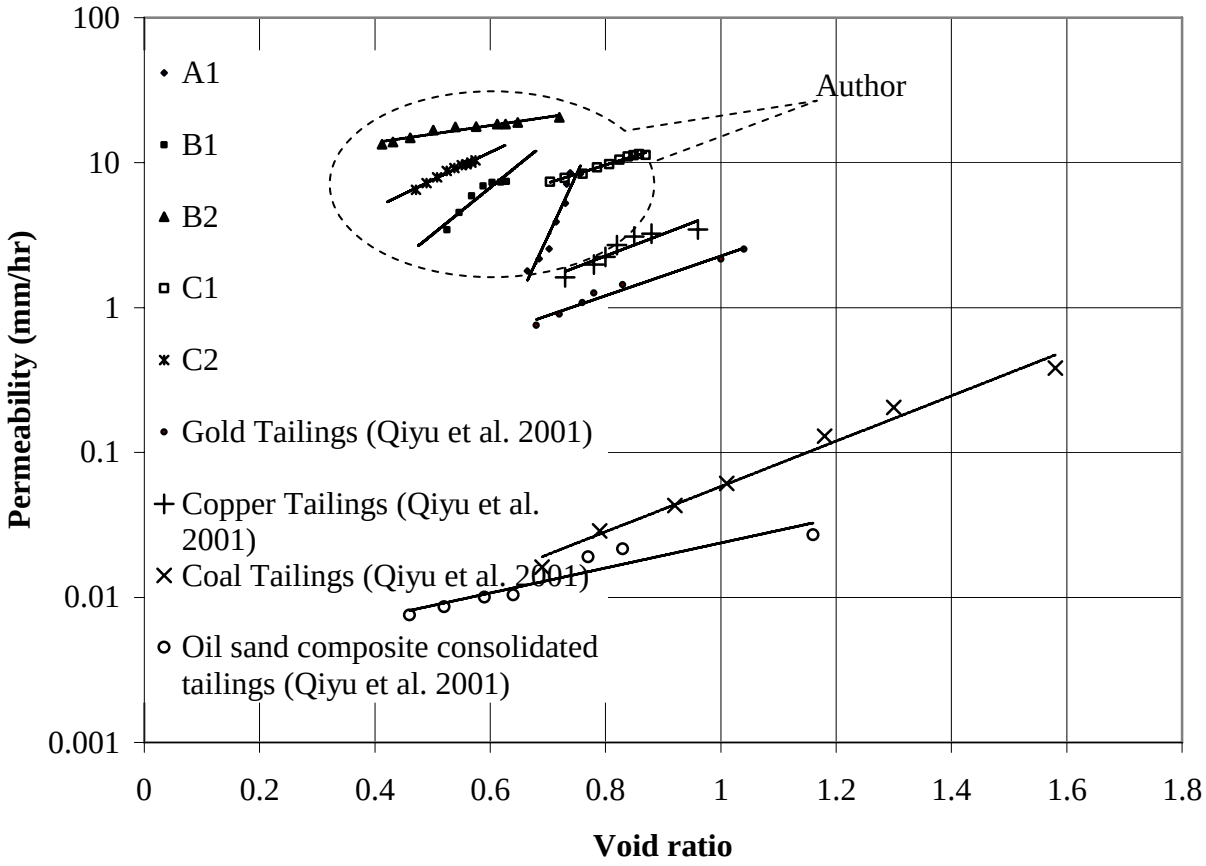

Figure 4.10 Variation of void ratio with permeability for hydraulic fills

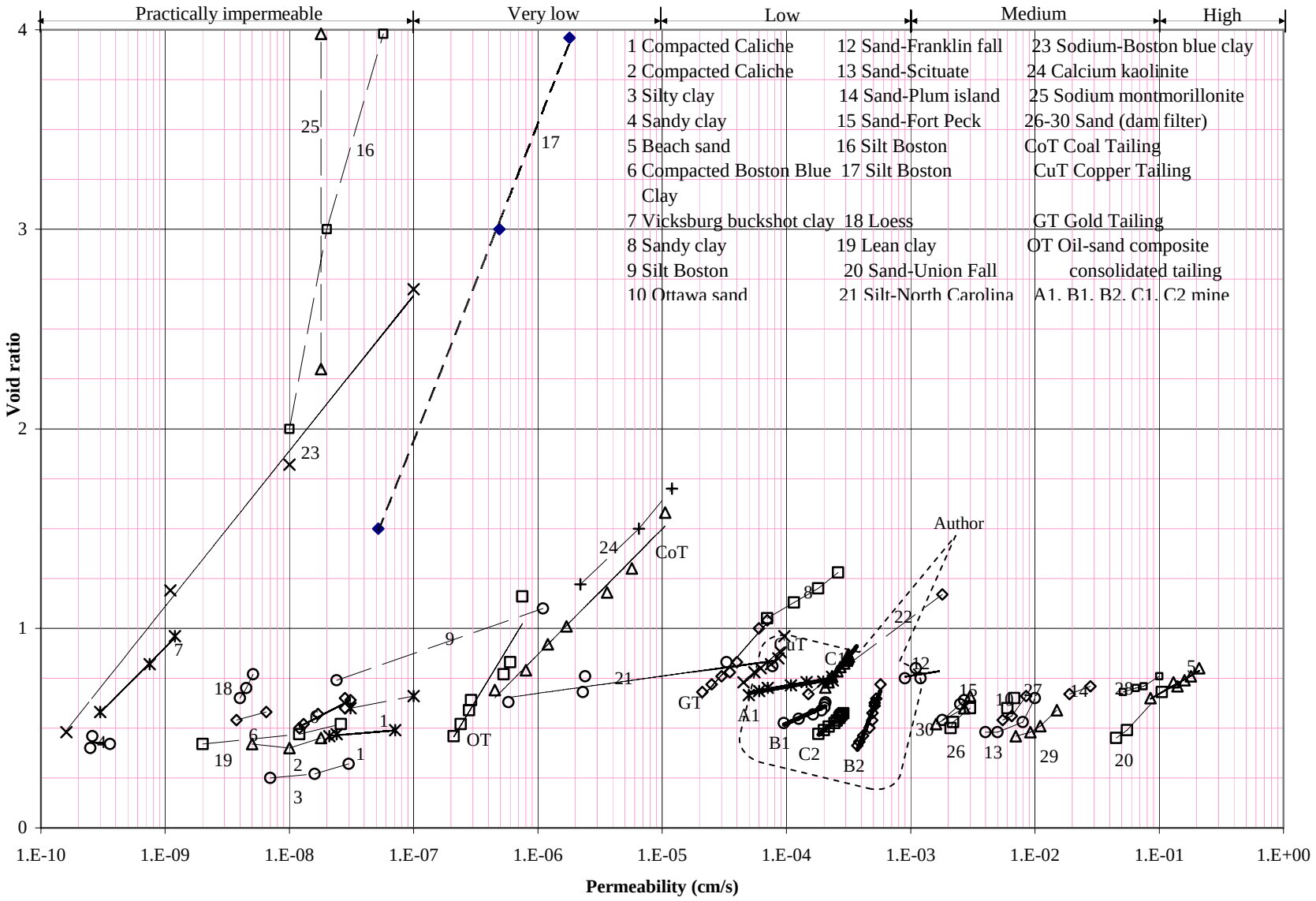

Figure 4.11 Void ratio versus permeability for different soil (Adapted from Lambe and Whitman, 1969)

4.4 Effect of specific gravity and other physical properties on permeability

The variations of 'a' and 'k_0' with Specific gravity (G_s) are shown in Figure 4.12. It is observed that the empirical coefficient 'a' is inversely proportional to the specific gravity (G_s) of the hydraulic fills. However, it is not possible to express k_0 solely as function of G_s (Figure 4.12).

The following empirical relationship is suggested for 'a' in terms of specific gravity

$$a = -2.1668\,G_s + 9.3085 \tag{4.4}$$

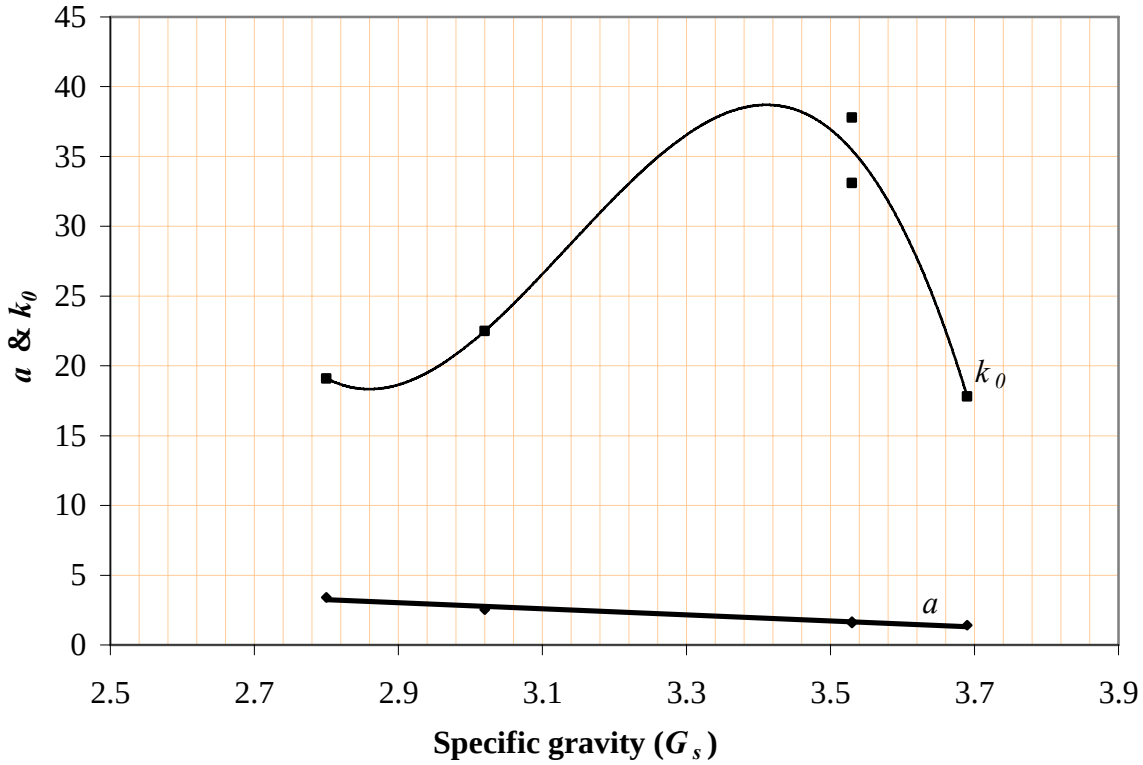

Figure 4.12 Empirical coefficients *a* and k_0

The permeability has been plotted against grain size distribution parameters such as relative density D_r, coefficient of uniformity C_u and coefficient of curvature C_Z of

hydraulic fills. A dimensionless term χ has been defined using relative density, specific gravity, coefficient of uniformity and coefficient of curvature, as following:

$$\chi = \frac{D_r C_u C_z}{G_s^5} \tag{4.5}$$

The permeability of hydraulic fills has been plotted against χ in Figure 4.13. It has been observed that the permeability varies linearly with this non-dimensional parameter χ. The test results show that permeability of hydraulic fills depends significantly on the specific gravity.

Following empirical equation has been established to estimate permeability of hydraulic fills using relative density and the particle size distribution curve of the hydraulic fills.

$$k_0(\text{mm/hr}) = -7.156\,\chi + 24.746 \tag{4.6}$$

Most of the permeability values fall in a range of ±10% of the permeability estimated using Equation 4.6. Relative density increases with decrease in void ratio in hydraulic fills, which reduces the tortuosity in the hydraulic fills and gives a lower permeability. This is in agreement with the Equation 4.6. Similarly it can be verified that increase in C_u and C_z will reduce the permeability of hydraulic fills. Increasing C_u makes the hydraulic fill well graded, with less voids and hence lower permeability. Higher values of C_z shows the presence of large number of particles of different sizes, which makes soil well graded, hence reduce permeability.

4.5 Permeability variation of hydraulic fill with moisture content

Drainage in a mine stope is a continuous process. Hydraulic fills are poured into the stopes in form of slurry with initial moisture content of 35-40%. Excess water ponds over the fill surface, as shown in Figure 3.1, then commences a vertical path of drainage due to gravity. In the absence of inflow of water in the stope, the moisture content of hydraulic

fill gradually decreases with time and hydraulic fills become unsaturated. It is too difficult to measure the change in moisture content and permeability of hydraulic fill with time and depth in a mine stope. In this dissertation, permeability variation with moisture content has been studied using soil-water characteristic curve of hydraulic fills. The details of soil-water characteristic curve have been discussed in Chapter 2. The empirical method, proposed by Arya and Paris (1981), has been used to estimate the permeability of 5 different hydraulic fill samples (A1, B1, B2, C1 and C2) that are unsaturated.

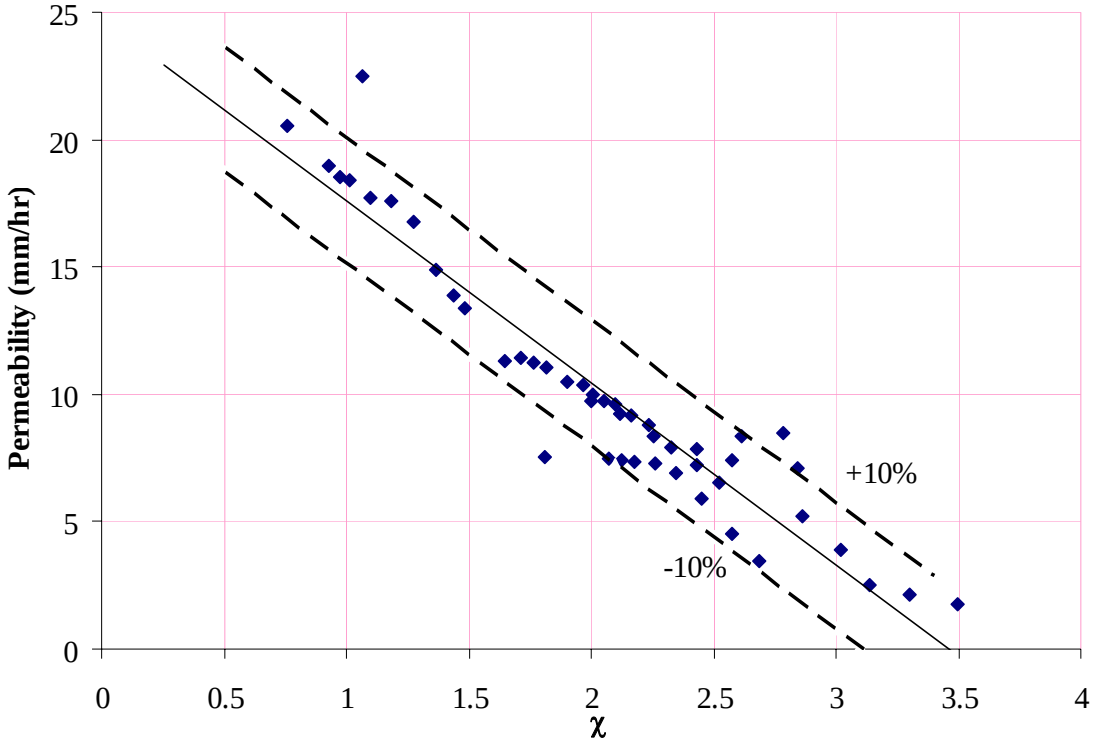

Figure 4.13 Variation of permeability with χ

4.5.1 Average moisture content variation within stope

Apparatus, discussed in Section 4.2.4, has been used to measure the average moisture content variation with time. Hydraulic fill was poured in form of slurry with initial moisture content of 35% and 40%. Apparatus was placed on a high precision balance and mass of fill-apparatus system was recorded with time. Since the top of apparatus was

covered to avoid any evaporation, the change in mass of fill-apparatus system was due to change in moisture content. The result of one of the samples is shown in Figure 4.14 for three different cylinder diameter (*D*) and drain diameter (*d*). It has been observed that there is no decant water after 120 – 150 min of drainage. In all three cases, moisture content reduces to 10% in 10 days of pouring the slurry. Similar behavior was seen for all 5 samples of hydraulic fills for cylinders of different aspect ratios. The test results for other samples are given in Appendix B.1.

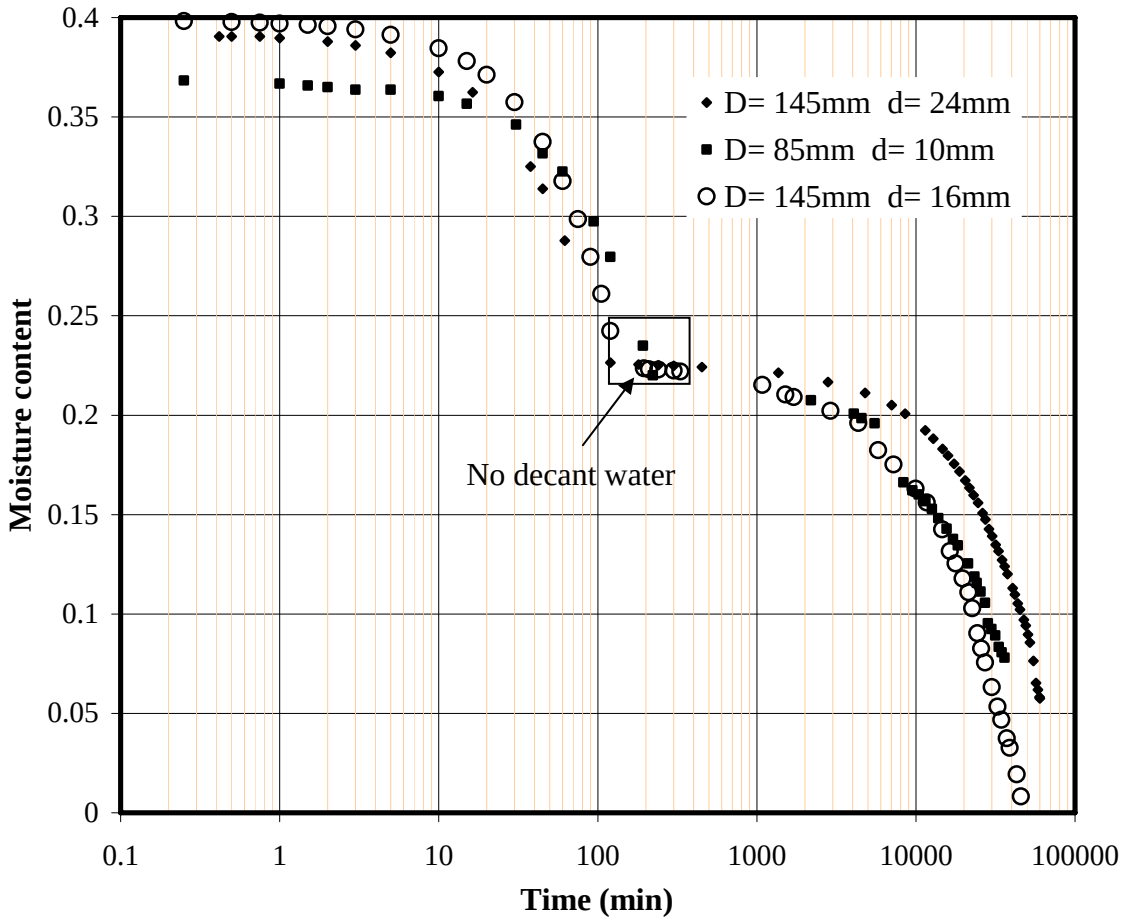

Figure 4. 14 Average moisture content variations for sample B2

4.5.2 Permeability variation with moisture content

The coefficient of permeability is significantly affected by the changes in the void ratio and moisture content of the soil. In unsaturated soils, air replaces water in larger pores,

and leaving the water to flow through smaller pores with increased tortuosity to flow path. The effect of degree of saturation of soil is more significant than the effect of void ratios on permeability. Singh et al. (2008a) and Qiyu and Sego (2001) have reported the permeability of hydraulic fills decreases with void ratio on permeability of hydraulic fills.

The permeability of soil decreases with increase in matric suction or decrease in moisture content. Several methods (Marshall, 1958; van Genuchten, 1980; Fredlund and Xing, 1994) have been proposed to estimate permeability of soil using matric suction curve. Methodology of computing permeability of unsaturated hydraulic from matric suction is explained in Appendix A.1.2. Vanapalli and Lobbezoo (2002) defined relative coefficient of permeability (k_{rel}) as ratio of unsaturated coefficient of permeability (k_{un}) and saturated coefficient of permeability (k_s). Figures 4.15 and 4.16 show the permeability variation of hydraulic fill with matric suction and moisture content of hydraulic fills respectively. Figure 4.17 shows the variation of logarithm of relative coefficient of permeability (k_{rel}) with moisture content. It has been observed that all the hydraulic fill samples follow the same trend. An empirical equation has been established to predict the relative coefficient of permeability of unsaturated hydraulic fills (Equation 4.9) in terms of degree of saturation.

Degree of saturation (S) is given by:

$$S = \frac{w}{w_s} \tag{4.7}$$

Relative coefficient of permeability (k_{rel}) is defined as:

$$k_{rel} = \frac{k_{un}}{k_s} \tag{4.8}$$

where w, w_s and k_s are moisture content, saturation moisture content and permeability of saturated hydraulic fills respectively. Saturation moisture content (w_s) of hydraulic fills varies from 22% - 27% (Chapter 2).

$$k_{rel} = 10^{-2\log S(\log S - 6)} \tag{4.9}$$

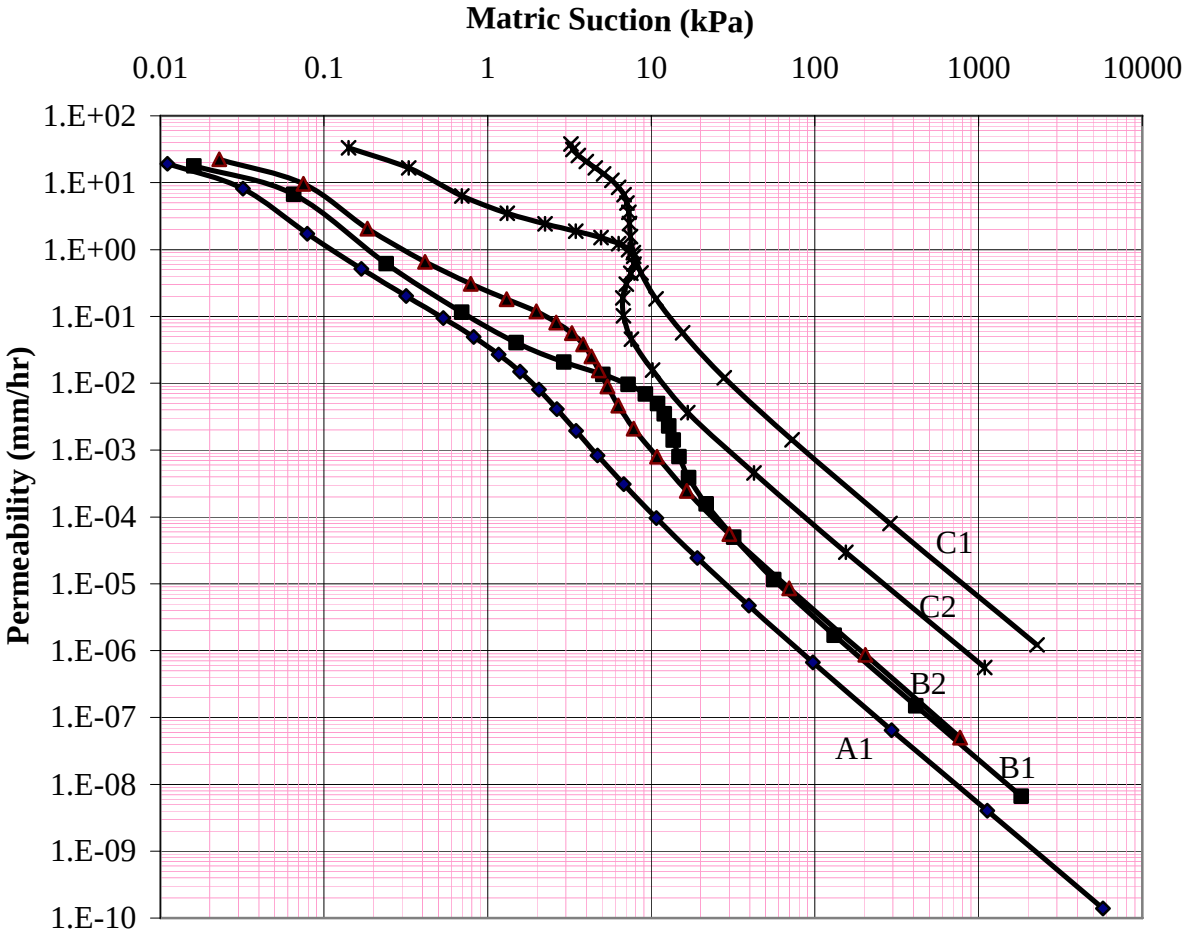

Figure 4.15 Permeability variations of hydraulic fills with matric suction

The continuous decrease in the coefficient of permeability with decrease in moisture content due to reduced degree of saturation produces a shut off of water flow. This moisture content is also known as residual moisture content. Ebrahimi et al. (2004) estimated the lower limit for permeability based on water vapour flow theory. They

suggested that the lowest value of water permeability is 3.6×10^{-8} mm/hr, regardless the type of soil. Figure 4.16, shows that the hydraulic fills will have permeability of 3.6×10^{-8} mm/hr at moisture content of 3 – 4 %. Due to lack of evaporation the minimum moisture content of the hydraulic fills within the stopes will be higher than the predicted value. Residual moisture content of hydraulic fill has been measured using vibrational apparatus (Chapter 2). Permeability of hydraulic fills at residual moisture content is 1×10^{-6} mm/hr, which is higher than 3.6×10^{-8} mm/hr.

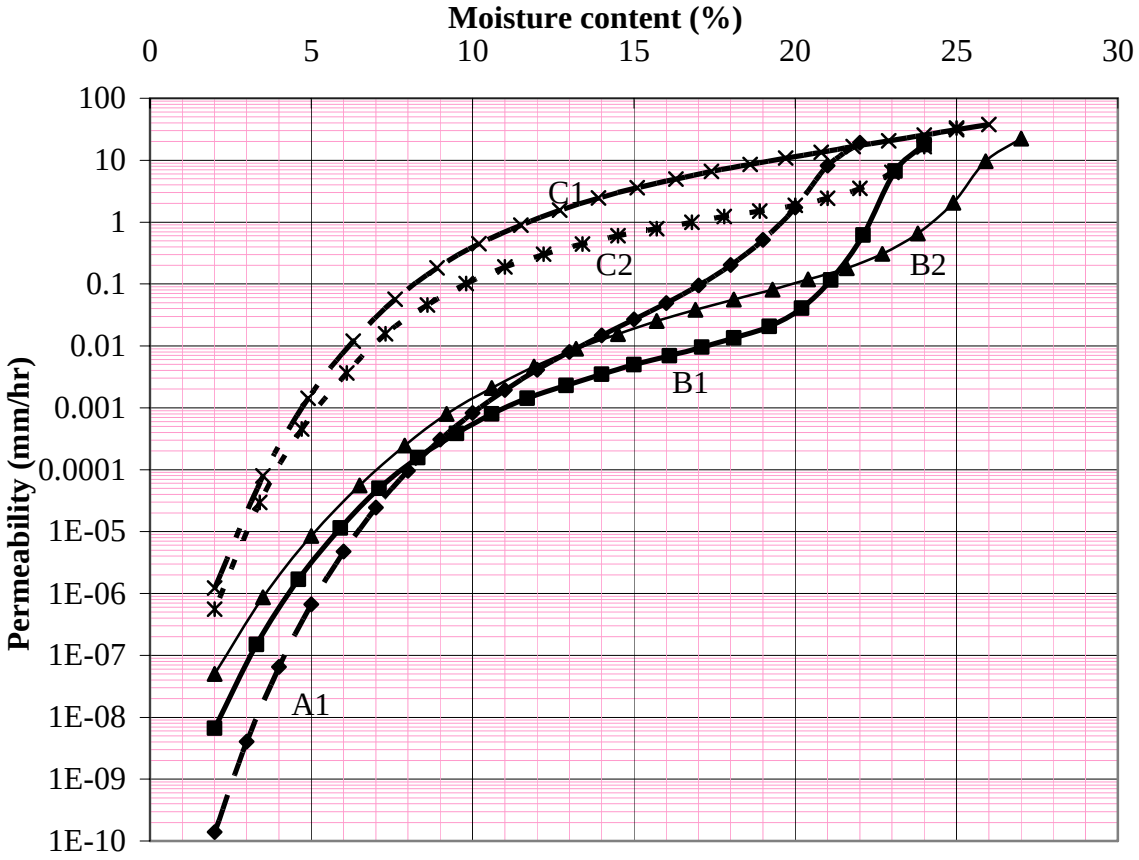

Figure 4.16 Permeability variations of hydraulic fills with moisture content

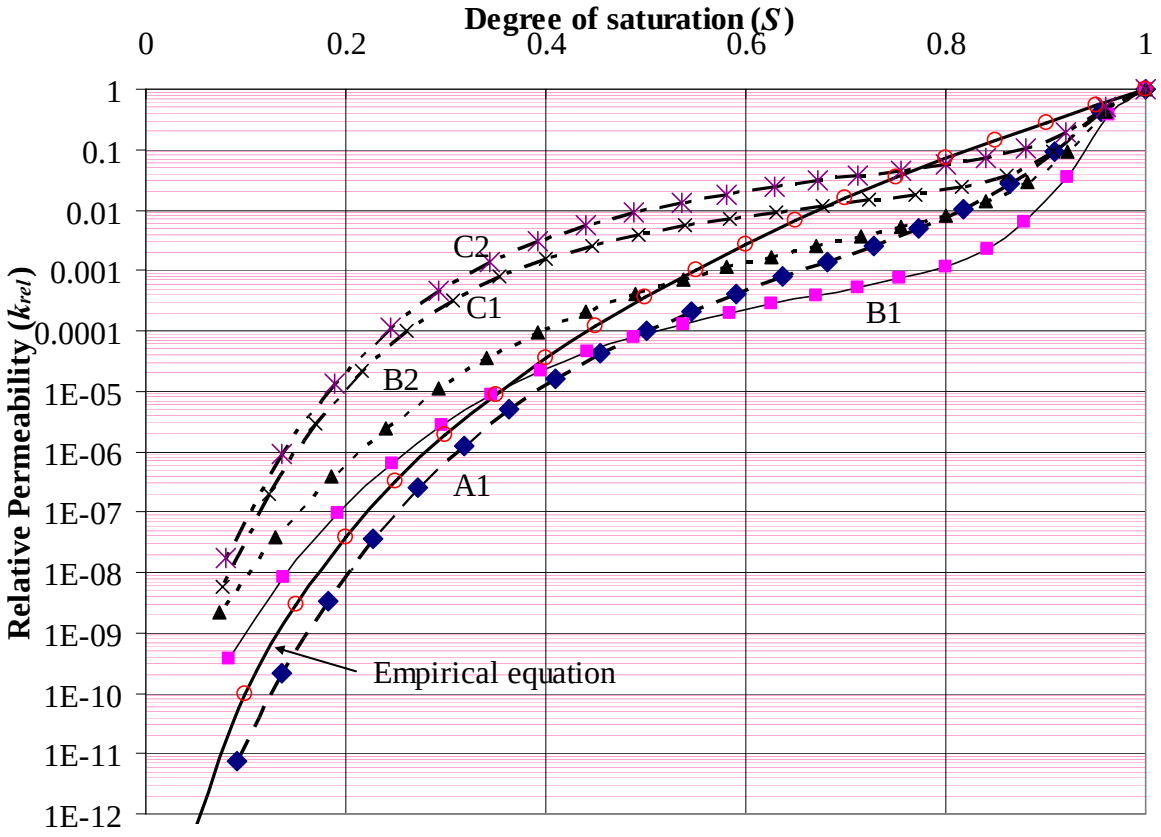

Figure 4.17 Variation of relative permeability with degree of saturation

4.6 Variation of permeability of hydraulic fill with depth in a stope

The stopes have a plan dimensions in the order of 20-60 m and heights in the order of 100- 200 m. In all previous drainage analysis, it has been assumed that moisture content, permeability and stresses within the stopes remains constant with time. These assumptions become unrealistic due to large height of stope. Stress variation with the depth of stope has been discussed in Chapter 3. In this dissertation, the moisture content variation has been studied through a series of laboratory tests for 5 different hydraulic fill samples. These tests were performed in a cylinder with separable rings. The details of the test methodology and apparatus are discussed in Section 4.2.3.

4.6.1 Stress and moisture content variation depth in stope

Hydraulic fills were poured in a cylinder with separable rings (Figure 4.5) with initial moisture content of 40%. The moisture content in each ring was measured at the end of each test. Drainage time of 4, 6, 10, 15 and 30 days were used for each sample. Height of sample was normalized in terms of height ratio. Result of sample C2 is shown in Figure 4.15. Height ratio is calculated as following:

$$Height ratio = \frac{h}{H} \tag{4.10}$$

where h is height of the center of the ring from the base of first ring and H is total height of the hydraulic fill.

Moisture content was measured at the center of each ring and it was assumed that it remains constant in that ring. Moisture content variation has been plotted against the height ratio (Figure 4.18). It has been observed that the moisture content remains almost constant from H/4 to 3H/4 in the apparatus for all the sample heights. The results of test are given in Appendix B.2. The moisture content in the apparatus remains decreases from saturation moisture content to residual moisture content. The moisture content near the barricades is always higher than the moisture content at the center. Permeability variation of the hydraulic fills has been computed assuming constant moisture content from 1/4 to 3/4 of the height of the stope.

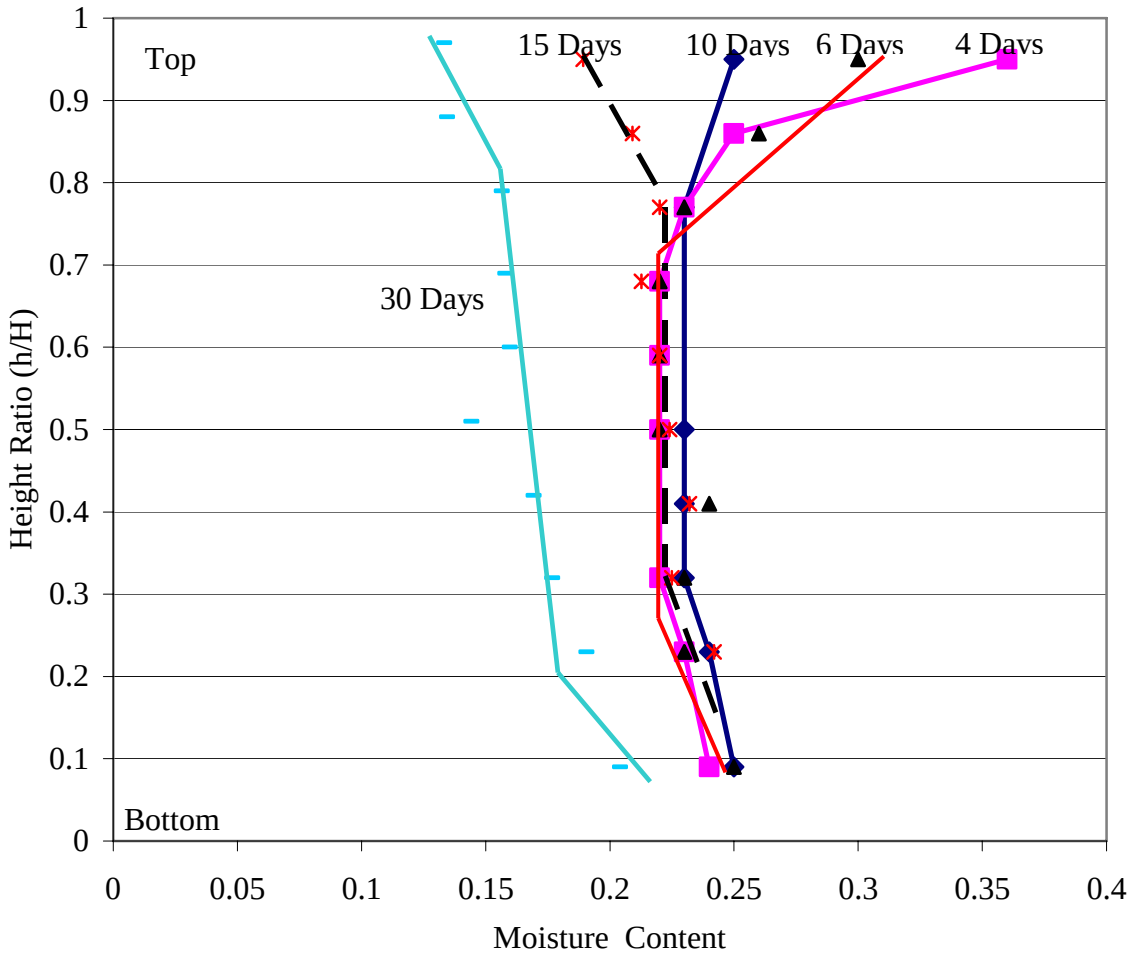

Figure 4.18 Moisture content variations with height ratio for sample B2 at end of 4, 6, 10, 15 and 30 days.

4.6.2 Permeability variation with depth

In all the previous analyses of drainage from a mine stope, a constant value of permeability has been used to simplify the analysis (Isaacs and Carter 1983; Traves and Isaacs 1991; Rankine et al. 2003; Sivakugan et al. 2006; Sivakugan and Rankine 2006). It has been observed that the permeability can be expressed as a logarithmic function of vertical effective stress in a mine stope (Singh et al. 2008). It was discussed in Chapter 3 that the vertical effective stress reduces to approximately 30% of the overburden pressure at depth of 5*B* in both vertical and inclined stope due to arching. Since the permeability of hydraulic fills is a logarithmic function of vertical effective stress, it change rapidly

with depth in a stope. Equations 3.33 and 4.3 have been used to compute the permeability variation for all five samples (A1, B1, B2, C1 and C2).

Variation of k/k_0 has been shown in Figure 4.19 for saturated hydraulic fill sample A1 for a vertical mine stope, where k is the permeability of saturated hydraulic fill at any depth for stope width of 10, 20, 30, 40 and 50 m. Results of other sample (B1, B2, C1 and C2) are shown in Appendix B.3. It has been observed that the permeability of a hydraulic fill changes rapidly to depth of $2B$ and then the variation is very slow with depth. It has been concluded that permeability can be assumed to be constant after depth of $2B$ in a vertical mine stope.

Similar analysis has been done to estimate the permeability variation of hydraulic fill in an inclined mine stope. k/k_0 variation for sample A1with depth is shown in Figure 4.20 for stope width of 20 m in an inclined stope. The variation has been shown for stope inclination (α) of 70^0, 75^0, 80^0, 85^0 and 90^0 with horizontal. The results for other samples (B1, B2, C1 and C2) are given in Appendix B.3. It has been observed that there is no significant change in permeability of hydraulic fill in an inclined stope with inclination of 80^0 to the horizontal compared to a vertical stope. It has been observed that permeability increases very slightly after inclination of 80^0 with horizontal in a mine stope. A significant change in the permeability has been observed for angle of inclination of 70^0, 75^0 and 80^0 (Figure 4.20). Sagawa and Yamotami (2003) reported that the stope can inclined up to 70^0 from horizontal. In this dissertation the permeability variation has been studied up to inclination of 70^0. It has been concluded that the there no significant effect of inclination on the permeability of hydraulic fills (Figure 4.20) for inclination up to 80^0 from horizontal.

It has been assumed that hydraulic fills are saturated in the process of estimating permeability of hydraulic fills in the vertical and horizontal stopes. Due to continuous drainage of water from stope, the hydraulic fills become partially saturated. Laboratory tests have been conducted to measure the average moisture variation from a stope (Section 4.2.3, 4.2.4, 4.5.1 and 4.6.1). It has been observed that the moisture content in

the stope remains almost constant from height ratio of 1/3 to 0.75. It increases at the bottom of the stope and decreases on the top of stope after a long time.

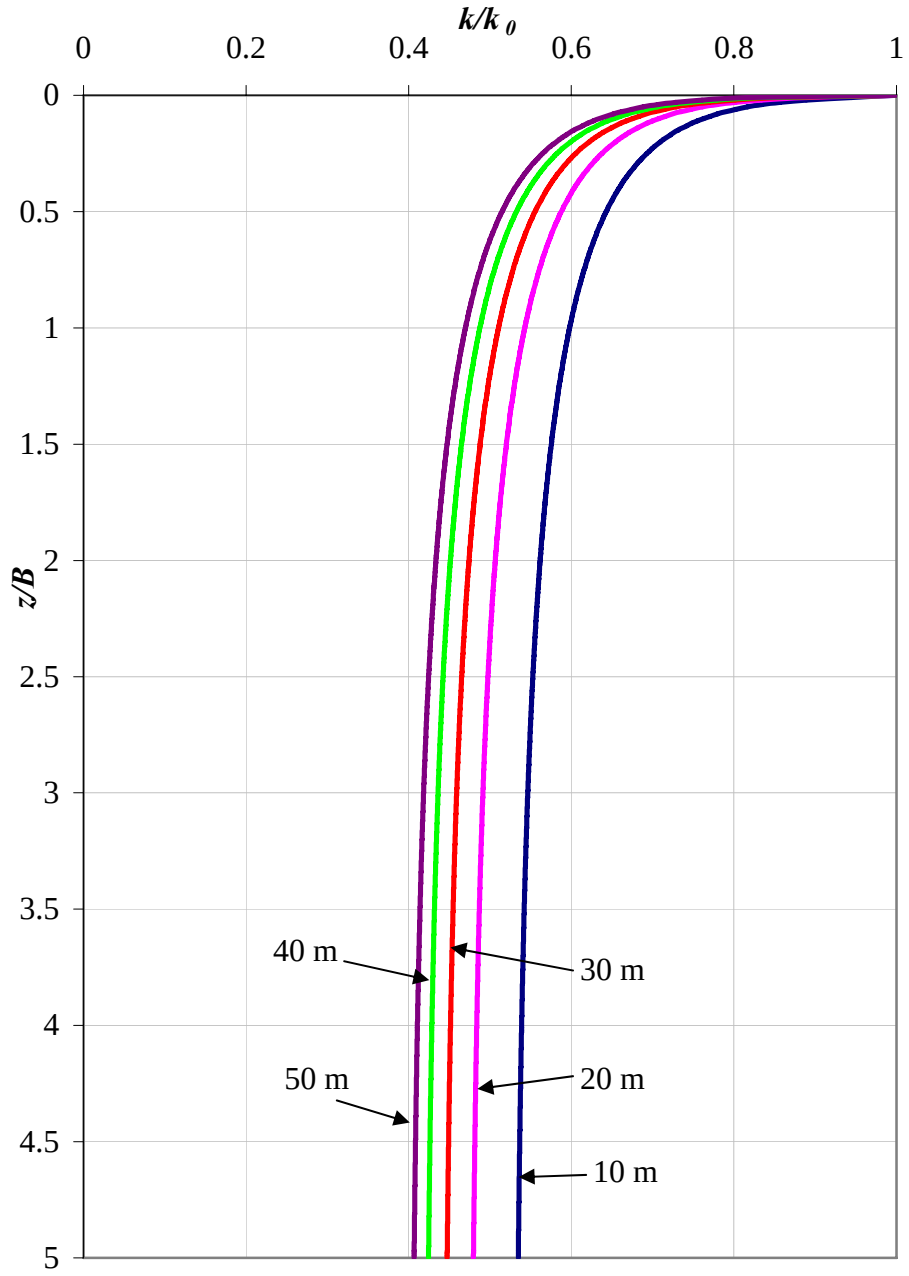

Figure 4.19 Permeability variation of saturated hydraulic fill sample A1 with depth for stope width (*B*) of 10, 20, 30, 40 and 50 m.

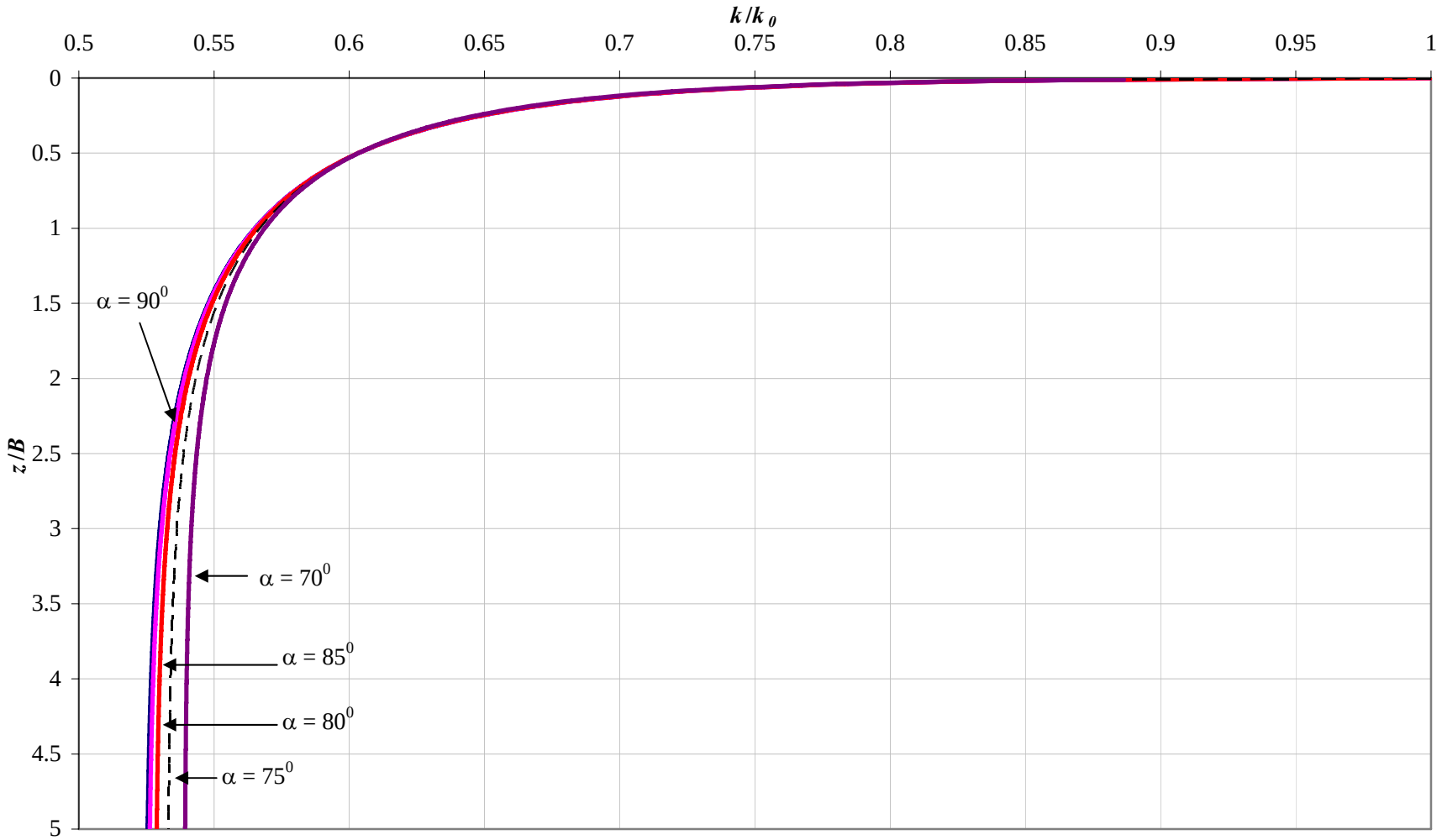

Figure 4.20 Permeability variation of saturated hydraulic fills sample A1 with depth for stope width (*B*) of 20m in stope of inclination (α) of 70^0,75^0, 80^0, 85^0 and 90^0 with horizontal.

Saturation moisture content and residual moisture content have been measured using soil-water characteristic curves and laboratory tests (Chapter 2). It has been observed that saturation moisture content of hydraulic fill varies from 22% to 27% and residual moisture content varies from 12% to 14%. Since mine stopes are not exposed to the atmosphere. It is realistic to assume that the evaporation is negligible. As shown in Figure 4.21 that moisture content is almost constant in model stope after 30 days, moisture content is constant through out the stope after a long time and is equal to residual moisture content. At residual moisture the permeability decreases by 8.5×10^{-5} times the permeability at saturation. Permeability variation of hydraulic fill has been estimated by considering the reduction in the stresses and change in moisture content along the depth of stope (Figure 4.21).

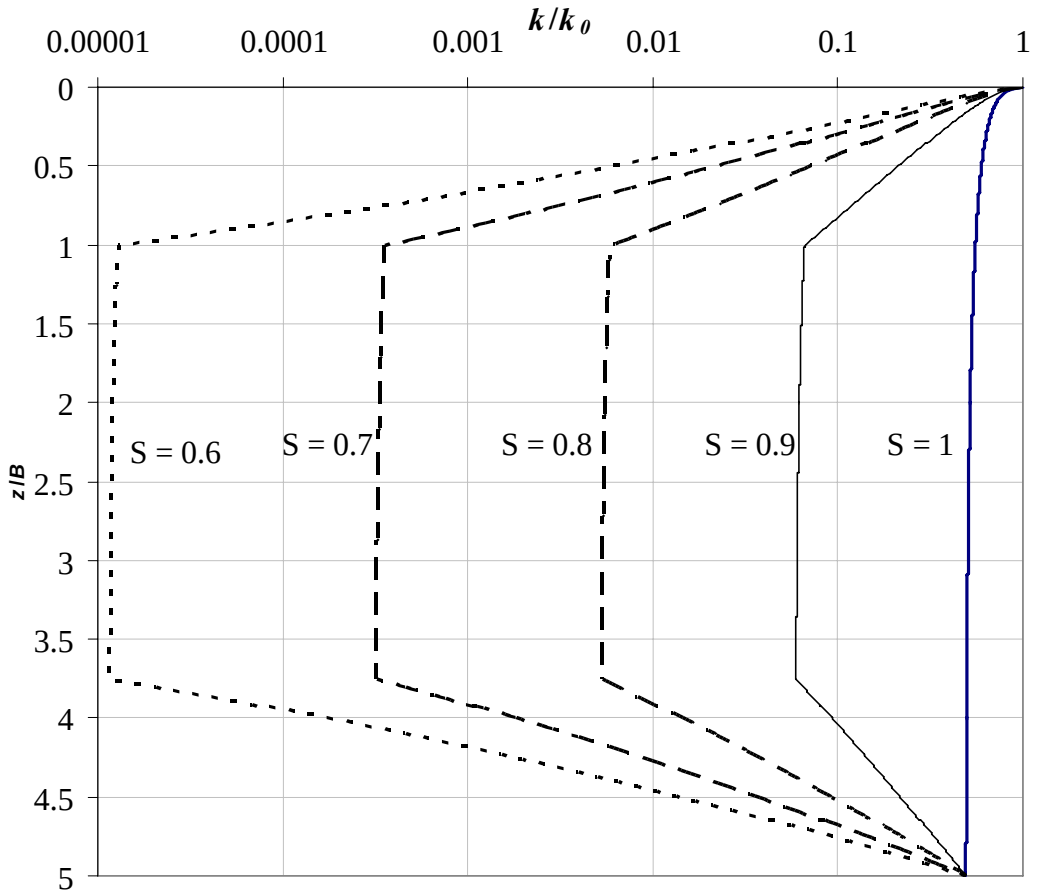

Figure 4.21 Permeability variations with depth of stope for stope width of 20 m and degree of saturation of 0.6, 0.7, 0.8, 0.9 and 1.0

In Figure 4.21, permeability has been calculated for degree of saturation of 0.6, 0.7, 0.8, 0.9 and 1.0 for stope width B = 20 m and stope height of 100 m by estimating permeability of saturated hydraulic fill and multiplying it by relative permeability as shown in Figure 4.17. Drainage and time required to achieve desired degree of saturation has been discussed in Chapter 6 using concept of equivalent permeability and method of fragments. It has been observed that the permeability reduces by 100000 times at degree of saturation of 0.6, which is very low in comparison to the value of saturated hydraulic fills.

The concept of equivalent permeability has been used to estimate the drainage from mine stope (Chapter 6) using the permeability variation discussed in this chapter. Cutoff permeability will help in determining the cutoff time of water (fluid) flow from the stope.

4.7 Summary and Conclusions

Most of the permeability of the hydraulic fills reported in the literature are not subjected to any surcharge. In reality, hydraulic fills are under several meter of overburden pressure therefore it is important to study the permeability of hydraulic fills under surcharge for design of drainage from mine stopes. Continuous drainage of water from mine stopes makes hydraulic fill unsaturated, which reduces the permeability of hydraulic fill. Soil-water characteristic curves have been used to study the permeability variation with moisture content (Chapter 2) especially when fill gets unsaturated.

In this chapter, a methodology for studying the permeability of hydraulic fills at different overburden pressures has been established. A modified oedometer has been used to determine the permeability of the hydraulic fills by falling head method after the sample has been consolidated at each stress increment. The variation of permeability with effective overburden pressure and void ratio is studied. Based on this study, the permeability of the mine tailing can be estimated using the empirical equations suggested. Permeability was related to the vertical effective stress through k (mm/hr) = - a log σ (kPa) + k_0, where is a is found to depend on the specific gravity of hydraulic fills and k_0 is

the permeability of hydraulic measured in laboratory using falling head or constant head method. An equation has been established to compute k_0 as a function of relative density, specific gravity and the particle size distribution characteristics of the hydraulic fills (Equation 4.6). This equation can be used to estimate the permeability of hydraulic fills under any surcharge loading.

Laboratory tests have been conducted to measure the average moisture content variation for hydraulic fill with time and moisture content variation with time and depth in a cylindrical and removal ring apparatus respectively. It has been observed that the moisture content in a stope remains constant from 1/3 of height to 3/4 of height of stope. The permeability of hydraulic fills has been computed using the vertical normal stress distribution in a stope. Arching effect has been considered in calculating the stress the variation. Permeability of hydraulic fill has been shown graphically for a mine stope, by considering continuous drainage from the stope for degree of saturation of 0.6, 0.7, 0.8 and 1.0. It has been observed that permeability reduced by 100000 (Sample A1) at center of stope for degree of saturation of 0.6, whereas permeability of saturated hydraulic fill without any surcharge in 19.1 mm/hr (Sample A1). Permeability and moisture content variation with depth of stope for all five samples are shown graphically in Appendix B. This permeability variation will be used to estimate drainage from mine stope using concept of equivalent permeability and method of fragments (Chapter 6).

Chapter 5

Time Dependent Settlement in Hydraulic Fills

5.1 General

Backfill is an increasingly important component of underground mining around the world. Different types of backfills are used on the basis of requirement and availability at mines. Hydraulic fill and paste fill are two most popular backfill types used world wide. Unlike the hydraulic fills, paste fills contain substantial fines and small percentage of binder which is mostly ordinary Portland cement. The maximum grain size in a paste fill is 300-400 μm and it is generally required that at least 15% of the grains are smaller than 20 μm. The drainage is one of the main concerns in the hydraulic fills which are uncemented classified tailings with not more than 10% by weight of size less than 10 μm, but is never a concern in paste fill. The excess water is absorbed by the fines and also used in the hydration process in paste fills.

The hydraulic fill settles within the stopes under its self-weight. The barricades made of free draining porous bricks, are used to block the horizontal access drives and thus retain the fill and prevent it from entering the drives (Figure 3.1). The free water is allowed to drain through the fill and the barricades into the empty drives. Rankine et al. (2006) and Sivakugan et al. (2006) measured the permeability of the barricade bricks and showed that it is 2-3 orders of magnitude greater than the permeability of hydraulic fills, implying that the barricades can be assumed to be free draining.

The grain size distribution of hydraulic fills of Australian mines fall within the shaded narrow band shown in Figure 2.4. In the Unified Soil Classification System (USCS), the hydraulic fills would be classified as silty sands (SM) or sandy silts (ML) with no plasticity. The mineralogy of the mine tailings is such they have quite high values of specific gravities from 2.80 to 4.50 (Table 2.1 and 4.1). This is significantly higher than the range of 2.60-2.80 reported for inorganic soils including sands, silts and clays. Rankine et al. (2006) and Sivakugan et al. (2005, 2006) discussed the geotechnical characteristics of typical hydraulic fills.

Paterson (2004) observed that solid and liquid phases of relatively fine materials may not separate during sedimentation until a long period in a quiescent state has passed. Similar behavior has been observed for the several hydraulic fills studied at JCU laboratory that are discussed in this paper.

5.2 Review of consolidation and secondary compression

When a soil mass is subjected to compressive stresses, it can undergo volumetric strains. Assuming the soil grains and water to be incompressible, the volumetric strains are primarily due to the expulsion of water and/or air from the voids. Lade and Liu (1998) suggested that any increase of stresses acting on a virgin soil element produces recoverable elastic deformation, non-recoverable plastic deformation and time dependent inelastic creep deformation.

The compression or settlement of soil can be divided into immediate settlement, consolidation settlement and secondary consolidation settlement. Immediate settlement, also known as distortion settlement or elastic settlement, occurs instantaneously on the application of the load, and is caused by the elastic deformation of soil under undrained conditions. The consolidation settlement, sometimes known as primary consolidation settlement to distinguish from the secondary compression, takes place due to the consolidation of the soil and is a time-dependent process. The secondary consolidation

settlement, also known as creep settlement, takes place under constant effective stress due to realignment of the soil grains.

Terzaghi (1941) and Taylor (1942) proposed a general hypothesis describing the continuous process of primary and secondary consolidation of clays. As per the hypothesis, primary and secondary consolidations are parts of a single continuous process. During primary consolidation of clay, the total stress is shared by the free pore water, highly viscous adsorbed double layer (film bond) and the grain bond in the form of solid-solid contact between clay particles. During secondary compression, the pore water pressure is negligible, and therefore the total stress is shared by the film and the grain bonds (Barden, 1968). Shen et al. (1973) and Lambe and Whitman (1969) observed a small excess pore water pressure within the soil even after the completion of primary consolidation. The secondary consolidation or creep effect is the gradual readjustment of soil skeleton following the disruption caused during primary consolidation. The rate of secondary compression is strongly influenced by viscous effect of the adsorbed double layers of the clay particles.

In the case of sands, due to their higher permeability, the primary consolidation process is almost immediate and any applied total stress in transferred to the soil skeleton almost instantaneously in the form of effective stress. Lade and Liu (1998) observed inelastic time dependent creep deformation in the sand immediately after stress changes and suggested that slippage between the grains and fracture of the particles as possible reasons for creep in the sand. Figure 5.1 shows the typical settlement variations for sands, silty sands and clays as seen in oedometer tests.

As seen in Figure 5.1, generally, the ratio of immediate settlement to total settlement is high in case of sands. The clays and silty-sands follow the typical ‘S’ curve on logarithmic time scale. Settlement curves for clays and silty sand have well-defined immediate, primary consolidation and creep components whereas sands have immediate and creep components only.

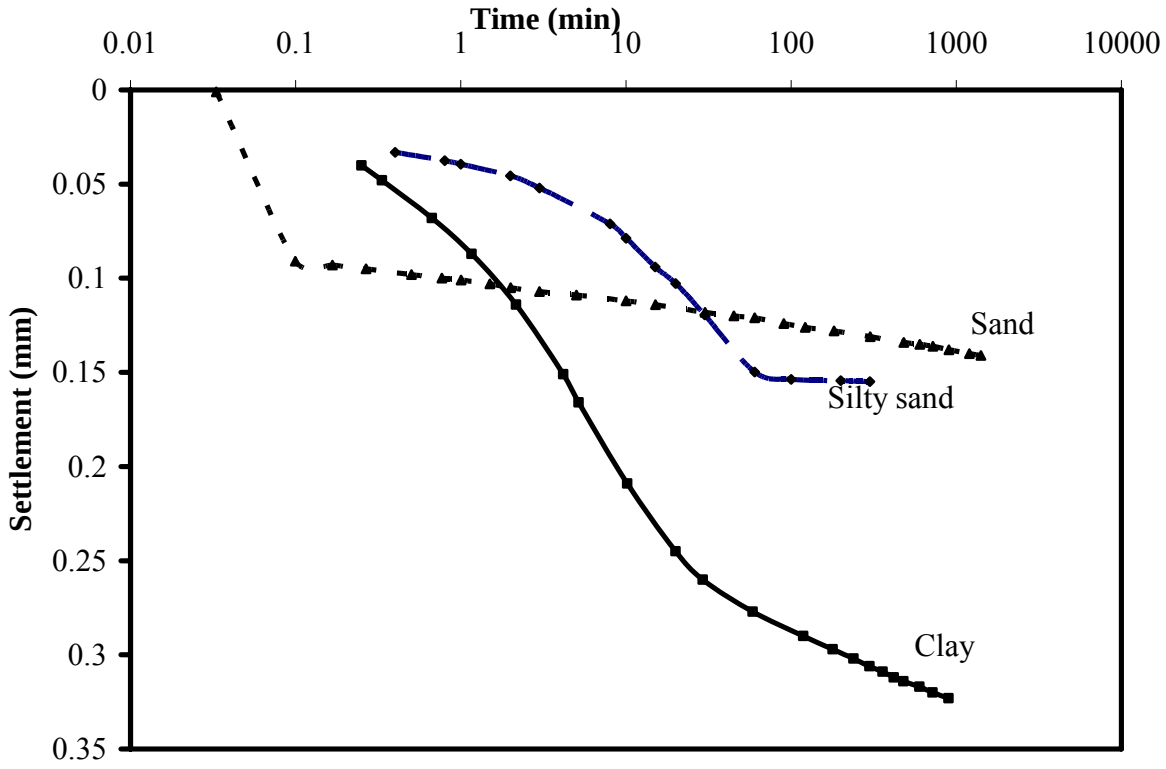

Figure 5.1 Typical settlement behaviors of clay, silty sand and sand

Terzaghi (1923) proposed the theory of one-dimensional consolidation for clays based on several simplifying assumptions such as linear relationship between void ratio and effective stress being independent of time and stress history, constant permeability during consolidation etc. Mesri and Rokhsar (1974) reformulated the existing consolidation theory for saturated soils using more realistic assumption with respect to permeability and compressibility of the soil as consolidation proceeds and incorporated compression index (C_c), recompression index (C_r) and permeability index (C_k) in compression analysis. Permeability index (C_k) is defined as $C_k = \Delta e / \Delta \log k$. For most of the clays C_k/C_c varies from 0.5 to 2 (Berry and Wilkinson, 1969). The condition of $C_k/C_c \neq 1$ has been considered by Raymond (1966) assuming small strain and Poskitt (1969) for finite strain. In these cases, rate of compression and pore pressure dissipation is governed by the value of C_k/C_c. Rate of compression and pore pressure dissipation decreases for $C_k/C_c < 1$ and it increases for $C_k/C_c < 1$.

Variation of secondary compression index (C_α) has been studied by many researchers. Newland and Alley (1960) showed that C_α is independent of consolidation stress whereas Wahls (1962) showed that it decreases with stress. Ladd and Preston (1965) found that the decrease or increase of C_α depends on the soil. Horn and Lambe (1964) concluded that ε_α, defined as $\frac{C_\alpha}{1+e}$, is independent of vertical effective stress. Adams (1965), Keene (1964) and Goldberg (1964) indicated that ε_α increases with increase in consolidation pressure.

Barden (1969) used spring and dashpot model to predict the behavior of soil skeleton subjected to vertical effective stress using Ostwald's power law, thrixtropic law and Murayama and Shibata's (1964) rate process theory, given by Equations 5.1, 5.2 and 5.3 below.

Ostwald's Power law:

$$\tau = b\left(\frac{\partial \varepsilon}{\partial t}\right)^{1/n} \tag{5.1}$$

Thrixtropic law (Barden 1969):

$$\tau = \frac{1+t}{b}\frac{\partial \varepsilon}{\partial t} \tag{5.2}$$

Murayama and Shibata's Rate process theory:

$$\frac{\partial \varepsilon}{\partial t} = \beta \tau_0 \sinh\left(\frac{\alpha \tau}{\tau_0}\right) \tag{5.3}$$

where t = time, τ = shear stress, τ_0 = shear stress at t = 0, ε = vertical strain, b = coefficient of viscosity, and α, β = rate process theory viscosity parameters.

Barden (1968) proposed the conceptual strain-vertical stress- time (ε-p-t) variations satisfying Equations 5.1, 5.2 and 5.3 as shown in Figure 5.2.

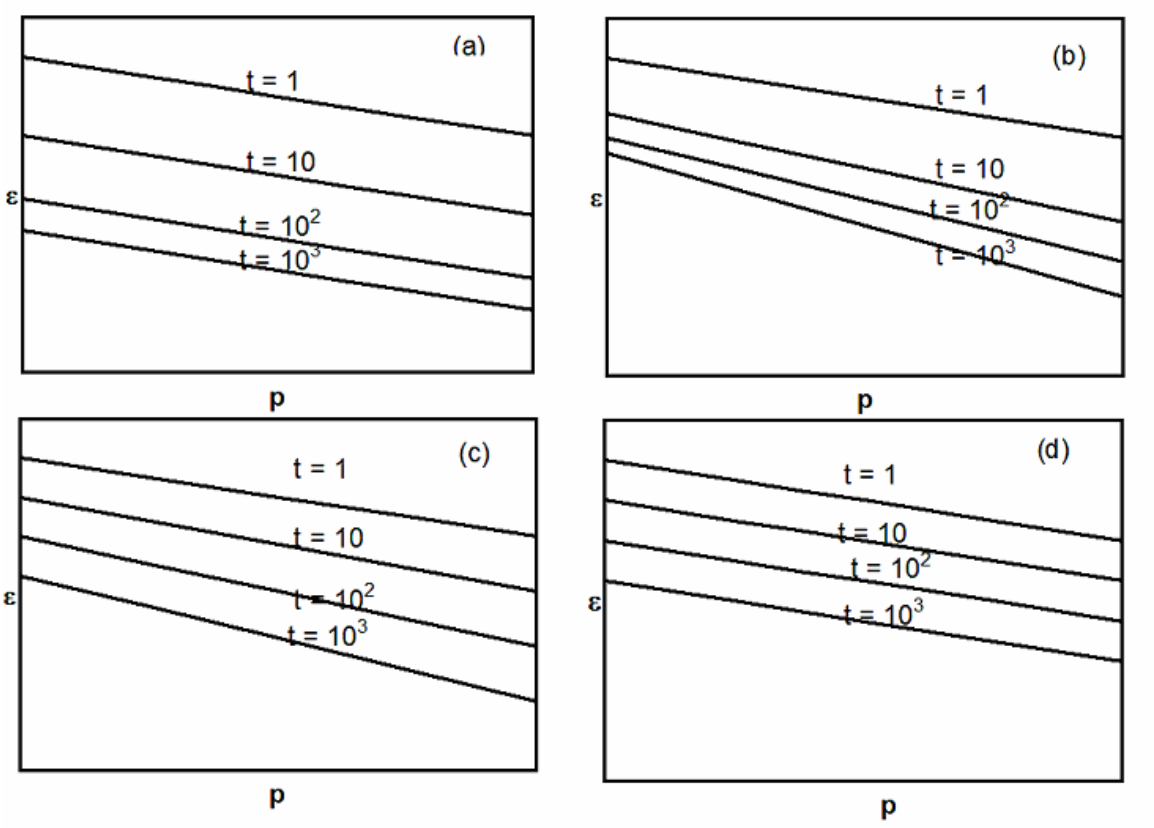

Figure 5.2 ε-p-t (strain – vertical stress – time) plots for clays (Adapted from Barden, 1969)

Barden (1968) showed that when C_α is independent of the vertical effective stress but decreases with time, the variation of strain with vertical effective stress will be similar to what is shown in Figure 5.2a. When C_α decreases with time and increases with the vertical effective stresses, the variation of strain with vertical effective stress will be similar to what is shown in Figure 5.2b. The variation shown in Figure 5.2c is the result of C_α being independent of time and increasing with the vertical effective stress. If C_α is

independent of time and vertical effective stress, the variation takes the form shown in Figure 5.2d.

5.3 Review Settlement of hydraulic fills

When hydraulic fill is placed in the underground voids in the form of slurry, the settlement takes place solely under the self weight. Wickland and Wilson (2005) performed self weight consolidation tests on mine tailing and rock mixture in a column of approximately 1 m diameter and 6 m height for disposal of mine wastes. Stone et al. (1994) used centrifuge modeling technique to replicate the staged filling of the tailings impoundment to assess both the short and long time consolidation behavior of tailings from Boddinston Gold Mine in Western Australia. Centrifuge modeling technique is very effective for assessment of self-weight consolidation. Stone et al. (1994) measured the long term variation of pore pressure within the different layers of tailing during self weight consolidation. Qiu and Sego (2001) performed consolidation test in a large-strain consolidation cell and permeability test using falling head method on copper, coal and gold mine tailings in Canada. The pressure increments of 0.5-100 kPa were applied on the sample within the consolidation cell. Coefficient of consolidation and coefficient of volume compressibility were calculated for these samples. It has been found that the coefficient of consolidation of tailings varied from 0.310 m^2/yr to 104.23 m^2/yr, while the permeability varied from 2.2×10^{-7} cm/s to 9.8×10^{-5} cm/s.

5.4 Comparison of settlement of sand and hydraulic fills

Settlement behavior of the hydraulic fills can be compared to that of fine sands. The particle size distribution curves of the fine sand and hydraulic fill used in this study are shown in Figure 5.3. The shaded area in the figure shows the range of particle size distribution of hydraulic fills of Australian mines, as reported by Rankine et al. (2006). There is no consolidation settlement in fine sands due to higher permeability. So the settlement behavior of sand had been used to compare with the settlement behavior of

hydraulic fills. Figure 5.3 show that hydraulic fills are even finer than the fine sand used for the test.

The settlements of sand and hydraulic fill were measured in an oedometer for both dry and saturated samples. Method of sample preparation for the test is discussed in Section 5.5. Figure 5.4 shows the variation of settlement with time when the vertical effective stress was increased from 80 kPa to 160 kPa.

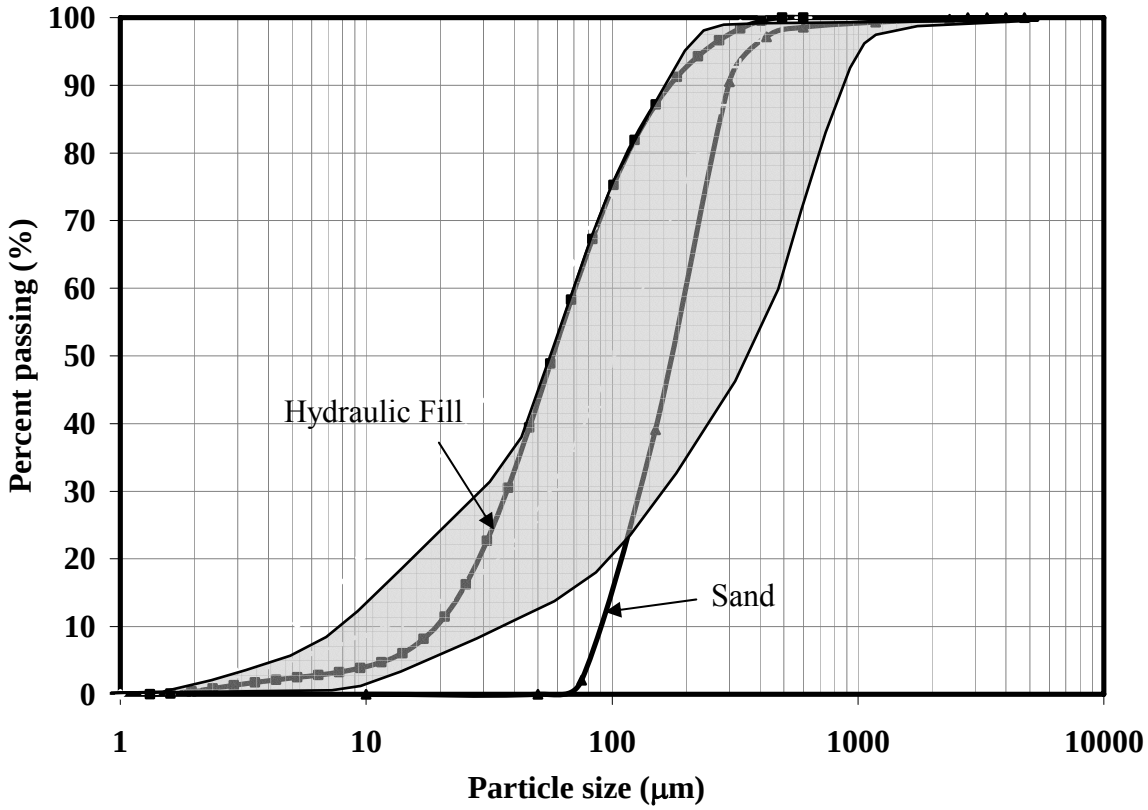

Figure 5.3 Particle size distribution curves for hydraulic fills of Australian mines

The rate of dissipation of pore water pressure in the sand is very high due to higher permeability. No significant difference between the settlement of dry and saturated sand has been observed (Figure 5.4) which shows that the consolidation settlement in sands is negligible. Immediate settlement and secondary compression are the major component of settlement in the sands. Secondary compression in sand occurs due to slippage between

grains as well as fracture of sand particles (Lade et al 1998). A significant difference in settlement has been observed between the saturated and dry hydraulic fills (Figure 5.4). In the case of saturated hydraulic fills, the settlements continue to take place for quite long time. It shows that the dissipation of pore water pressure within the hydraulic fills takes time. Primary consolidation and secondary compression occur simultaneously, following the immediate settlement of hydraulic fill, and it is difficult to separate the two. Extensive laboratory tests have been conducted to study the behavior of settlement of hydraulic fills. In this dissertation, attempts have been made to separate out consolidation and secondary compression. Tests and apparatus used to study the settlement of hydraulic fills are discussed later in this chapter.

5.5 Laboratory tests

The settlements of five hydraulic fills from three different mines of Australia had been studied at James Cook University. Oedometer, cylindrical cell and modified triaxial cell have been used to measure the settlement of hydraulic fill samples of different heights varying from 19 mm to 170 mm. The properties of the samples that have been used for laboratory tests are given in Table 4.1 and Figure 4.4 and 5.3.

Several tests have been performed to separate immediate settlement, consolidation settlement and secondary compression in hydraulic fills. One of the major cause barricades failures is attributed to the build-up of high pore water pressure behind the barricades resulting the liquefaction due to blasting or piping (Bloss et al., 1998). It increases the importance of estimating consolidation time or time required for pore water pressure dissipation in a mine stope. Since, settlement tests performed on classical oedometer are inconclusive about consolidation settlement and pore water pressure dissipation due to smaller sample height, triaxial cell has been modified to measure the pore water pressure. Method of preparing samples and laboratory test methodology has been discussed in this section.

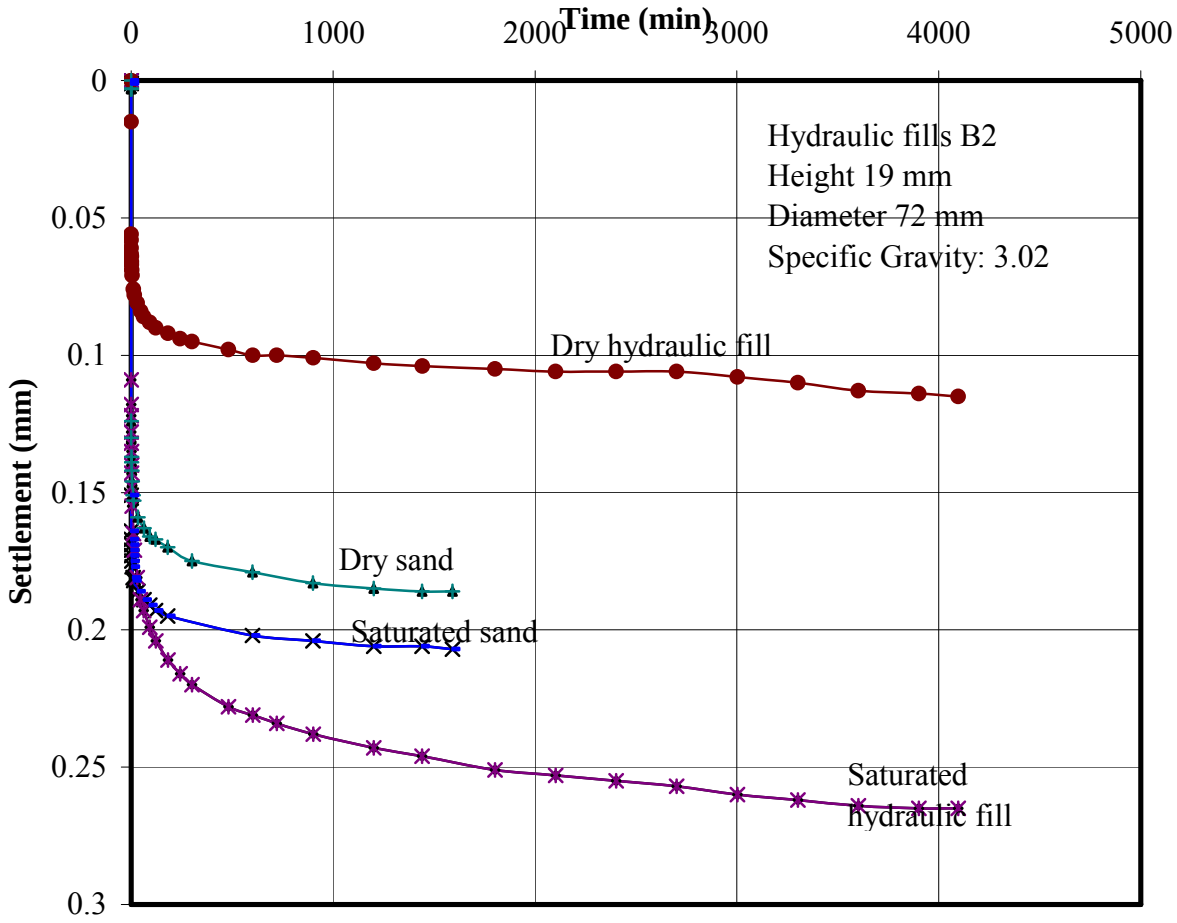

Figure 5.4 Comparison of settlement behavior of hydraulic fill and sand

5.5.1 Sample preparation for settlement tests

It is very difficult to prepare saturated hydraulic fill samples for oedometer. Since hydraulic fills are silty sands or sandy silts as per Unified Soil Classification System, it is very difficult to transfer the saturated samples into the oedometer ring or other apparatus in an undisturbed state. The samples for measuring settlement on the conventional oedometer (Figures 5.5, 5.6, 5.7, and 5.8) were prepared from slurry of the hydraulic fills with initial moisture content of 35 – 40%. The slurry was poured in a cylinder with downward drainage. It was allowed to settle under self-weight for 24 hours. Sample was extruded into the oedometer ring after 24 hours.

Samples for the cylindrical cell and modified triaxial cell were prepared from pouring the slurry of hydraulic fills with initial moisture content of 35 – 40% in the sample cell, as shown in Figures 5.9, 5.10 and 5.11. Hydraulic fills were allowed to drain and settle under its self weight. The top surface was trimmed the sample smooth on both top and bottom.

5.5.2 Oedometer tests for hydraulic fills

Settlement test were performed on the oedometer as per Australian Standard AS 1289.6.6.1 and American Standard ASTM D2435 – 04. The conventional oedometer apparatus and its schematic diagram are shown in Figure 5.5. Since hydraulic fills have very large permeability, the time required for consolidation is small. Conventional oedometer rings at James Cook University laboratory have a drainage length of 9.5 and 19 mm with drainage on one and both sides respectively. An arrangement was made to increase the drainage length in the oedometer by using a thicker sample and allowing the drainage from only one side. Figure 5.6 shows the arrangement that was used for allowing only one side drainage.

The settlement tests have been performed on the conventional oedometer for saturated and dry hydraulic fills. Test results from conventional oedometer are inconclusive about the consolidation settlement in hydraulic fills. Samples of different height have been used to increase the drainage path and consolidation time in the conventional oedometer using cylindrical tubes as shown in Figure 5.8. Settlements of dry and saturated sand have been measured and settlement behavior has been compared with hydraulic fills. The results of these tests are discussed later in this chapter.

Figure 5.5 Conventional oedometer apparatus

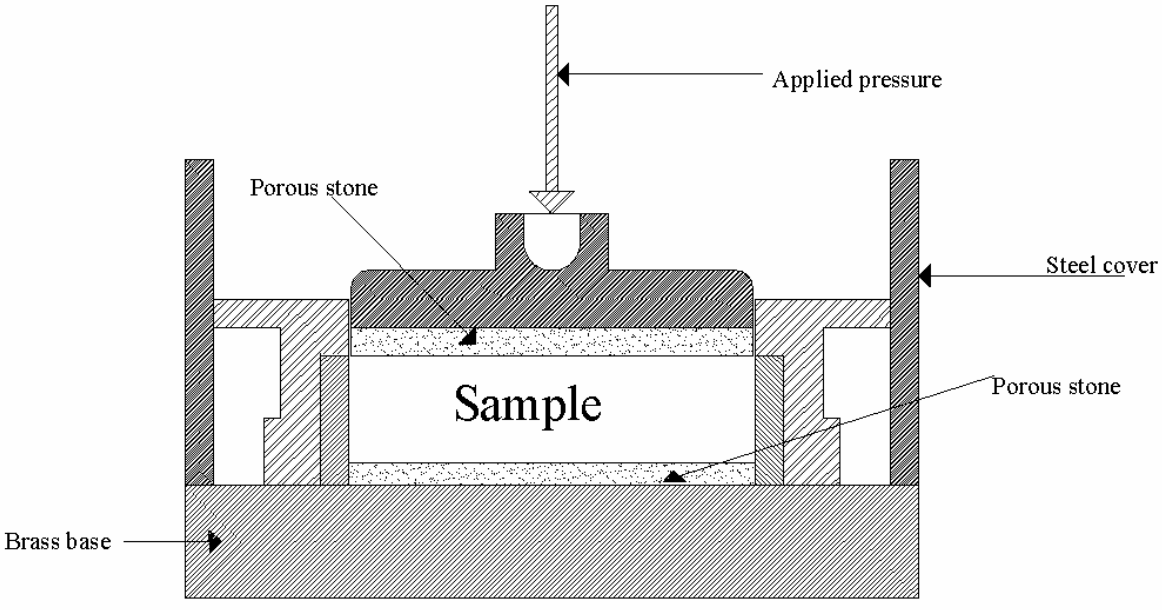

Figure 5.6 Schematic diagram of Oedometer

Figure 5.7 One side drainage in oedometer

Figure 5.8 Arrangement to increase the sample height in the conventional oedometer

5.5.3 Tests on large cylindrical cell to measure settlement

Oedometer tests were inconclusive about the existence of consolidation settlement in the hydraulic fills. Since the time required for consolidation is directly proportional to the square of drainage height (Das, 2005; Lambe and Whitman, 1969), larger cylindrical cell were designed to increase the consolidation time. A steel cylinder of 80 mm diameter and 150 mm height (Figure 5.9) was used to perform consolidation test. The sample was sealed from the top to increase the drainage path. The loading arrangement is shown in Figure 5.8b. A dial gauge was used to measure the settlement of hydraulic fills under a specific load. Drainage was allowed from the bottom of apparatus. This test gave an indication of consolidation in hydraulic fills. Since load was applied directly on the top of sample and there was no lever arm arrangement, as we get in oedometer, large amount of load (approximately 1600 kg-f) was required to increase the pressure up to 320 kPa on the sample.

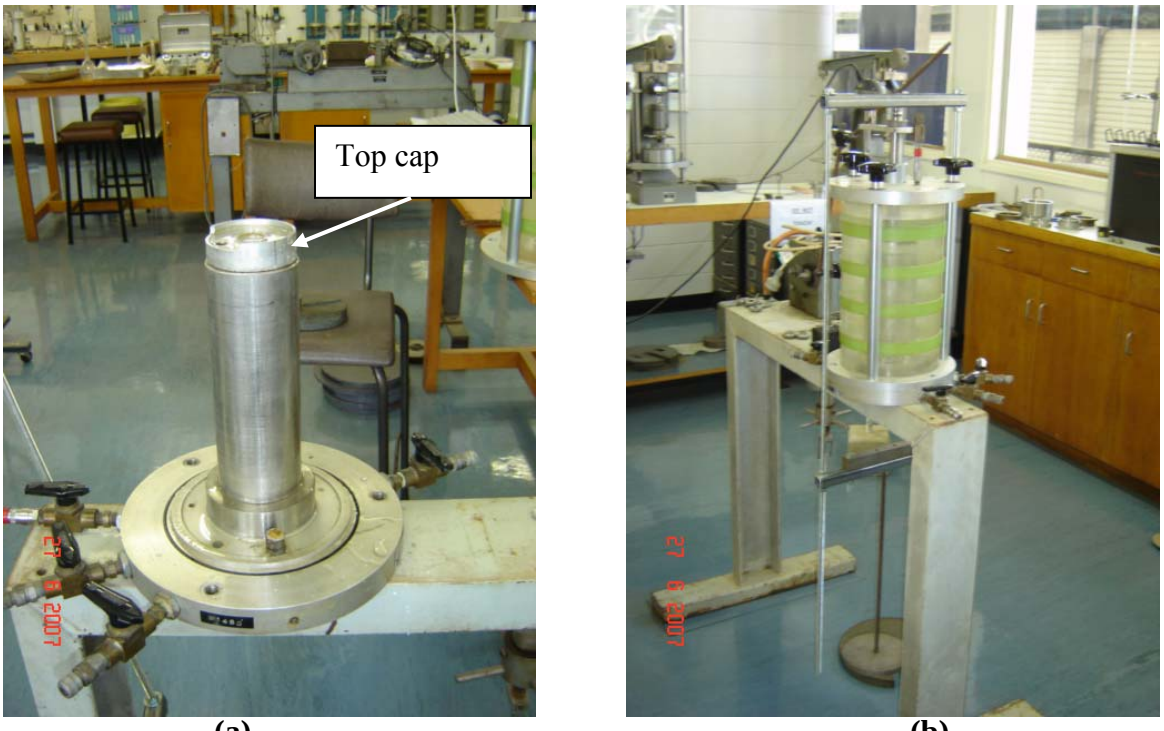

(a) **(b)**

Figure 5.9 Large apparatus to measure settlement of hydraulic fills

5.5.4 Modified triaxial cell to measure consolidation and pore pressure

It has been difficult to separate consolidation from immediate settlement and secondary compression using the settlement tests on oedometer and large cylindrical cell. Triaxial cell was modified to perform settlement test and measure pore pressure. Hydraulic fills are silty sands or sandy silts so the rate of pore pressure dissipation is very high. Triaxial cell was modified to perform the test for a drainage length of 85 mm (total length = 170 mm) which will increase the pore pressure dissipation time by 80 times compared to the 19 mm sample with drainage on both side. The schematic diagram and arrangement of modified triaxial cell are shown in Figure 5.10 and Figure 5.11 respectively.

Samples were prepared by pouring hydraulic fill slurries into the triaxial cylinder and allowing them to settle under self weight. Samples were trimmed from both ends before saturating in the apparatus by allowing the water to flow from the bottom to top (as shown in Figure 5.10) under the weight of top cap. Pore pressure of the sample was measured at the central bottom of the sample using pressure gauge. Sample was saturated after completion of each load increment.

Very large load was required to increase the vertical effective pressure on the cell due to the large diameter of cell and 1:1 load transfer. For example, 80 kg-f was required to increase the vertical effective pressure in the sample from 160 kPa to 320 kPa. Settlement of sample was recorded using data logger connected to the computer and readings were taken manually for pore pressure transducer.

5.6 Laboratory test results

Several tests have been performed to determine the settlement behavior of hydraulic fills at James Cook University. Laboratory tests results from oedometer tests, tests on the cylindrical cell and modified triaxial cell have been discussed in this section. Coefficients

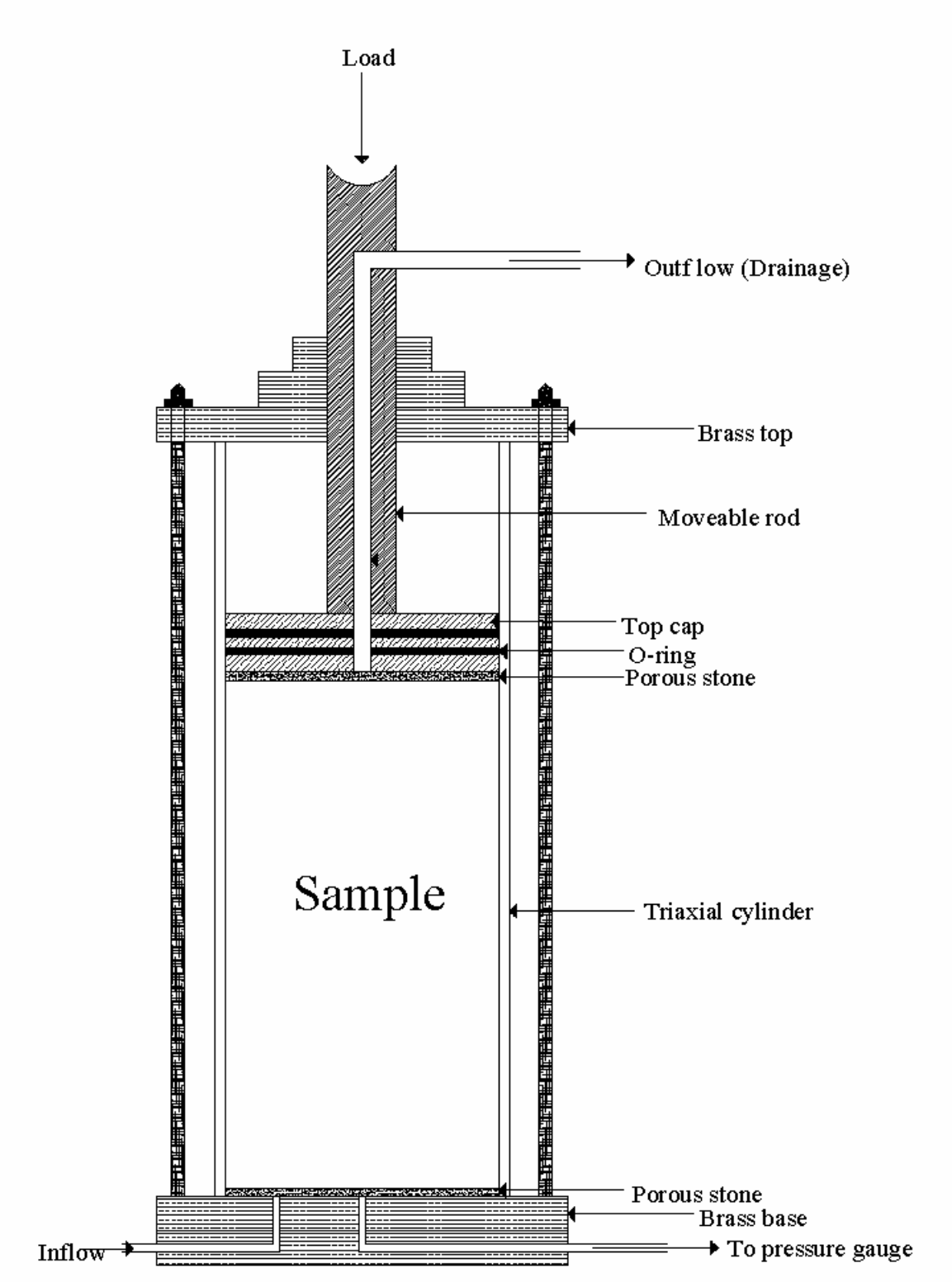

Figure 5.10 Schematic diagram of modified triaxial cell

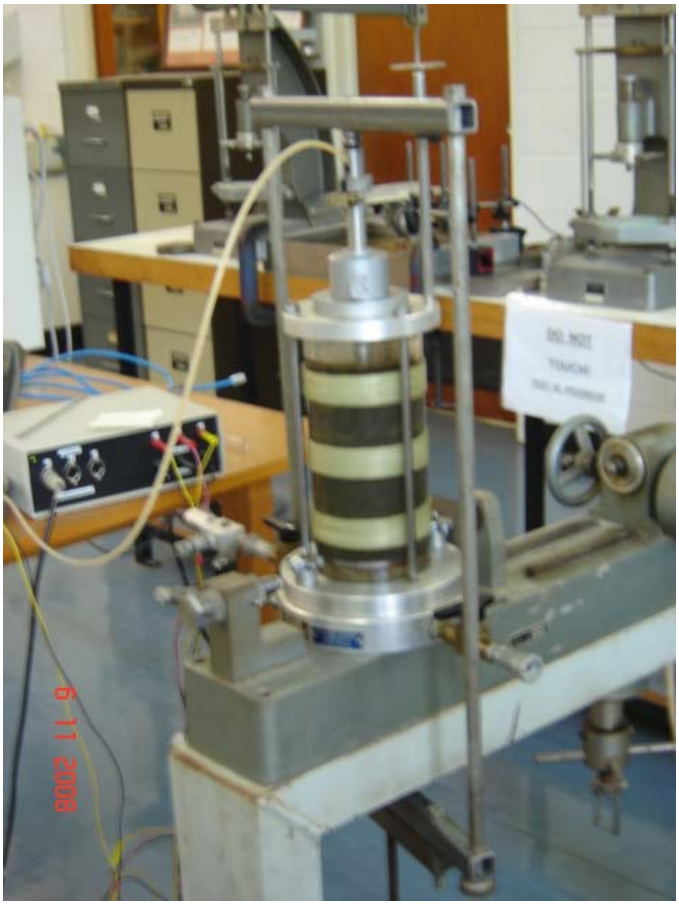

Figure 5.11 Modified triaxial cell arrangement

of consolidation of hydraulic fills have been computed by measuring pore water pressure dissipation from modified triaxial cell samples. Test results have been compared with data available in the literature.

5.6.1 Oedometer test

Several tests have been performed to measure the settlement of hydraulic fills using oedometer test. Samples of 19 mm, 40 mm and 78 mm height were used for the oedometer tests. Both one side and two-side drainages were used for 19 mm and 40 mm samples to increase the drainage path and consolidation time. Figure 5.12 shows the typical settlement curves for different vertical stress of a 19 mm high saturated sample (Sample B2) in an oedometer, under the vertical pressures of 80 kPa, 160 kPa and 320 kPa. The tail ends of the plots are shown in the inset. The laboratory tests show the

bilinear behavior of settlements of hydraulic fills on logarithmic scale. Immediate settlement in the hydraulic fill is completed within a minute in an oedometer. It is followed by primary consolidation and secondary compression. It has been observed that there is no significant change in the settlement after long time.

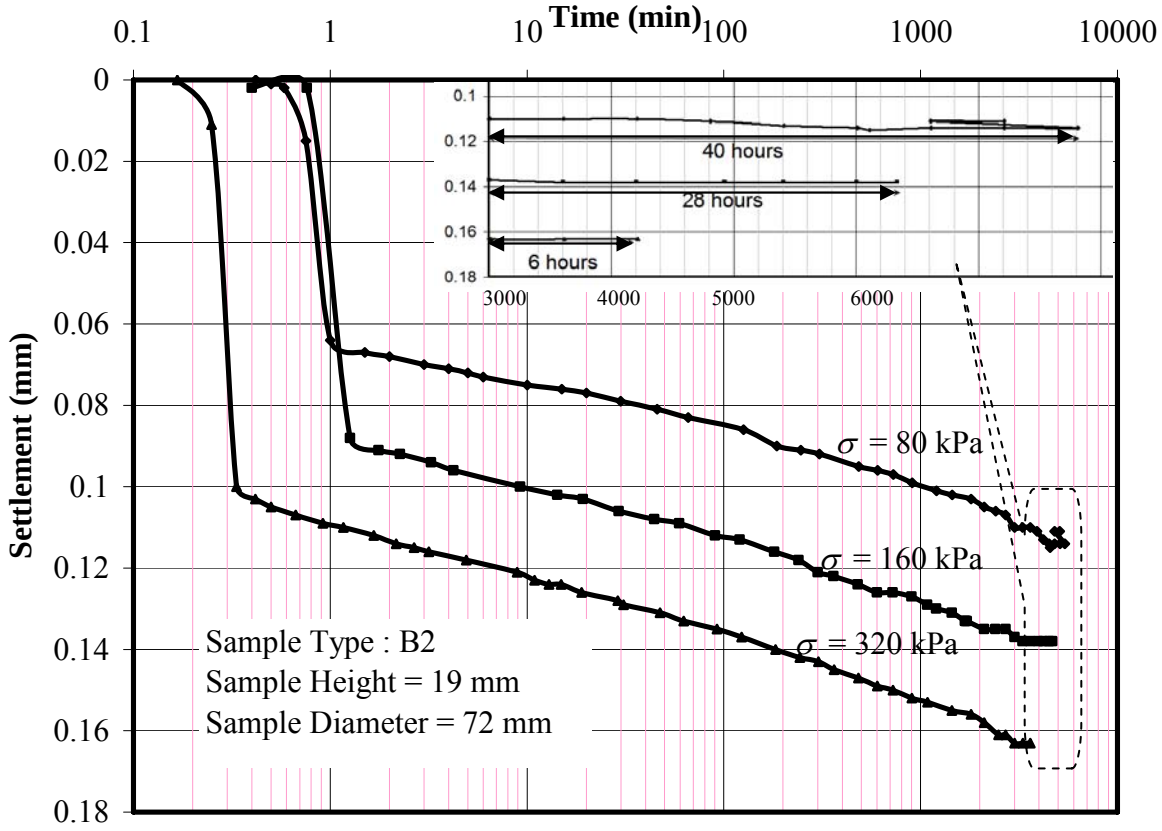

Figure 5.12 Typical settlement curves for hydraulic fills

Results of the other samples are shown in Appendix C1. Oedometer tests were inconclusive in separating consolidation settlement from secondary compression. No significant change was observed in the secondary compression after long time, as shown in Figure 5.12. Immediate settlement and secondary compressions contributes equally to the total settlement. Immediate and secondary compressions of hydraulic fills are discussed later in this chapter.

It has been observed that the settlements of hydraulic fills are bilinear logarithmic functions of time (Figure 5.12). Total settlement of hydraulic fills can be expressed as:

$s(\text{mm}) = s_0\,(\text{mm}) + a \log t\,(\text{min})$ (5.4)

where, s is the total settlement and a is the slope of the line which varies in the range of 0.003 to 0.03 for the different hydraulic fills studied. s_0 is the settlement at t = 1 minute (the unit used in the time axis) that is approximately the immediate settlement.

Tests have been conducted on different heights of samples in the oedometer. It has been observed that all sample heights show similar trends of settlement. Figure 5.13 shows settlement of sample B2 for sample height of 19 mm, 40 mm and 80 mm at initial void ratio of 0.81 and vertical effective stress increased from 80 kPa to 160 kPa. Figure 5.13 verifies the linear variation of settlement with logarithmic of time.

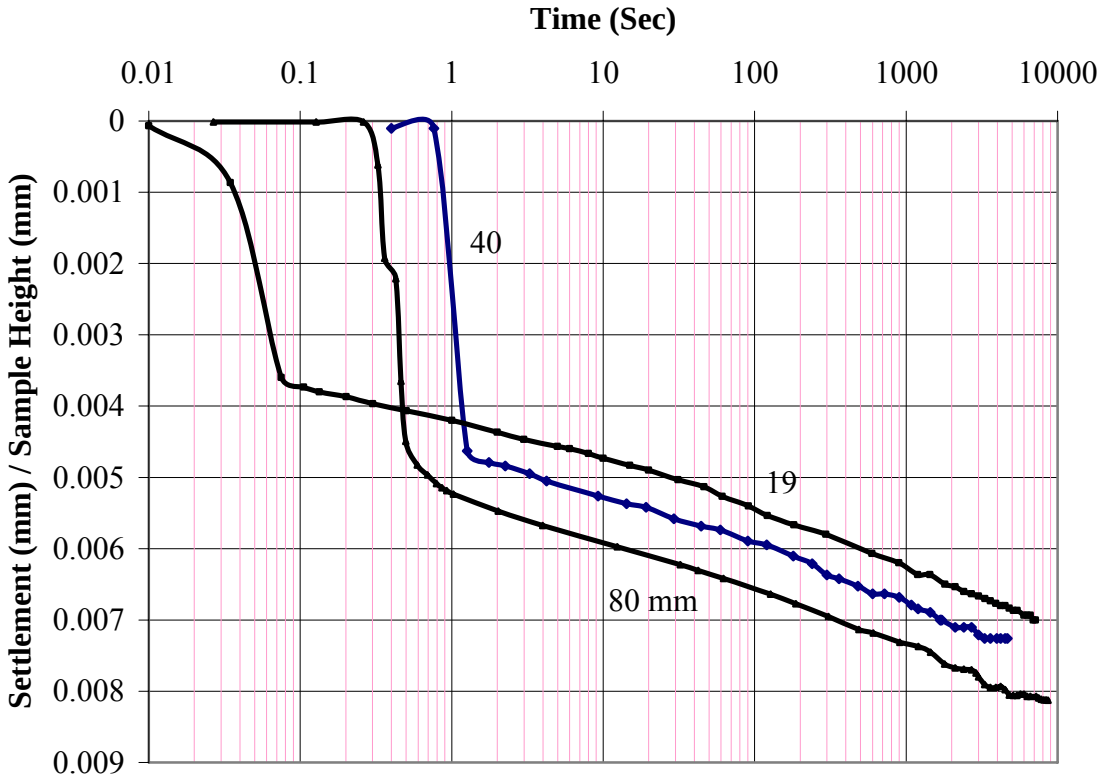

Figure 5.13 Typical settlement curves for hydraulic fills for different height of sample at vertical effective stress increased from 80 kPa to 160 kPa (Sample B2)

5.6.2 Tests on large cylindrical apparatus

A large apparatus, as shown in Figure 5.9, was used to measure the settlement of hydraulic fills. A steel cylinder of 80 mm diameter was used to hold 150 mm high samples for the test. The load was applied using a top cap as shown in Figure 5.9. The settlement of sample B2 is shown in Figure 5.14 for final vertical stress of 80, 160 and 320 kPa at load increment ratio of 1. 320 kPa was the maximum load than can be applied on this apparatus. The settlement measured using large cylindrical cell, have similar trends as the settlement measured using oedometer. Immediate settlement was contributing 50 – 60% of total settlement. It was difficult to separate the consolidation from secondary compression using large apparatus. It was inconclusive in separating consolidation and secondary compression.

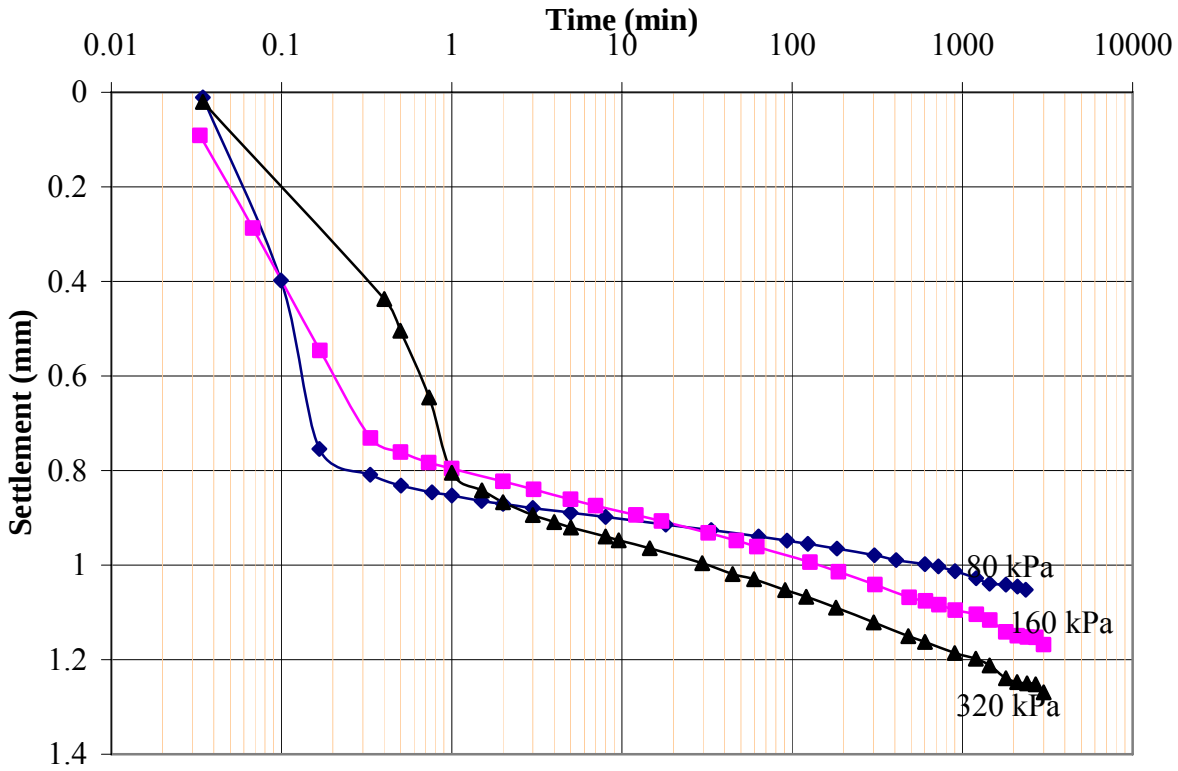

Figure 5.14 Settlement of hydraulic fills sample B2 in large cylindrical cell with final loads of 80 kPa, 160 kPa and 320 kPa

5.6.3 Modified triaxial cell test

Triaxial cell was modified (Figure 5.9) to measure the settlement and pore water pressure dissipation in the hydraulic fill sample. Pore water pressure was measured using pressure transducer. Settlement was measured using dial gauge. Maximum 320 kPa load was applied to the sample with load increment ratio of 1. A sample of 170 mm height and 80 mm diameter was used for the test. Settlement and pore water pressure variations with time for sample C2 are shown in Figure 5.15 and 5.16 respectively. It has been observed that the consolidation is over within 12 min. Results from modified triaxial cell have been used to estimate coefficient of consolidation using Logarithm-of-Time method proposed by Casagrande (1936); and Casagrande and Fadum (1940).

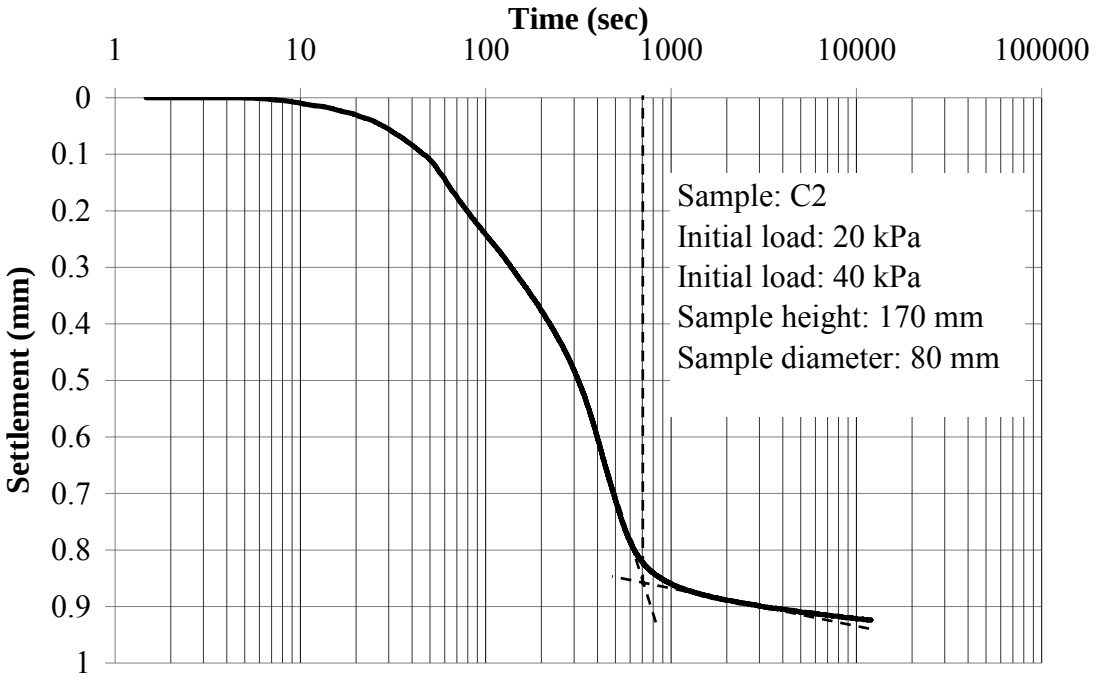

Figure 5.15 Settlement of hydraulic fill sample C2 in modified triaxial cell

Pore water pressure dissipation curve was used to calculate the coefficient of consolidation settlement by estimating consolidation time of hydraulic fills. Consolidation behavior of hydraulic fills is discussed in section 5.7.

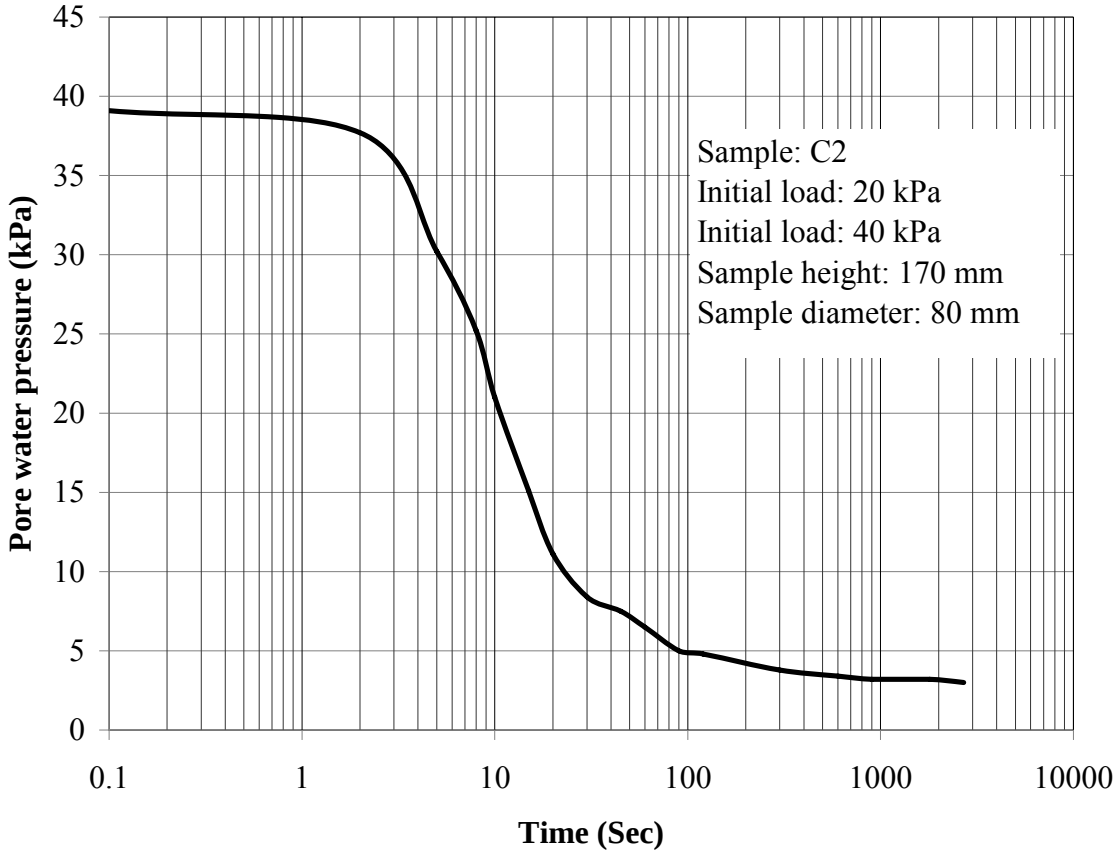

Figure 5.16 Pore water pressure variation of sample C2 in modified triaxial cell

5.7 Immediate settlement

It has been observed that the immediate settlement contributes 45-65% of the total settlement as shown in Figures 5.12, 5.13 and 5.14. Variation of immediate settlement with total settlement as observed from several tests has been shown in Figure 5.15. Immediate and total settlement of samples of different heights under different vertical effective stress was used to plot Figure 5.15. From the line of best bit, obtained through linear regression, it can be shown that 62.83% of the total settlement is immediate settlement, and it can be written as:

$$\text{Immediate settlement} = 0.6283\,\text{Total settlement} \tag{5.5}$$

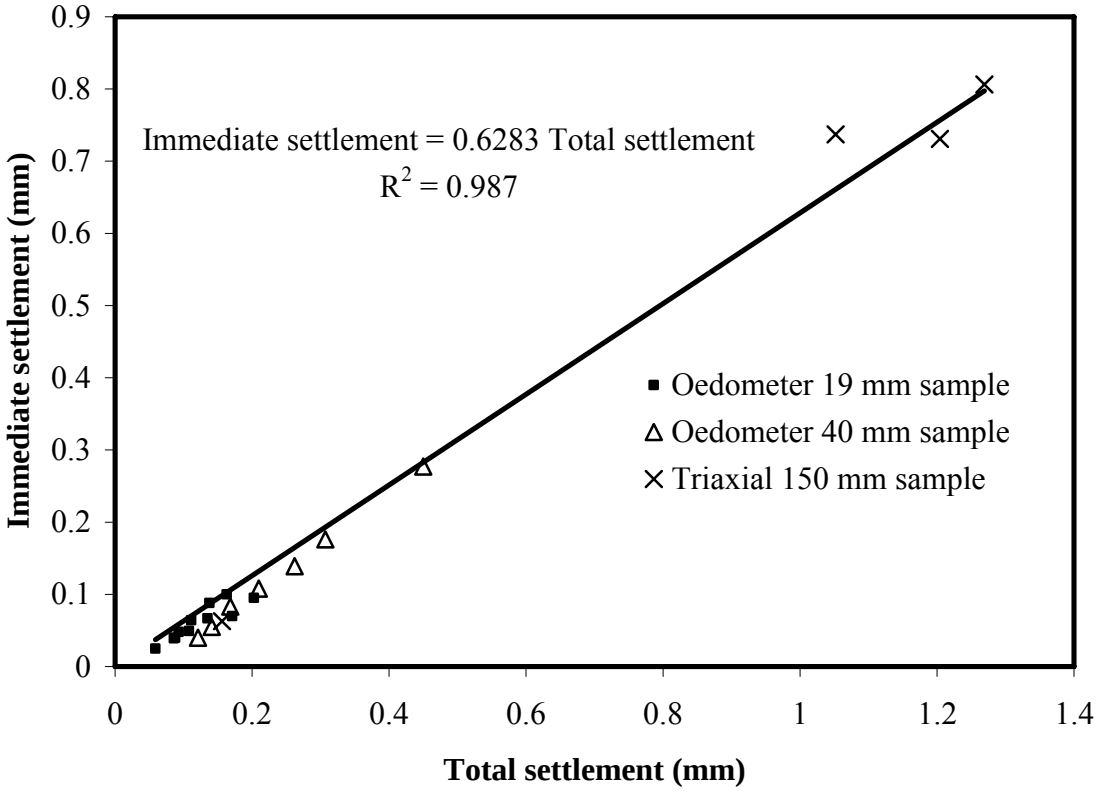

Figure 5.17 Immediate settlement versus total settlement

Coefficient of determination (R^2) was estimated for linear correlation between immediate settlement and total settlement of hydraulic fills. R^2 for this correlation was 0.987, which is very close to exact correlation. Even though immediate settlements are not actually elastic, they are usually estimated using elastic theory (Holtz and Kovacs 1981). Immediate settlement variation with applied vertical stress was studied for verification of elastic theory. Immediate settlement variation with applied stress for sample B2 is shown in Figure 5.18. It has been observed that immediate settlement bilinear function of vertical effective stress. Large immediate settlement at load 5 kPa is observed due to rearrangement of hydraulic fills under top cap load and applied load. Since the stress on hydraulic fill in a mine stope is very high, immediate settlement can be estimated using elastic theory.

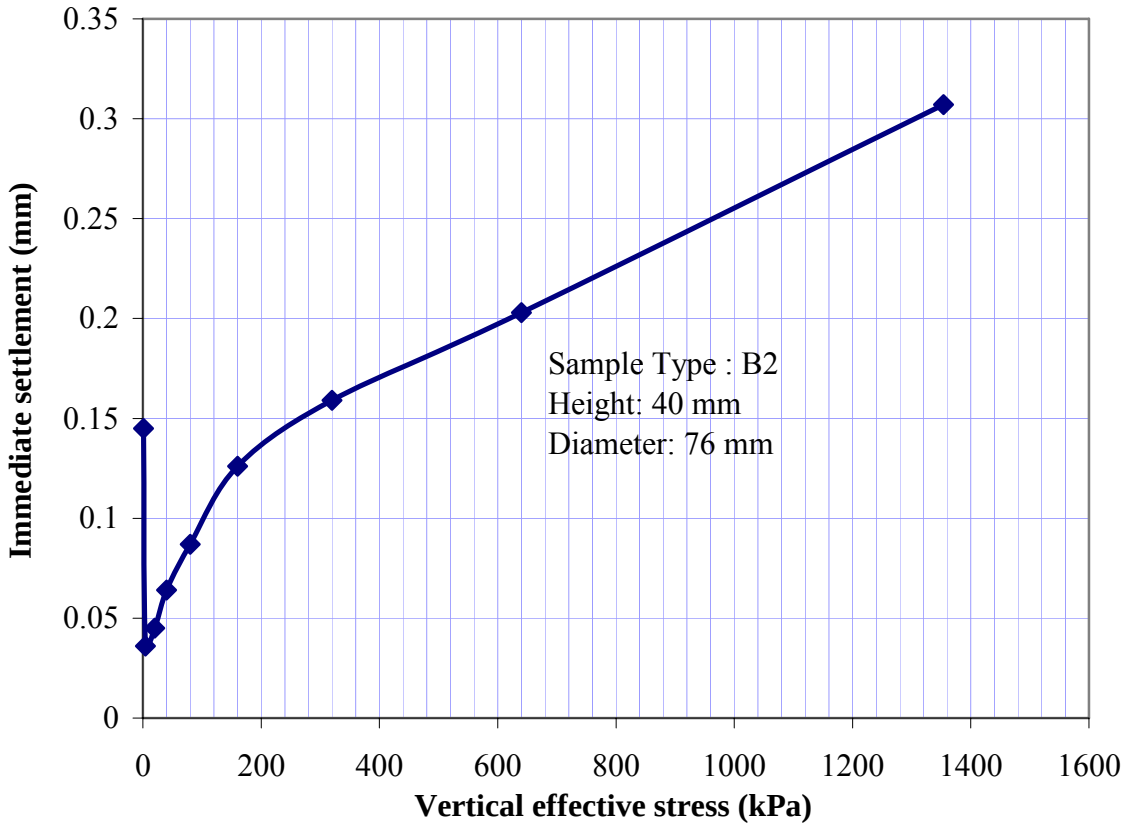

Figure 5.18 Immediate settlement variation with vertical effective stress for sample B2

5.8 Consolidation settlement

Modified triaxial cell was used to estimate consolidation settlement for hydraulic fills using a sample of 170 mm height. Time required for a certain degree of consolidation is directly proportional to the drainage height of the sample. Time required for 90% consolidation in 170 mm sample has been measured in laboratory using modified Triaxial cell. It has been used to compute the time required for 90% consolidation in other sample heights using $t_{90} \alpha H^2$, where H is drainage length. Table 5.1 summarizes the time required for 90% consolidation for samples of different heights. Table 5.1 shows that the time required for 90% consolidation in oedometer cell for 19 mm (both side drainage), 19 mm (one side drainage) and 40 mm (one side drainage) are 1.2, 5 and 22 sec respectively.

It supports the inconclusive test results in separating consolidation from secondary compression using oedometer test.

Table 5.1 Time required for 90% consolidation of hydraulic fills

Sample height	Apparatus	90% consolidation time
170 mm	Modified triaxial cell*	400 sec
19 mm	Oedometer (two side drainage)	1.2 sec
19 mm	Oedometer (one side drainage)	5 sec
40 mm	Oedometer (one side drainage)	22 sec
100 m	Mine stope	1600 days

* Measured in laboratory

Table 5.1 show that the time required for 90% consolidation in mine stope is 1600 days which is a large time. Samples were saturated during the tests on modified triaxial test. Mine stopes have continuous drainage without any inflow of water. It reduces degree of saturation in a mine stope. Simultaneous study of pore water pressure dissipation and pore air pressure dissipation is required to estimate the consolidation time of unsaturated hydraulic fills in the mine stope (Fredlund and Rahardjo 1993). Even though theoretical studies show that the pore water pressure dissipation will take more than 4 years in a 100 m high stope but due reduction in the saturation due to continuous drainage, pore water pressure dissipation will not take that long time.

Coefficients of consolidation have been computed for all five samples. It was observed that coefficient of consolidation for hydraulic fills varies from 0.5 mm^2/sec to 2.6 mm^2/sec as shown in Table 5.2. Qiu and Sego (2001) measured the coefficient of consolidation for mine tailing in tailing dams and found that it varies from 9.8×10^{-3}

mm^2/sec to 3.3 mm^2/sec. Stone et al. (1994) measured coefficient of consolidation for gold tailing and found that it varies from 0.19 mm^2/sec to 0.8 mm^2/sec. Table 5.2 shows coefficient of consolidation for hydraulic fills and other soils.

Table 5.2 Coefficient of consolidation for hydraulic fills and other soils

Sample	Coefficient of consolidation (mm^2/sec)
A1	0.5–1.5
B1	0.5–1.7
B2	0.5–1.9
C1	0.5–2.1
C2	0.5–2.6
Mine Tailings*	9.8×10^{-3}–3.3
Gold Tailing†	0.19–0.80
Silts‡	2×10^{-3}– 6×10^{-3}
Clays‡	1×10^{-3}– 6×10^{-3}

*Qiyu and Sego (2001), †Stone et al. (1994), ‡ Taylor (1948)

Coefficients of consolidation variation with vertical effective stress have been studied. Figure 5.19 shows the c_v variation with vertical effective stress of hydraulic fill samples. This variation has been compared with the c_v variation of gold tailing studied by stone et al. (1994). It has been observed that coefficient of consolidation of hydraulic fill increases with vertical effective stress.

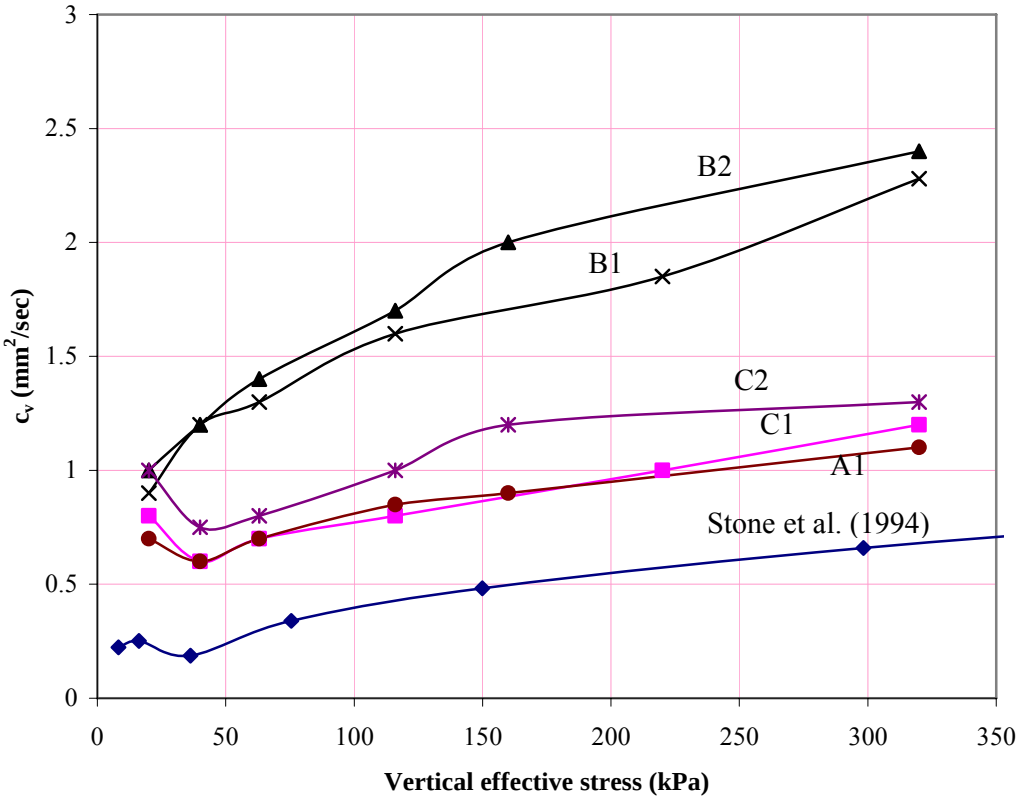

Figure 5.19 Coefficient of consolidation variation with vertical effective stress

5.9 Secondary compression settlement

In all previous studies of settlement the soil parameters such as linear compressibility and viscosity parameters were assumed as constant. The viscosity of soils decreases with increase in vertical effective stress. Barden (1969) suggested following equation for coefficient of secondary compression (C_α).

$$C_\alpha = 2.3\frac{a_v}{\alpha} \tag{5.6}$$

where a_v is coefficient of compressibility of soil and 'α' is the rate process theory viscosity parameter introduced by Murayama and Shibata (1964). α is inversely

proportional to vertical effective stress (Barden, 1969). Coefficient of compressibility (a_v) can be expressed as:

$$a_v = \frac{C_c}{2.303\sigma} \tag{5.7}$$

where C_c is compression index and σ is vertical effective stress. Permeability index (C_k) and compression index are defined as:

$$C_k = \frac{\partial e}{\partial \log k} \tag{5.8}$$

$$C_C = -\frac{\partial e}{\partial \log \sigma} \tag{5.9}$$

Total settlement of the hydraulic fill (Sample C1) has been plotted against vertical effective stress at the end of 1 min, 5 min, 25 min, 625 min and 3125 min, in Figure 5.20 for a sample of 19 mm thickness. Comparing this figure with the ones postulated by Barden and shown in Figure 5.2c, it is quite clear that C_α increases with the vertical effective stress for the hydraulic fills. The difference in change in settlement of hydraulic fill is approximately constant for a given vertical effective stress. It shows that C_α is independent of time.

The settlement-vertical stress – time plot for two different thicknesses of hydraulic fill samples (Sample B2) is shown in Figure 5.21. It shows that the secondary compression depends on sample thickness which is well supported by Barden (1968).

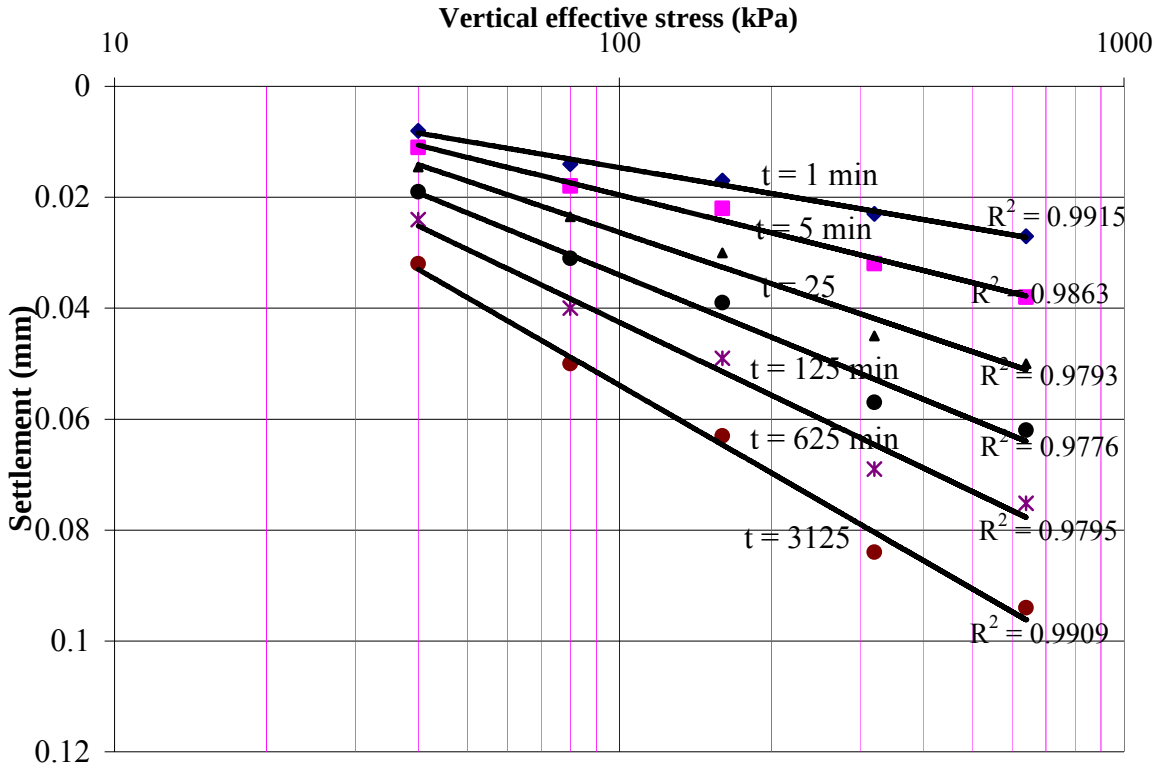

Figure 5.20 Settlement -vertical stress-time plot for sample C1

5.10 Permeability – vertical effective stress – settlement relationship

When the underground voids are backfilled by hydraulic fills, self-weight consolidation takes place, and the excess water is drained through the porous barricades at the horizontal access drives. These hydraulic fill stopes can be approximated as rectangular prisms, with heights as much as 200 m or even more. Pirapakaran and Sivakugan (2007a, 2007b) studied the stress developments within the minefill stopes, with due considerations of arching that takes place within the minefills. In spite of the significant reduction in the vertical normal stresses due to arching, the stresses within the minefill stopes can be quite high, which can reduce the void ratio and hence permeability.

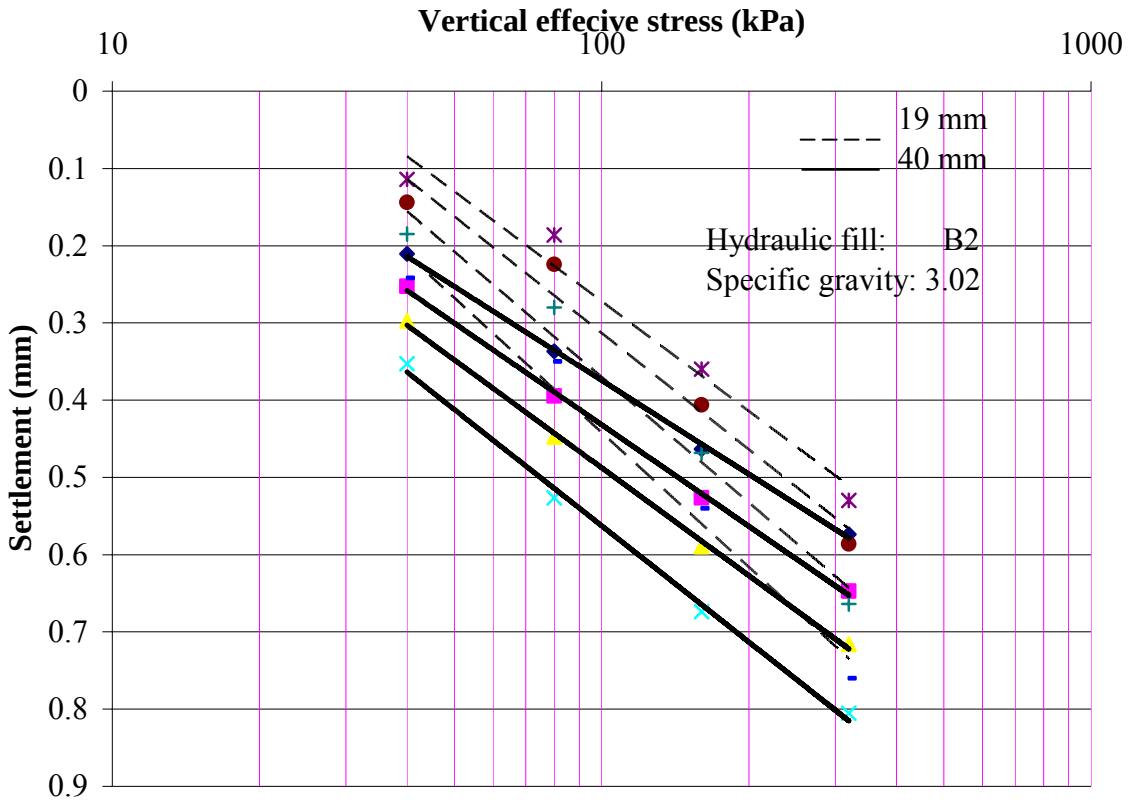

Figure 5.21 Settlement-vertical stress – time plot for samples of different thickness

In all the studies carried out to date on drainage through hydraulic fill stopes, it has been assumed that the permeability remains constant with depth and time (Isaacs and Carter 1983, Traves and Issacs 1991, Rankine et al. 2006). The permeability variation with stress and moisture content is discussed in Chapter 4.

Hydraulic fills were placed in an oedometer submerged in water, and were subjected to vertical pressures. The details of this special oedometer test setup are given in Singh et al. (2008). The coefficient of consolidation (c_v), coefficient of volume compressibility (m_v) and permeability (k) are related by:

$$c_v = \frac{k}{m_v \gamma_w} \tag{5.10}$$

Theoretically, it is possible to estimate k from the values of c_v and m_v measured in an oedometer test using the above definition of c_v. However, it is well known that such estimates are often unrealistic (Tavenas et al. 1983). Therefore, a special oedometer setup (Singh et al. 2008) was used to measure permeability at every pressure increment through a falling head permeability test, without using Equation 5.10. Figure 5.20 shows the permeability variation of typical hydraulic fills and sands with vertical effective stress, measured using falling head permeability setup in the special oedometer.

It can be seen from Figure 5.23 that the permeability of hydraulic fills and sand decreases with increase in vertical effective stress, and the variation is linear when the vertical effective stress is presented on logarithmic scale. The void ratio of the hydraulic fills has been calculated at different effective vertical stress levels. Variation of void ratio with effective vertical stress, for five different hydraulic fills, from three different mines A, B and C, is shown in Figure 5.23. The void ratio varies linearly with vertical stress on logarithmic scale as expected for a self-weight settled hydraulic fill that has not experienced a preconsolidation pressure. Similar trend has been observed for sands.

There is a reduction of less than 20% in the void ratio when vertical effective stress increased from 10 kPa to 1280 kPa. The compression index values computed from the virgin consolidation lines shown in Figure 5.23 were in the range of 0.04-0.11, similar to those seen for granular soils and significantly less than the values reported for clays.

Singh et al. (2008) measured the variation of void ratio with logarithm of permeability of different hydraulic fills samples. Permeability index (C_k) of each sample has been calculated from void ratio and permeability plots. These values are shown in Table 5.3 along with the values reported by Qiu and Sego (2001) for other mine tailings from Canada. Also shown in the table are selected values for sands and clays and silts, as reported by Lambe and Whitman (1979). The permeability index of hydraulic fills varies from 0.108 to 1.597. C_k/C_c of different mine tailings (Qiu and Sego 2001) and hydraulic fills are given in Table 5.4.

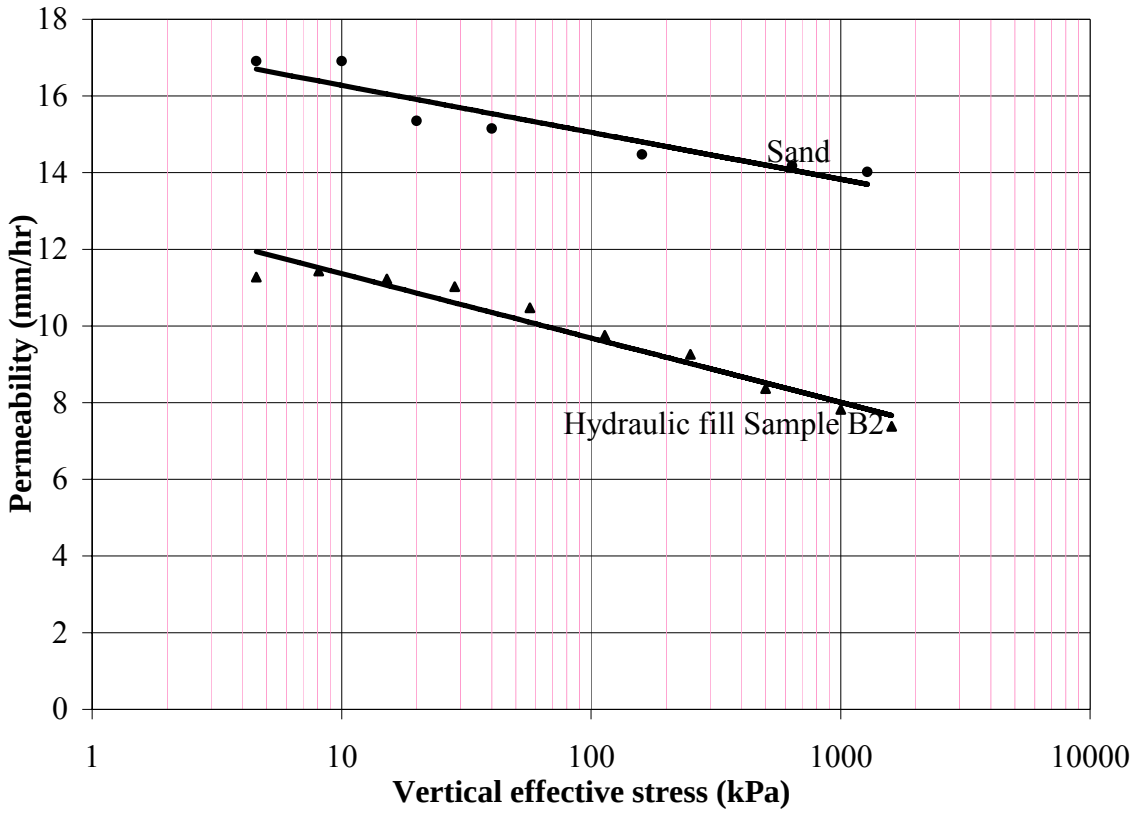

Figure 5.22 Permeability versus vertical effective stresses

If the vertical effective stress on hydraulic fills is increased from σ_0 to σ_1, the permeability of the hydraulic fills will change from k_0 to k_1 due to change in void ratio. Using Equation 5.8 and 5.9,

$$k_1 = \frac{k_0}{\left(\frac{\sigma_1}{\sigma_0}\right)^{C_C/C_k}} \tag{5.11}$$

Coefficient of consolidation (c_v) can be calculated using Equations 5.7, 5.10 and 5.11 as:

$$c_v = \frac{2.303 k_0 \sigma_1 (1+e_0)}{C_C \left(\frac{\sigma_1}{\sigma_0}\right)^{C_C/C_k}} \tag{5.12}$$

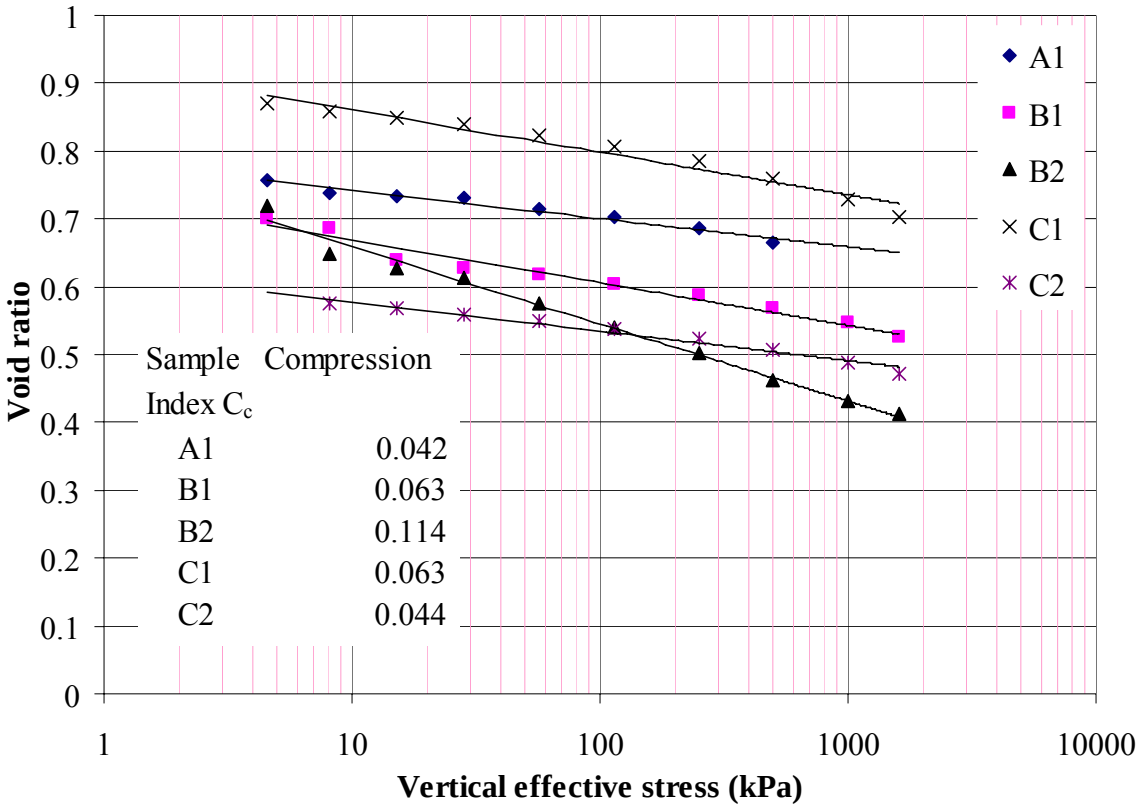

Figure 5.23 Void ratio versus vertical effective stresses

Equation 5.12 shows that if C_k/C_c will increase then the rate of consolidation and pore pressure dissipation will also increase. When C_k/C_c = 1, then c_v is constant during consolidation and is independent of σ and same as Terzaghi's definition of c_v. The rate of consolidation and dissipation decreases for C_k/C_c < 1 (Mesri and Rokhsar, 1974; Berry and Wilkinson, 1969). C_k/C_c of hydraulic fills varies from 2.57 to 14 as shown in Table 5.4. C_k/C_c for bentonite is 0.52 and it varies from 0.12 – 0.2 (Raymond, 1966) for Boston Blue clay (Holtz and Kovacs, 1981). It indicates that rate of settlement and pore pressure dissipation are higher for hydraulic fills and lower for bentonite and clays.

Table 5.3 C_k values for hydraulic fills, mine tailings, and other soils

Soil type	Permeability index (C_k)
Silty sand*	0.108
Beach Sand*	0.359
Sandy clay*	0.397
Lean clay*	0.085
Boston silt*	1.592
Sodium Boston blue clay*	0.78
Coal Tailing**	0.629
Copper Tailing**	0.556
Gold Tailing**	0.713
A1	0.108
B1	0.278
B2	1.597
C1	0.818
C2	0.513

* Lambe and Whitman (1979), ** Qiu et al. (2001)

Table 5.4 C_k/C_c for hydraulic fills and mine tailings

Sample	C_k/C_c
A1	2.57
B1	4.41
B2	14.01
C1	12.98
C2	11.66
Coal Tailing*	1.52
Copper Tailing*	3.33
Gold Tailing*	4.28
Bentonite†	0.52
Boston Blue Clay‡	0.12 – 0.2

** Qiu and Sego (2001), † Raymond (1966), ‡ Holtz and Kovacs (1981)

5.11 Summary and conclusions

Hydraulic fills are transferred to the mine stope in form slurry at initial moisture content of 35 – 40%. It settles within the stope under its self-weight and free water is allowed to drain through fill and barricades into empty drives. Settlement and pore water pressure dissipation from the mine stopes are two major issue in designing barricades and stopes. In previous studies, it has been assumed that there is no consolidation settlement in hydraulic fills. In this dissertation, several apparatus have been designed to study time dependent settlement of hydraulic fills and pore water pressure dissipation from mine stope. Several tests have been conducted to measure the settlement of hydraulic fills. It has been observed that the settlement of hydraulic fill is a bilinear logarithmic function of time. Primary consolidation and secondary compression follows the immediate settlement. It is difficult to separate the primary consolidation and secondary compression using traditional oedometer tests. Triaxial cell has been modified to study the pore pressure dissipation and consolidation of hydraulic fills. An empirical equation (Equation 5.4) has been proposed to estimate the settlement variation of hydraulic fills with time.

Immediate settlement contributes about 63% of the total settlement. It has been observed that the immediate settlement of hydraulic fill varies linearly with vertical effective stress for higher vertical effective stress (more than 160 kPa) whereas it is non-linear for lower vertical effective stress (less than 160 kPa). It has been recommended that the elastic theory of calculating settlement can be used to estimate immediate settlement in hydraulic fill stopes.

Consolidation settlement of hydraulic fill has been measured using modified triaxial cell by measuring pore water pressure dissipation from the sample. It has been observed that consolidation time for the 170 mm sample is 12 min, which explains the reason for inconclusive settlement results from oedometer. Coefficient of consolidation has been computed for 5 hydraulic fill samples and its variation with vertical effective stress is shown graphically (Figure 5.19).

Settlement- effective stress- time plot has been used to investigate the variation of coefficient of secondary compression (C_α). C_α of the hydraulic fill increases with effective stresses and is independent of time. Ratio of permeability index and compression index (C_k/C_c) of hydraulic fills varies from 2.57 to 14 for hydraulic fills as shown in Table 5.4. It indicates that rate of settlement and pore pressure dissipation is higher for hydraulic fills. Compression index of all five hydraulic fill has been estimated and reported in Table 5.3. It can be used in estimating total settlement of hydraulic fills.

Chapter 6

Drainage and Pore Pressure Development within a Stope

6.1 General

When mine stopes are backfilled using hydraulic fills, the solid particles of hydraulic fills settle rapidly after entering the stopes. Excess water initially tends to pond on the surface building up from the lowest corners of the mine stope and then commences a vertical path of drainage due to gravity. Since hydraulic fills are placed as slurry, there is substantial amount of water entering the stope. Design of barricades should be such that they enable the excess water from hydraulic fill to be removed as quickly as possible, so that the pore water pressure within the stope is minimized. Magnitude and distribution of pore water pressure developed during the backfilling of mine stope is required for design of backfilling operation and barriacades (Isaac and Carter, 1983).

Five hydraulic backfill barricades failed in Australian mines in 1997 due to delivery of excess quantity of transport water from low density slurry (Grice, 1998). The major cause of barricades failure was attributed to the build-up of high pore water pressure behind the barricades, resulting the liquefaction due to blasting or piping (Bloss et al., 1998). Another brick barricade failed after 3 weeks of filling at Normandy Bronzewing Mine in Western Australia in June 2000. It killed 3 workers at the site. In the same year, two barricades failed at Osborne Mine in Queensland (Brady and Brown 2002; Sivakugan et al., 2006; and Rankine 2007).

Mine stopes are backfilled in batches. After filling for a certain time in the mine stope, backfilling is stopped to allow the drainage of the excess water from the stope. There are several approaches to design the backfilling schedule. Mitchell et al. (1975) proposed a method of filling on the basis of monitoring the water balance the stope. At any given time the total water in the stope should not exceed 60% of the water placed in the slurry (Mitchell et al., 1975). Cowling (1998) proposed a guideline for mine stope at Mount Isa. Filling schedule proposed by Cowling (1998) were based on fill rate of 300 t/h at 72 ± 2% solid content and specific gravity of 2.90. Isaac and Carter (1983) used filling rate of 125 t/hr to 250 t/hr for drainage and pore water pressure analysis using numerical method with pouring (filling) and rest time of 100 hrs and 50 hrs respectively. Grice (2005) adviced that to have a definite rate of fill placement and rest time for each mine stope, and it should not be exceeded.

In this dissertation, filling rate of 150 t/hr, pouring time of 100 hrs and rest time of 50 hrs have been used to compute drainage and maximum pore pressure in the stope (Section 6.4.1). The rate of drainage is a function of permeability of the hydraulic fill and driving head (Cowling, 1998 and Traves and Isaacs, 1991). Sivakugan and Rankine (2006) and Sivakugan et al. (2006) used method of fragments to estimate drainage and maximum pore water pressure. In this chapter, form factors introduced by Harr (1962); Sivakugan and Rankine (2006); and Sivakugan et al. (2006) have been used to develop drainage and pore water variation in mine stope.

6.2 Method of fragments

Pavlovsky (1956) developed method of fragments to study drainage and pore-water pressure in the soils. Fundamental assumption of method of fragments is that the equipotential lines at various critical parts of the flow can be approximated by vertical or horizontal straight lines (Harr, 1962; and Sivakugan and Rankine, 2006). These equipotential lines divide the flow region into sections (or fragments). Method of fragments provides an approximate solution but it is widely used because it enables the computation of drainage, pore-water pressure and exit hydraulic gradient without

drawing any flow net. Sivakugan and Al-Aghbari (1993) computed the seepage beneath concrete dam and sheet piles using method of fragments and flow net and observed that both methods give similar results.

Sivakugan et al. (2006) and Sivakugan and Rankine (2006) developed a numerical model using FLAC to study drainage and pore water pressure development within a two dimensional rectangular stope and proposed a simple solution to determine discharge and maximum pore water pressure using method of fragments.

6.2.1 Method of fragment for 2-D mine stope

Sivakugan et al. (2006), Sivakugan and Rankine (2006), and Rankine (2007) used finite difference software FLAC to develop the flow nets in a two dimensional mine stope as shown in Figure 6.1. Few selected equipotential lines are shown in Figure 6.2. Equipotential lines are horizontal above the height of B, where B is width of stope, which shows that flow is vertical. These lines are vertical in the drain or drives beyond a distance of $0.5D$, where D is height of drive. It implies that flow is horizontal in the drains. Equipotential lines change its direction from horizontal to vertical from height of B from bottom of the stope to the bottom.

Ratio of euipotential drops to the flow channel within the fragments is known as form factor (Φ). Discharge (q) in i^{th} fragment can be computed as:

$$q = \frac{k h_i}{\Phi_i} \tag{6.1}$$

where h_i and Φ_i are head loss and form factor in i^{th} fragment and k is permeability of soil. Since discharge through all fragments must be same, discharge can be estimated as:

$$q = \frac{k \sum h_i}{\sum \Phi_i} = \frac{k h}{\sum \Phi_i} \tag{6.2}$$

where h is total head loss.

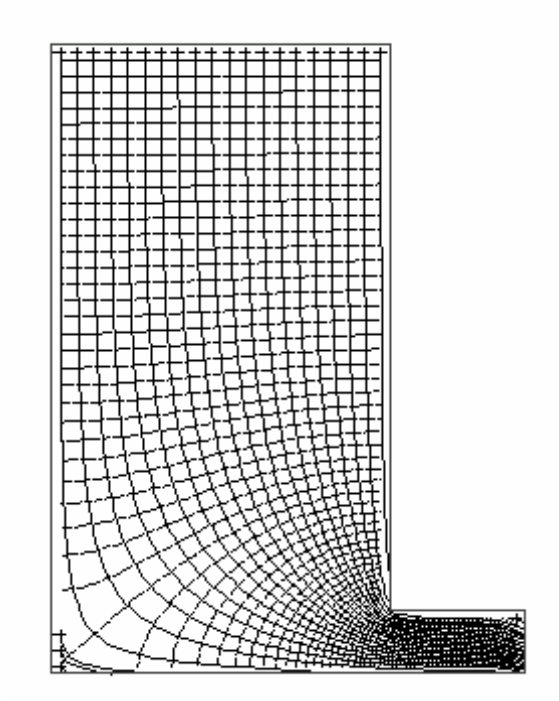

Figure 6.1 Flow net of two dimensional mine stope from FLAC (Sivakugan and Rankine 2006)

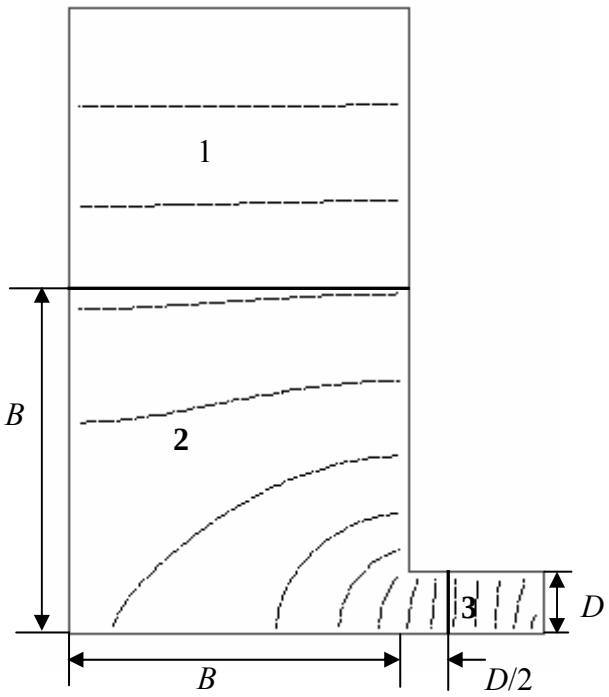

Figure 6.2 Selected equipotential lines from FLAC (Sivakugan and Rankine 2006)

Harr (1962) summarized six fragment types and form factors for one dimensional flow. Sivakugan et al. (2006), Sivakugan and Rankine (2006), and Rankine (2007) divided flow domain in two dimensional mine stope in three (3) fragments on the basis direction of equipotential lines (Figure 6.3). Fragment 1 is from height of B to the top of mine stope where equipotential lines are horizontal. Fragment 2 is from bottom of stope to height of B and fragment 3 is from distance of 0.5 *D* in the drain or drive. As shown in Figure 6.2 and 6.3, fragments 1 and 3 in two dimensional mine stope are of Type I (Harr, 1962; Sivakugan and Rankine, 2006). The form factors of fragments 1 and 3 can be calculated as follows:

$$\Phi_1 = \frac{H_w - B}{B} \tag{6.3}$$

$$\Phi_3 = \frac{X - 0.5D}{D} \tag{6.4}$$

where, Φ_1 *and* Φ_3 are form factor of fragment 1 and 3 respectively and X is drive length.

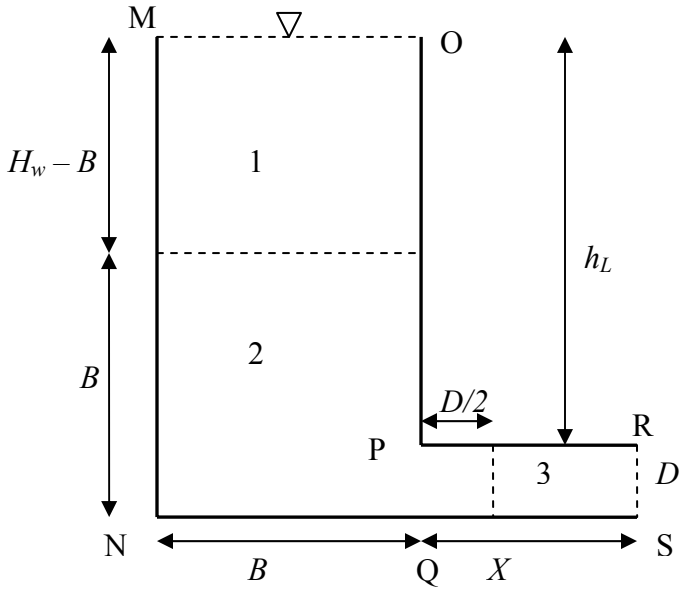

Figure 6.3 Fragments in a 2-D mine stope (Adapted from Sivakugan et al. 2006)

Form factor (Φ_2) for fragment 2 cannot be approximated using any of Harr (1962) six fragments. Sivakugan and Rankine (2006) used numerical model on FLAC to determine Φ_2 for two dimensional stope with height (H_w) in the stope. Variation of Φ_2 with D/B for H_w/B of 0.1, 0.2, 0.4, 0.6, 0.8 and 1.0 is shown in Figure 6.4. Following empirical equation has been proposed to estimate form factor (Φ_2) for $H_w/B \geq 1$.

$$\Phi_2 = -1.414 \log \frac{D}{B} + 1.2752 \qquad (6.5)$$

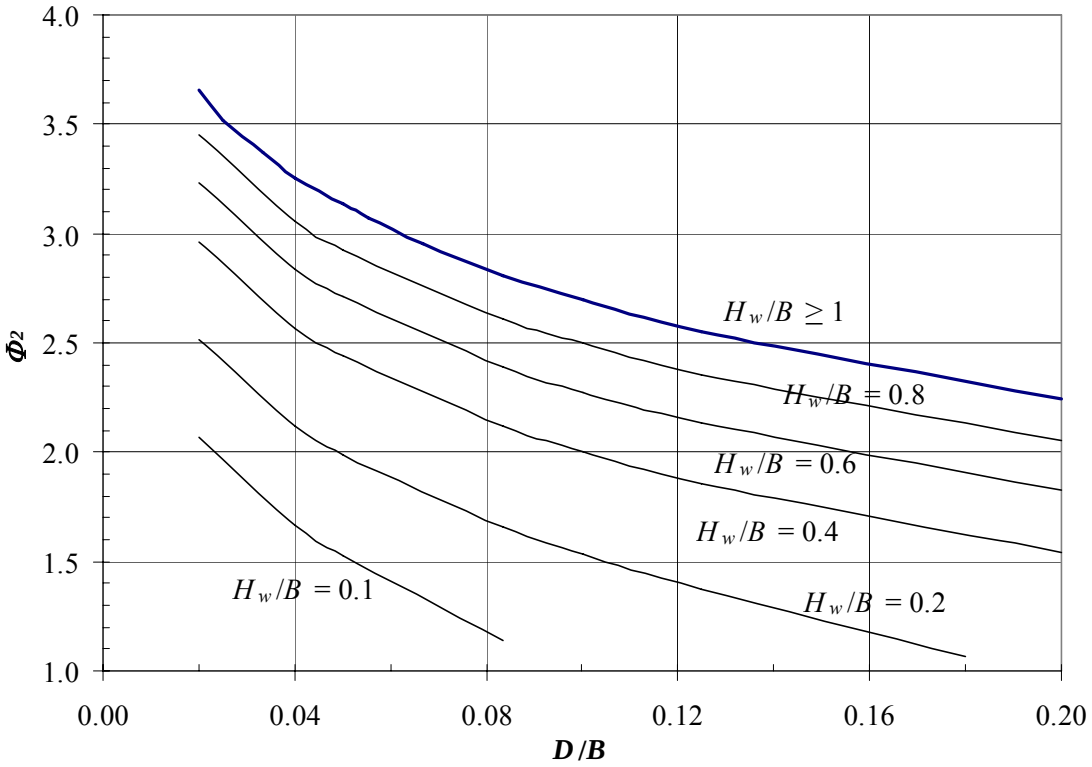

Figure 6.4 Form factor Φ_2 for fragment 2

It can be seen from Figure 6.4 that form factors are almost parallel for different H_w/B ratios. It has been observed that difference in Φ_2 is almost independent of D/B. Φ_2 remains constant for $H_w/B \geq 1$ and fragment above $H_w > B$ is Φ_1. Form factor 2 (Φ_2) for $H_w < B$ can be computed as following:

$$\Phi_2 = -1.414 \log \frac{D}{B} + 1.2752 - \left[0.75 \left(\frac{H_w}{B} \right)^2 + 1.65 \right] \log \frac{H_w}{B} \qquad (6.6)$$

Φ_2 have been calculated using Equation 6.6 and has been compared with Φ_2 computed from numerical model (Sivakugan et al., 2006; and Sivakugan and Rankine, 2006) for H_w/B = 0.4, 0.6 and 0.8 (Figure 6.5). It can be seen from the Figure 6.5 that empirical equations 6.5 and 6.6 give same results. Coefficient of determination for aforementioned empirical equation is 0.99, which shows very good correlation with existing data.

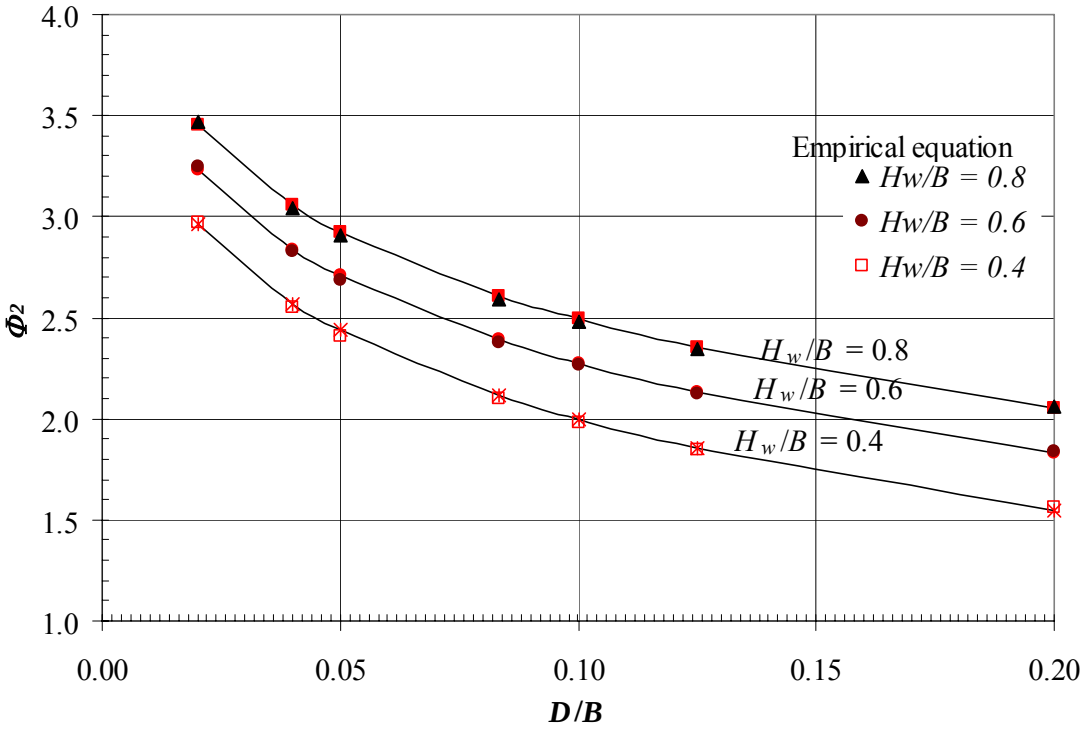

Figure 6.5 Comparison of form factor Φ_2 for fragment 2 computed using numerical method and empirical equation

6.3 Equivalent permeability

In most of the numerical modeling work carried out to date, simulating the drainage through hydraulic fills, it is assumed that the permeability of the fill remains constant

with depth (Isaacs and Carter, 1982; Sivakugan et al., 2006; Sivakugan and Rankine, 2006; and Rankine, 2007). The hydraulic fills at the mine stopes are under several meters of overburden. As discussed in Chapter 4 and Singh et al. 2008, that the permeability of hydraulic fills varies linearly with logarithmic of vertical effective stresses. Hydraulic fills transfer a part of its self weight to the adjacent rock mass in the process of self-weight settlement due their friction between hydraulic fill and adjacent rock wall (Sivakugan 2008). This process of reduction in vertical normal stress is known as arching. Stress reduction in a two dimensional vertical and inclined mine stope is discussed in Chapter 3 and Singh et al. (2008). Permeability variation with depth in a vertical mine stope are shown in Figures 4.16 and 4.17. It can be computed using Equations 3.29 and 4.3.

Sivakugan et al. (2006), Sivakugan and Rankine (2006), and Rankine (2007) estimated drainage and pore water pressure in a mine stope assuming that the permeability of hydraulic fills remains constant in the stope and method of fragments. Natural soils are laid down in layers so exhibit anisotropic properties. Usually the permeability in horizontal direction is higher than permeability in vertical direction (Lambe and Whitman, 1969; and Azizi, 1999). In this analysis, it has been assumed that hydraulic fills ate isotropic and vertical permeability is equal to horizontal permeability. As shown in the Figure 6.3, flow in mine stope is vertical in MNQPO region and it is horizontal in PQRS. Since horizontal permeability is always higher than vertical permeability, the assumption of equal permeability at P and R will underestimate the drainage from the stope. In this dissertation, permeability variation from P to Q in Figure 6.3 will be same as the permeability variation from R to S.

Permeability in a mine stope varies with depth as discussed in Chapter 4. As shown in Figure 4.19, permeability of saturated hydraulic fill varies with depth. It can be assumed that the permeability of hydraulic fills be constant in a differential depth of Δh, as shown in Figure 6.6. Mine stope has been divided in n segments of equal permeability and depth Δh (Figure 6.6). In this dissertation, concept of equivalent permeability has been

proposed to use a single value of permeability for computing drainage and pore-water pressure in the mine stope.

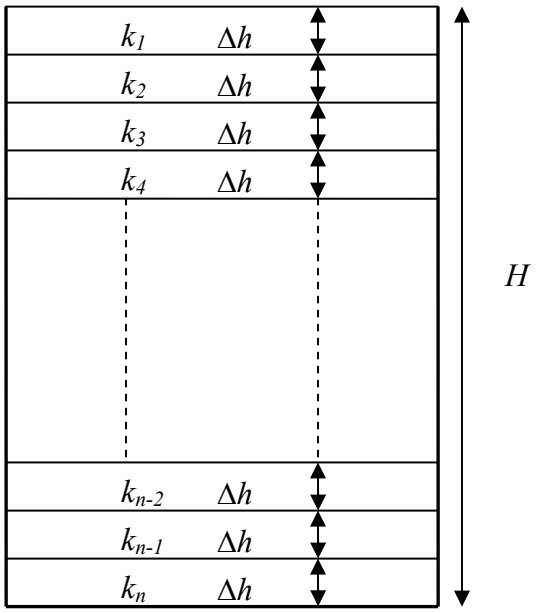

Figure 6.6 Schematic diagram showing permeability variation in a mine stope

If the permeability of individual layers are k1, k_2, k_3,… k_{n-2}, k_{n-1}, k_n, the equivalent permeability (k_{eq}) in a mine stope can be calculated as (Das, 2005):

$$\frac{H}{k_{eq}} = \frac{\Delta h}{k_1 + k_2 + \cdots + k_{n-1} + k_n} \tag{6.7}$$

or $$k_{eq} = \frac{H}{\sum_{i=1}^{n} \frac{\Delta h}{k_i}} \tag{6.8}$$

Substituting Equation 4.3 in Equation 6.8,

$$k_{eq} = \frac{H}{\int_0^H \frac{1}{a \log \sigma_v + k_0} dh} \tag{6.9}$$

where, a is permeability coefficient (Equation 4.4), σ_v is vertical effective stress in kPa under no surcharge, which varies with depth, and k_0 is permeability of hydraulic fills measured in laboratory from slurry sedimented sample.

Equivalent permeability of 5 hydraulic fills has been calculated using aforementioned methodology and the resulting stress reduction under no surcharge. It has been assumed that the hydraulic fill is saturated in the stope. Effects of arching have been considered while calculating the vertical effective stress in the stope. Variation of ratio of k_{eq}/ k_0 have been shown in Figure 6.7 and 6.8. As shown in Figure 6.7, the equivalent permeability can be reduce to 20% of permeability measured in laboratory for saturated hydraulic fills. So use of equivalent permeability is required in all drainage and pore water pressure analysis. Effect of equivalent permeability on drainage and pore water pressure is discussed later in this chapter.

Effect of stope width on equivalent permeability for sample A1 is shown in Figure 6.8. Equivalent permeability of hydraulic fills decreases with increases in stope width. When stope width is changed from 10 m to 50 m, equivalent permeability decreases to 0.44 from 0.6 at aspect ratio of 5. Equivalent permeability variation for other samples (B1, B2, C1 and C2) is shown in Appendix D.1.

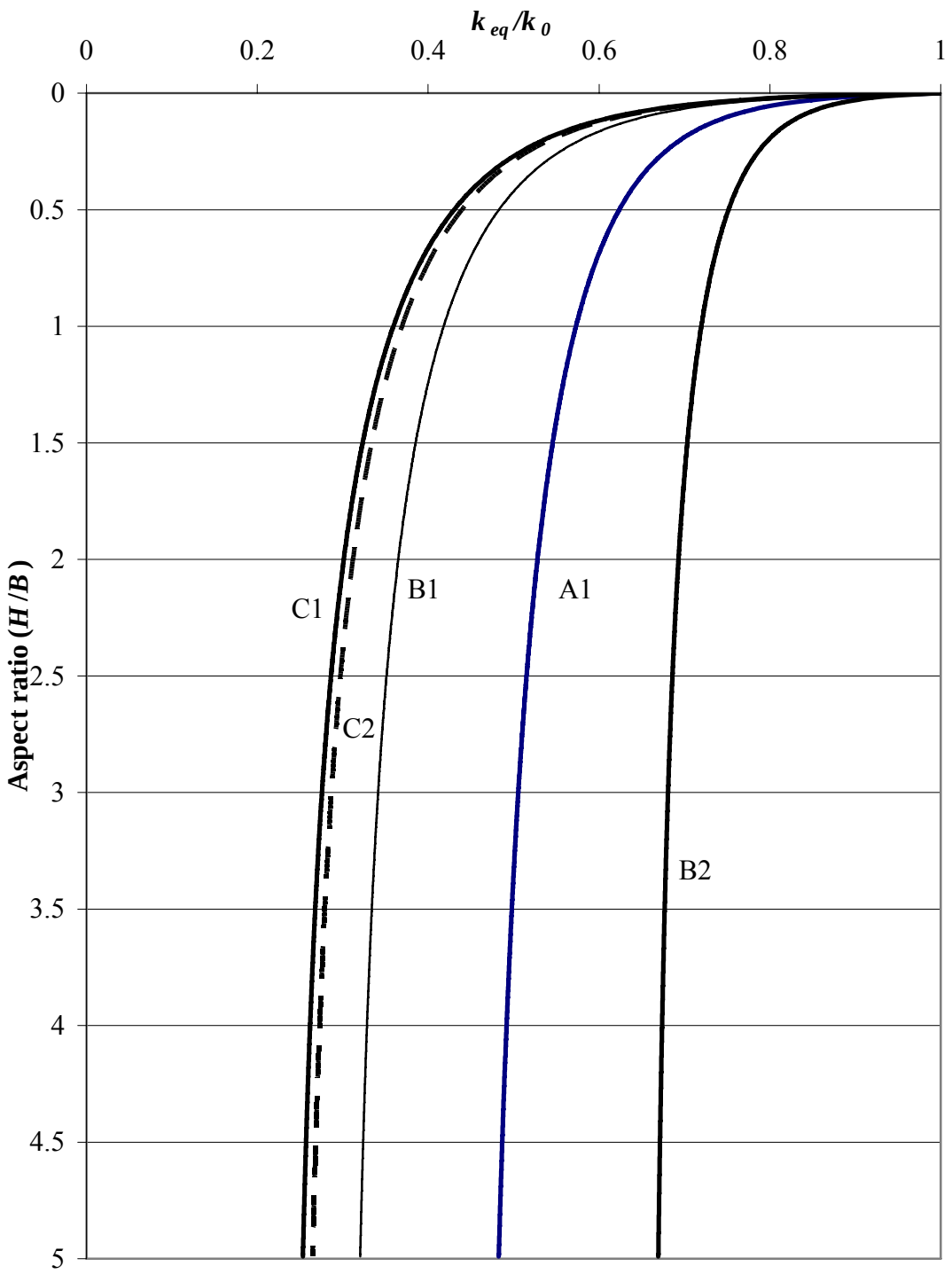

Figure 6.7 Variation of equivalent permeability (k_{eq}) in a mine stope for stope width of 30 m

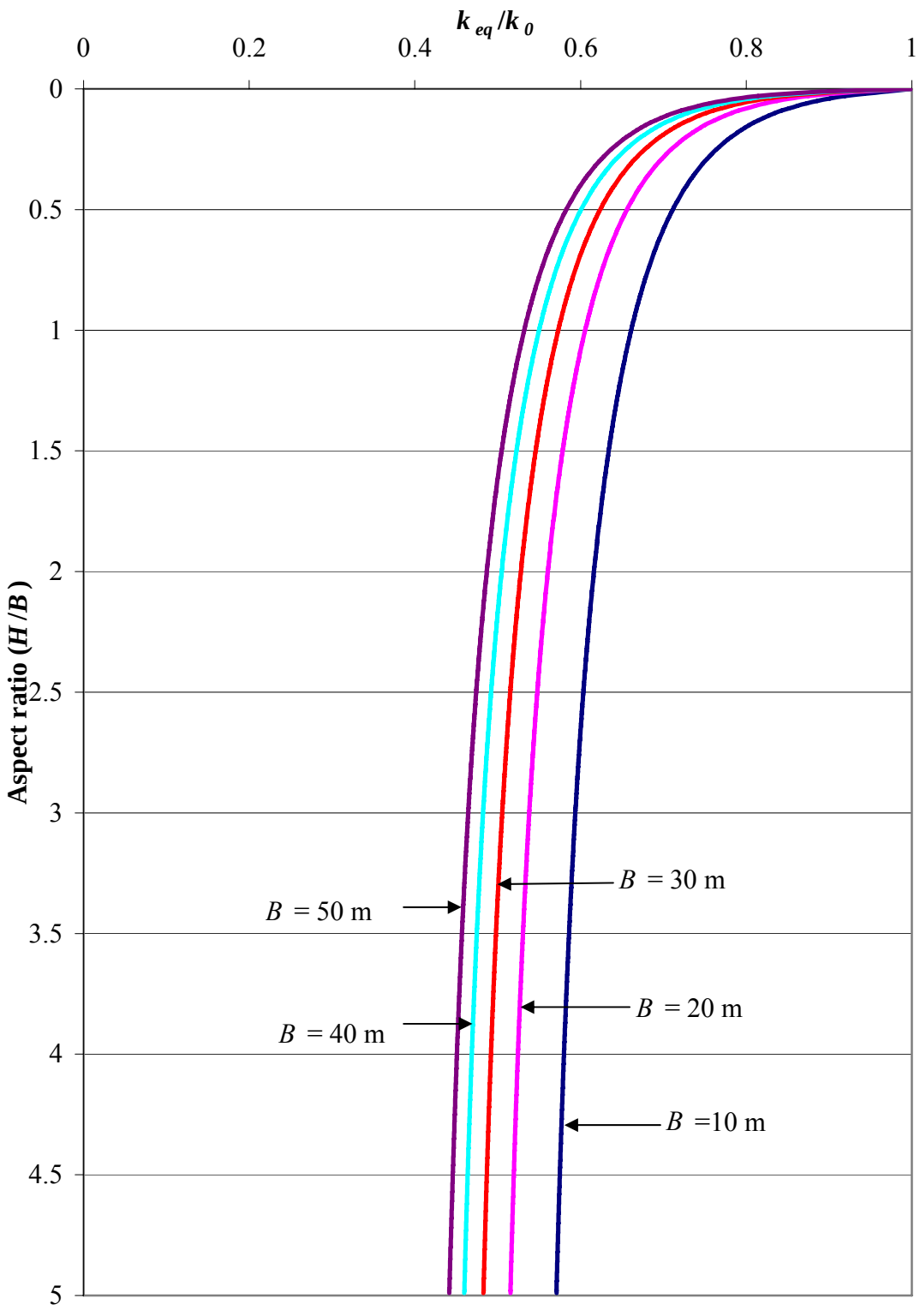

Figure 6.8 Effect of width of stope on equivalent permeability for hydraulic fill sample A1

6.4 Drainage from mine stope

It is essential to study the drainage and maximum pore water pressure in a mine stope for design of barricades. Backfilling and drainage are the simultaneous process. Drainage from mine stopes start as soon as the hydraulic fill is poured into the stope. In this section, analysis has been carried out to compute drainage and maximum pore water pressure from the stope. Backfilling and drainage are an unsteady state problem but series of steady state analysis has been used with adjusting the fill height and equivalent permeability. Fill height can be divided into solid height and water height. Isaacs and Carter (1983), Sivakugan and Rankine (2006), and Rankine (2007) assumed height of water (H_w) in a mine stope as the height of top surface of fill when the entire fill is saturated and upper boundary of saturated surface when fill is not saturated over full height. Above H_w, the fill was assumed dry (Isaacs and Carter, 1983; Sivakugan and Rankine, 2006; and Rankine, 2007). Since there is no clear separation between solid and water in the backfills and no clear separation line for saturated and unsaturated fill surface so use of height of water in the analysis is irrelevant and misleading. In this analysis, height of solid and water have been not separated as they were considered in the literature (Rankine, 2004; and Rankine, 2007). Fill height in the stope is considered as the combined height of hydraulic fill and water in the stope. In this dissertation, it is assumed that H_w is the height of top surface hydraulic fill for saturated hydraulic fill and H_w time degree of saturation for unsaturated hydraulic fills. Fill height increases during filling or pouring whereas it decreases at time of rest due to time dependent settlement and drainage of water.

Following assumptions have been made in estimating drainage and maximum pore water pressure in a mine stope.

i. Darcy's law is applicable;
ii. Hydraulic fills are isotropic;
iii. Top surface of hydraulic fill is horizontal; and

iv. Head loss through fragments (h_L) is the total height of fill (including decant water) for saturated hydraulic fills and total height of fill times degree of saturation for unsaturated hydraulic fill.

If rate of filling per hour is W and initial moisture content of the hydraulic fill slurry is w, then volume of fill entering the stope per hour (V_{in}) can computed as:

$$V_{in} = \frac{W}{G_s \gamma_w (1-n)(1+w)} \tag{6.10}$$

where, G_s is specific gravity of hydraulic fill, γ_w is unit weight of water and n is porosity of hydraulic fills (not in percentage).

Volume of water draining out the stope (V_{out}) can be calculated as following:

$$V_{out} = k_{eq}\, i\, A \tag{6.11}$$

where i is hydraulic gradient and A (=BL) is cross sectional area of stope. Sivakugan and Rankine (2006) established an empirical equation for hydraulic gradient as following:

$$i = \frac{1}{\Phi_1 + \Phi_2 + \Phi_3} \frac{H_{w(t)} - D}{B} \tag{6.12}$$

From Eqs. 6.11 and 6.12,

$$V_{out} = \frac{1}{\Phi_1 + \Phi_2 + \Phi_3} \frac{H_{w(t)} - D}{B} k_{eq} A \tag{6.13}$$

Where $H_{w(t)}$ is height of fill at a given time t, Φ_1, Φ_2 and Φ_3 are form factors for fragments 1, 2 and 3 respectively.

The height of fill $H_{w(t)}$, can be computed as:

$$H_{w(t)} = \frac{W}{B\,L\,G_s\,\gamma_w\left(1-n\right)\left(1+w\right)} \tag{6.14}$$

If the height of fill at time $t = t + \Delta t$ is $H_{w(t+\Delta t)}$,

$$H_{w(t+\Delta t)} = H_{w(t)} + \frac{W}{B\,L\,G_s\,\gamma_w\left(1-n\right)\left(1+w\right)}\Delta t - k_{eq} i_{(t)} \Delta t \tag{6.15}$$

where $i_{(t)}$ is hydraulic gradient at time $t = t$.

or $$H_{w(t+\Delta t)} = H_{w(t)} + \Delta\, H_{w(t)} \tag{6.16}$$

or $$\frac{\Delta H_{w(t)}}{\Delta t} = \frac{W}{B\,L\,G_s\,\gamma_w\left(1-n\right)\left(1+w\right)} - k_{eq} i_{(t)} \tag{6.17}$$

or $$\frac{dH_{w(t)}}{dt} = \frac{W}{BLG_s\gamma_w\left(1-n\right)\left(1+w\right)} - k_{eq}\frac{H_{w(t)}-D}{B}\frac{1}{\frac{H_{w(t)}-B}{B}+\frac{X-0.5D}{D}+\Phi_2} \tag{6.18}$$

where, equivalent permeability (k_{eq}), moisture content (w) and Φ_2 are function of fill height $H_{w(t)}$.

Head loss (h_L) at any time (t)can be computed as:

$$h_L\left(t\right) = H_{w(t)} - D \tag{6.19}$$

Sivakugan and Rankine (2006) proposed following equation to estimate maximum pore water pressure which occurs at the bottom corner of the mine stope as:

$$u_{\max} = \left[h_L \frac{\alpha \Phi_2 + \Phi_3}{\Phi_1 + \Phi_2 + \Phi_3} + D \right] \gamma_w \tag{6.20}$$

where, α is an empirical coefficient which can be calculated using following equation (Sivakugan and Rankine, 2006):

$$\alpha = \begin{cases} 0.84 - 0.54 \dfrac{D}{B} & \text{for } B \le H_w \\ -0.7788 \left(\dfrac{H_w}{B} \right) \left(\dfrac{D}{B} \right) + 0.2473 \left(\dfrac{D}{B} \right) - 0.2193 \left(\dfrac{H_w}{B} \right) + 1.0689 & \text{for } B > H_w \end{cases} \tag{6.21}$$

Aforementioned methodology can be used to estimate the variation of drainage, fill height, equivalent permeability, average moisture content and pressure head or hydraulic gradient with time in a vertical mine stope. An example has been discussed in section 6.4.1.

6.4.1 Problem definition

In this section, development of pore water pressure and drainage from a mine stope have been studied using aforementioned methodology. Analysis has been carried out for two-dimensional stope as shown in Figure 6.9. Stope geometry is shown in Figure 6.9, where width of stope is 20 m, length is 40 m, drainage height is 2 and drive length is 2 m.

Average moisture content in the stope has been calculated by deducting the amount of drained water from the total water in the stope. Permeability of hydraulic fill has been calculated using Equations 4.3 and 4.4. Equivalent permeability has been computed using Equation 6.9. Input parameters of analysis are shown in Table 6.1. It has been assumed that saturation moisture content of hydraulic fills is 27%.

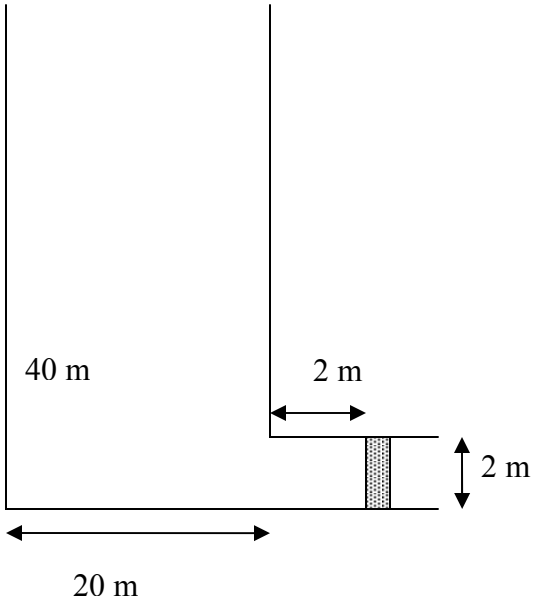

Figure 6.9 Stope geometry for drainage and maximum pore water pressure analysis

Table 6.1 Input parameter for drainage and maximum pore water pressure analysis

Input parameter	Value
Permeability without any surcharge (k_0)	33 mm/hr
Specific gravity (G_s)	3.1
Porosity (n)	0.45
Rate of filling (W)	150 t/hr
Filling time	100 hr
Rest time	50 hr
Saturation moisture content (w_s)	27%
Initial moisture content of slurry (w)	40%

Hydraulic fill slurry is poured for 100 hr and rest time is 50 hr. In this example, pouring is done in three (3) cycles. Figures 6.10 show the fill height (slurry) in the stope without drainage and fill height (with continuous drainage). If drainage is not allowed from the stope then fill height increases linearly during filling time and it remains constant during rest. Due to continuous drainage from the stope the fill height (hydraulic fill solid and

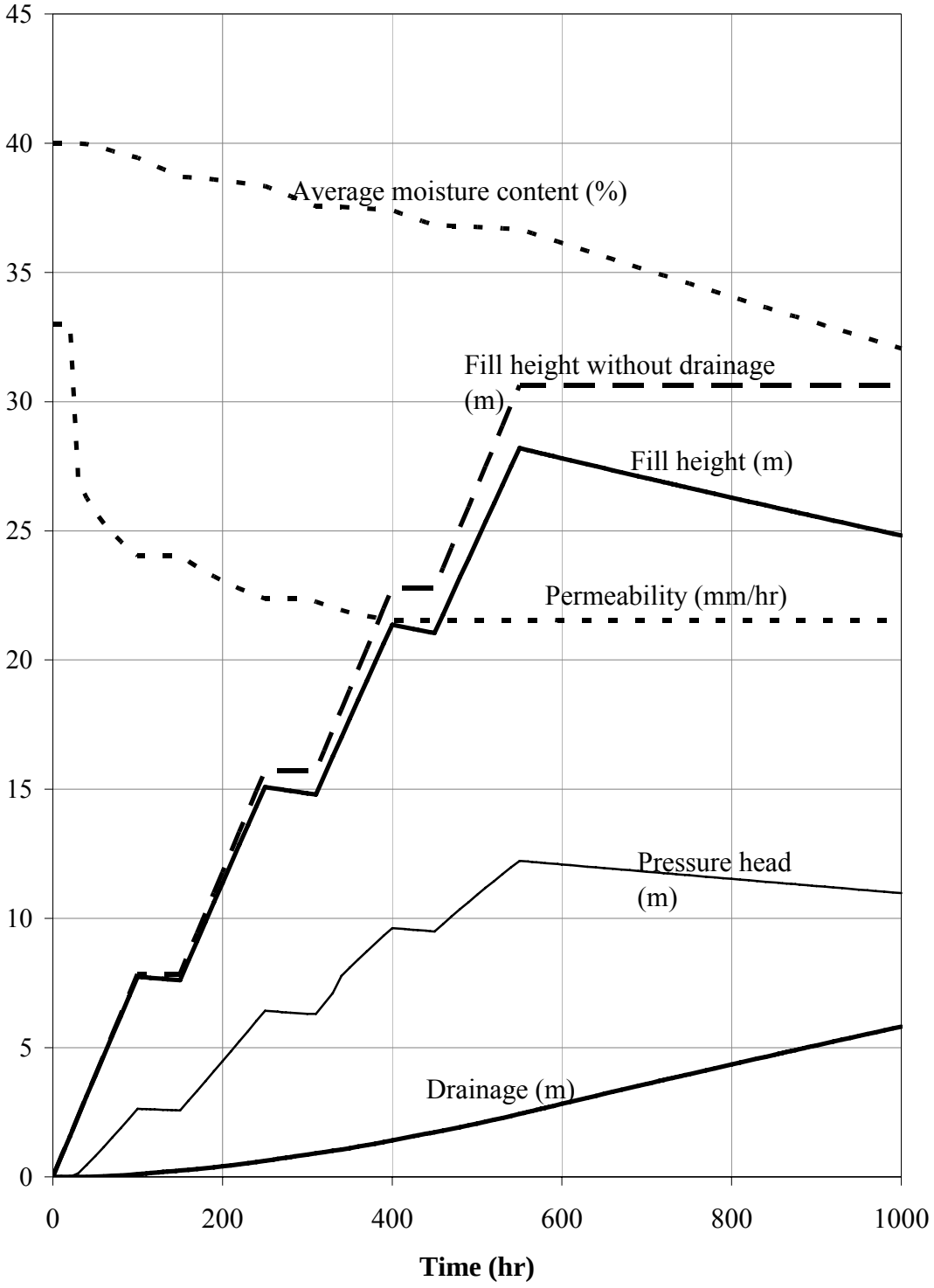

Figure 6.10 Variation of drainage and other parameters with time in a mine stope

water) gradually decreases and it always less than the fill height with out drainage. Volume of water draining out of the stope has been calculated and represented in form of

height by dividing volume by cross sectional area (Figure 6.10). Sum of drainage height and fill height will give the height of fill without the drainage. It can be verified from Figure 6.10.

Permeability of hydraulic fill (in this example) without any surcharge is 33 mm/hr. As discussed in Chapter 4, the permeability of hydraulic fill decreases with increase in vertical effective stress. It has been calculated at different depth due increase in the surcharge. Equivalent permeability has been computed using Eq. 6.9. It has been observed that equivalent permeability of hydraulic fills decreases with increase in the fill height. Equivalent permeability reduced to 22 mm/hr after 400 hr of filling, which is 33% reduction in the permeability. Effect of equivalent permeability on maximum pore water pressure has been discussed later in this section.

Moisture content of the hydraulic fill is another major property that influences the permeability and drainage. Average moisture content has been estimated by deducting the drained water from the stope (Figure 6.10). Saturation moisture content (w_s) of hydraulic fill varies from 22% – 27%. It has been observed that average moisture content continuously decreases with time in the stope. After 1000 hr (total 300 hr of filling and 700 hr of rest) the average moisture content reduced from initial moisture content of 40% to 33%, which is higher than saturation moisture content. It shows that more time is required for draining out the water from mine stope. If degree of saturation is less than 1 then permeability should be adjusted with moisture content, as discussed in chapter 4. In this example, degree of saturation is 1 so permeability is not adjusted with degree of saturation.

Maximum pore water pressure in the mine stope has been computed using Equation 6.20. Pressure head for calculating pore water pressure is shown in Figure 6.10 and maximum pore water pressure variation with time is shown in Figure 6.11. It has been observed that the maximum pore water pressure develops during backfilling of the stope and it decreases during rest (Figure 6.10 and 6.11). Maximum pore water pressure has been compared with constant permeability of 33 mm/hr (permeability without any surcharge,

k_0) throughout the stope and equivalent permeability estimated using the methodology discussed in Section 6.3. Since equivalent permeability is lower than the 31 mm/hr, so rate of drainage from stope will be slower. Maximum pore water pressure is lower in case of constant permeability throughout the stope. It shows that equivalent permeability should be used to improve the design of barricades and estimate the pore water pressure.

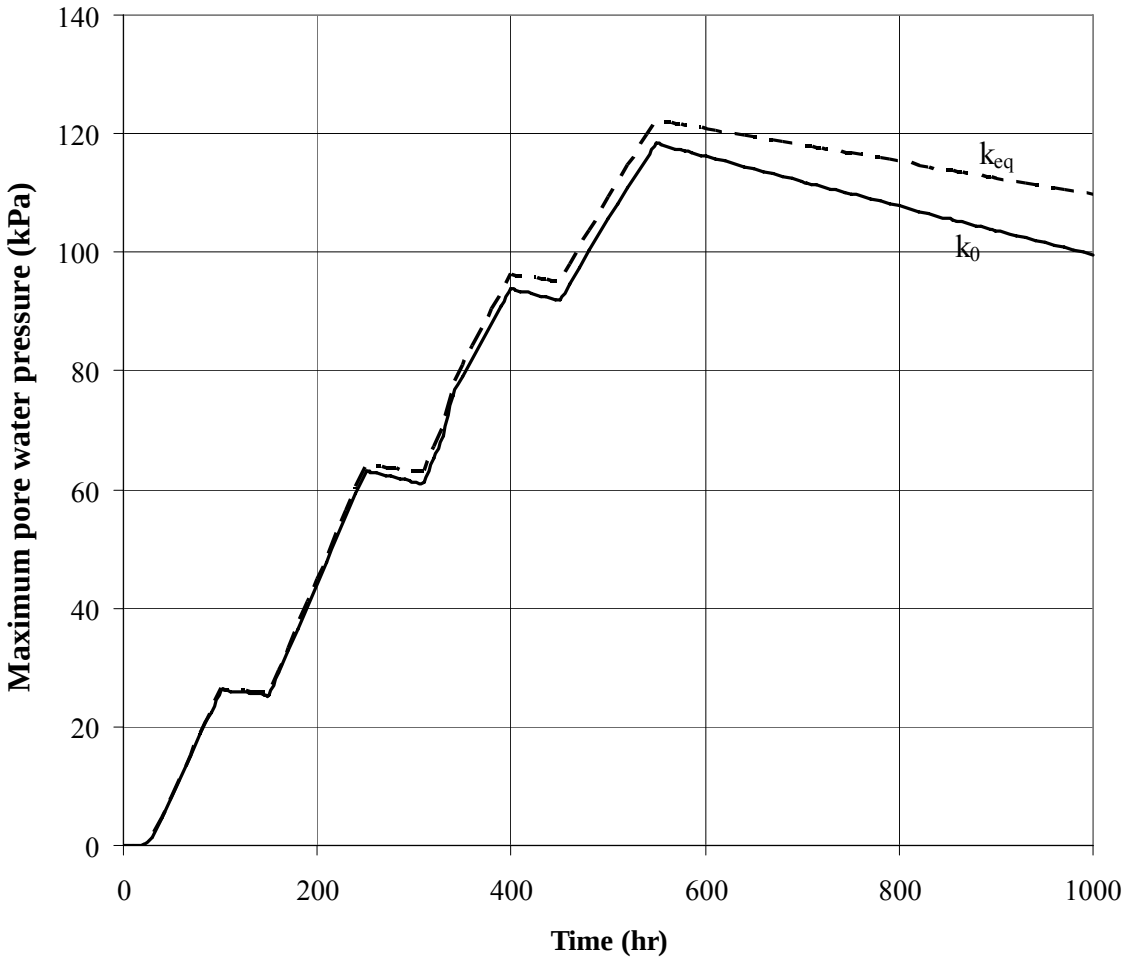

Figure 6.11 Effect of permeability on maximum pore water pressure

6.5 Summary and conclusions

Excess water in hydraulic fill slurry initially tends to pond on the surface building up from lowest corner of the stope and then commences a vertical path of drainage due to

gravity. Barricades, high permeably bricks (of permeability 2 – 3 order of the permeability of hydraulic fills), allow water to drain quickly and retain the backfills. Buildups of high pore water pressure behind the barricades have been a major cause for several mine failures. Mine stopes are backfilled in batches. Normally filling time is more than rest time.

Method of fragments have been used in the literature to compute drainage and maximum pore water pressure in a mine stope. Two dimensional mine stopes can be divided into three fragments (Figure 6.2 and 6.3). Sivakugan and Rankine (2006), Sivakugan et al. (2006) and Rankine (2007) established empirical equations for form factors Φ_1 and Φ_3 using equipotential lines in terms of stope geometry using flow net in two dimensional stope. Sivakugan and Rankine (2006) developed numerical model using finite difference software FLAC to compute Φ_2. In this dissertation, an empirical equation has been proposed for form factor Φ_2 (Equation 6.6). Equation 6.2 can be used to calculate drainage from the stope.

In most of the numerical and analytical solutions of drainage in a mine stope, it is assumed that permeability of hydraulic fills remains constant throughout the stope depth. The hydraulic fills at the mine stopes are under several meters of overburden. As discussed in Chapter 4, the permeability of hydraulic fills varies linearly with logarithmic of vertical effective stresses. Concept of equivalent permeability has been proposed to use a single value of permeability for computing drainage and pore-water pressure in the mine stope. Equation 6.9 can be used to compute equivalent permeability in a mine stope. Equivalent permeability variation of five hydraulic fill samples is shown graphically (Figures 6.7 and 6.8). It may reduces to 20% at aspect ratio of 5.

Drainage and maximum pore water pressure variation in a mine stope has been derived using method of fragments. Effect of drainage of water during filling has been considered in estimating fill height in the stope. Equations 6.20 and 6.21 have been used to calculate maximum pore water pressure in the stope. Due to continuous drainage from the stope the fill height (hydraulic fill solid and water) gradually decreases and it always less than

the fill height without drainage. Since there is no clear separation between solid and water in the backfills so it will be misleading to estimate them separately. In this analysis, height of solid and water have been not separated as they were considered in the literature.

An example has been solved (Section 6.3.1) to show the effect of different parameters on the drainage and maximum pore water pressure. It has been observed that the use of constant permeability underestimates the maximum pore water pressure. Permeability and average moisture content in mine stopes decreases rapidly as shown in Figure 6.10. After this analysis, it has been concluded that equivalent permeability should be used to estimate drainage and maximum pore water pressure. Height of fill and permeability of hydraulic fill should be adjusted with the change in moisture content.

Chapter 7

Reliability of Drainage and Pore Water Pressure Analysis

7.1 General

Drainage and pore water pressure are two major concerns in design of barricades and stopes. Several mines have failed due to excess drainage and higher pore water pressure during backfilling. In this dissertation, method of fragments has been used to estimate maximum pore water pressure and drainage. Sivakugan and Rankine (2006), and Sivakugan et al. (2006) verified method of fragments using finite difference software FLAC and FLAC^{3D}. These analyses are based on the several empirical equations and laboratory measurements. Since, it is very difficult to get in-situ data for verification, it is required to study the error or uncertainty in the analysis. Errors and uncertainties in modeling and in measurement data make it difficult to predict a single value for the physical variables involved. It is more desirable to present a likely or probable interval, and ideally specify a reliability measure associated with each prediction. Therefore a methodology based on first order uncertainty analysis to estimate these uncertainties is presented. There are two type of uncertainty in any analysis based on empirical equations. First type of uncertainty is model error, which is imperfection or error in theoretical relationships in the modeling. Parameter uncertainty or error in estimation of the parameter is second type of uncertainty. Total uncertainty (error) in drainage and pore water pressure analysis should be computed using probability models.

Several probabilistic methods have been developed to measure the distribution functions of random variables. Exact Method, First Order Second – Moment Method are most common. Exact Method requires probability distribution function of all component variables to be known initially. Numerical integrations and Monte Carlo Methods are exact method of reliability analysis. In this methodology, complete probability functions of dependent variables are estimated. The second method is known as First Order Second-Moment Method (FOSM). Taylor series expansion of the function form is the basis of FOSM (Sagar, 1978; Dettinger and Wilson, 1981; Townley and Wilson, 1985; Connel, 1995; and Glasgow et al., 2003). Inputs and outputs are expressed as expected value (mean value) and standard deviation (Harr, 1987). First Order Second-Moment Method and Monte Carlo Method are explained later in this chapter. In this dissertation, FOSM has been used to determine probability distribution function of the variable values. Monte Carlo method has been used to verify the developed approach.

7.2 First Order Second-Moment Analysis

First Order Second-Moment provides two moments, mean and covariance to estimate the probability distribution function. This method is based on Taylor series expansion, where second and higher order terms are truncated (Glasgow et al., 2003). McLaughlin and Wood (1988a, b) used a Taylor series to derive expressions for the two moments (mean and covariance) of a discretised model. It combines the sensitivity of a model and covariance of the input data to covariance of output. Sensitivity represents how sensitive the model output is to a small change in the input. It is computed by taking derivatives of output $\left(\frac{doutput}{dinput}\right)$. The covariance of the model describes the spatial uncertainty associated with either input or output data. Banerjee and Datta (1991) explained the methodology to estimate covariance and mean of a model. It has been used to compute total uncertainty in drainage and pore water analysis. The basic methodology is briefly discussed below.

It is assumed that A can be approximated by a function of several random variable X_1, X_2, ... , X_n as follows:

$$A = \hat{F}\left(X_1, X_2, ..., X_n\right) \tag{7.1}$$

where, $\hat{F}$ is approximation of unknown exact theoretical expression F.

Total uncertainty in the prediction of any quantity depends on uncertainty associated with the approximate nature of function $\hat{F}$, and uncertainties associated with the estimate parameters, which are the random variables such as X_1, X_2, ... , X_n in Equation 7.1. If predicted value of the parameters is $\hat{X}_i$ and mean of predicted value is $\overline{X}_i$, the coefficient of variation of parameter X_i is:

$$\delta_{X_i} = \frac{\sigma_{\hat{X}_i}}{\overline{X}_i} \tag{7.2}$$

where $\sigma_{\hat{X}_i}$ is the standard deviation of the predicted values of $\hat{X}_i$. The coefficient of variation can be estimated from a set of laboratory or field test or data available in literature. In this dissertation, coefficients of variation of geotechnical parameters given by Harr (1987) have been used. If the parameters are determined through empirical equations or theoretical correlations that involves approximation, then actual parameter value of X_i can be given by following:

$$X_i = N_{X_i} \hat{X}_i \tag{7.3}$$

where N_{Xi} is assumed to be random variables with a mean of 1.0 and coefficient of variation (COV) of Δ_{Xi} (Banerjee and Datta, 1991). It represents estimated error in parameter X_i. Δ_{Xi} is zero when the predictions are very accurate or the parameters are

measured in the laboratory. Total uncertainty (Ω_{Xi}) in the prediction of parameter of X_i can be computed as follows:

$$\Omega_{X_i} = \sqrt{\delta_{X_i}^{\ 2} + \Delta_{X_i}^{\ 2}} \tag{7.4}$$

Standard deviation (σ_{X_i}) of actual parameter X_i is given by

$$\sigma_{X_i} = \Omega_{X_i} \overline{X}_i \tag{7.5}$$

The exact theoretical expression (F) of A and its approximate expression ($\hat{F}$) can be related as:

$$F = N_F \hat{F} \tag{7.6}$$

where N_F is a random variable with mean of 1.0 and coefficient of variation of Δ_F. It represents estimation error due to imperfect functional relationship. Coefficient of variation (δ_F) can be calculated as:

$$\delta_F = \frac{\sigma_{\hat{F}}}{\overline{A}} \tag{7.7}$$

where $\overline{A}$ is the mean of predicted value of A and $\sigma_{\hat{F}}$ is the standard deviation of predicted value A. Total uncertainty (Ω_F) in exact function F can be given by

$$\Omega_F = \sqrt{\delta_F^{\ 2} + \Delta_F^{\ 2}} \tag{7.8}$$

Total uncertainty of A can be estimated as (Banerjee and Datta, 1991):

$$\Omega_A^2 = \Omega_F^2 + \frac{1}{\bar{A}^2}\left(\sum_i C_i \sigma_{X_i}^2 + \sum_{i \neq j}\sum \rho_{ij} C_i C_j \sigma_{X_i} \sigma_{X_j}\right) \tag{7.9}$$

where $\bar{A}$ is mean of predicted value of *A*; $C_i = \left.\frac{\partial \hat{F}}{\partial X_i}\right|_{X_i}$; and ρ_{ij} is cross-correlation between parameters X_i and X_j. Standard deviation (σ_A) of predicted value of A can be written as

$$\sigma_A \cong \Omega_A \bar{A} \tag{7.10}$$

These standard deviation and coefficient of variation are used to estimate the probability distribution function for the actual value of the variable, given a predicted value. In this chapter, FOSM has been used to estimate uncertainty and reliability in the empirical analysis of drainage and maximum pore pressure.

7.3 Monte Carlo Simulation

Monte Carlo simulation is one of the most common method for calculating uncertainty (Wagner and Gorelick, 1987, 1992; Lee and Kitanidis, 1991; and Glasgow et al., 2003). In this method, coefficient of variance of model output are estimated from a set of random generated input variables. Monte Carlo simulation is used for nonlinear or multivariable parameters. Random values are selected to conform with assumed distribution of each variable. It shows that all values are equally likely with appropriate limit for a uniform distribution. In this dissertation, Microsoft Excel has been used to generate random numbers for beta distribution. It has been used to verify reliability analysis performed using the First Order – Second Moment Method.

7.4 Reliability of drainage analysis of stope

Methodology for estimating drainage and maximum pore water pressure has been discussed earlier in Chapter 6. Method of fragments is used to compute the form factors

and drainage parameters. Form factors for calculating drainage depends on the geometry of stope and hydraulic fill properties such as permeability, specific gravity, etc (Sivakugan and Rankine , 2006; and Sivakugan et al., 2006). Rate of drainage (q) in a mine stope can be computed as:

$$q = \frac{W}{G_s \gamma_w (1-n)(1+w)} - k_{eq} \frac{H-D}{B} \frac{BL}{\frac{H-B}{B} + \frac{X-0.5D}{D} + \Phi_2} \tag{7.11}$$

where, k_{eq} is equivalent permeability, w is moisture content and Φ_2 is the form factor 2 (as discussed in Chapter 2), H is height of saturated fill, G_s is specific gravity of hydraulic fill, γ_w is unit weight of water, n is porosity of hydraulic fills, B is width of stope, L is length of stope, D is drainage height and X is drive length of stope.

Maximum pore water pressure (u_{max}) in a mine stope can be calculated as follows (Chapter 6):

$$u_{\max} = \left[(H-D) \frac{\alpha \Phi_2 + \frac{H-B}{B}}{\frac{H-B}{B} + \Phi_2 + \frac{X-0.5D}{D}} + D \right] \gamma_w \tag{7.12}$$

where, α is an empirical coefficient which can be calculated using following equation (Sivakugan and Rankine, 2006). Equations 7.11 and 7.12 are based on several empirical equations. Uncertainty in the above models for estimating the rate of drainage and maximum pore water pressure are discussed in following section.

7.4.1 Uncertainty in permeability

Permeability of hydraulic fill, measured in laboratory is generally under no surcharge, whereas hydraulic fills at the mine stopes are under several meters of overburden (surcharge). Empirical equation has been developed using laboratory models to predict the permeability variation with stress (Chapter 3; Singh et al., 2008). Equivalent

permeability that has been used in Equation 7.11, has both modeling uncertainty (error associated with the empirical equation) and parameter estimation uncertainty (error in laboratory tests and measurement). Permeability of hydraulic fill (k) in a mine stope can be estimated as:

$$k = a\log\left(\frac{\gamma\,\delta\,B\,\mathrm{cosec}\,\delta}{2\left(\sin^2\delta + K\cos^2\delta\right)\tan\delta}\left\{1-\exp\left(-\frac{8H\left(\sin^2\delta + K\cos^2\delta\right)\tan\delta\sin\delta}{B\left[2\left(1+K\right)\delta+\left(1-K\right)\sin 2\delta\right]}\right)\right\}\right)+k_0 \quad (7.13)$$

where, a is permeability coefficient, γ is unit weight of hydraulic fills, B is width of stope, δ is hydraulic fill – stope wall interface angle, K is earth pressure coefficient, H is height of stope, and k_0 is permeability measured in laboratory. Stress reduction in the mine stope due to arching has been taken into consideration in estimating permeability in Equation 7.13. Permeability of hydraulic fill depends on γ, B, K, H, δ and k_0. Because, Since width of stope and height of fill can be measured accurately, it has been assumed that uncertainty in measuring B is zero. Permeability of hydraulic fill can be expressed as following:

$$k = f\left(a,\gamma,k_0,\delta,K\right) \quad (7.14)$$

where, f is a function defining the predicted value of permeability. Coefficients of variation of $a,\gamma,k_0,\delta,$ and K are given in Table 7.1 (Harr, 1987). These are used in estimating standard deviation and coefficient of variation of permeability. Cross correlation of parameters can be computed using linear regression (Benjamin and Cornell, 1970). Figure 7.1 shows a typical example of cross correlation variables. Cross correlation coefficient of parameter $a,\gamma,k_0,\delta,$ and K , obtained from laboratory test data and data available in literature, are given in Table 7.2. Using Equation 7.9, total uncertainty in the estimation of permeability can be given by:

$$\Omega_k^2 = \Omega_{\hat{F}}^2 + \frac{1}{k^2}\left(\sum_i C_i^2\sigma_{Xi}^2 + \sum_{i\neq j}\sum\rho_{ij}C_iC_j\sigma_{Xi}\sigma_{Xj}\right) \quad (7.15)$$

where C_i is derivative of permeability with respect to parameters, ρ is cross correlation coefficient, σ_{xi} is standard deviation of parameter x_i, $\hat{F}$ is the function for predicting permeability and $\Omega_{\hat{F}}$ is uncertainty in modeling. In the illustrative solution presented here, it has been assumed that $\Omega_{\hat{F}}$ for permeability analysis is 0.1, which is a measure of the modeling or functional uncertainty, based on accuracy of the model.

Table 7.1 Coefficient of variation of parameters used in estimating permeability of hydraulic fills

Parameter	Coefficient of variation (COV)
A	0.05
γ	0.1
K	0.05
δ	0.05
K_0	0.05

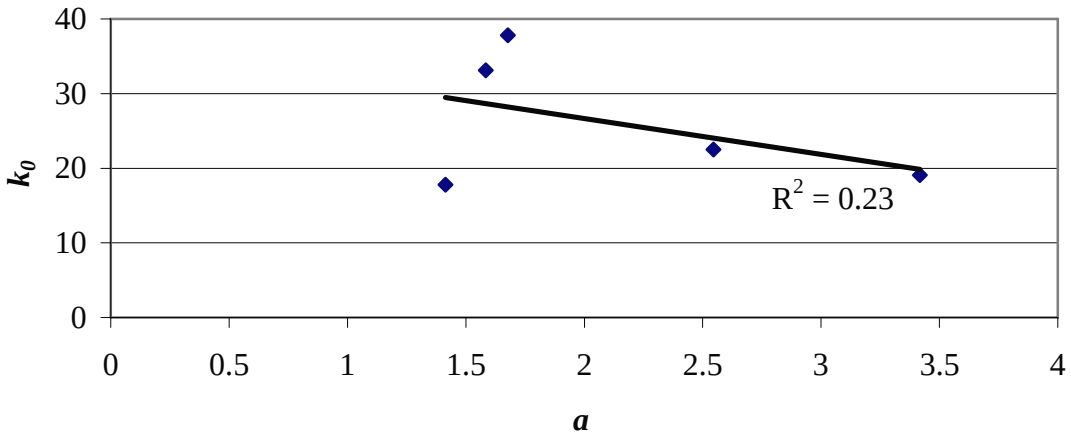

Figure 7.1 Correlation between a and k_0

Table 7.2 Cross correlation coefficient of parameter $a, \gamma, k_0, \delta,$ and K

for hydraulic fill

ρ	A	γ	K	δ	k_0
a	1	–0.985	–0.203	–0.203	–0.23
γ	–0.985	1	–0.235	–0.235	–0.258
K	–0.203	–0.235	1	0.507	0.507
δ	–0.203	–0.235	0.507	1	0.507
k_0	–0.23	–0.258	0.507	0.507	1

Total uncertainty in permeability has been calculated using methodology discussed in this section and by using Equation 7.15. It has been assumed subjectively that coefficient of variation of random variable (N_{xi}) of parameters is 0.15 for unit weight, and 0.1 for other parameters. Total uncertainties in permeability for hydraulic fill samples have been computed and it has been used to estimate standard deviation. Variation of standard deviation of permeability has been computed using Equations 7.10 and7.15, and its variation with depth of mine stope is shown in Figure 7.2. Standard deviation of hydraulic fill samples decreases with increase in depth and width ratio (z/B) as shown in Figure 7.2. These obtained values have been used in estimating total uncertainty in drainage and pore water pressure analysis.

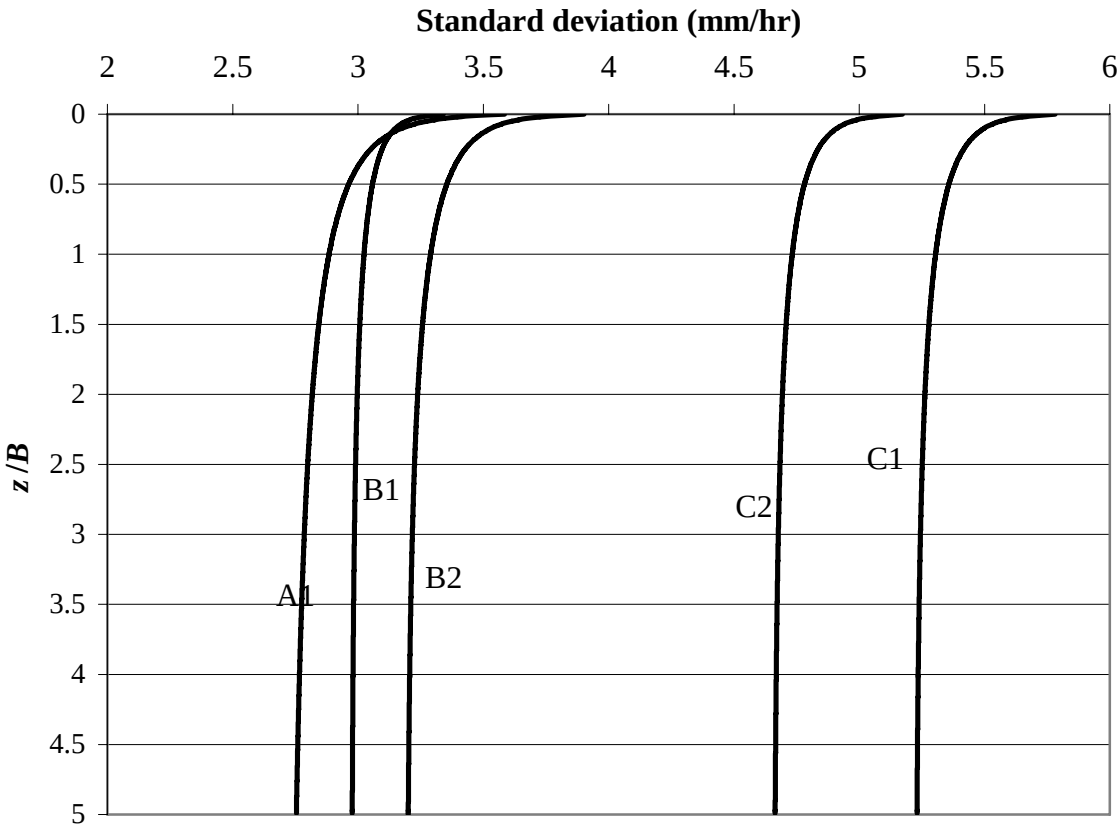

Figure 7.2 Standard deviation of permeability for hydraulic fill samples

7.4.2 Uncertainty in drainage

Drainage (q) from mine stope of fill height H, width B and length L can be computed using Equation 7.11. Uncertainty in drainage is function of uncertainties in rate of filling (W), specific gravity (G_s), porosity (n), moisture content (w) and equivalent permeability (k_{eq}). It has been assumed that parameters associated with stope geometry are measured accurately and they do not have any error. Since all form factors (Φ_1, Φ_2, and Φ_3) are based on empirical equation so coefficient of variance for Φ_1, Φ_2, and Φ_3 is assumed as 0.1. Coefficient of variance and standard deviation (Sample B2) for specific gravity (G_s), porosity (n), moisture content (w) and equivalent permeability (k_{eq}) are shown in Table 7.3. It has been assumed that the coefficient of variance of these parameter will not change with change in stope geometry and other fills used for backfilling. Since mean of

equivalent permeability and moisture content varies with depth of stope and time, they have not been included in Table 7.3.

Table 7.3 Coefficient of variation and standard deviation of parameters for Sample B2 for uncertainty analysis in drainage

Parameter	Coefficient of variation (COV)	Mean	Standard deviation (σ_{xi})
G_s	0.02	3.02	0.0604
n	0.1	0.45	0.045
w	0.1		
$k_{eq\ (mm/hr)}$	0.21		
W(tonne/hr)	0.05	150	7.5

Uncertainty in drainage analysis has been computed using First Order – Second Moment as discussed in section 7.2. Since rate of filling (W) is independent of stope geometry and other parameters so cross correlation coefficient for W is assumed to be zero with all other parameters in Equation 7.11. Cross correlation coefficient and derivatives have been computed as discussed earlier. For illustrative purpose, it has been assumed that uncertainty in modeling error of drainage is 10%. Total uncertainty in drainage for fill height of 25 m, stope width 20 m, stope length 40 m, barricade height of 2 and drive length of 2m for slurry with initial moisture content of 40% and fill rate of 150 t/hr is 0.154. Beta distribution has been used to estimate the probability distribution function of drainage using mean and standard deviation calculated using FOSM. The probability distribution function of drainage is shown in Figure 7.3. Monte Carlo method has been used to verify probability distribution function. Probability distribution has been plotted for a normalized variable q*, which is given as:

$$q^* = \frac{q - q_{\min}}{q_{\max} - q_{\min}} \tag{7.16}$$

where q_{max} and q_{min} are maximum and minimum drainage from stope respectively. As it has been shown in Figure 7.3, FOSM and Monte Carlo simulation have good agreement with probability distribution function.

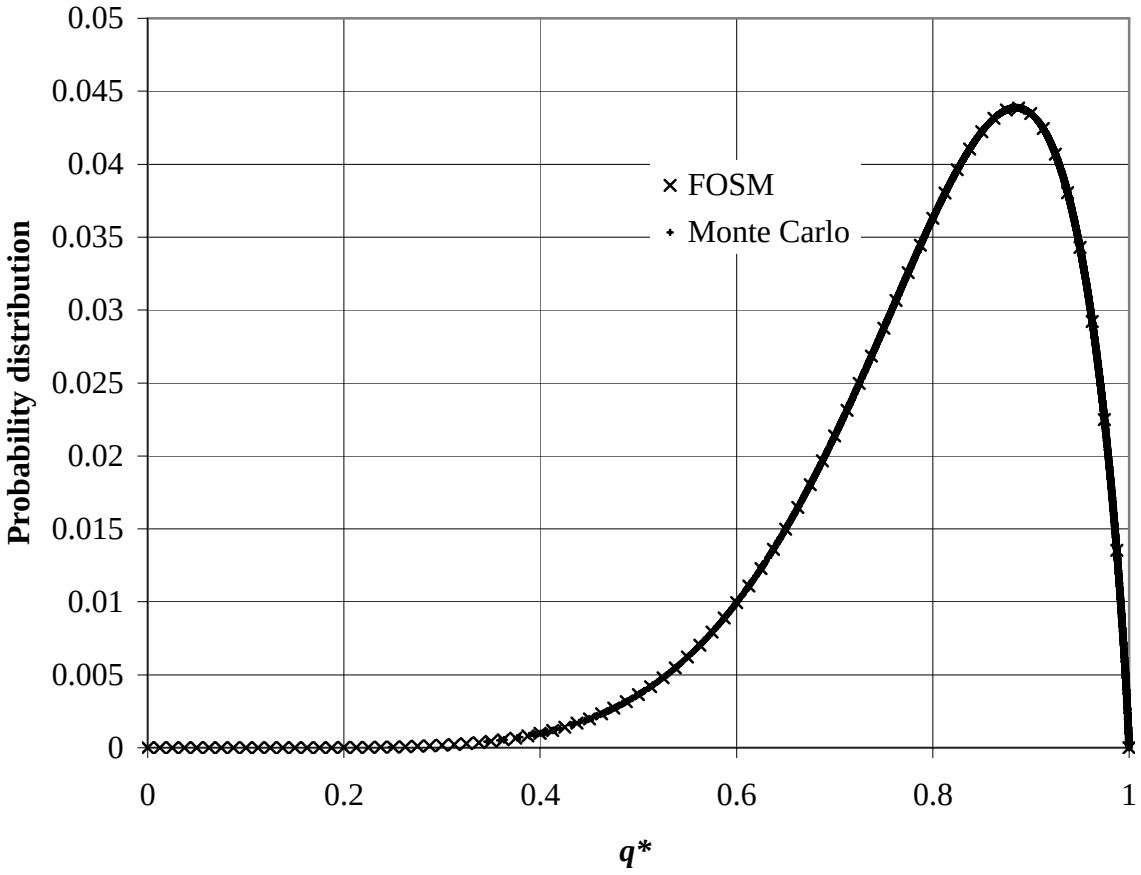

Figure 7.3 Probability distribution function for drainage from mine stope

7.4.3 Uncertainty in pore water pressure

In this dissertation, method of fragments has been used to estimate maximum pore water pressure in a mine stope. It has been discussed in Chapter 6. Equation 7.12 has been recommended to calculate maximum pore water pressure. It can be seen from Equation 7.12, maximum pore water pressure is a function of fill height (H), height of barricades (D), form factors Φ_1, Φ_2, and Φ_3 and unit weight of water. Drainage and height of fill

have same degree of uncertainty. Uncertainty in fill height is 0.154. It has been assumed that uncertainty in empirical equation of pore water pressure is 0.1. First Order – Second Moment method has been used to estimate total uncertainty in pore water pressure. Uncertainty in modeling of empirical coefficient of pore water pressure is assumed to be 0.1. Total uncertainty in maximum pore water analysis is 0.11. Beta distribution has been used to estimate the probability distribution function of maximum pore water pressure has been plotted the normalized variable u^* (Figure 7.4), which is given as:

$$u^* = \frac{u - u_{\min}}{u_{\max} - u_{\min}} \tag{7.17}$$

where u, u_{max}, u_{min} are pore water pressure, maximum pore water pressure and minimum pore water pressure respectively.

Cumulative probability distribution of pore water pressure $u < u^*$ has been shown in Figure 7.5. It has been observed that the probability range of pore water pressure has a narrow band. It shows that probability of measuring $u^* < 0.5$ is zero. It shows that the degree of uncertainty in pore water pressure analysis is low.

After defining probability distribution function, it is possible to estimate confidence interval for predicted value of pore water pressure. Confidence limit of 80% has been used to compute confidence interval for example in Chapter 6 (Section 6.4.1). Central confidence interval has been used in this analysis. It means the limit has been calculated for probability of 10% and probability of 90%. It has been shown in Figure 7.5. As discussed earlier pore water pressure falls in a narrow band for confidence limit of 80%. Confidence interval of pore water pressure has been plotted for confidence limit of 90% and is shown in Figure 7.6. The band width increases with time and increase in fill height. For the data used for the illustrative purpose, it appears that uncertainty of 0.09 – 0.12 may be reasonable for estimation of pore water pressure.

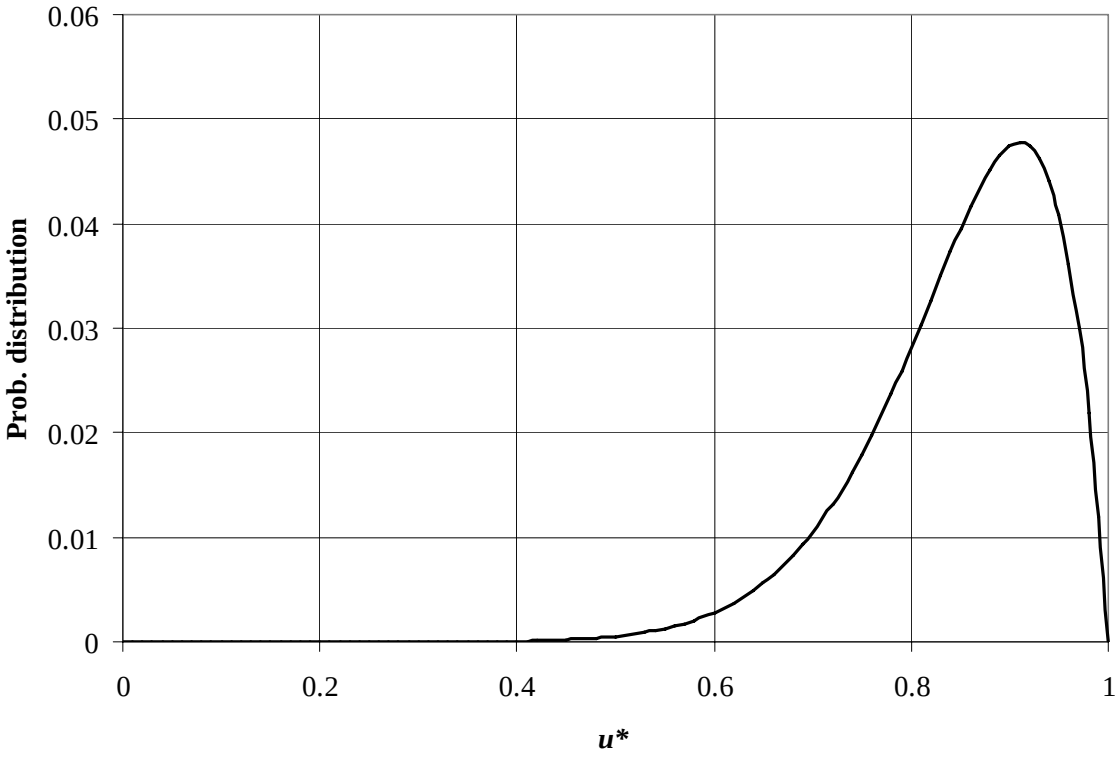

Figure 7.4 Probability distribution function for pore water pressure

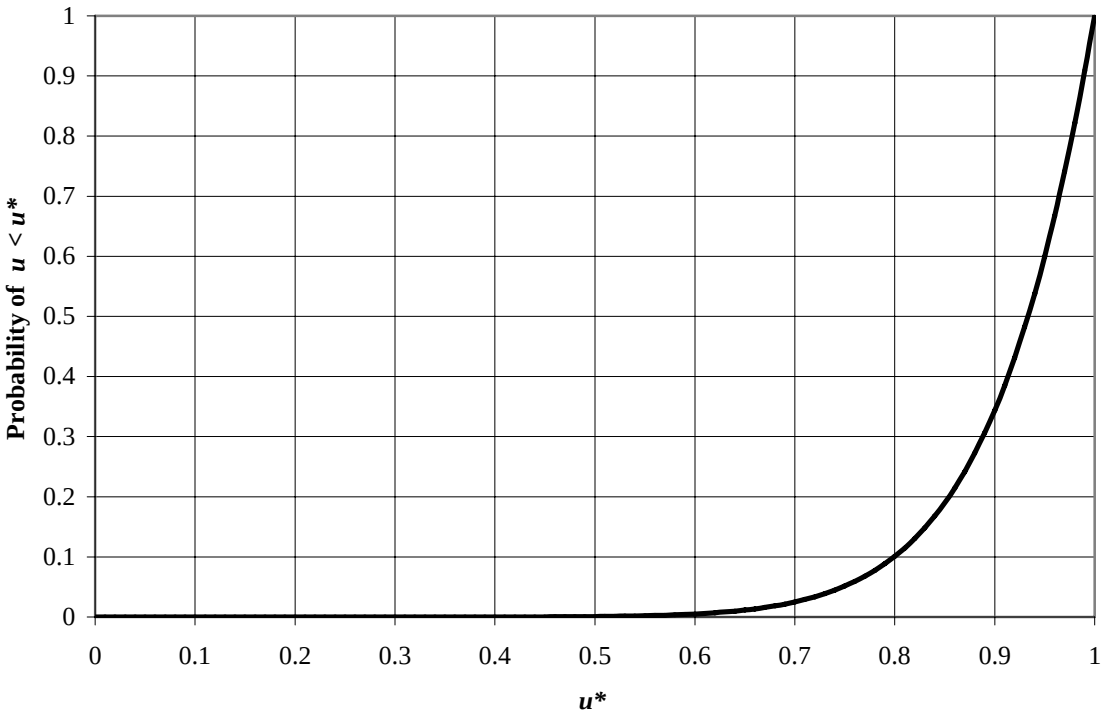

Figure 7.5 Cumulative probability of distribution of $u < u^*$

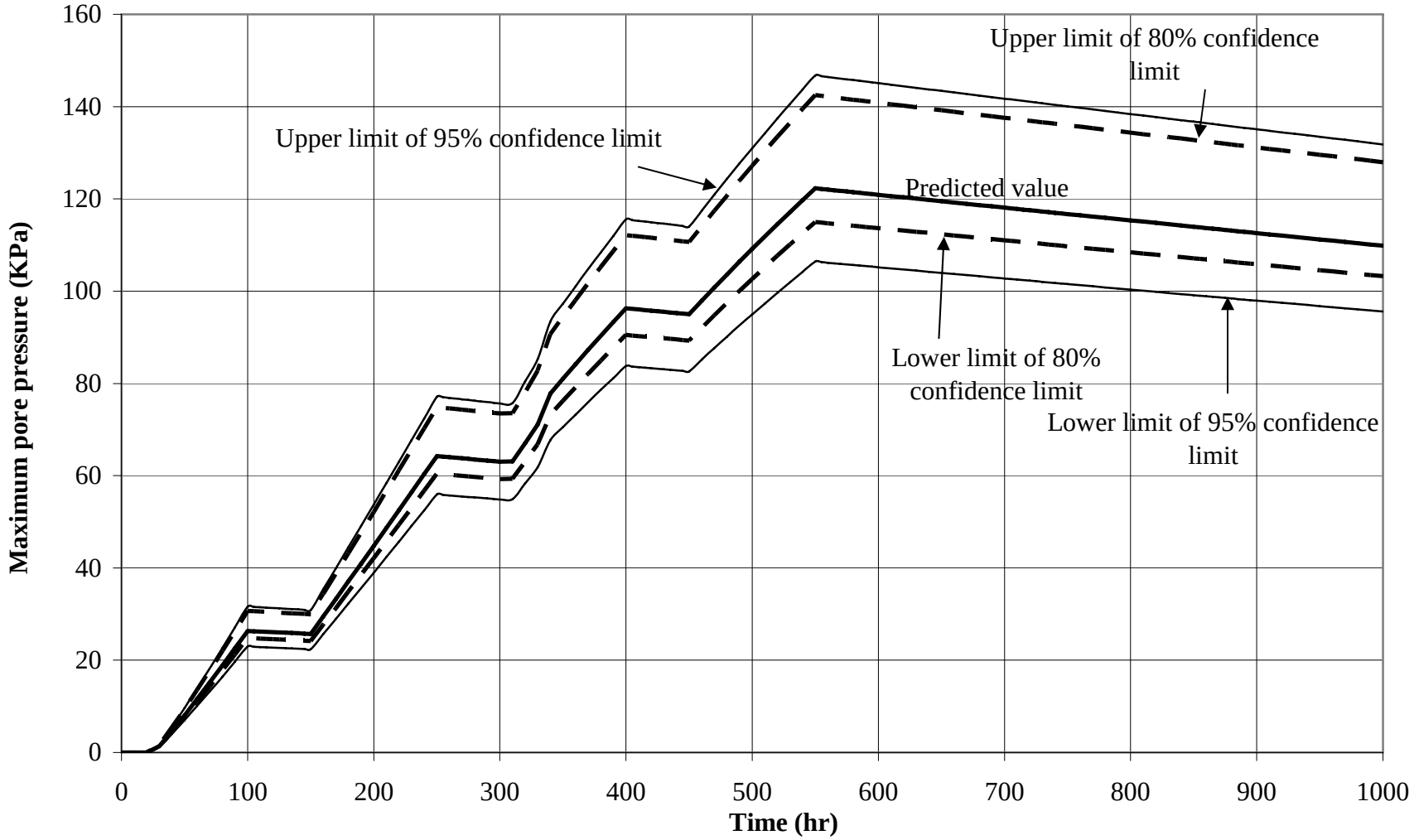

Figure 7.6 Range of pore water pressure for confidence limit of 80% and 90%

7.5 Summary and conclusions

Method of fragments that has been used to estimate drainage and pore water pressure from a mine stop. It is based on several empirical equations that have been developed from laboratory tests and numerical modeling. Analyses based on empirical equations have uncertainty due to modeling and uncertainty in parametric analysis. It is required to measure total uncertainty in drainage and pore water analysis based on random variable. There are several probabilistic methods that measure total uncertainty in modeling by measuring probability distribution function of random variables.

Exact method, First Order – Second Moment Method and Monte Carlo Simulation are most methodologies that are used to develop probability distribution function. In this dissertation , First Order – Second Moment method has been used to compute total uncertainty in permeability, drainage and pore water pressure analysis. It has been verified with Monte Carlo method. Harr (1987) have reported coefficient of variation of geotechnical parameters such as specific gravity, permeability, porosity, etc. and these values are utilized in illustrating the developed methodology. The methodology of computing total uncertainty has been explained in Section 7.2.

Standard deviation variations of permeability of hydraulic fills are shown graphically. Total uncertainties in the drainage and pore water pressure analysis have been computed and used to plot probability distribution function for normalized drainage and normalized pore water pressure (Figures 7.3 and 7.4). Figure 7.3 shows that FOSM and Monte Carlo simulation have good agreement. Confidence interval for pore water pressure example (Section 6.4.1) has been shown for confidence limit of 80% and 90%. It has been observed that confidence interval has a very narrow band. Based on the illustrative solution, it appears that the total uncertainty measure in the pore pressure analysis is in the range of 0.09 – 0.12.

Chapter 8

Summary, Conclusions and Recommendations

Summary of this dissertation, conclusions and recommendations for the future work have been discussed in this chapter.

8.1 Summary

Backfilling of the mine stopes is one of the major operations of mining industry. Hydraulic fill and paste fill are the two popular backfill types used world-wide. Hydraulic fills are transported through pipelines in the form of slurry, at 65-75% solids content, implying water contents of 33-54%. Fill slurry enters the stope and overlies the existing fills. It segregates both horizontally and vertically. The excess water tends to pond on the surface building up from the lowest corners of a stope. Water drains through the barricades. Hydraulic fill settles within the stope under its self-weight, draining through the barricades that cover the horizontal access drives. Drainage and pore water pressure are major concern in hydraulic backfilled stope.

Due to continuous drainage from stope, degree of saturation of hydraulic fill decreases. Geotechnical properties of partially saturated soils (hydraulic fills) are different from saturated soils. In this research, Filter paper method has been used to develop soil-water characteristic curve (SWCC) for hydraulic fills. An empirical equation has been established to develop particle size distribution curve, which has been used to estimate matric suction and SWCC for hydraulic fills. Permeability of unsaturated hydraulic fills is lower than permeability of saturated fills. Mine stopes are closed to atmosphere which

reduces rate of evaporation. Drainage of water mainly occurs due to higher permeability of hydraulic fills. Laboratory tests have been carried out to measure saturation and residual moisture content of hydraulic fills in the stope.

Hydraulic fills transfer a part of their self weight to the adjacent rock mass in the process of self-weight settlement due the friction between hydraulic fill and adjacent rock wall. This process of reduction in vertical normal stress is known as arching. In this dissertation, a continuous compression arch of principal stresses has been used to estimate the vertical stress within an inclined and vertical mine stope. Effects of hydraulic fill friction angle (ϕ) and wall-backfill interface angle (δ) on vertical stress have been studied, as a part of this research. It has been observed that arching is almost insensitive to the friction angle ϕ of the backfill. In this research, concept of stress reduction factor (α_s) has been introduced as the ratio of the actual vertical normal stress to the surcharge at that depth to estimate vertical stress at any depth.

Most permeability measurements reported in the literature are from hydraulic fill samples prepared in the laboratory by sedimentation and subjected to no surcharge (Rankine et al. 2006, Sivakugan et al. 2006a, 2006d). In reality, the hydraulic fills at the mine are under several meters of overburden and therefore it is useful to study the effects of surcharge on the measured permeability. In this dissertation, extensive laboratory tests using modified oedometer have been carried out to measure effect of vertical effective stress on permeability. Laboratory tests have been conducted to measure the average moisture content variation for hydraulic fill with time and moisture content variation with time and depth in a cylindrical and removable ring apparatus respectively. It has been observed that the moisture content in a stope remains constant from 1/4 of height to 3/4 of height of stope for unsaturated hydraulic fills. The permeability of hydraulic fills has been computed using the average vertical normal stress variation with depth in a stope considering arching effect and moisture content variation in stope.

Hydraulic fill in a stope settle under its self-weight. Settlement and pore water pressure dissipation from the mine stopes are two major issues in designing barricades and stopes.

In previous studies, it has been assumed that there is no consolidation settlement in hydraulic fills. In this dissertation, several apparatus have been designed to study time dependent settlement of hydraulic fills and pore water pressure dissipation from mine stope. Several tests have been conducted to measure the settlement of hydraulic fills. It has been observed that the settlement of hydraulic fill is a bilinear logarithmic function of time. In this research, modified triaxial cell has been used to measure pore water pressure dissipation. Coefficient of consolidation has been computed for five hydraulic fill samples representing hydraulic fills in Australian mine and its variation with vertical effective stress has been studied. Settlement – effective stress – time plot has been used to investigate the variation of coefficient of secondary compression (C_α). C_α of the hydraulic fill increases with effective stresses and is independent of time. Rate of settlement and pore pressure dissipation is higher for hydraulic fills.

Many barricades have failed due to excessive pore water pressure and early stage drainage. Mine stopes are backfilled in batches. After filling for a certain time in the mine stope, backfilling is stopped to allow the drainage of the excess water from the stope. Sivakugan and Rankine (2006) and Sivakugan et al. (2006) used method of fragments to estimate drainage and maximum pore water pressure in a stope assuming constant permeability in the stope. It has been discussed in Chapter 4 that permeability in a stope varies with depth. In this research, equivalent permeability in stope has been computed and recommended to use in calculating drainage and maximum pore water pressure. In this dissertation, a methodology has been proposed to estimate time dependent drainage and pore water pressure. Moisture content variation is also studied in this research.

Drainage and pore water pressure analysis are based on many empirical equations and laboratory test results. In this research, reliability analysis has been carried out to estimate uncertainty in the analysis using First Order – Second Moment simulation and it has been verified using Monte Carlo simulations. Permeability and other design parameters depend on many empirical coefficients. Total uncertainty in equivalent permeability, drainage and pore water pressure has been computed.

8.2 Conclusions

In this dissertation, research has been carried out on characteristic properties of drainage and settlement of hydraulic fills. Geotechnical phenomenon and parameters such as arching, behavior of unsaturated hydraulic fill, permeability, settlement, etc. have been studied. Following conclusions have been made from this research.

8.2.1 Properties of saturated and unsaturated hydraulic fills

Hydraulic fills are prepared from crushing of waste rock or waste products from mining operation from the milling process. They are transported to mine stope through gravity through boreholes and pipelines. Physical properties of saturated and dry hydraulic fills have been given in literature. In this research, filter paper method has been used to establish soil-water characteristic curves (SWCC) for hydraulic fills. Some of physical properties of hydraulic fills are as follows:

- Hydraulic fills consist of classified mine tailing with not more than 10% by weight of size less than 10 μm. They are classified as silty sands (SM) or sandy silts (ML) with no plasticity. Hydraulic fills have high values of specific gravities from 2.80 to 4.50 due to presence of heavy minerals.
- Friction angle of hydraulic fills varies from 27^0 to 44^0. An empirical equation has been proposed to compute friction angle from relative density (Eq. 2.6). It has been observed that hydraulic fills are cohesionless.
- An empirical equation has been proposed to establish particle size distribution of hydraulic fills that has been used to develop SWCC numerically. It has been compared with SWCC developed using filter paper method by measuring matric suction of hydraulic fills.
- Saturation moisture content of hydraulic fills varies from 22% – 27 %. Residual moisture content has been measured using laboratory tests. It has been observed that residual moisture content of hydraulic fill varies from 12% – 14%.

8.2.2 Effect of arching on vertical stresses

For stability and drainage analysis, the mine stopes are often assumed to be vertical rectangular prisms. In reality, the mine stopes are inclined, where the walls are no more vertical. Arching is a process in which hydraulic fills transfer a part of their self-weight to the adjacent rock mass in the process of self-weight settlement due the friction between hydraulic fill and adjacent rock wall. Several theories have been proposed to estimate vertical normal stress in a vertical mining stope. In this dissertation, a continuous compression arch of principal stresses has been used to estimate the vertical stresses within inclined and vertical mine stopes. Following conclusions have been made from arching analysis in a mine stope.

- Wall surface of mine stopes consist of broken rock in the form of large undulations. Failure within the backfills will take place few grain diameters away from wall surface. Fill – stope wall surface angle (δ) is equal to internal friction angle of fills (ϕ).
- Circular compression arch of principal stresses has been used for arching analysis in vertical and inclined stope. Wall friction angle is fully mobilized at the foot wall whereas it is partially mobilized at the hanging wall. An equation has been proposed to estimate the vertical stresses within the inclined stope for any backfill under a surcharge. It has been observed that present analysis gives higher stresses than the stresses reported by Aubertin et al. (2003), Pirapakaran and Sivakugan (2007a) and Handy (1985) and lower than Marston (1930).
- A methodology has been proposed to calculate the vertical stress distribution along the width of inclined stope. The variation of stresses along the width of stope is skewed toward footwall.
- It has been observed that arching is almost insensitive to the friction angle ϕ of the backfill.
- Concept of stress reduction factor (α_s) has been introduced as the ratio of the actual vertical normal stress to the overburden at that depth. It has been used to estimate stress at any depth in an inclined and vertical stope.

8.2.3 Permeability of hydraulic fills

Mining accidents due to barricade failures are often catastrophic, resulting in sudden flow of wet slurry into the drives, trapping the miners and machinery in the vicinity. Most of the failures take place in the early hours of filling and are caused by the presence of excess water within the mine fill. Most permeability measurements reported in the literature are from reconstituted hydraulic fill samples subjected to no surcharge (Rankine et al. 2006, Sivakugan et al. 2006a, 2006d). In reality, the hydraulic fills at the mine are under several meters of overburden and therefore it is useful to study the effects of surcharge on the measured permeability. In this dissertation, laboratory tests have been conducted in modified oedometer to estimate permeability variation with stress. This section concludes the finding of this research on permeability.

- Permeability of hydraulic fills varies linearly with logarithmic of vertical effective stress.
- Continuous drainage of water from mine stopes makes hydraulic fill unsaturated, which reduced the permeability of hydraulic fill. Soil-water characteristic curves have been used to study the permeability variation with moisture content. It has been observed that the permeability reduces by 1/100000 times at degree of saturation of 0.6, which is very low in comparison to permeability of saturated hydraulic fills.
- Laboratory tests have been conducted to measure the average moisture content variation for hydraulic fill with time and moisture content variation with time and depth in a cylindrical and removable ring apparatus respectively. It has been observed that the moisture content in a stope remains constant from 1/3 of height to 3/4 of height of stope.
- At residual moisture the permeability decreases by 8.5×10^{-5} times the permeability at saturation without surcharge.
- Equivalent permeability has been computed and it has been observed that the equivalent permeability of saturated hydraulic fill reduces to 0.2 time the permeability of saturated hydraulic fill without surcharge at aspect ratio of 5.

Equivalent permeability has been used to compute drainage and maximum pore water pressure using method of fragments.

8.2.4 Settlement of hydraulic fills

The hydraulic fill settles within the stopes under its self-weight. Laboratory tests have been conducted using oedometer and modified triaxial cell to measure settlement and pore water dissipation in hydraulic fills. Following conclusions have been made from this research.

- Settlement of hydraulic fill is a bilinear logarithmic function of time. Immediate settlement contributes about 63% of the total settlement. It has been observed that the immediate settlement of hydraulic fill varies linearly with vertical effective stress for higher vertical effective stress (more than 160 kPa) whereas it is non-linear for lower vertical effective stress (less than 160 kPa).
- Settlement- effective stress- time plot has been used to investigate the variation of coefficient of secondary compression (C_α) of the hydraulic fill which increases with effective stresses and is independent of time.
- Ratio of permeability index and compression index (C_k/C_c) of hydraulic fills varies from 2.6 to 14 for hydraulic fills which indicates that rate of settlement and pore pressure dissipation are higher for hydraulic fills. Compression index of hydraulic fill has been recommended to use in estimating total settlement of hydraulic fills.
- Consolidation settlement of hydraulic fill has been measured using modified triaxial cell by measuring pore water pressure dissipation from the sample. Coefficient of consolidation of hydraulic fills varies from 0.5 – 2.6 mm^2/sec.

8.2.5 Drainage and Reliability analysis

Mine stopes are backfilled in batches. After filling mine stope for a certain time, backfilling is stopped to allow the drainage of the excess water from the stope. The rate

of drainage is a function of permeability of the hydraulic fill and head loss (Cowling et al., 1988 and Traves et al., 1991). Sivakugan and Rankine (2006) and Sivakugan et al. (2006) used method of fragments to estimate drainage and maximum pore water pressure. In this dissertation, method of fragments has been used to compute drainage and maximum pore water pressure using equivalent permeability. Since all these analysis are based on several empirical equations so uncertainty analysis has been carried out in this research to study the modeling and parametric errors.

- An empirical equation has been proposed for form factor Φ_2 that has been used to calculate drainage from the stope.
- A methodology has been proposed to estimate pore water pressure and drainage variation with time.
- It is suggested that equivalent permeability should be used to estimate drainage and maximum pore water pressure. Height of fill and permeability of hydraulic fill should be adjusted with the change in moisture content.
- Total uncertainties in equivalent permeability, drainage and pore water pressure analysis have been computed and used in developing probability distribution function.

8.3 Recommendations for future research

There have been considerable achievements through this dissertation in understanding drainage and settlement characteristics of hydraulic fills. State of stresses has been studied in inclined and vertical stopes using arching analysis. This dissertation discusses permeability variation with depth in mine stope. Settlement of hydraulic fills has been measured using laboratory tests and coefficient of consolidation has been reported. Drainage and pore water pressure are also computed. All these analysis are based on several assumptions and there are many areas that deserve further study. Some of them are discussed below.

8.3.1 Non-homogenous hydraulic fills in stope

In all the drainage and settlement analysis, it has been assumed that the hydraulic fill are homogenous. Hydraulic fill is poured in the stope in form of slurry with initial moisture content of approximately 40%. Hydraulic fill settles in stope under its self weight. A laboratory test has been conducted in a cylindrical cell of height 300 mm with rings of 25 mm height (as shown in Figure 4.5). Particle size distribution has been measured using electronic particle size analyzer. Particle size distribution of hydraulic fills in each ring has been shown in Figure 8.1. It has been observed that the gradation of the hydraulic fill varies with depth. While estimating permeability in mine stope, the variation of internal friction angle (ϕ) has been ignored. Friction angle (ϕ) of hydraulic fills will change due to non-homogeneity of hydraulic fill. Laboratory tests should be conducted to study ϕ variation with uniformity coefficient and coefficient of gradation.

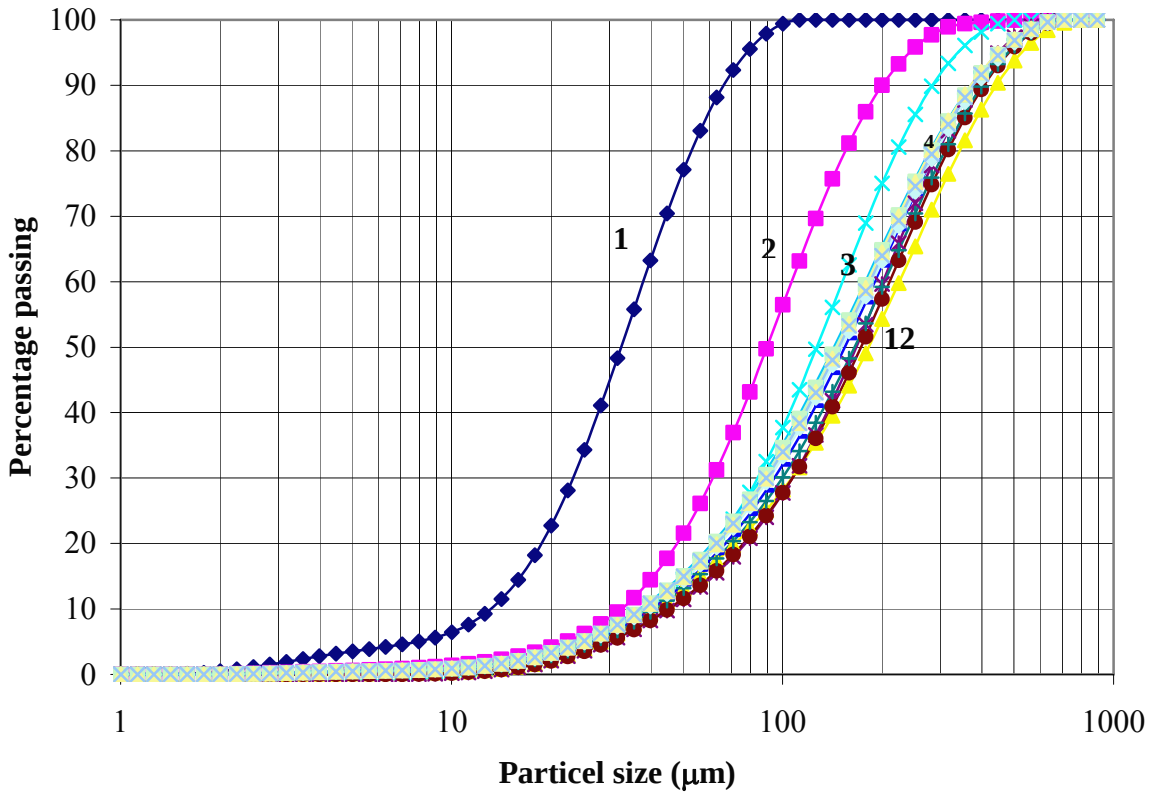

Figure 8.1 Particle size distribution of hydraulic fills variation with depth

8.3.2 Arching analysis in a 3-D stope

In this dissertation, analysis has been carried for two – dimensional stope for inclined in vertical stope. In reality, mine stopes are three dimensional so it has been recommended to extend the 2-D modeling to three dimension inclined stope. Extensive laboratory tests and numerical modeling is required to study the mobilization of friction angles on hanging wall and foot wall. Laboratory tests should be conducted to study the effect of pouring slurry in the mine stope. Influence of water pressure on the vertical effective stress in a 3-D stope should be considered to predict the actual stresses in mine stope. Effect of degree of saturation of hydraulic fill on total effective stresses should be considered in estimating permeability of hydraulic fills.

References

AS 1289.3.5.1 (1995) – Methods of testing soils for engineering purposes – Soil classification tests.

AS 1289.6.6.1 Method 6.6.1: Soil strength and consolidation tests—Determination of the one-dimensional consolidation properties of a soil—Standard method

ASTM D2435 - 04 Standard Test Methods for One-Dimensional Consolidation Properties of Soils Using Incremental Loading

ASTM D5298 - 03 Standard Test Method for Measurement of Soil Potential (Suction) Using Filter Paper

Adams J. (1965). "The engineering behavior of a Canadian muskeg." *Proceedings of 6th International Conference on Soil Mechanics and Foundation Engineering, Montreal Canada,* Vol. 1, pp. 3-7.

Arya L.M. and Paris J.F. (1981). "A physicoempirical model to predict the soil moisture characteristic from particle size distribution and bulk density data." *Soil Science Society of America Journal,* Vol. 45, pp. 1023-1030.

Aubertin, M., Li L., Arnoldi S. and Simon R. (2003). "*Interaction between Backfill and Rock mass in narrow stopes*", Soil and Rock mechanics America, pp. 1157-1164.

Azizi F. (1999). *Applied analyses in geotechnics*. Taylor and Francis Publications.

Banerjee S. and Datta B. (1991). "Reliability analysis of thaw-induced pore pressure." Journal of Cold Regions Engineering, Vol. 5, No. 3, pp. 125-141.

Barden L. (1968). "Consolidation of clay with non-linear viscosity." *Geotechnique,* Vol. 15, pp. 267-286.

Barden L. (1969). "Time dependent deformation of normally consolidated clays and peats." *Journal of the Soil Mechanics and Foundation Division, ASCE,* Vol. 95, pp. 1-31.

Benjamin J.R. and Cornell C.A. (1970). *Probability, statistics, and design for civil engineers.* McGraw-Hill Book Company.

Berdnt C.C., Rankine K.J. and Sivakugan N. (2007). "Material properties of barricade bricks for mining applications." *Geotechnical and Geological Engineering*, Vol. 25, No. 4, pp. 383- 393.

Berry, P.L. and Wilkinson, W.B. (1969). "The radial consolidation of clay soils." *Geotechnique*, Vol. 19, No. 2, pp. 253-284.

Bloss, M.L. (1992). "Prediction of cemented rock fill stability design procedures and modelling techniques," PhD Thesis, *Department of Mining and Metallurgical Engineering,* University of Queensland, Brisbane, Australia, 265.

Bloss M.B. and Chen J. (1988). "Drainage research at Mount Isa Mines Limited 1992-1997", *Proceedings of 6th International Symposium on Mining with Backfill: Minefill '98,* Ed. M. Bloss, 111-116.

Brady A.C. and Brown J.A. (2002). "Hydraulic fill at Osborne mine." *Proceedings of 7th underground Operators Conference, Townsville*, Australia, pp. 161-165.

Brooks R.H. and Corey A.T. (1964). "Hydraulic properties of porous media." *Hydrologic Papers,* No. 3, Colorado State University, Fort Collins, Colorado.

Caceres, C. (2005). "Effect of Backfill on Longhole Open Stoping." *MASc Thesis*, Mining Engineering, University of British Columbia.

Carrier D.W., Bromwell L.G. and Somogyi F. (1983). “Design capacity of slurried mineral waste ponds.” *Journal of Geotechnical Engineering*, Vol. 109, No. 5, pp. 699-716.

Casagrande A. (1936). “Determination of the preconsolidation load and its practical significance.” *1st International Conference on Soil Mechanics and Foundation Engineering*, Cambridge, M.A., Vol. 3, pp. 60-64.

Casagrande A. and Fadum R.E. (1940). *Notes on soil testing for engineering purposes. Harvard University Graduate Engineering Publication*, No. 8.

Cedergren H.R. (1967). *Seepage, Drainage, and Flow nets. John Wiley and Sons, Inc. Canada.*

Chandler R.J. and Gutierrez C.I.(1986). "The filter paper of suction mesurement." *Geotechnique*, Vol. 36 pp. 265-268.

Clarke I.H. (1988). “The properties of hydraulically placed backfill.” *Proceedings of Backfill South African Mines*, Johannesburg, SAIMM, pp. 15-33.

Connell L.D. (1995). “An analysis of perturbation based methods for treatment of parameter uncertainty in numerical groundwater models.” *Transport in Porous Media*, Vol. 21, pp. 225-240.

Cooke R. (2001). “Design procedure of hydraulic backfill distribution systems.” *Journal of the South African Institute of Mining and Metallurgy*, pp. 97-102.

Corson D.R., Dorman R.K., and Sprute R.H. (1981). “Improving the support characteristics of hydraulic fills.” *Application of Rock Mechanics to Cut and Fill Mining*, The Institute of Mining and Metallurgy, Eds. O. Stephansson and M.D. Jones, pp. 93-99.

Cowling R. (1998). "Twenty Five years of mine filling: developments and directions." *Proceedings of Minefill* 1998, Brisbane, pp. 3-10.

Das B.M. (2005). *Fundamentals of geotechnical engineering*. Thomson Publications.

Delleur J. W. (1999). The handbook of ground water engineering. CRC Press

Dettinger M.D. and Wilson J.L. (1981). "First order analysis of uncertainty in numerical models of underground flow. Part 1, Mathematical development." *Water Resources Research*, Vol. 17, No. 1, pp. 215-232.

Digging Deeper (2003). AMC News Letter.

Ebrahimi B.N., Gitirana Jr. G.F.N., Fredlund D.G., Fredlund M.D. and Samarasekera L. (2004). "A lower limit for the water permeability coefficient." *57th Canadian Geotechnical Coneference, 4th Joint IAH-CNC/CGS Conference, Geo Quebec 2004, Canada.*

Fawcett R.G. and Collis-George N. (1967). "A filter-paper method for determining the moisture characteristics of soil." *Australian Journal Experimental Agriculture and Animal Husbandry*, Vol. 7, pp. 162 – 167.

Fredlund M.D., Fredlund D.G. and Wilson G.W. (2000). " An equation to represent grain-size distribution." *Canadian Geotechnical Journal*, Vol. 37, pp. 817-827.

Fredlund D.G. and Rahardjo H. (1993). *Soil mechanics for unsaturated soils*. John Willey and Sons, Inc.

Fredlund D.G. and Xing A. (1994). "Equations for the soil-water characteristic curve." *Canadian Geotechnical Journal*, Vol. 31, pp. 521-532.

Gardner R. (1937). " A method of measuring the capillary tension of soil moisture over a wide moisture range." *Soil Science*, Vol. 43, No. 4, pp. 277-283.

Gardner W.R. (1956). "Representation of soil aggregate size distribution by a logarithmic-normal distribution." *Soil Science Society of America Proceedings*, Vol. 20, pp. 151-153.

Gitirana Jr. G.F.N. and Fredlund D.G. (2004). "Soil water characteristic curve equation with independent properties." *Journal of Geotechnical and Geoenvironmental Engineering*, Vol. 130, pp. 209-212.

Glasgow H.S., Fortney M.D., Lee J., Graettinger A.J. and Reeves H.W. (2003). "MODFLOW 2000 head uncertainty, a First – Order Second Moment Method." *Ground Water*, Vol. 41, No. 3, pp. 342-350.

Goldberg T. (1964). Discussion of "Design of foundations for control of settlement." *Proceedings of ASCE, Evanston, III.*

Grice A.G. (1998). "Stability of hydraulic backfill barricades." *Sixth International Symposium on Mining with Backfill*, AusIMM.

Grice A. G. (1988a). "Underground mining with back fill." *The 2nd Annual Summit-Mine tailing disposal system.*

Grice, A.G. (2001). "Recent minefill developments in Australia.", *Proceedings of the 7th International Symposium on Mining with Backfill*, Seattle, USA. In: Minefill (2001), Ed. Stone D., pp. 351–357.

Grice T. (2005). *Introduction to hydraulic fill.* Chapter 5, In: Handbook on Mine Fill, Eds. Y. Potvin, E. Thomas and A. Fourie, ACG Australian Centre for Geomechanics.

Gupta S.C. and Larson W.E. (1979a). “Estimating soil-water retention characteristics from particle size distribution, organic matter percent, and bulk density.” *Water Resources Research*, Vol. 15, No. 6, pp. 1633-1635.

Gupta S.C. and Larson W.E. (1979b). “A model for predicting packing density of soils using particle-size distribution.” *Soil Science Society of America Journal*, Vol. 43, pp. 758-764.

Hagen L.J., Skidmore E.L. and Fryrear D.W. (1987). “Using two sieves to characterize dry soil aggregate size distribution.” *Transaction of the American Society of Agriculture Engineers*, Vol. 30, No. 1, pp. 162-165.

Hamblin A.P. (1981). "Filter-Paper method for routine measurement of field water potential." *Journal of Hydrology*, Vol. 53, pp. 355-360

Hamrin H. (2001). “Underground Mining Methods and Applications”, Chapter 1, In: Hustrulid W.A. and Bullock R.L. (Eds), Underground Mining Methods: Engineering Fundamentals and International Case Studies, Published by Society for Mining, Metallurgy, and Exploration.

Handy R.L. (1985). “The Arch in Soil Arching.” *Journal of Geotechnical Engineering*, Vol. 111, No. 3, pp. 302-318.

Handy, R.L. (2004). “Anatomy of an error.” *Journal of Geotechnical and Geoenvironmental Engineering*, ASCE, 130(7), pp. 768-771.

Handy, R.L., and Spangler, M.G. (2007). *Geotechnical Engineering – Soil and Foundation Principles and Practice*, 5th Edition, McGraw Hill, New York.

Harr M.E. (1987). *Reliability- based design in civil engineering*. McGraw-Hill Book Company.

Harr M. E. (1962). "*Ground Water and Seepage*." McGraw Hill Book Company, USA.

Harrop-Williams K. (1989). "Arch in Soil Arching." *Journal of Geotechnical Engineering*, Vol. 11, No. 3, pp. 415-419.

Hazen A. (1930). *Water Supply*. American Civil Engineering Handbook, Wiley, New York.

Herget G. and De Korompay V. (1988). "In situ drainage properties of hydraulic backfills." *Proceedings of Mining with Backfill, Research and Innovations*, CIM, No. 19, pp. 117-123.

Hinde A.L. (1993). "Advances in particle sizing of backfill." *Minefill 93*, Johannesburg, SAIMM, pp. 181-188.

Holtz W.G. and Gibbs H.J. (1956). " Shear strength of pervious gravelly soils." *Proceedings of American Society of Civil Engineering*, Paper No. 867.

Holtz R.D. and Kovacs W.D. (1981). *An introduction to geotechnical engineering*. Prentice Hall, Inc.

Horn H.M. and Lambe T.W. (1964). "Settlement of buildings on the MIT campus." *Journal of Soil Mechanics and Foundation Division, ASCE*, Vol. 90, No. SM5, pp. 181-196.

Houston S.L. , Houston W.N. and Wagner A. (1994). "Laboratory filter paper suction measurements." *Geotechnical Testing Journal*, Vol. 17, No. 2, pp. 185-194.

Hunt R.E. (1986). *Geotechnical Engineering Analysis and Evaluation*. McGraw-Hill Book Company.

Isaacs L.T. and Carter J.P. (1983). “Theoretical study of pore water pressure developed in hydraulic fill in mine stopes.” *Transactions of Institution of Mining and Metallurgy* (Section A: Mining Industry), Vol. 92, pp. A93-A102.

Janssen H.A. (1895). “Versuche über Getreidedruck in Silozellen.” *Zeitschr. d. Vereines deutscher Ingenieure*, 39: pp. 1045-1049.

Jaky, J. (1944). “The coefficient of earth pressure at rest.” *Journal of the Society of Hungarian Architect and Engineering*, 7, pp. 355-358.

Keene P. (1964). Discussion of “Design of foundations for control of settlement.” *Proceedings ASCE, Evanston, III.*

Krynine D.P. (1945). Discussion of "Stability and Stiffness of Cellular Cofferdams." by K. Terzaghi, *American Society of Civil Engineers, Transactions*, Vol. 110, pp. 1175-1178.

Kuganathan K. (2001). “Mine backfilling, backfill drainage and bulkhead construction – a safety first approach”, *Australian Mining Monthly*, pp. 58-64.

Kuganathan K. (2002). “Design and construction of shotcrete bulkhead with engineered drainage system for mine backfilling.” *International Seminar on Surface Support Liner, Australian Centre for Geomechanics*, Section 8, pp. 1-15.

Kulhawy, F.H., and Mayne, P.W. (1990). *Manual on estimating soil properties for foundation design, Final Report* submitted to Electric Power Research Institute (EPRI), Palo Alto, California.

Ladanyi B. and Hoyaux B. (1969). “A study of the trap-door problem in a granular mass.” *Canadian Geotechnical Journal*, Vol. 6, No. 1, pp. 1-14.

Ladd C.C. and Preston W.E. (1965). “On the secondary compression of saturated clays.” *Soil publication 181, Massachusetts Institute of Technology, Cambridge, Massachusetts.*

Lade P.V. and Liu C. (1998). “Experimental study of drained creep behavior of sand.” *Journal of Engineering Mechanics, ASCE,* Vol. 124, No. 8 pp. 912-920

Lambe T.W. and Whitman V. R. (1969). “*Soil Mechanics*.” John Wiley and Sons, Inc. Canada.

Leong E.C., He L. and H. Rahardjo (2002). “Factors affecting the filter paper method for total and matric suction measurements.” *Journal of Geotechnical Testing*, Vol. 25, No. 3, pp. 322-333.

Li L., Aubertin M. and Belem T. (2005). “Formulation of a three dimensional analytical solution to evaluate stresses in backfilled vertical narrow openings.” *Canadian Geotechnical Journal*, Vol. 42, No. 6, pp. 1705- 1717.

Low, B.K., Tang, S.K., and Choa, V. (1994). “Arching in Piled Embankments.” *Geotechnical Engineering Journal*, ASCE, Vol. 120, No. 11, pp. 1917-1937.

Luckner L., van Genuchten M.Th. and Nielsen D.R. (1989). “A consistent set of parametric model for the two pahse flow of immiscible fluid in the subsurface.” *Water Resources Research*, Vol. 25, pp. 2187-2193.

Marshall T.J. (1958). “A relation between permeability and size distribution of pores.” *Journal of Soil Science*, Vol. 9, No. 1, pp. 1-8.

Marston A. (1930). “The theory of external loads on closed conduits in the light of latest experiments.”, *Bulletin No. 96, Iowa Engineering Experiment Station*, Ames, Iowa.

Marston A. and Anderson A.O. (1913). “The theory of loads on pipes in ditches and tests of cement and clay drain tile and sewer pipe.” *Bulletin No. 31, Iowa Engineering Experiment Station*, Ames, Iowa.

McCarthy, D.F. (1988). *Essentials of Soil mechanics and Foundations: Basic Geotechnics.* Prentice Hall.

McLaughin D. and Wood E.F. (1988a). “A distributed parameter approach for evaluating the accuracy of groundwater model predictions 1: Theory.” *Water Resources Research*, Vol. 24, No. 7, pp. 1037-1048.

McLaughin D. and Wood E.F. (1988b). “A distributed parameter approach for evaluating the accuracy of groundwater model predictions 2: Application to groundwater model predictions” *Water Resources Research*, Vol. 24, No. 7, pp. 1048-1060.

Mesri G. and Rokhsar A. (1974). “Theory of consolidation for clay.” *Journal of Geotechnical Engineering Division*, Vol. 100, pp. 889-904.

Meyerhof, G.G. (1957). “Discussion on research on determining the density of sands by penetration testing,” *Proc., the 4th International Conference on Soil Mechanics and Foundation Engineering*, London, UK, 3, 110.

Miller R.J. and Low P.F. (1963). “Threshold gradient for water flow in clay system.” P*roceedings of soil science Society of America*, Vol. 27, No. 6, pp. 605-609.

Mitchell R.J., Smith J.D., and Libby D.J. (1975).”Bulkhead Pressures Due to Cemented Hydraulic Mine Backfills,” *Canadian Geotechnical Journal*, Vol. 12 No. 3, pp. 362-371.

Newland P.L. and Alley B.H. (1960). “A study of consolidation characteristics of a clay.” *Geotechnique*, Vol. 10, pp. 62-74.

Murayama S. and Shibata T. (1964). “Flow stress relaxation of clays.” *I.U.T.A.M. Symposium Rheology and Soil Mechanics, Grenoble, France.*

Nicholson D.E. and Wayment W.R. (1964). *Properties of hydraulic backfills and preliminary vibratory compaction tests*. United States Department of the Interior, Bureau of Mines, pp. 6477.

Paterson A.J.C. (2004). “High slurry density and paste tailings, transport system.” *International Platinum Conference ‘Platinum Adding Value’,The South African Institute of Mining and Metallurgy* , pp. 159-165.

Pettibone H.C. and Kealy C.D. (1971). “Engineering properties of mine tailings.” *Journal of Soil Mechanics and Foundation Division,* ASCE, 97(SM9), pp. 1207-1225.

Pirapakaran, K. and Sivakugan, N. (2007a). “Arching within hydraulic fill stopes.” *Geotechnical and Geological Engineering*, 25(1): pp. 25-35.

Pirapakaran, K. and Sivakugan, N. (2007b). “A laboratory model to study arching within a hydraulic fill stope.” *Geotechnical Testing Journal*, ASTM, Vol. 30, No. 6, pp. 496-503.

Pirapakaran K. (2008). “*Load-deformation characteristics of mine fills with particular reference to arching and stress developments.*” PhD Thesis, School of Engineering, James Cook University, Townsville, Australia.

Pirapakaran, K. and Sivakugan, N. (2007a). “Arching within hydraulic fill stopes,” *Geotechnical and Geological Engineering*, Springer, 25(1), 25-35.

Pirapakaran, K. and Sivakugan, N. (2007b). "A laboratory model to study arching within a hydraulic fill stope," *Geotechnical Testing Journal*, ASTM, 30(6), 496-503.

Poskitt T.J. (1969). "The consolidation of saturated clay with variable permeability and compressibility." *Geotechnique*, Vol. 19, No. 2, pp. 234-252.

Potvin Y., Thomas E. and Fourie A. (2005). "*Handbook on Mine Fill*" ACG Australian Centre for Geomechanics.

Pavlovsky N. N. (1956). "*Collected Works*", Akad Nauk USSR, Lenningrad.

Qiu Y. and Sego D.C. (2001). "Laboratory properties of mine tailings." *Canadian Geotechnical Journal*, Vol. 38, No. 1, pp. 183-190

Rankine, W.M.J. (1857). "On stability on loose earth." *Philosophic Transactions of Royal Society*, London, Part I, 9-27.

Rankine K.J., Rankine K.S. and Sivakugan N. (2003). "Three dimensional drainage modelling of hydraulic fill mines." *Proceedings of 12th Asian Regional Conference on Soil Mechanics and Geotechnical Engineering*, World Scientific Publishing, pp. 937–940.

Rankine, R.M. (2004). *The geotechnical and static stability analysis of Cannington mine paste backfill*. PhD Thesis, School of Engineering, James Cook University, Townsville, Australia.

Rankine, K.J., Sivakugan, N. and Rankine, K.S. (2004). "Laboratory tests fro mine fills and barricade bricks," *Proceedings of 9th Australian New Zealand Conference on Geomechanics*, Auckland, pp. 218-224.

Rankine, K.J., Sivakugan, N. and Cowling, R. (2006). "Emplaced characteristics of hydraulic fills in a number of Australian mines," *Geotechnical and Geological Engineering*, Springer, Vol. 24, No. 1, pp. 1-14.

Rankine K.S. (2007). *Development of two and three-dimensional method of fragments to analyse drainage behavior in hydraulic fill stope*. PhD Thesis, School of Engineering, James Cook University, Townsville, Australia.

Raymond G.P. (1966). "Laboratory consolidation of some normally consolidated soils." *Canadian Geotechnical Journal*, Vol. 3, No. 4, pp. 217-234.

Richards B.G. (1965). "Measurement of the free energy of soil moisture by the pasychrometric using thermistor." *Moisture Equilibria and Moisture changes in Soil beneath covered areas*. Editor: G.D. Aitchinson, Butterworth & Co. Ltd., pp. 39-46.

Sagar B. (1978). "Galerkin finite element procedure for analyzing flow through random media." *Water Resources Research*, Vol. 14, No. 6, pp. 1035-1044.

Sagawa Y. and Yamatomi J. (2003). "Stope design in the Hishikari Gold Mine, Japan, by using numerical analysis." *ISRM 2003 - Technology Roadmap for Rock Mechanics*, South African Institute of Mining and Metallurgy, 2003.

Sallfors G and Oberg-Hostga A. (2002). "Determination of hydraulic conductivity of sand-bentonite mixture for engineering purposes." *Geotechnical and Geological Engineering* No. 20, pp. 65-80.

Shen C., Arulanandan K. and Smith W.S. (1973)."Secondary consolidation and strength of clay." *Journal of Soil Mechanics and Foundation Division, ASCE*, Vol. 99, No. SM1, pp. 95-110.

Shukla, S.K., Gaurav and Sivakugan, N. (2008). "A simplified extension of the conventional theory of arching in soils." *International Journal of Geotechnical Engineering,* (communicated).

Singh S., Sivakugan N. and Chandra S. (2008). "The permeability of hydraulic fills under surcharge." *International Journal of Geotechnical Engineering,* Vol. 2, No. 2, pp. 77-87.

Singh S. and Sivakugan N. (2008). "Time dependent settlement in hydraulic fills." *International Journal of Geotechnical Engineering,* Vol. 2, No. 4, pp. 293 – 303.

Singh S., Shukla S.K. and Sivakugan N. (2008a). "Arching in an inclined stope." *Canadian Geotechnical Journal* (Review).

Singh S., Sivakugan N. and Shukla S.K. (2008b). "Can soil arching be insensitive to ϕ." *Journal of Geotechnical and Geoenvironmental Engineering*, (Review).

Singh S., Sivakugan N., and Shukla S.K. (2008c). "Stress reduction factor for a mine stope." *International Journal of Geomechanics,* ASCE, (under review)

Sillers W.S. (1997). *The mathematical representation of the soil water characteristic curve*. M.Sc. Thesis, University of Saskatchewan.

Sivakugan N. and Al-Aghbari M.Y.S. (1993). "Method of fragments – quick solution to seepage problems." *Environmental Management, Geowater and Engineering Aspects*, Balkema, pp. 491-496.

Sivakugan, N., Rankine, K.J. and Rankine, R.M. (2005). Geotechnical Aspects of Hydraulic Filling of Underground Mine Stopes in Australia, Chapter 18, *Ground Improvements - Case Histories*, Eds. B. Indraratna and J.Chu, Elsevier, 515-540.

Sivakugan N. and Rankine K.S. (2006a). “A simple solution for drainage through a 2-dimensional hydraulic fill stope.” *Geotechnical and Geological Engineering*, Springer, Vol. 24, pp. 1229-1241.

Sivakugan N., Rankine K.J. and Rankine K.S. (2006b). “Study of drainage through hydraulic fill stopes using methods of fragments.” *Geotechnical and Geological Engineering*, Springer, Vol. 24, pp. 77-89.

Sivakugan, N., Rankine, R.M., Rankine, K.J. and Rankine, K.S. (2006c). “Geotechnical considerations in mine backfilling in Australia,” *Journal of Cleaner Production*, Elsevier, 14(12-13), 1168-1175.

Sivakugan N., Rankine K.S. (2006). “A simple solution for drainage through a 2-dimensional hydraulic fill stope.” *Geotechnical and Geological Engineering*, Vol. 24, pp. 1229–1241.

Sivakugan N., Rankine K. and Rankine R. (2006d). “Permeability of hydraulic fills and barricade bricks.” *Geotechnical and Geological Engineering*, Vol. 24, No. 3, pp. 661-673.

Sivakugan, N. (2008). "Drainage issues and stress developments within hydraulic fill mine stopes," *Australian Journal of Civil Engineering*, Engineers Australia, Vol. 5, No. 1, pp. 61-70.

Skempton, A.W. (1986). “Standard penetration test procedures and the effects in sands of overburden pressure, relative density, particle size, aging and overconsolidation,” *Geotechnique*, Vol. 36, No. 3, pp. 425-447.

Sokolovoskii V.V. (1965). “*Statics of Granular Media*.” Peramogan Press, Translated from Russian by J.K. Lusher.

Spangler, M.G. (1962). *Culverts and conduits. chapter 11, Foundation Engineering.*, Leonards, G.A. McGraw-Hill, pp. 965-999.

Stone K.J.L, Randolph M.F., Toh S. and Sales A. A. (1994). "Evaluation of consolidation behavior of mine tailings." *Journal of Geotechnical Engineering*, Vol. 120, No. 3, pp. 473-490.

Take, A.W., and Valsangkar, A.J. (2001). "Earth Pressures on Unyielding Retaining Walls of Narrow Backfill Width." *Canadian Geotechnical Journal*, Vol. 38, No. 6, pp. 1220-1230.

Tavenas F., Jean P., Leblond P. and Lerouell S. (1983)."The permeability of natural soft clays. Part I: Methods of laboratory measurement." *Canadian Geotechnical Journal* Vol. 20, 645-660.

Taylor D.W. (1942). "Research on consolidation of clays." *M.I.T. Dept. of Civil and Sanitary Engineering.* Serial 82.

Taylor D.W. (1948). *Fundamentals of Soil Mechanics*. John Willey and Sons Inc., London.

Terzaghi K. (1923)."Die Berechnug der durchlassigkeitsziffer des tones aus dem verlauf der hydrodynamischen spannungserscheinungen." *Siltz, Akademre der Wissenscgaften, Mathematishnatur Wissenschaftliche, Klasse, Vienna Austria, Part IIa*, Vol. 132, pp. 125-138.

Terzaghi K. (1941)."Undisturbed clay samples and undisturbed clays." *Journal of Boston Society of Civil Engineers*, Vol. 28, No. 3, pp. 211-231.

Terzaghi, K., (1943). *Theoretical Soil Mechanics.*, John Wiley and Sons, Inc., New York.

Terzaghi K. (1945). “Stability and Stiffness of Cellular Cofferdams.” *American Society of Civil Engineers, Transactions*, Vol. 110, pp. 1083-1119.

Thomas E.G., Nantel J.H. and Notley K.R. (1979).” *Bacfill technology in underground metalliferous mines*.” International Academic Services.

Thomas E.G. and Holtham P.N. (1989). “The basics of preparation of desilimed mill tailing hydraulic fill.” *Innovations in Mining Backfill Technology*, Ed. Hassani et al., Rotterdam, Balkerna, pp. 425-431.

Townley L.R. and Wilson J.L. (1985). “Computationally efficient algorithms for parameter estimation and uncertainty propogation in numerical models of ground water flow.” *Water Resources Research*, Vol. 21, No. 12, pp. 1851-1860.

Traves W.H. and Isaacs L.T. (1991). “Three dimensional modeling of fill drainage in mine stopes.” *Transactions of Institution of Mining and Metallurgy (Section A: Mining Industry)*, 100, pp. A66-A72.

Vanapalli S.K., Siller W.S. and Fredlund M.D. (1998). “The meaning and relevance of residual state of unsaturated soils.” *Proceedings of 51st Canadian Geotechnical Conference Edmonton Alberta*, pp. 101-108.

Vanapalli S.K., Salinas L.M., Avila D. and Karube D. (2002). “Suction and storage characteristics of unsaturated soils.” *Proceedings of the Third International Conference on Unsaturated Soils*, UNSAT 2002, Recife, Eds. J.F.T. Juca, T.M.P. de Campos and F.A.M. Marinho, A.A. Balkema Publishers, pp. 1045-1070.

Wagner B.J. and Gorelick S. (1987). “Optimal ground water quality management under parameter uncertainty.” *Water Resources Research*, Vol. 23, No. 7, pp. 1162-1174.

Wagner B.J. and Gorelick S. (1992). "Ground water quality management under uncertainty: Stochastic programming approaches and the value information." *Water Resources Research*, Vol. 28, pp. 1233-1246.

Westraad D. (2005). *Suction induced shear strength of gold mine tailings*. Master of Engineering, Dissertation, University of Pretoria.

Wickland E. Benjamin and Wilson G. W. (2005). "Self-weight consolidation of mixtures of mine waste rock and tailings." *Canadian Geotechnical Journal*, Vol. 42 No. 2 pp. 327-329.

Wahls H.E. (1962). "Analysis of primary and secondary consolidation." *Journal of Soil Mechanics and Foundation Division, ASCE*, Vol. 88, No. SM6, pp. 207-231.

van Genuchten M.T. (1980). "A closed form equation for predicting the hydraulic conductivity of unsaturated soils." *Soil Science Society of America Journal*, Vol. 44, pp. 892-898.

Vanapalli S.K. and Lobbezoo J.P. (2002). "A normalized function for predicting the coefficient of permeability of unsaturated soils." *Proceedings of the Third International Conference on Unsaturated Soils*, UNSAT 2002, Recife, Eds. J.F.T. Juca, T.M.P. de Campos and F.A.M. Marinho, A.A. Balkema Publishers, pp. 839-844.

http://www.mininglife.com/Miner/Backfill/Types_of_%20Mine_Backfill.htm [Accessed: July 2007].

http://www.tfhrc.gov/hnr20/recycle/waste/mwst4.htm [Accessed: 15 December 2008].

Appendix A

Soil-water characteristic curve and residual moisture content

A1.1 Development of matric suction curve from particle size distribution

Arya and Paris (1981) developed a model to predict soil – water characteristic curve of soil from its particle size distribution, bulk density and particle density parameter. Shape of particle size distribution curve and soil – water characteristic curves are similar. Following assumption were made for establishment of soil – water characteristic curves from particle size distribution:

1. Bulk density of natural – structured sample applies to assemblage formed by *n* fraction uniformly.
2. Particles in each size fraction pack are in a discrete domain. When all domains are assembled together, the resulting assemblage has a bulk density measured on natural sample.
3. Solid volume in any given assemblage can be approximated as uniform spheres with radius of mean particle size.
4. Volume of resulting pores can be approximated as that of uniform size cylindrical capillary tube whose radius is mean of particle size.

Particle size distribution curve for hydraulic fill sample A1, is shown in Figure A1.1. Divide particle size distribution curve in *n* fractions. In this case, particle size distribution curve has been divided in 10 fractions. Volume of pore or void associated with each fraction can be computed as:

$$V_{vi} = \left(\frac{W_i}{\rho_p} \right) e \qquad \text{(A1.1)}$$

where V_{vi} is the pore volume per unit sample mass associated with hydraulic fill particles in the i^{th} particle size range, W_i is the solid mass per unit sample in the i^{th} particle size range, ρ_p is the dry density and e is the void ratio of hydraulic fills. Difference in particle

size distribution corresponding to successive particle size is divided by 100, result in values of W_i such that the sum of all W_i is unity.

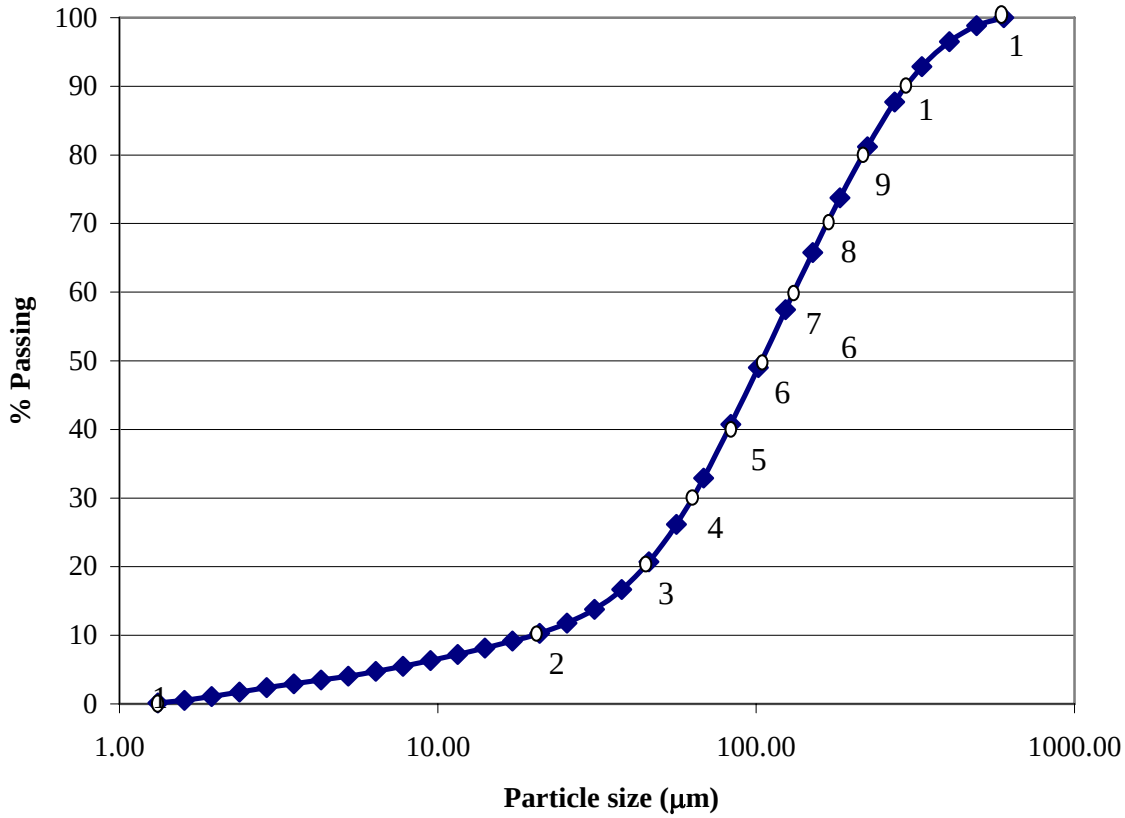

Figure A1.1 Particle size distribution of hydraulic fill sample A1

Pore volume V_{vi} generated by each particle size fraction are progressively accumulated. It is assumed that these pores are filled with water. Volumetric water content (θ_{vi}) corresponding to a pore volume can be computed as:

$$\theta_{vi} = \sum_{j=1}^{i} \frac{V_{vj}}{V_b} \tag{A1.2}$$

where V_b is bulk volume per unit sample, which can be calculated as:

$$V_b = \sum_{i=1}^{n} \frac{W_i}{\rho_b} = \frac{1}{\rho_b} \tag{A1.3}$$

Average volumetric moisture content (θ_{vi}^{*})corresponding to the midpoint of any particle size range can be approximated as:

$$\theta_{vi}^{*} = \frac{\theta_{vi} + \theta_{vi+1}}{2} \tag{A1.4}$$

Total solid volume (V_{pi}) and volume of void (V_{vi}) in any particle range *i* are given by:

$$V_{pi} = n_i \frac{4\pi R_i^3}{3} = \frac{W_i}{\rho_p} \tag{A1.5}$$

$$V_{vi} = \pi r_i^2 h_i = \frac{W_i}{\rho_p} e \tag{A1.6}$$

where R_i is mean particle radius, r_i is mean pore radius and h_i is the total pore length. Dividing Equation A1.6 by A1.5 gives:

$$\frac{r_i^2}{R_i^3} = \frac{4 n_i e}{3 h_i} \tag{A1.7}$$

Value of n_i can be obtained from Equation A1.5. Pore length has been approximated as number of particles lie along the pore path times length contributed by each particle. Since actual particles in hydraulic fills are angular, it has been assumed that each particle will contribute more than particle length. Total pore length can be approximated as:

$$h_i = 2 n_i^{\lambda} R_i \tag{A1.8}$$

where λ is an empirical coefficient and is greater than 1. In this analysis λ = 1.5 has been used. Substituting h_i in Equation A1.7.

$$r_i = R_i \sqrt{\frac{2 e n_i^{1-\lambda}}{3}} \tag{A1.9}$$

Pore radius can be used to compute suction of a soil (ψ_i) can be computed as following.

$$\psi_i = \frac{2\tau \cos\varphi}{\rho_w g r_i} \tag{A1.10}$$

where τ is surface tension, φ is contact angles, ρ_w is water density and g is acceleration due to gravity. At 25^0C it has been assumed that contact angle is zero (Arya and Paris, 1981). Matric suction of hydraulic fill samples have been computed using Equations 2.13, 2.14 and A1.10. Matric suction computed from particle size distribution has been compared with test results. Figure A1.2 shows comparison of matric suction measured using filter paper and computed using aforementioned methodology.

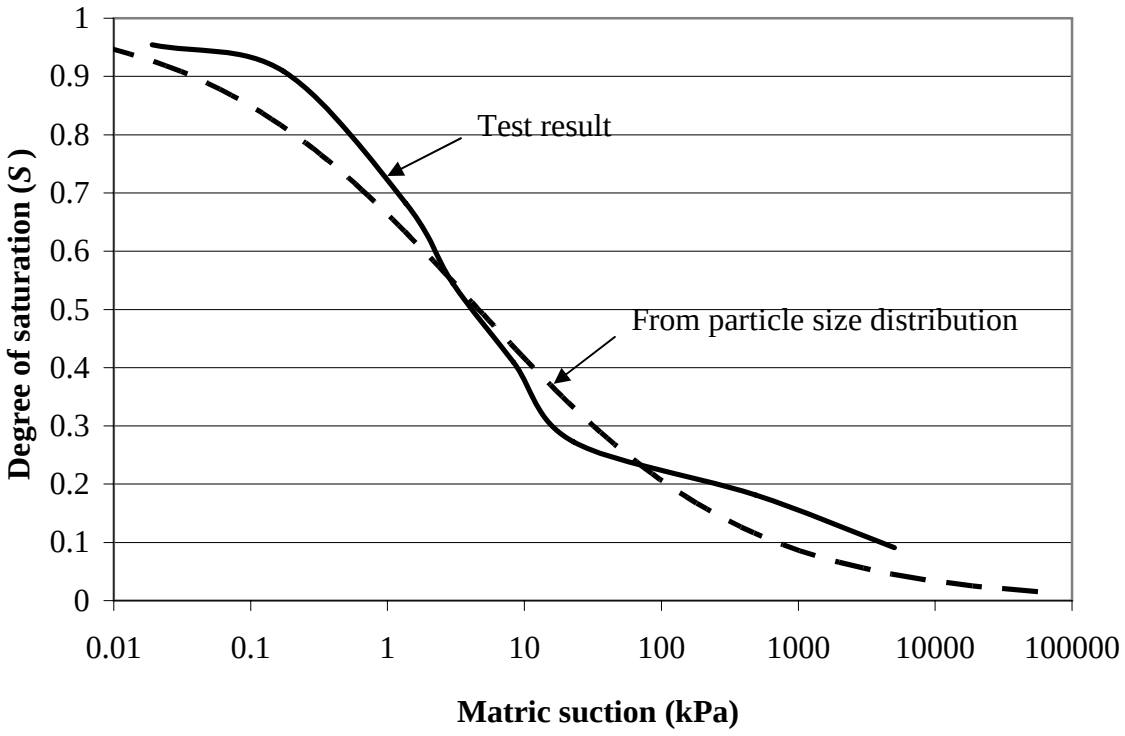

Figure A1.2 Comparison of matric suction measured in laboratory and computed from particle size distribution for hydraulic fill sample A1.

A1.2 Computation of permeability of unsaturated soil using soil-water characteristic curves

Soil water characteristic curve have been established using Filter Paper method. Laboratory test procedure has been explained in Chapter 2. Permeability of unsaturated hydraulic fills have been computed using the methodology proposed by Marshall (1958); and Kunze et al. (1968). Soil water characteristic curve has been established between volumetric moisture content (θ) and matric suction (u_a-u_w) as shown in Figure A1.3. Volumetric saturation moisture content of hydraulic fill in this example is 40%.

Soil-water characteristic curve are divided into n equal intervals of volumetric moisture content. First volumetric moisture content corresponds to saturated condition. Midpoint of each volumetric moisture content interval and matric suction corresponding on midpoint of volumetric moisture contents are marked in the Figure A1.3 and denoted by $(\theta_w)_i$ and $(u_a\text{-}u_w)_i$ respectively. Following empirical equation has been used to compute permeability of unsaturated hydraulic fills (Kunze et al. 1968):

$$k_w\left(\theta_w\right)_i = \frac{k_s}{k_{sc}} A_d \sum_{j=i}^{n}\left[\left(2j+1-2i\right)\left(u_a-u_w\right)_j^{-2}\right] \qquad \text{(A1.11)}$$

where $k_w\left(\theta_w\right)_i$ is predicted permeability of unsaturated hydraulic fill for water $(\theta_w)_i$, i is number of interval, j is a counter from i to n, k_s is permeability of saturated hydraulic fills, k_{sc} is computed coefficient of permeability for saturated hydraulic fill, which can be calculated as following:

$$k_{sc} = A_d \sum_{j=i}^{n}\left[\left(2j+1-2i\right)\left(u_a-u_w\right)_j^{-2}\right] \qquad \text{(A1.12)}$$

where adjusting constant (A_d) is given as:

$$A_d = \frac{T_s^2 \rho_w g \theta_s^p}{2\mu_w N^2} \qquad \text{(A1.13)}$$

where T_s is surface tension of water, ρ_w is water density, g is gravitational acceleration, μ_w is absolute viscosity of water, θ_s is volumetric saturation moisture content, p is a constant which account for interaction of pores. Green and Correy (1971a, 1971b) recommended that p should be taken as 2. N is total number of interval. $\sum_{j=i}^{n}\left[\left(2j+1-2i\right)\left(u_a-u_w\right)_j^{-2}\right]$ is aforementioned equations describes the shape of soil-water characteristic curve. Adjusting constant (A_d) remains constant in computing permeability.

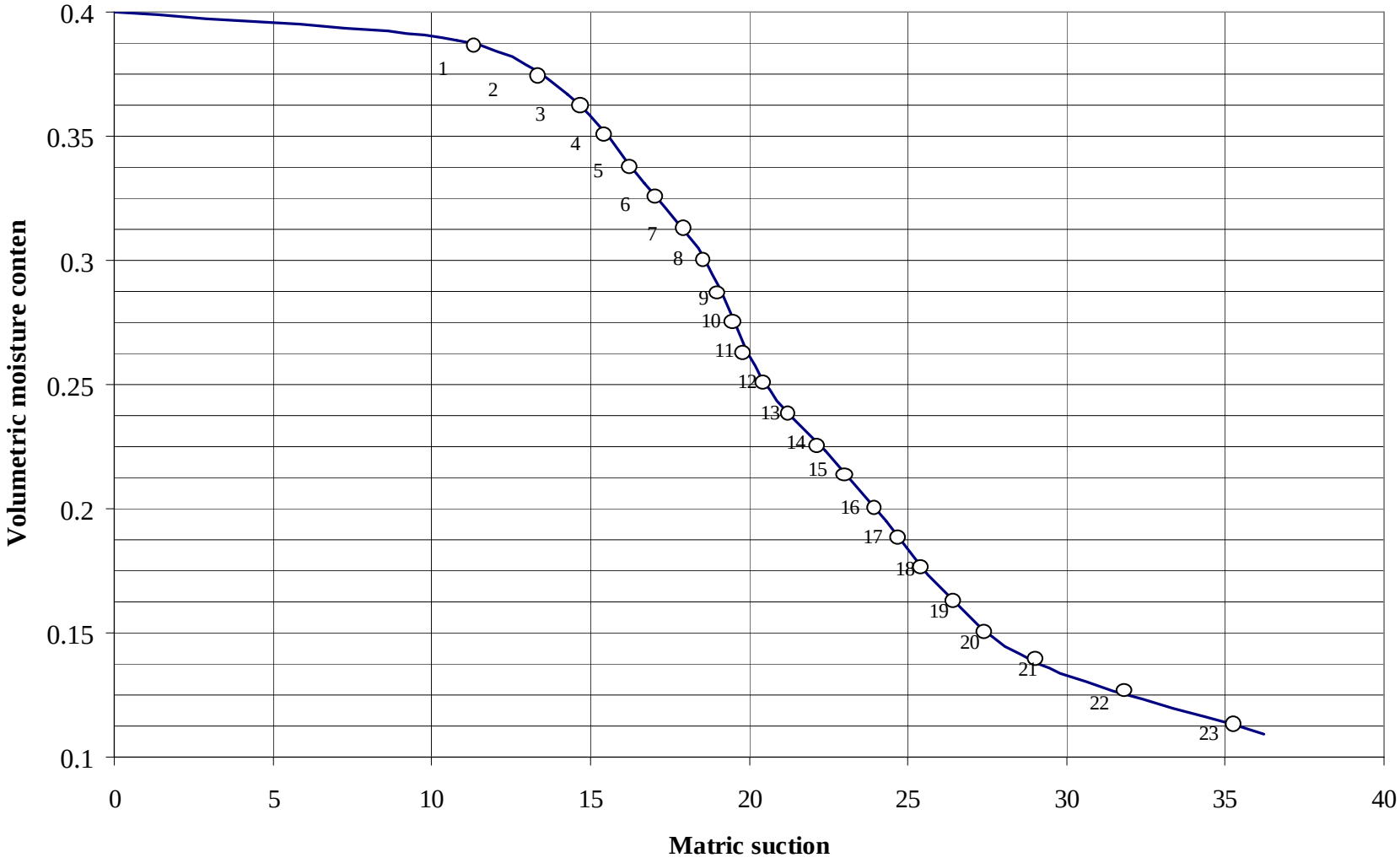

Figure A1.3 Soil-water characteristic curve to estimate permeability of hydraulic fills

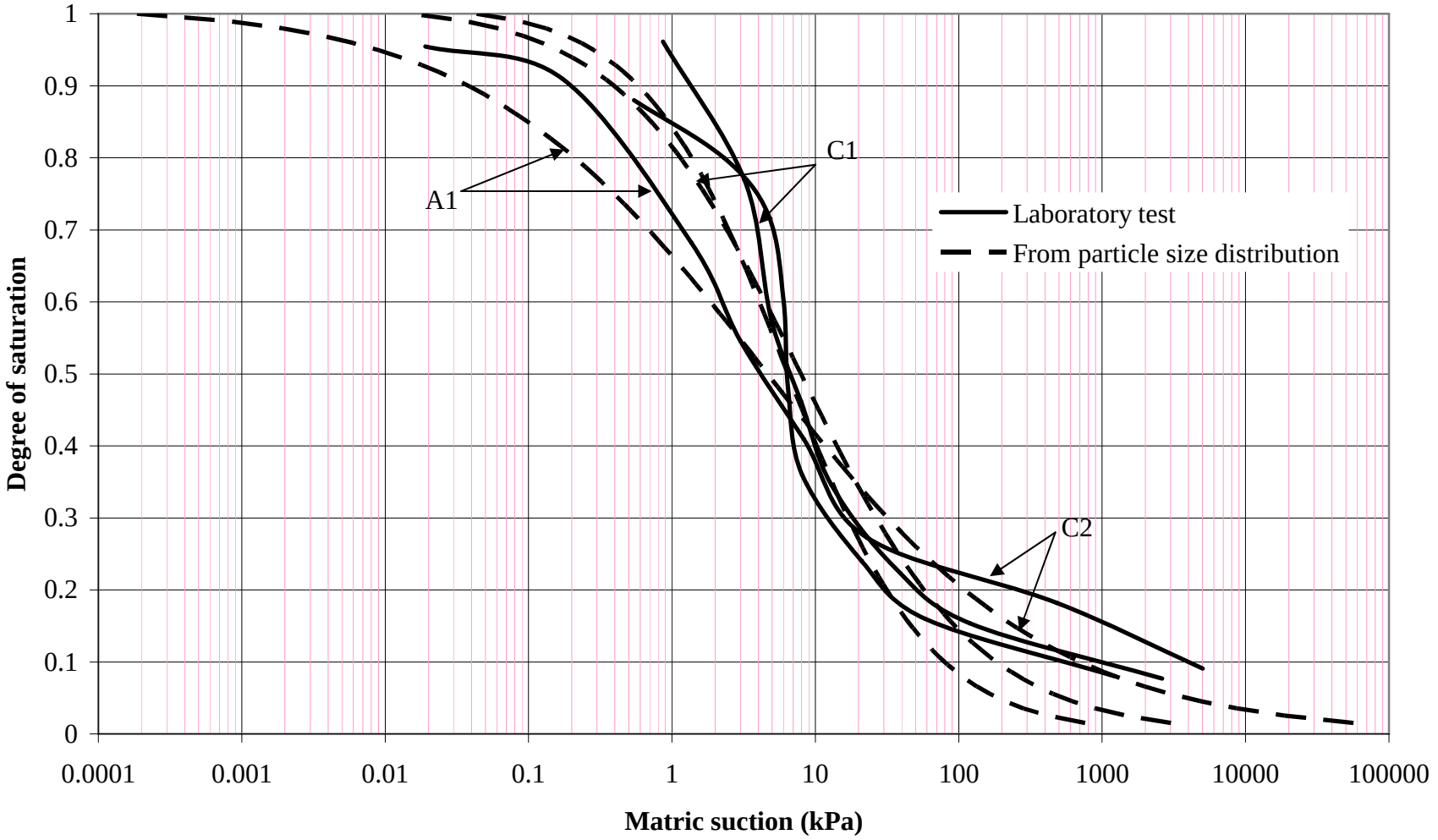

A2.1 Comparison of matric suction of hydraulic fills samples A1, C1 and C2 measured in laboratory and computed using particle size distribution

A2.2 Final moisture content of hydraulic fill samples on sieve vibrator

Table A2.1 Measurement of final moisture content of A1 for 23.9 mm high sample

Initial moisture content (%)	Final moisture content (%)		
	Vibration time		
	30 min	60 min	120 min
20	12.9	12.5	12.2
25	12.8	12.8	12.5
30	12.6	12.7	12.4
35	12.7	12.7	12.3
40	12.9	12.9	12.6

Table A2.2 Measurement of final moisture content of A1 for 47.7 mm high sample

Initial moisture content (%)	Final moisture content (%)		
	Vibration time		
	30 min	60 min	120 min
20	12.5	12.3	12.4
25	12.7	12.6	12.3
30	12.8	12.2	12.1

35	12.1	12.4	12.3
40	12.6	12.4	12.2

Table A2.3 Measurement of final moisture content of A1 for 71.6 mm high sample

Initial moisture content (%)	Final moisture content (%)		
	Vibration time		
	30 min	60 min	120 min
20	12.8	12.4	12.3
25	12.8	12.2	12.2
30	12.7	12.6	12.5
35	12.6	12.5	12.4
40	12.4	12.7	12.2

Table A2.4 Measurement of final moisture content of A1 for 95.4 mm high sample

Initial moisture content (%)	Final moisture content (%)		
	Vibration time		
	30 min	60 min	120 min
20	12.4	12.4	12.2

25	12.3	12.5	12.1
30	12.5	12.6	12.3
35	13.1	12.2	12.2
40	12.8	12.4	12.3

Table A2.5 Measurement of final moisture content of B1 for 23.9 mm high sample

Initial moisture content (%)	Final moisture content (%)		
	Vibration time		
	30 min	60 min	120 min
20	13.9	13.7	13.5
25	14.0	13.8	13.6
30	13.7	13.5	13.3
35	13.9	13.7	13.5
40	13.6	13.4	13.2

Table A2.6 Measurement of final moisture content of B1 for 47.7 mm high sample

Initial moisture content (%)	Final moisture content (%)		
	Vibration time		
	30 min	60 min	120 min
20	13.9	13.8	13.7
25	14.0	14.1	13.8
30	13.7	13.7	13.6
35	13.9	13.9	14.0
40	13.6	13.6	13.6

Table A2.7 Measurement of final moisture content of B1 for 71.6 mm high sample

Initial moisture content (%)	Final moisture content (%)		
	Vibration time		
	30 min	60 min	120 min
20	13.6	13.7	13.5
25	13.2	13.6	13.0
30	13.2	13.7	13.7
35	13.4	13.9	13.1
40	14.1	13.7	13.5

Table A2.8 Measurement of final moisture content of B1 for 95.4 mm high sample

Initial moisture content (%)	Final moisture content (%)		
	Vibration time		
	30 min	60 min	120 min
20	13.9	13.6	13.7
25	13.5	13.7	13.8
30	13.7	13.9	13.6
35	13.3	13.4	13.5
40	13.6	13.7	13.6

Table A2.9 Measurement of final moisture content of B2 for 23.9 mm high sample

Initial moisture content (%)	Final moisture content (%)		
	Vibration time		
	30 min	60 min	120 min
20	14.4	14.7	14.6
25	14.6	14.8	14.5
30	14.7	14.5	14.7
35	14.7	14.6	14.6
40	14.8	14.6	14.6

Table A2.10 Measurement of final moisture content of B2 for 47.7 mm high sample

Initial moisture content (%)	Final moisture content (%)		
	Vibration time		
	30 min	60 min	120 min
20	14.4	14.7	14.3
25	14.6	14.8	14.5
30	14.7	14.5	14.3
35	14.7	14.1	14.4
40	14.8	14.4	14.8

Table A2.11 Measurement of final moisture content of B2 for 71.6 mm high sample

Initial moisture content (%)	Final moisture content (%)		
	Vibration time		
	30 min	60 min	120 min
20	14.4	14.5	14.3
25	14.6	14.2	14.5
30	14.1	14.5	14.3
35	14.4	14.1	14.4
40	14.3	14.2	14.8

Table A2.12 Measurement of final moisture content of B2 for 95.4 mm high sample

Initial moisture content (%)	Final moisture content (%)		
	Vibration time		
	30 min	60 min	120 min
20	14.4	14.5	14.3
25	14.2	14.0	14.5
30	14.3	14.3	14.3
35	14.1	14.1	14.4
40	13.9	14.2	14.1

Table A2.13 Measurement of final moisture content of C1 for 23.9 mm high sample

Initial moisture content (%)	Final moisture content (%)		
	Vibration time		
	30 min	60 min	120 min
20	13.7	13.5	13.4
25	13.4	13.9	13.6
30	13.5	13.6	13.1
35	13.8	13.5	13.2
40	13.8	13.2	13.4

Table A2.14 Measurement of final moisture content of C1 for 47.7 mm high sample

Initial moisture content (%)	Final moisture content (%)		
	Vibration time		
	30 min	60 min	120 min
20	13.4	13.5	13.4
25	13.7	13.4	13.6
30	13.8	13.6	13.6
35	13.3	13.9	13.8
40	13.6	13.5	13.5

Table A2.15 Measurement of final moisture content of C1 for 71.6 mm high sample

Initial moisture content (%)	Final moisture content (%)		
	Vibration time		
	30 min	60 min	120 min
20	13.3	13.2	13.2
25	13.5	13.5	13.3
30	13.2	13.4	13.5
35	13.4	13.3	13.4
40	13.2	13.3	13.1

Table A2.16 Measurement of final moisture content of C1 for 95.4 mm high sample

Initial moisture content (%)	Final moisture content (%)		
	Vibration time		
	30 min	60 min	120 min
20	13.2	13.3	13.1
25	13.6	13.4	13.2
30	13.2	13.2	13.4
35	13.1	13.3	13.3
40	13.3	13.2	13.2

Table A2.17 Measurement of final moisture content of C2 for 23.9 mm high sample

Initial moisture content (%)	Final moisture content (%)		
	Vibration time		
	30 min	60 min	120 min
20	13.4	13.2	13.2
25	13.5	13.3	13.5
30	13.3	13.5	13.5
35	13.5	13.4	13.2
40	13.2	13.2	13.3

Table A2.18 Measurement of final moisture content of C2 for 47.7 mm high sample

Initial moisture content (%)	Final moisture content (%)		
	Vibration time		
	30 min	60 min	120 min
20	13.3	13.1	13.2
25	13.4	13.4	13.2
30	13.2	13.2	13.1
35	13.5	13.1	13.3
40	13.1	13.1	13.5

Table A2.19 Measurement of final moisture content of C2 for 71.6 mm high sample

Initial moisture content (%)	Final moisture content (%)		
	Vibration time		
	30 min	60 min	120 min
20	13.2	13.3	13.2
25	13.4	13.4	13.1
30	13.5	13.2	13.2
35	13.1	13.14	13.3
40	13.1	13.2	13.1

Table A2.20 Measurement of final moisture content of C2 for 95.4 mm high sample

Initial moisture content (%)	Final moisture content (%)		
	Vibration time		
	30 min	60 min	120 min
20	13.1	13.2	12.8
25	12.9	13.1	13.1
30	13.3	13.3	13.3
35	13.2	13.1	13.1
40	13.1	13.1	13.2

Appendix B

Moisture content and permeability variation in a mine stop

B1 Average moisture content variation of hydraulic fill samples

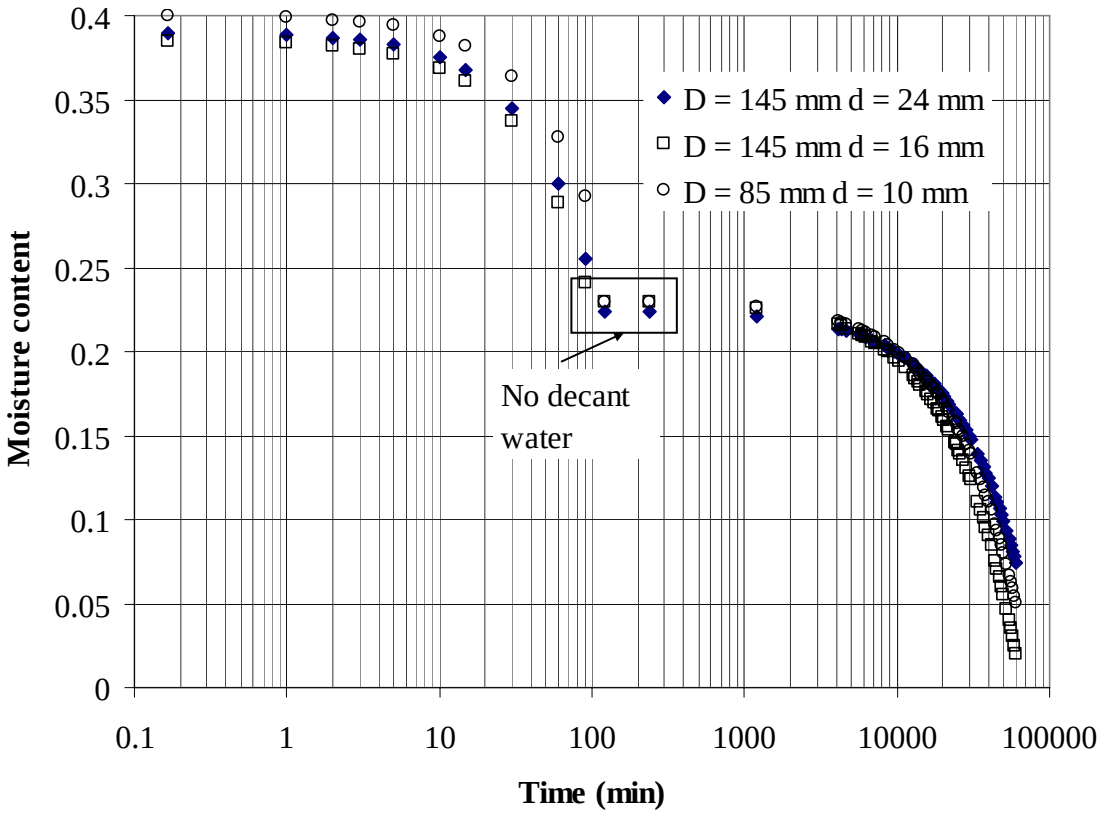

Figure B1.1 Average moisture content variation for sample A1

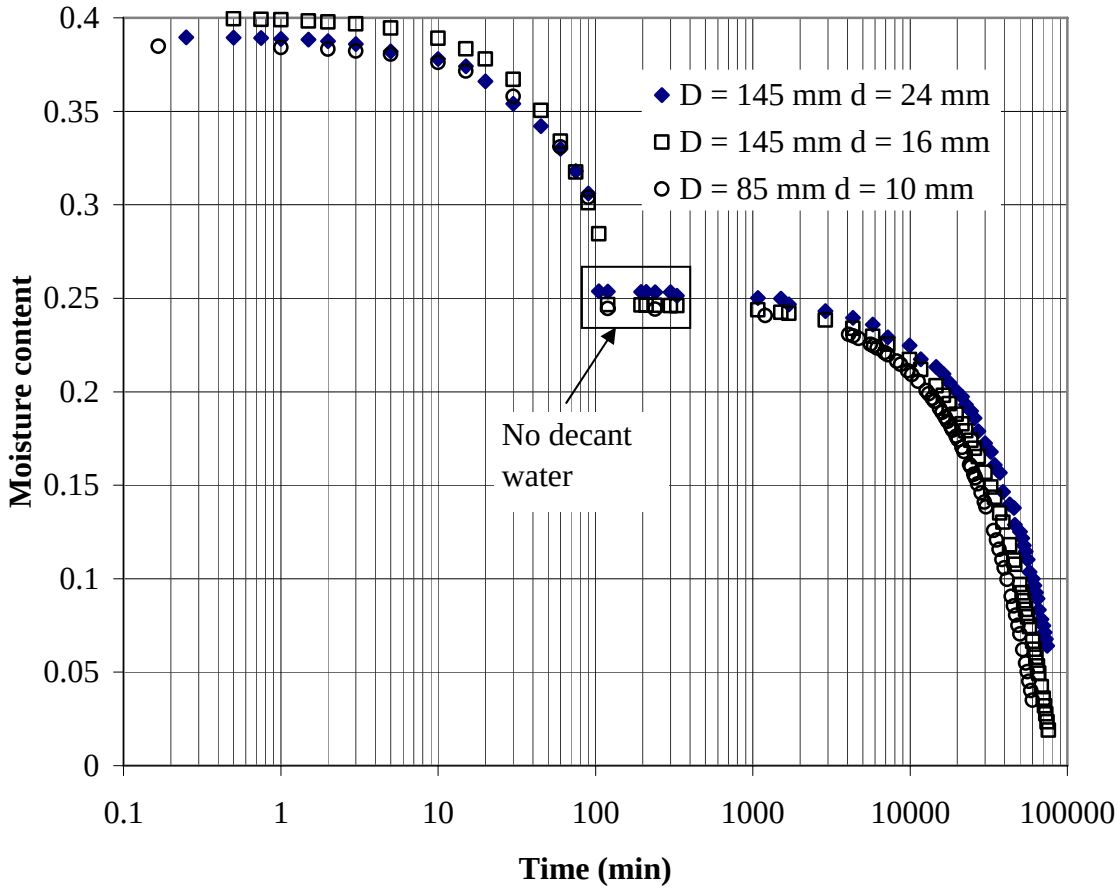

Figure B1.2 Average moisture content variation for sample B2

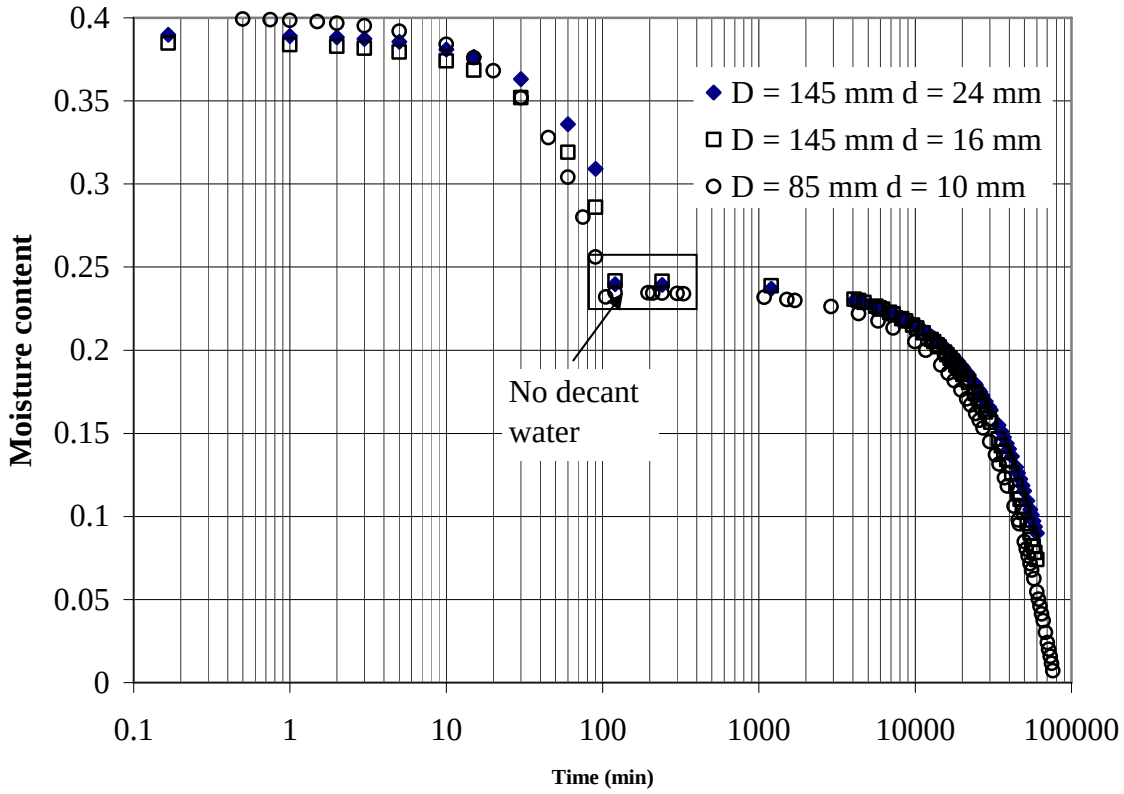

Figure B1.3 Average moisture content variation for sample C1

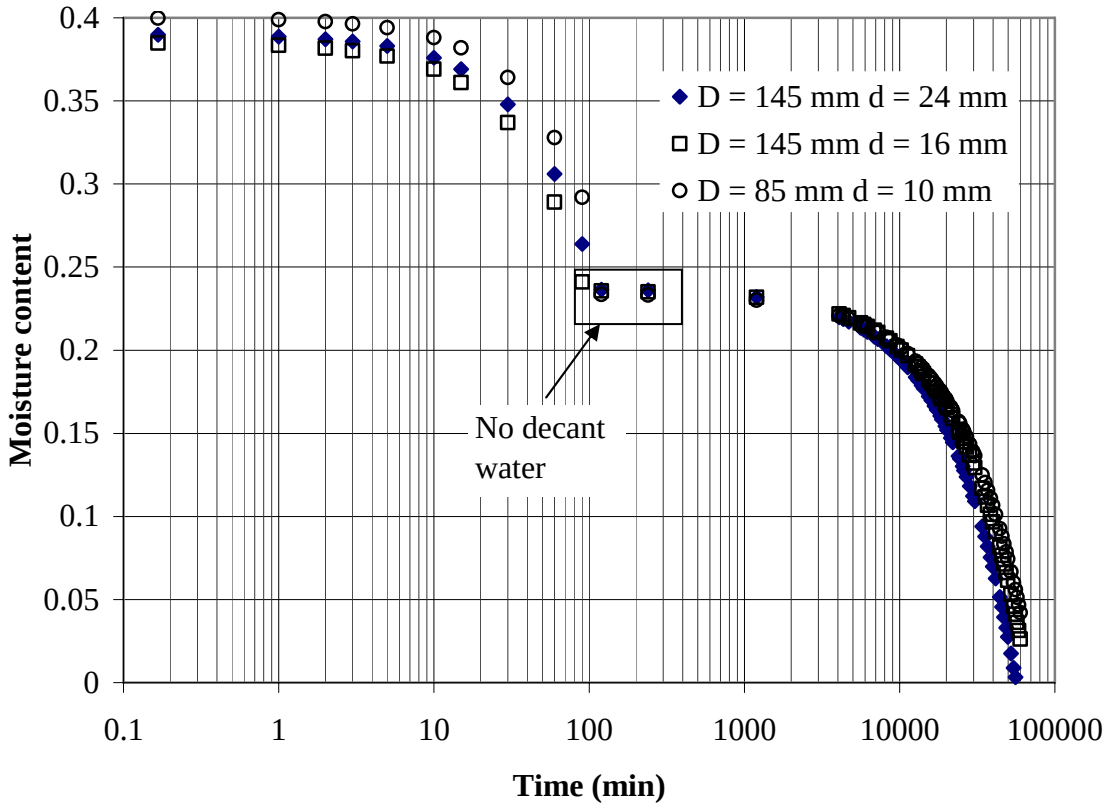

Figure B1.4 Average moisture content variation for sample C2

B2 Moisture content variation width depth and time

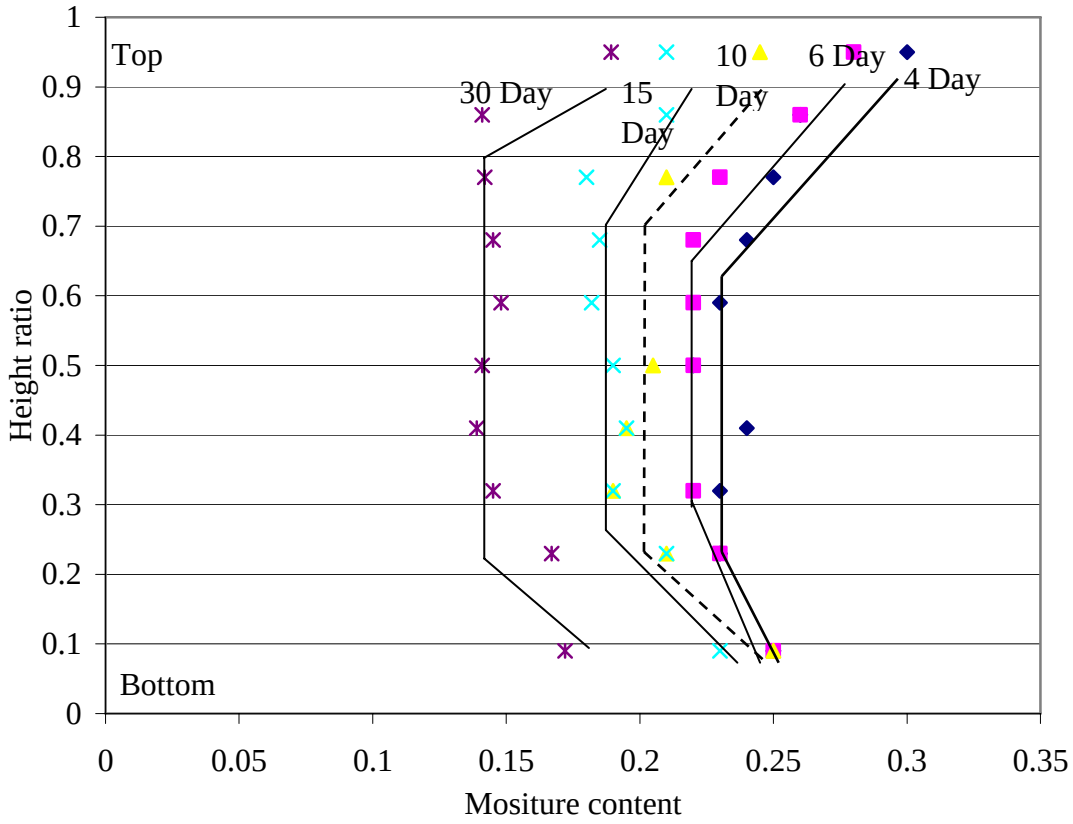

Figure B2.1 Moisture content variations with height ratio for sample A1 at end of 4, 6, 10, 15 and 30 days.

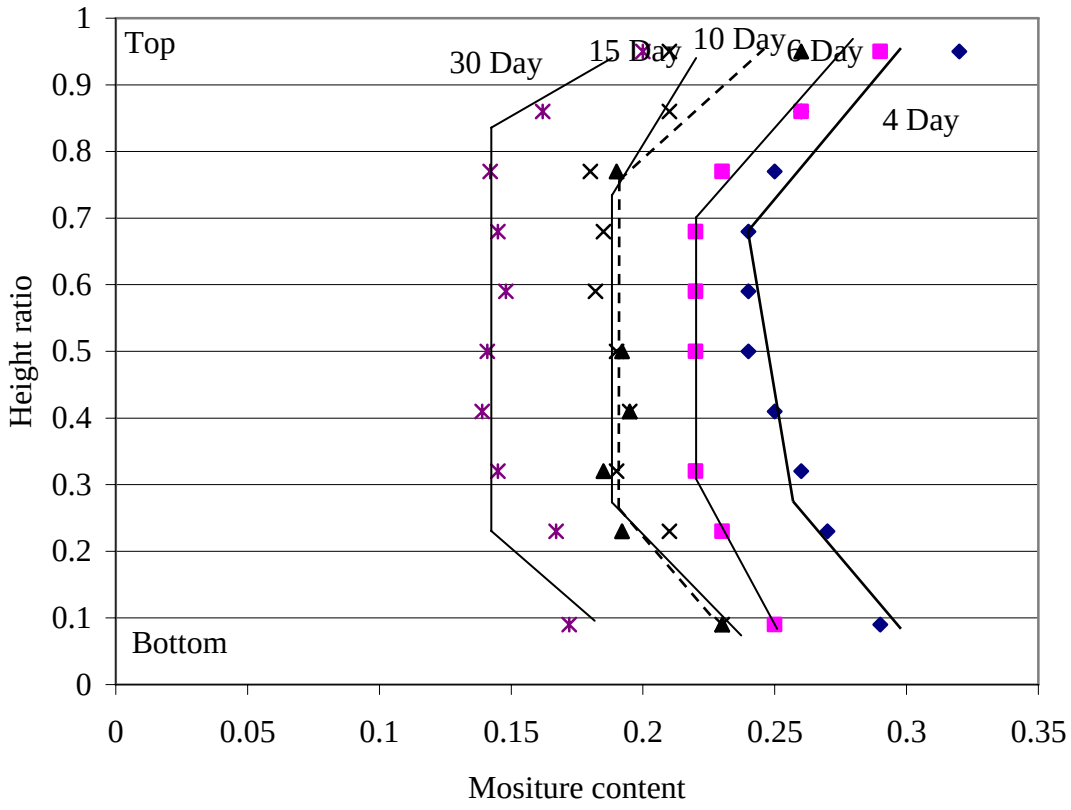

Figure B2.2 Moisture content variations with height ratio for sample B1 at end of 4, 6, 10, 15 and 30 days.

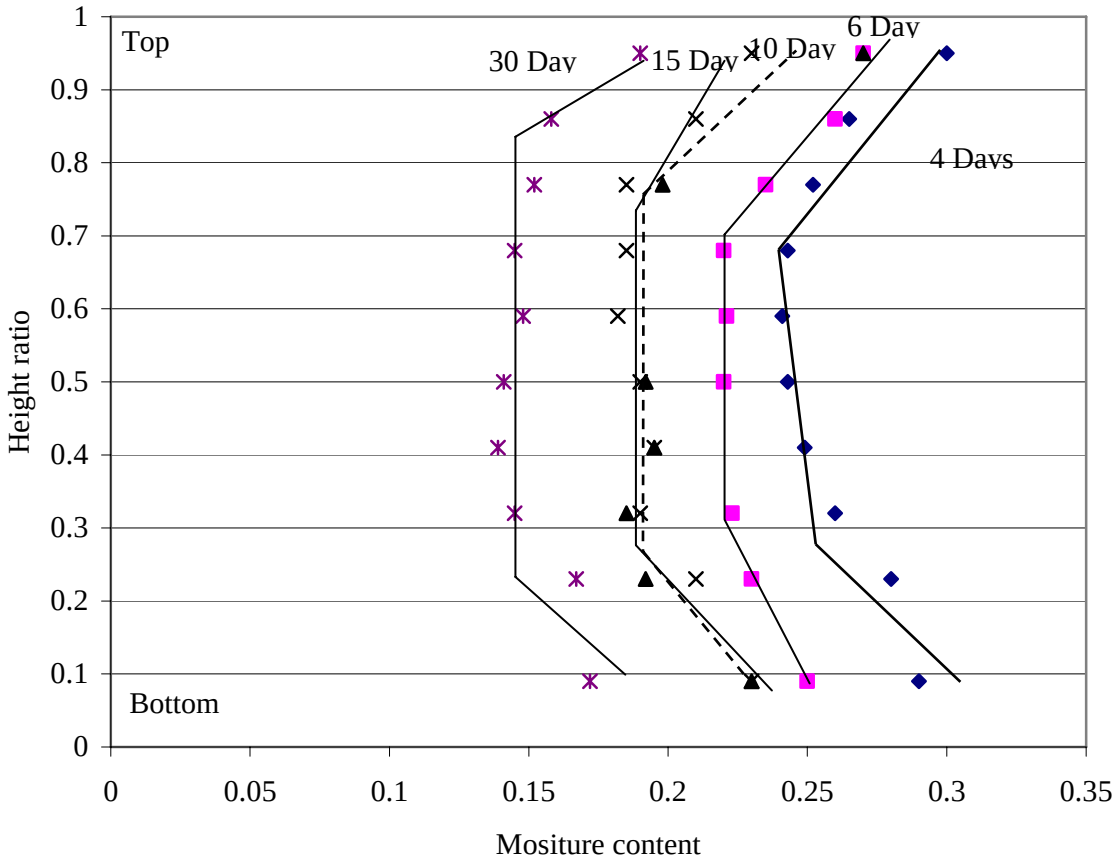

Figure B2.3 Moisture content variations with height ratio for sample C1 at end of 4, 6, 10, 15 and 30 days.

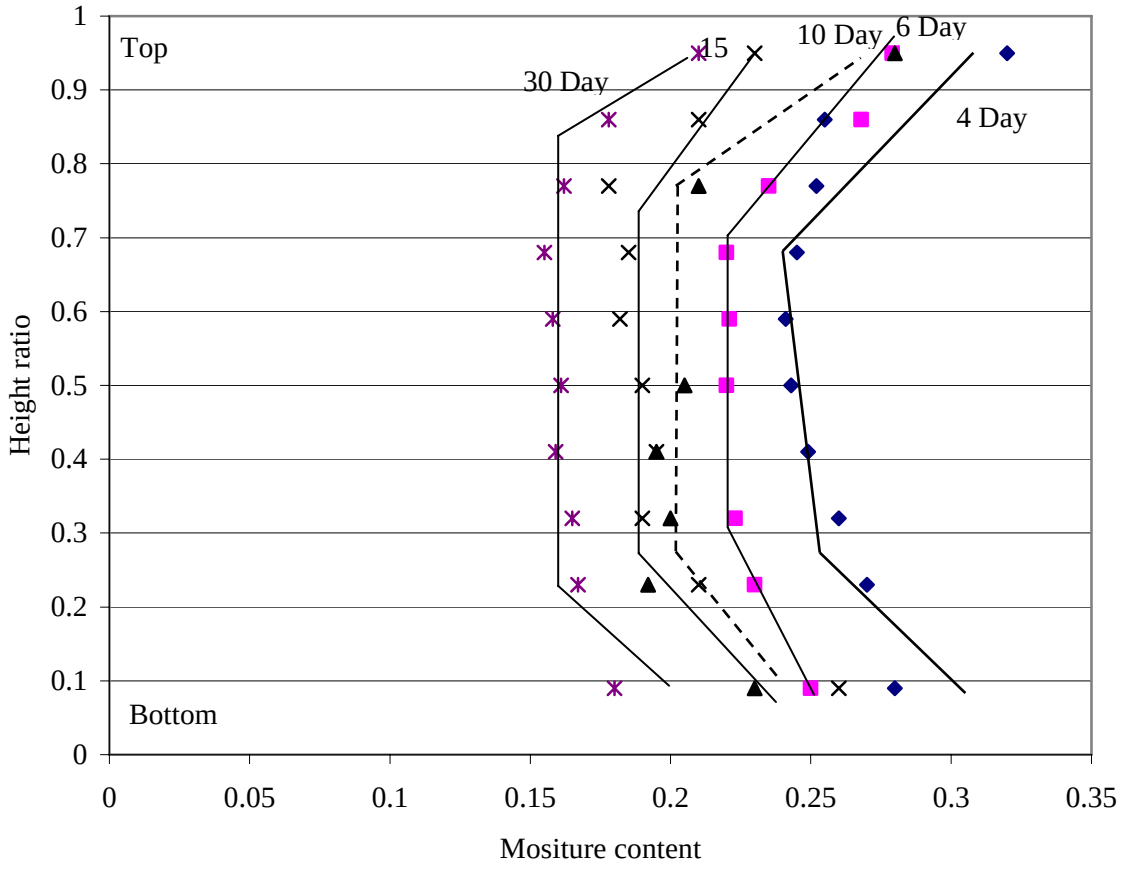

Figure B2.4 Moisture content variations with height ratio for sample C2 at end of 4, 6, 10, 15 and 30 days.

B3 Permeability variation with depth

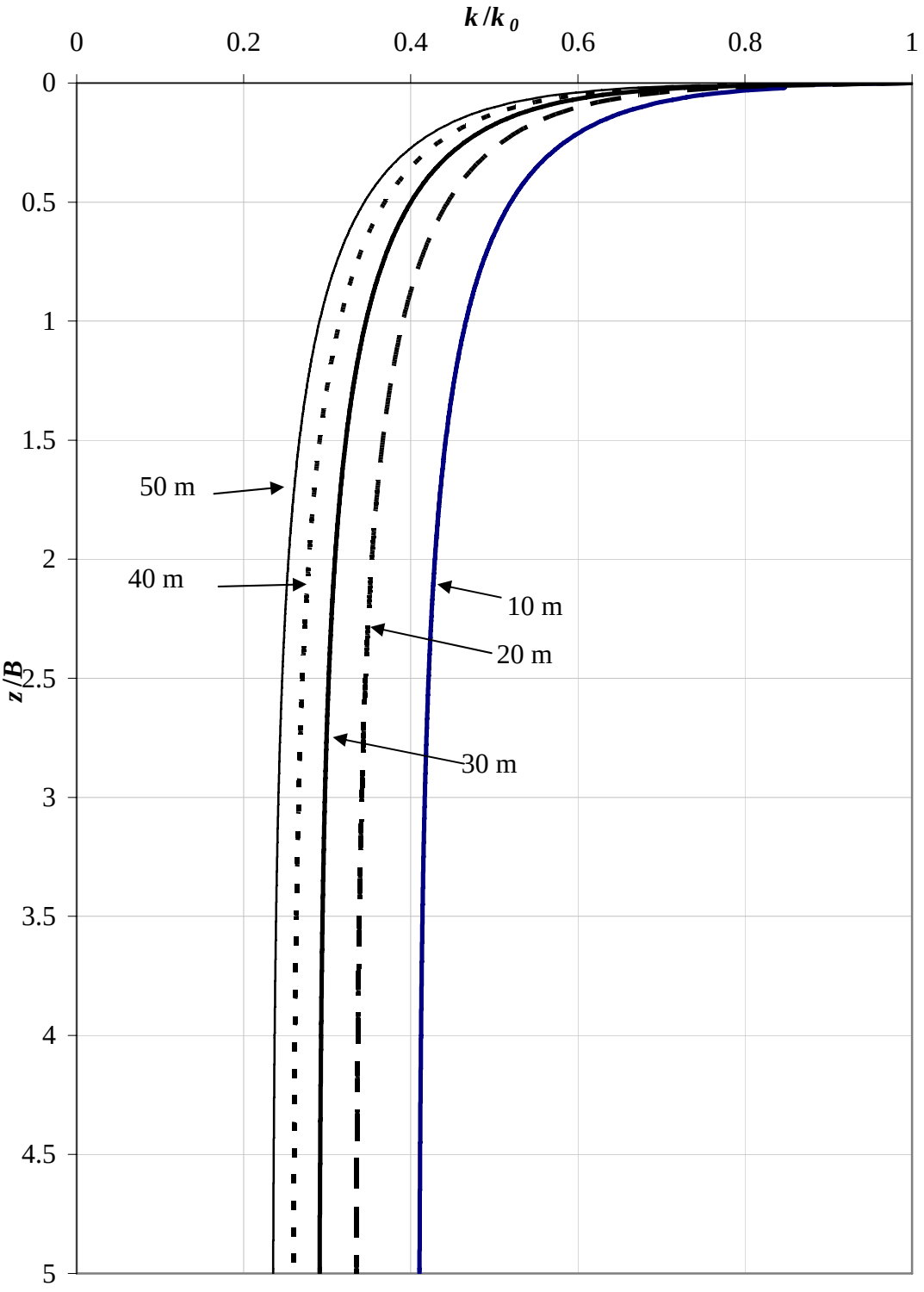

Figure B3.1 Permeability variation of saturated hydraulic fill sample B1 with depth for stope width (*B*) of 10, 20, 30, 40 and 50 m.

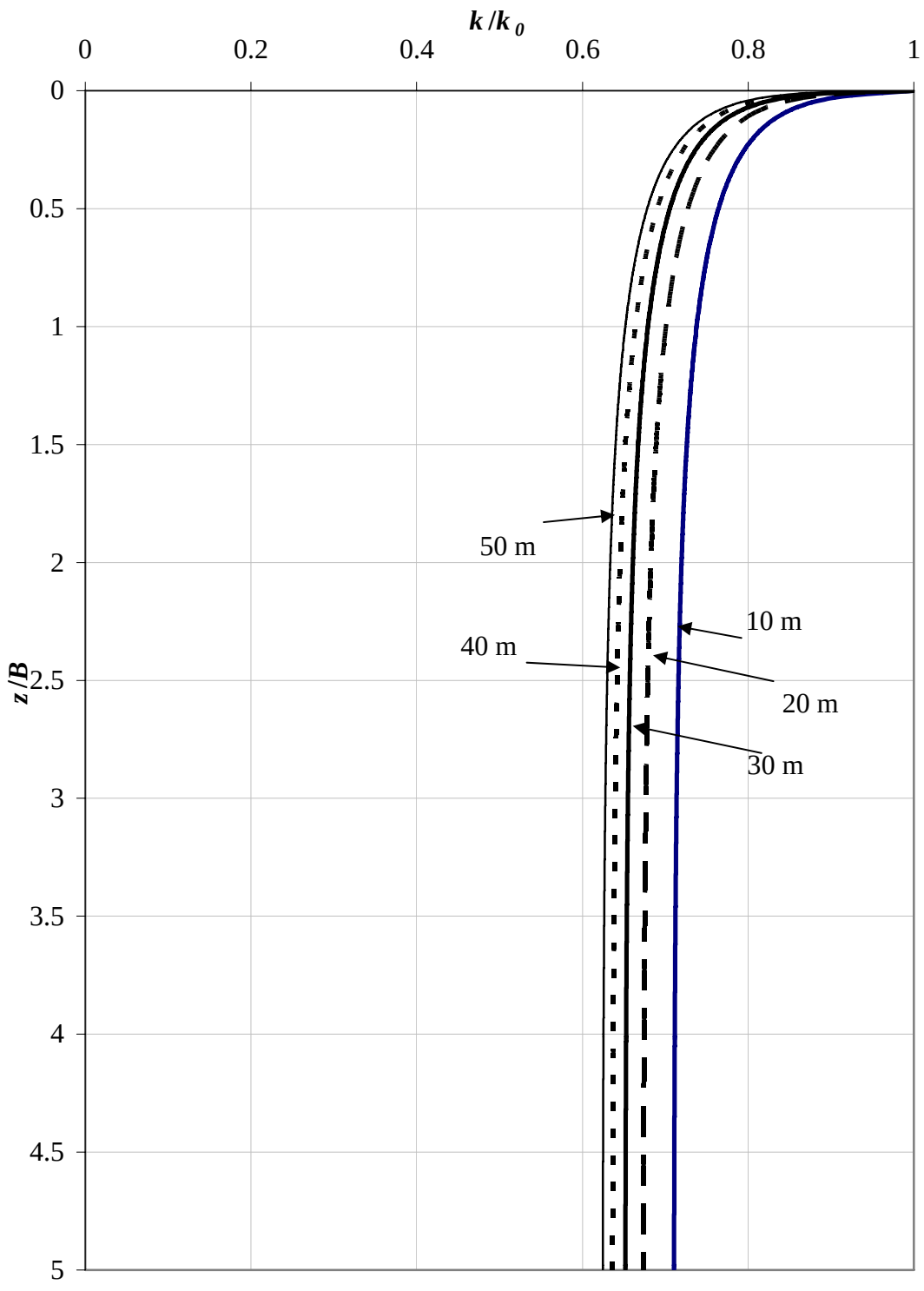

Figure B3.2 Permeability variation of saturated hydraulic fill sample B2 with depth for stope width (*B*) of 10, 20, 30, 40 and 50 m.

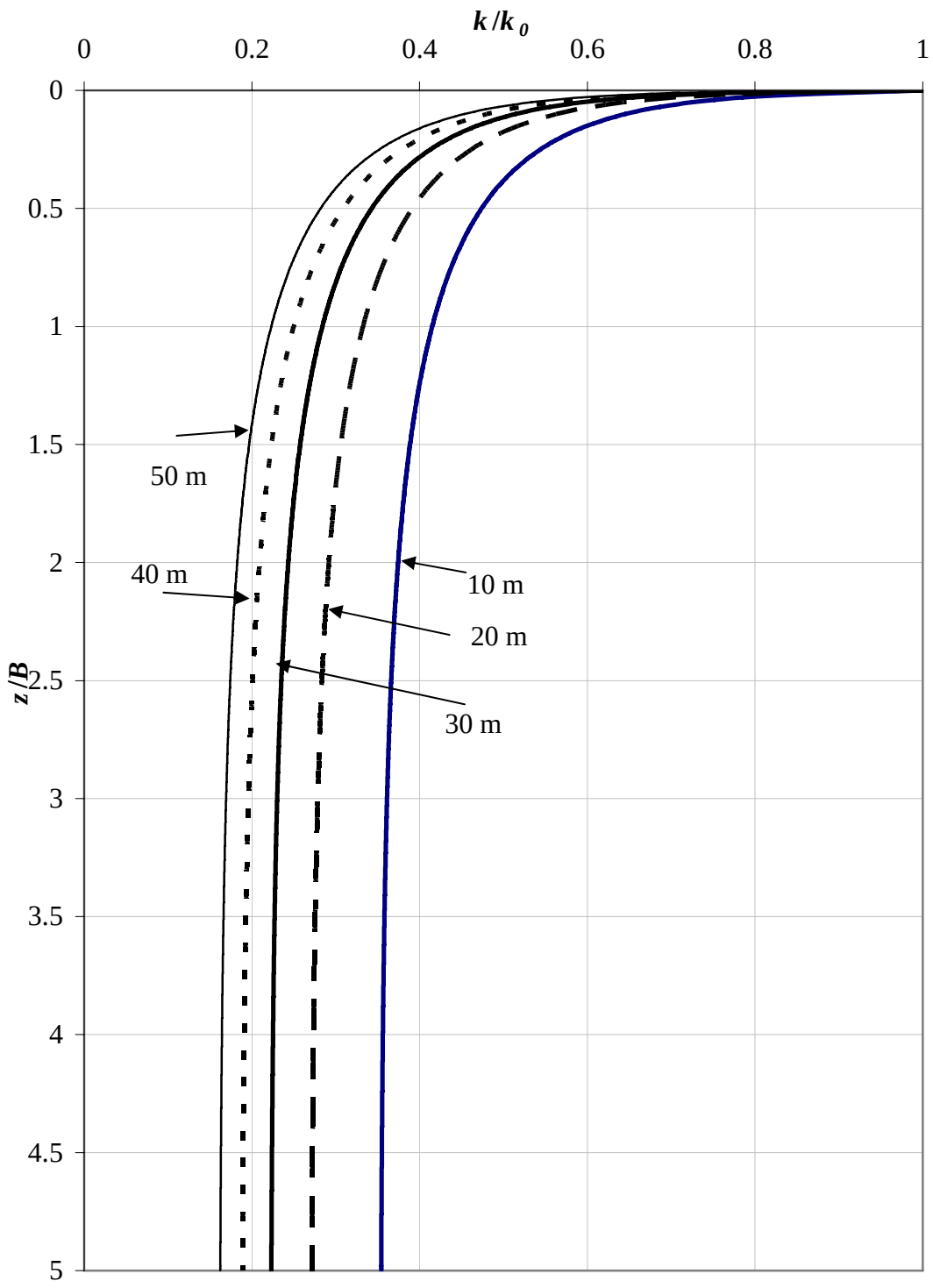

Figure B3.3 Permeability variation of saturated hydraulic fill sample C1 with depth for stope width (*B*) of 10, 20, 30, 40 and 50 m.

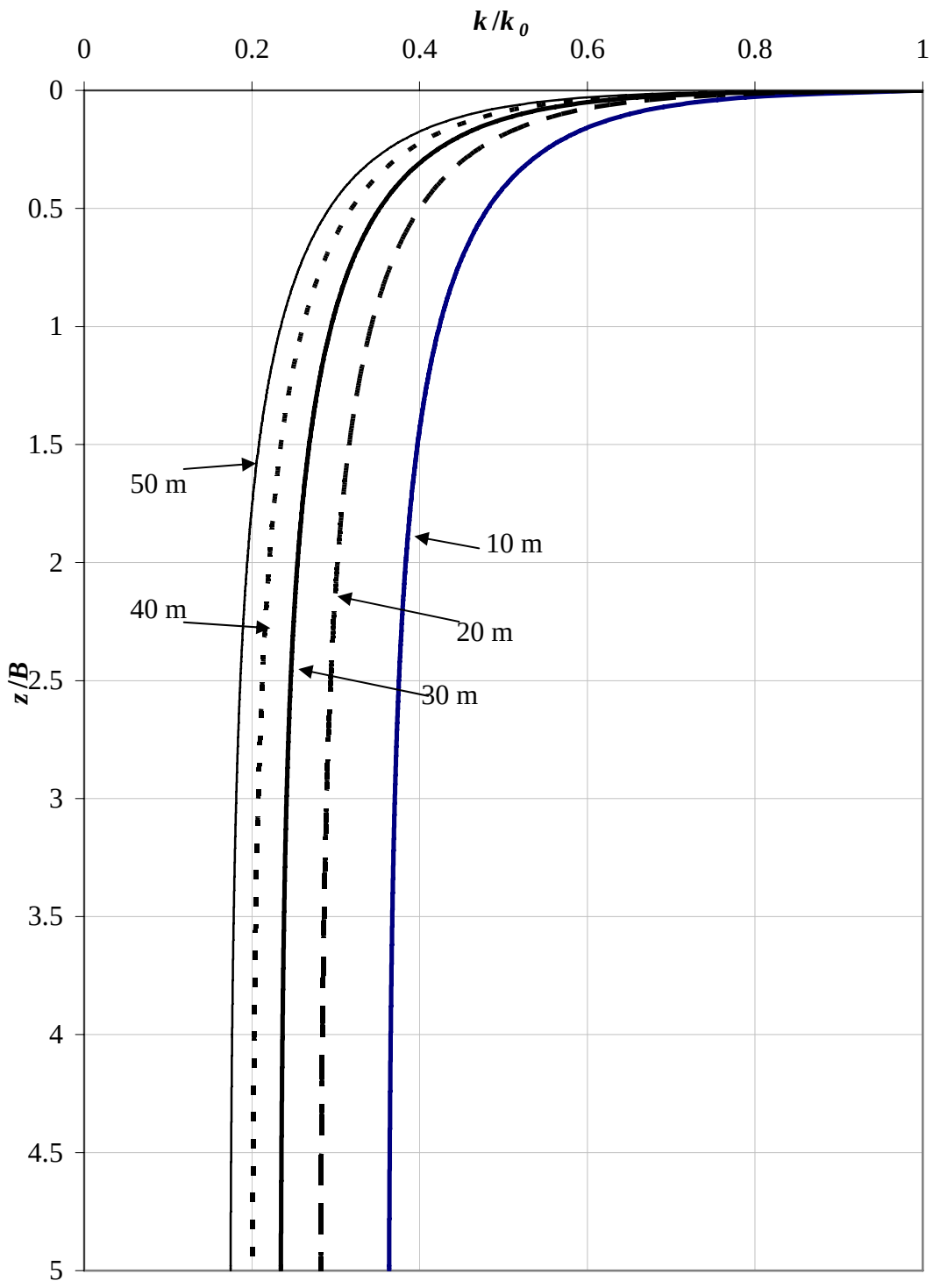

Figure B3.4 Permeability variation of saturated hydraulic fill sample C2 with depth for stope width (*B*) of 10, 20, 30, 40 and 50 m.

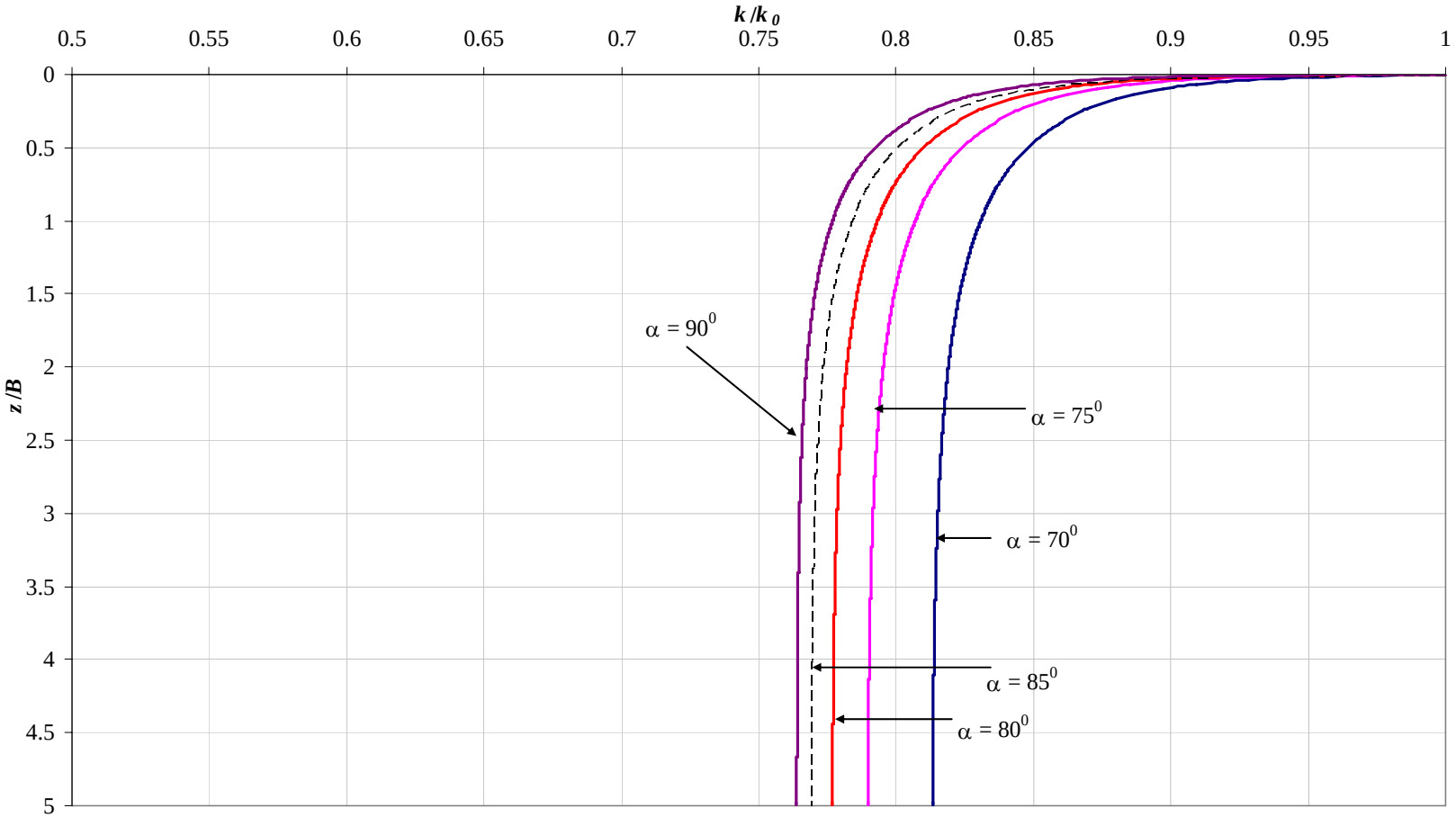

Figure B3.5 Permeability variation of saturated hydraulic fills sample B1 with depth for stope width (*B*) of 20m in stope of inclination (α) of 70^0,75^0, 80^0, 85^0 and 90^0 with horizontal

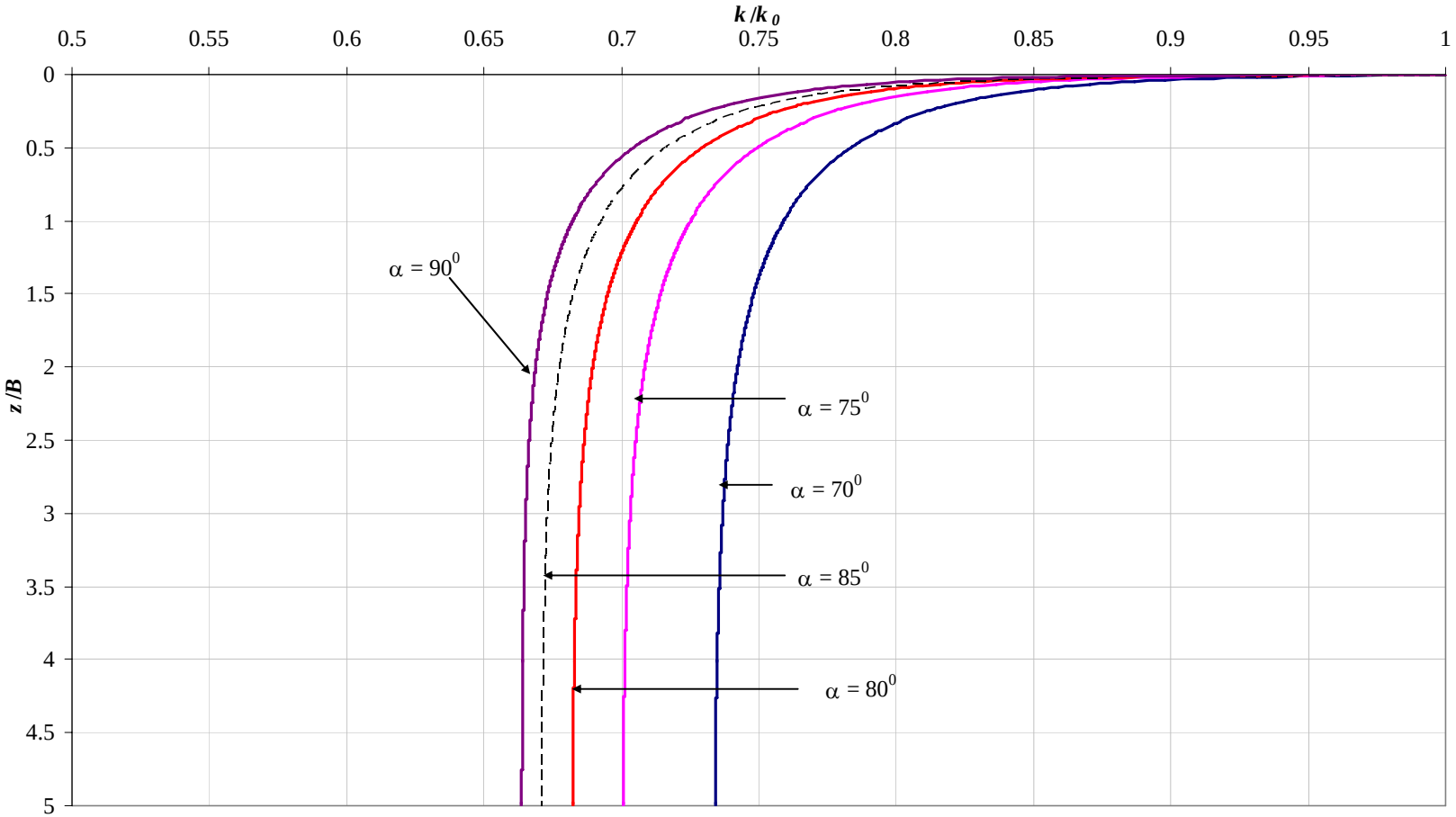

Figure B3.6 Permeability variation of saturated hydraulic fills sample B2 with depth for stope width (*B*) of 20m in stope of inclination (α) of 70^0,75^0, 80^0, 85^0 and 90^0 with horizontal

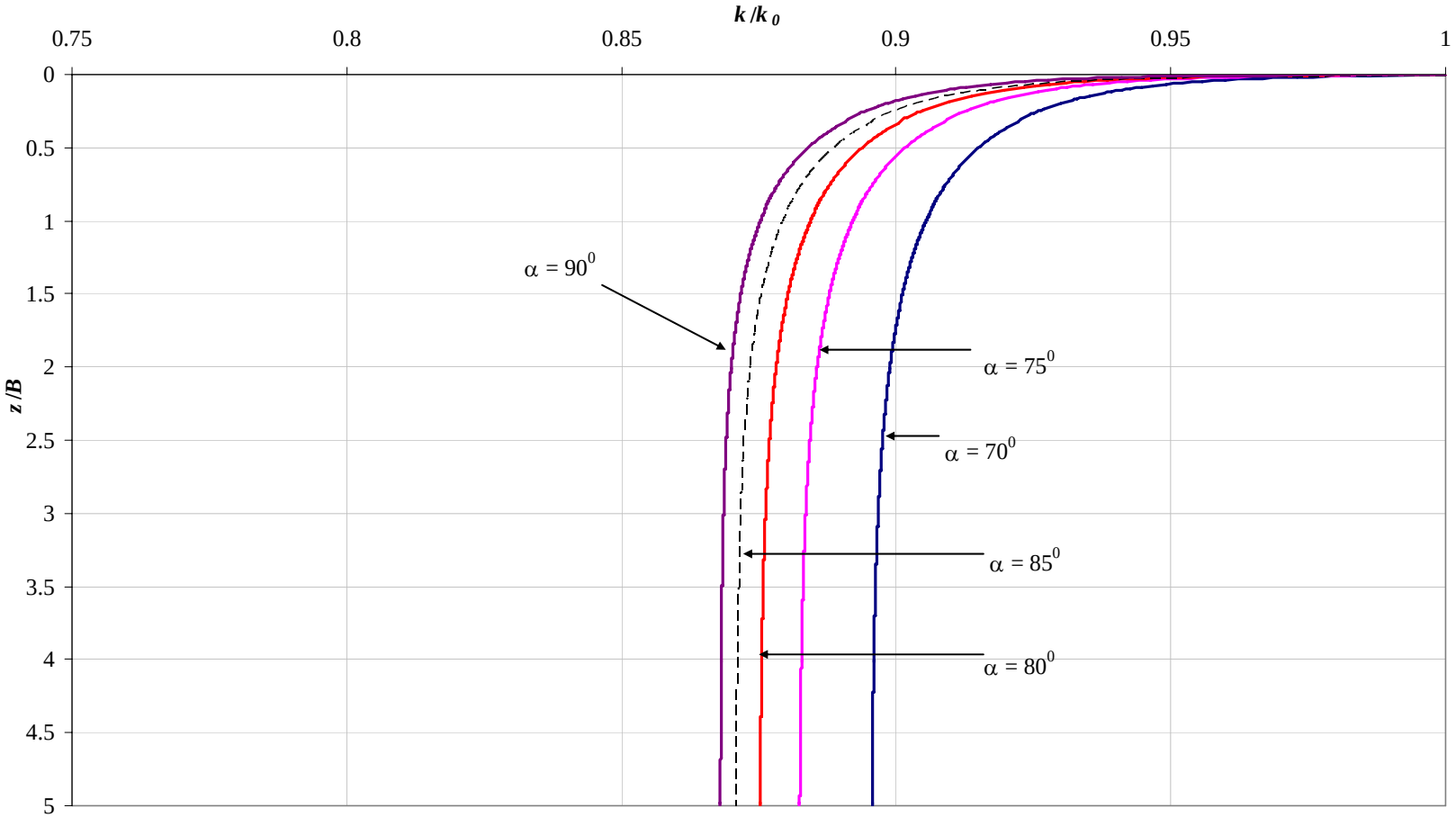

Figure B3.7 Permeability variation of saturated hydraulic fills sample C1 with depth for stope width (*B*) of 20m in stope of inclination (α) of 70^0,75^0, 80^0, 85^0 and 90^0 with horizontal

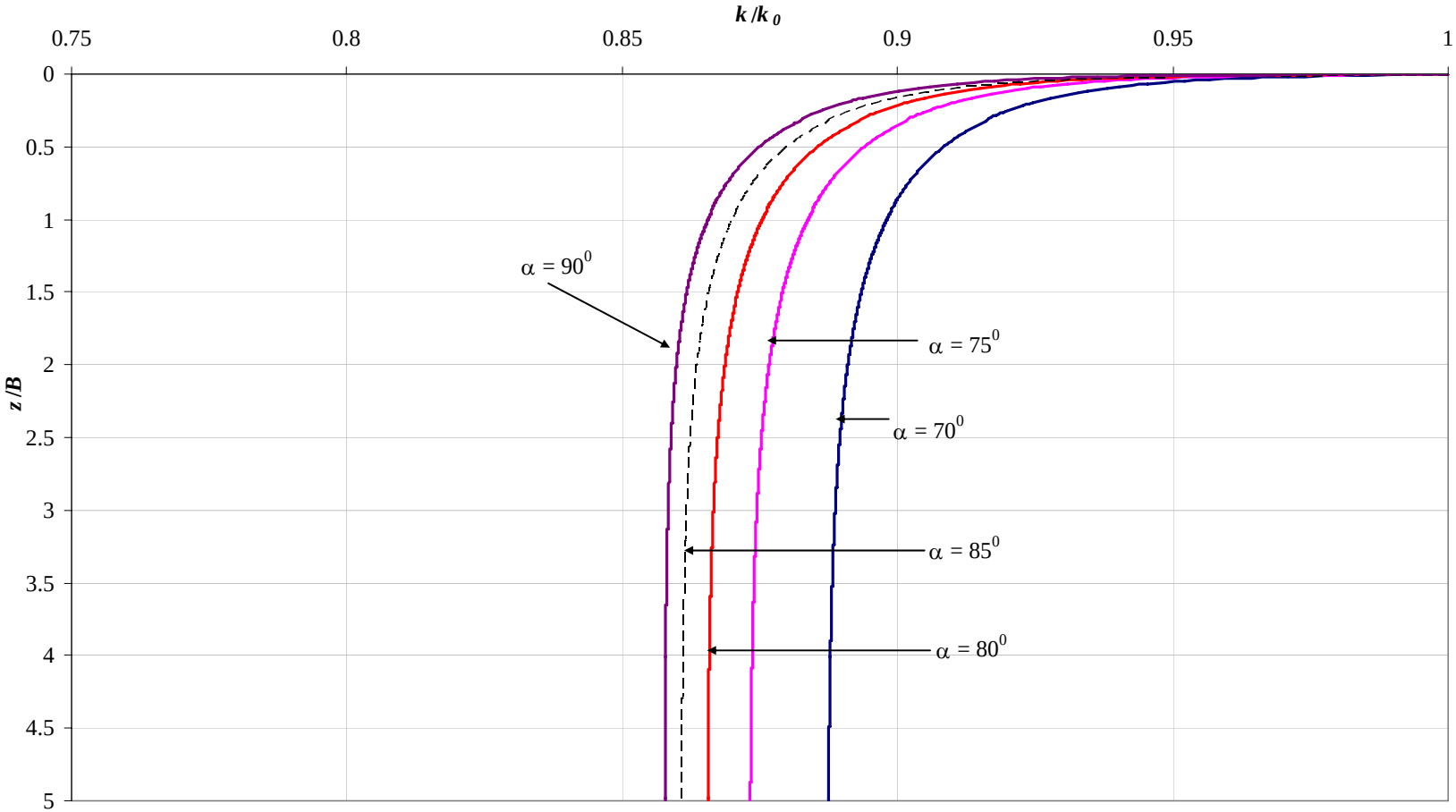

Figure B3.8 Permeability variation of saturated hydraulic fills sample C2 with depth for stope width (*B*) of 20m in stope of inclination (α) of 70^0,75^0, 80^0, 85^0 and 90^0 with horizon

Appendix C

Settlement of Hydraulic fills

C1 Typical settlement of hydraulic fills

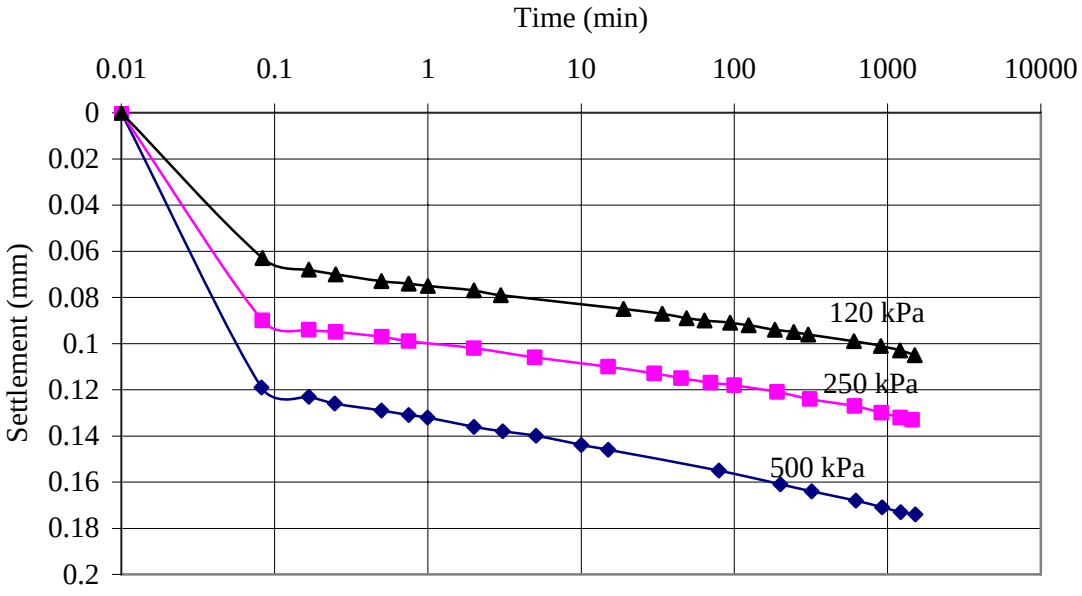

Figure C1.1 Settlement curve of hydraulic fill sample A1

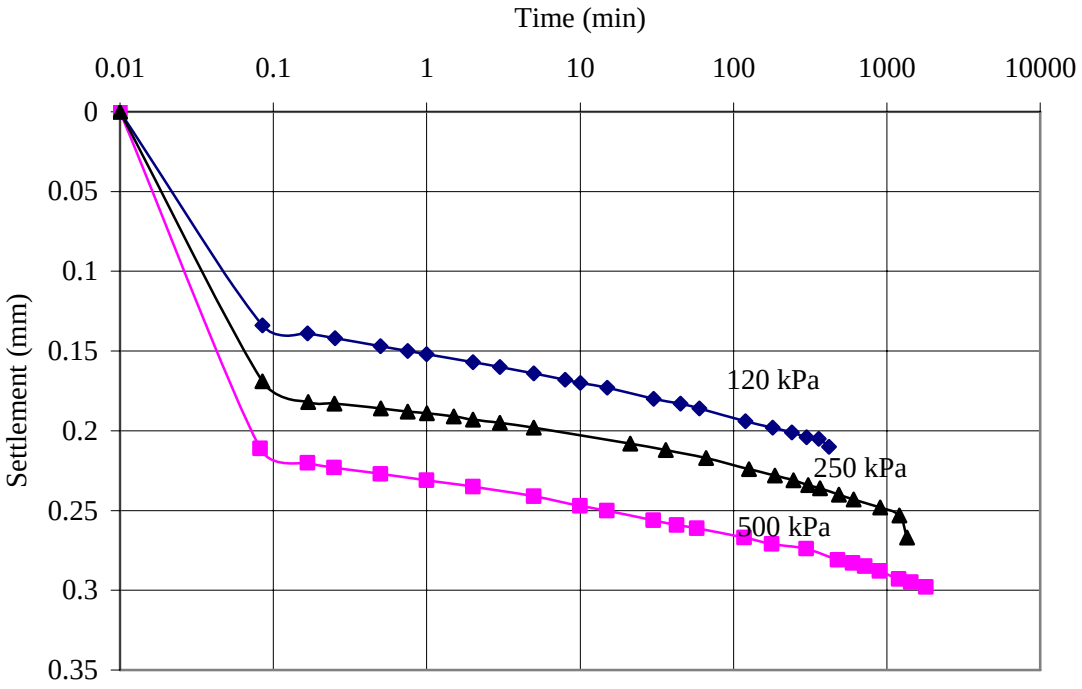

Figure C1.2 Settlement curve of hydraulic fill sample B1

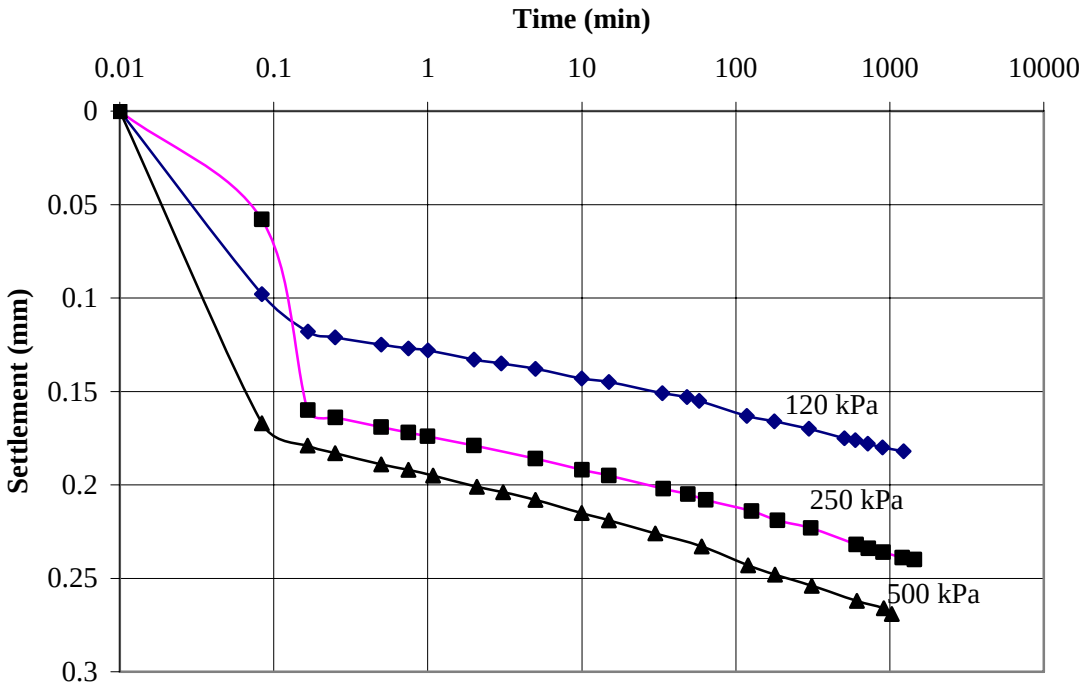

Figure C1.3 Settlement curve of hydraulic fill sample C1

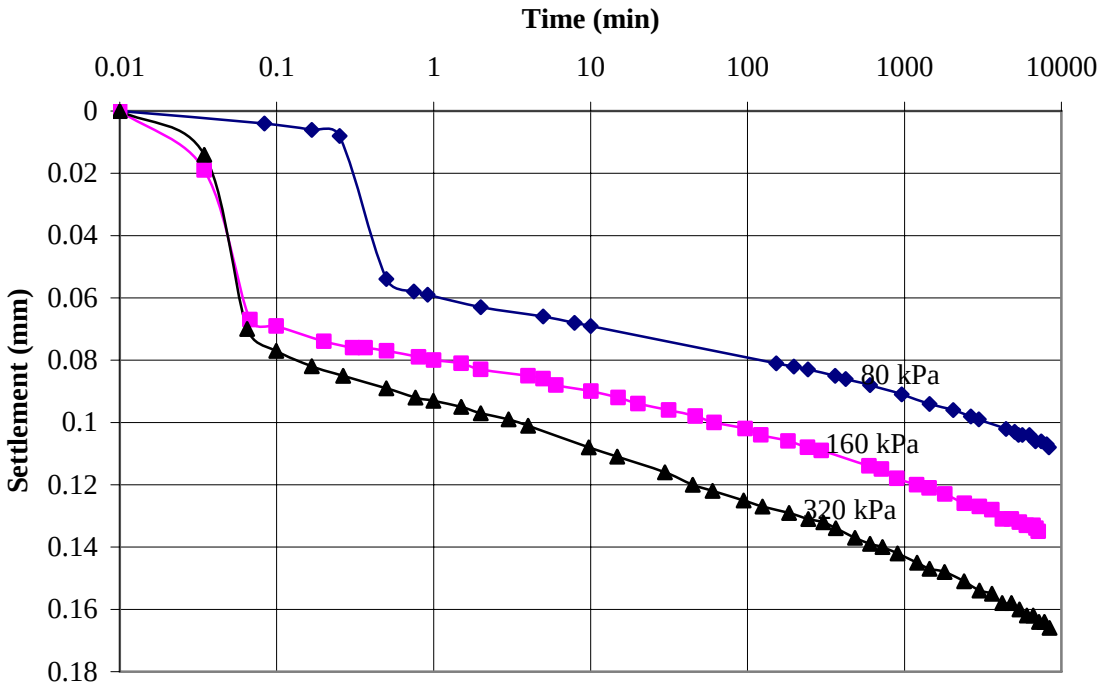

Figure C1.4 Settlement curve of hydraulic fill sample C2

Appendix D

Equivalent permeability variation of hydraulic fill in the mine stope

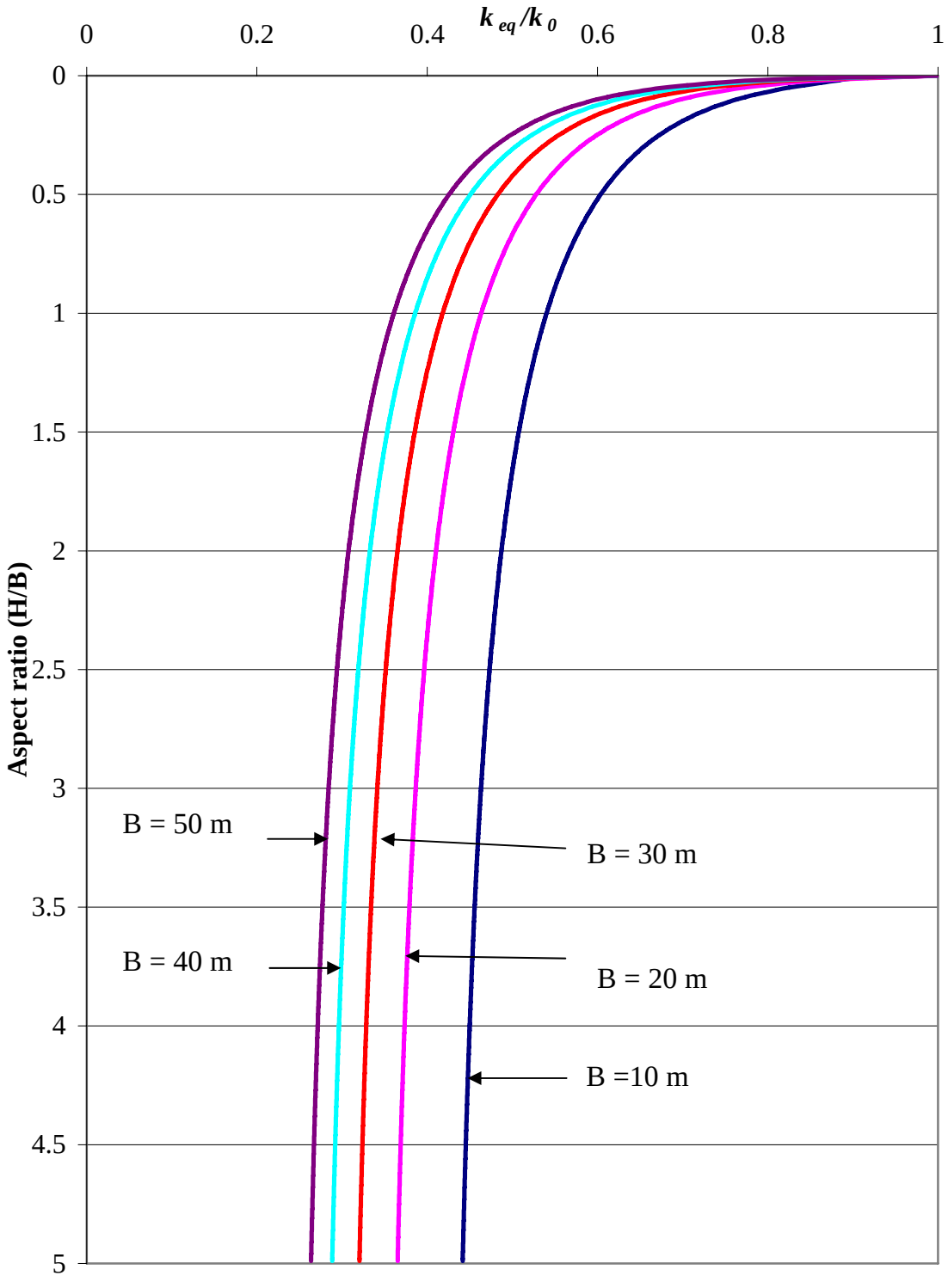

Figure D1.1 Variation of equivalent permeability for hydraulic fill sample B1 with depth

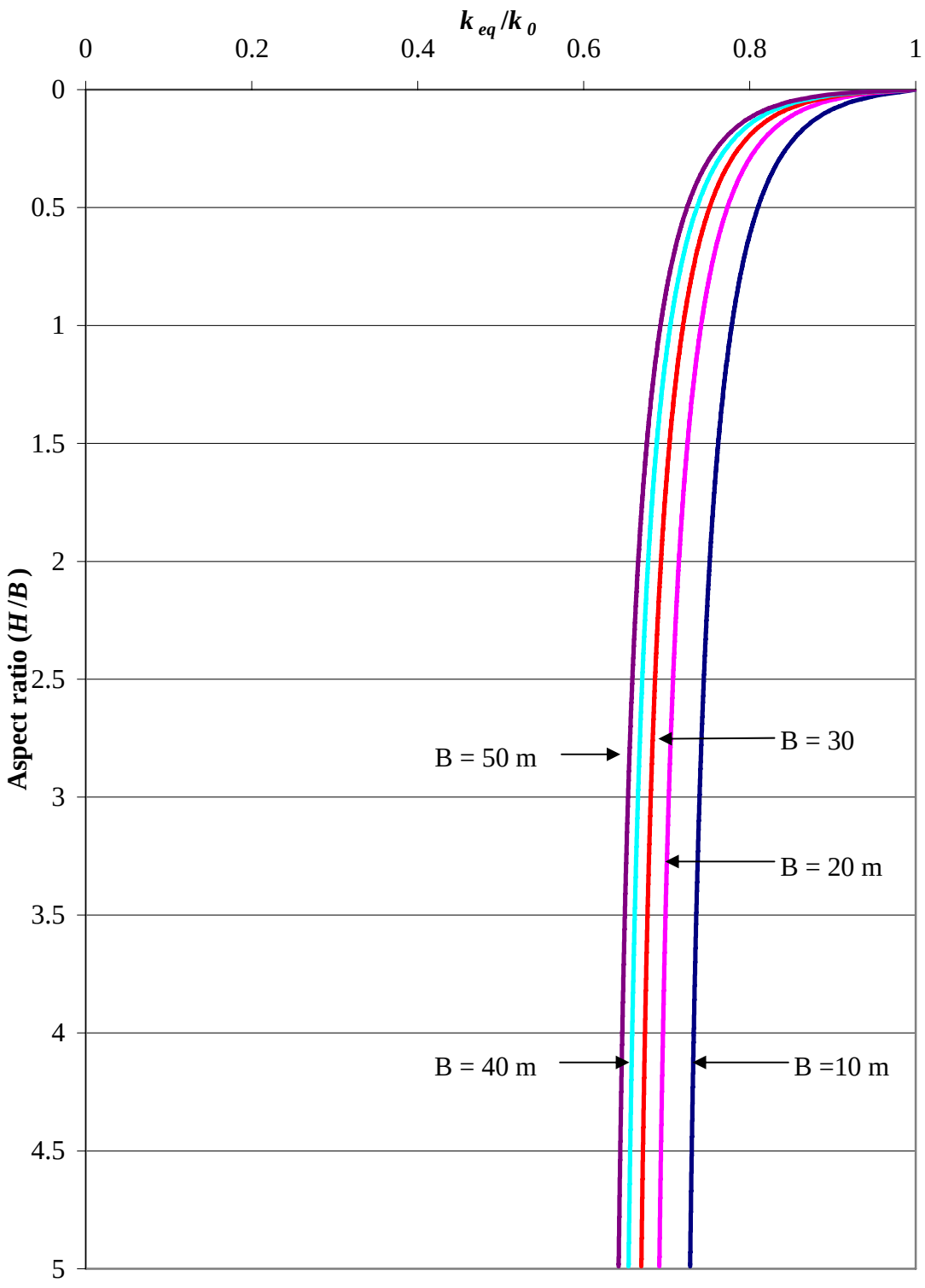

Figure D1.2 Variation of equivalent permeability for hydraulic fill sample B2 with depth

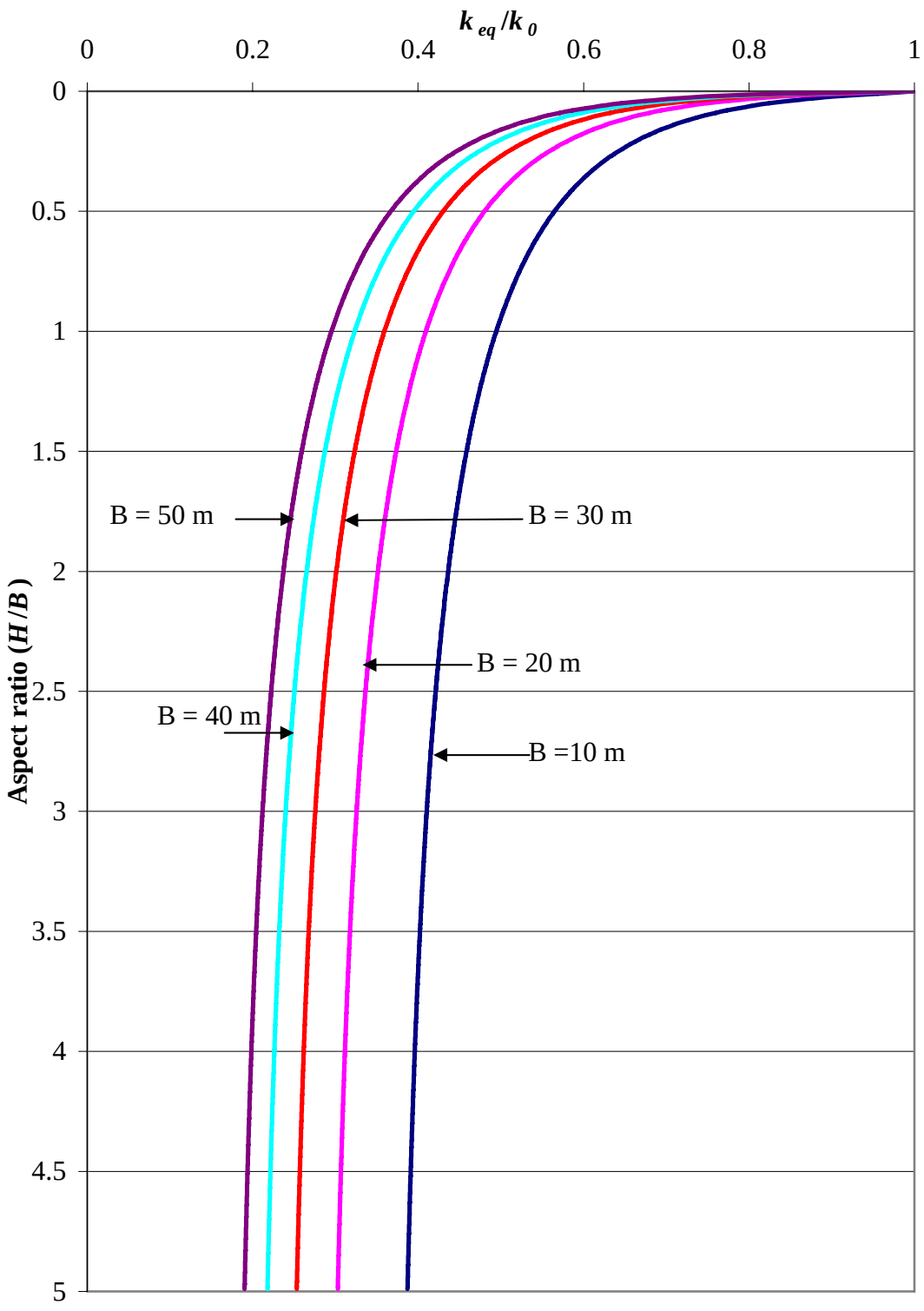

Figure D1.3 Variation of equivalent permeability for hydraulic fill sample C1 with depth

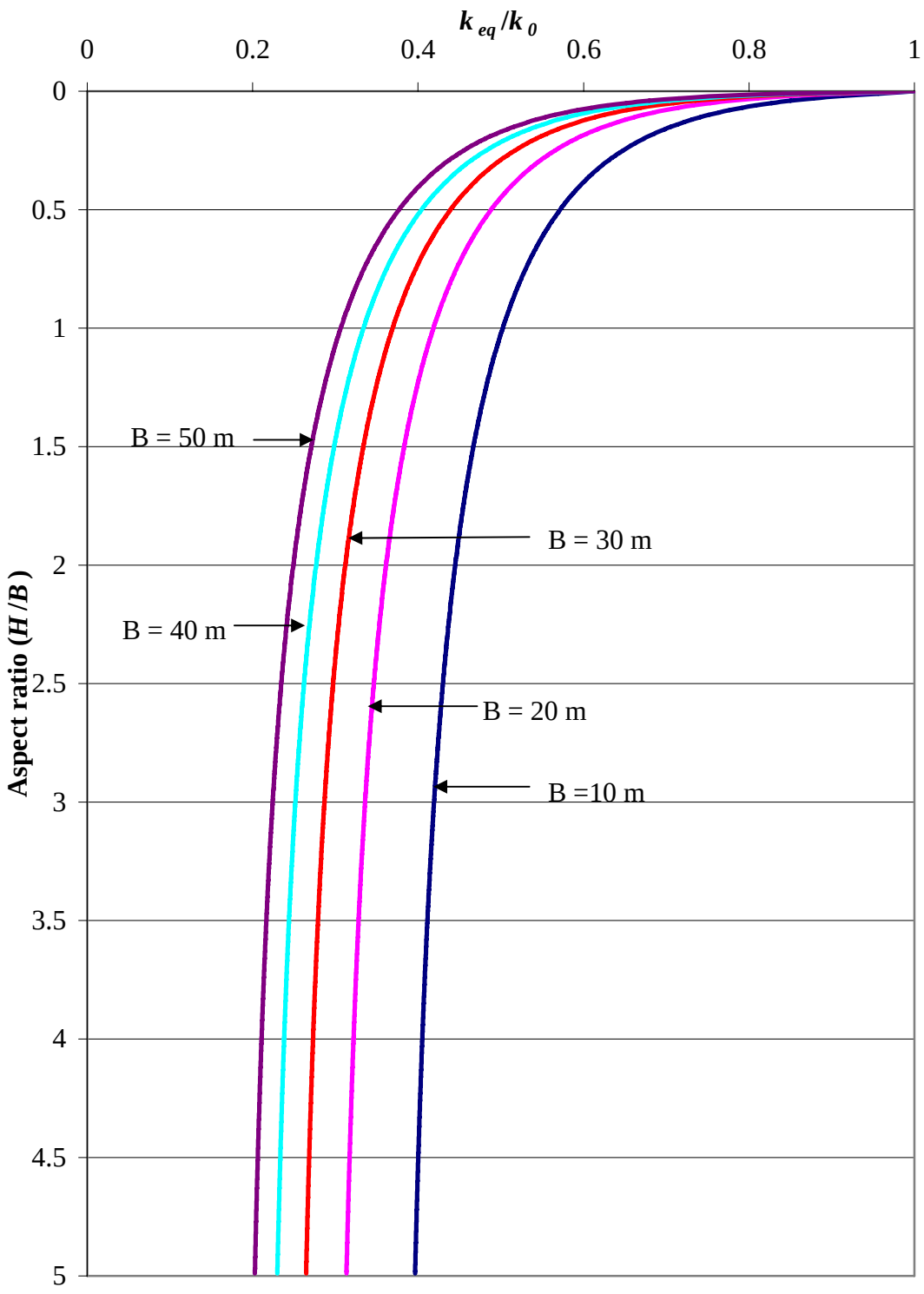

Figure D1.4 Variation of equivalent permeability for hydraulic fill sample C2 with depth